ARCHITECTURE OF THE MAMMALIAN CIRCADIAN REPRESSIVE COMPLEX

APPROVED BY SUPERVISORY COMMITTEE

Carla B. Green, PhD

Ryan E. Hibbs, PhD

Joseph S. Takahashi, PhD

Genevieve Konopka, PhD

DEDICATION

This work is dedicated first and foremost to my wife, Abby, who enriches my life beyond belief every day. I cannot imagine a better partner in life. I would also like to dedicate this work to my parents, Nora and Larry, and my brother, Drew, for their unconditional support and love. In addition, I would like to dedicate this work to Drs. Gena Konopka and Lisa Monteggia for pushing a reluctant admissions committee to give me a chance. Without their intervention, I never would have had the opportunity to do this work — work that has been life-changing for me. Finally, I would like to dedicate this work to my mentor, Dr. Carla Green, for giving me the opportunity to pursue what has long been a dream project for me. Her steadfast support and guidance has allowed me to mature and grow as a scientist in ways that I never imagined.

ARCHITECTURE OF THE MAMMALIAN CIRCADIAN REPRESSIVE COMPLEX

by

CLARK JEFFREY ROSENSWEIG

DISSERTATION / THESIS

Presented to the Faculty of the Graduate School of Biomedical Sciences

The University of Texas Southwestern Medical Center at Dallas

In Partial Fulfillment of the Requirements

For the Degree of

DOCTOR OF PHILOSOPHY

The University of Texas Southwestern Medical Center at Dallas

Dallas, Texas

August, 2017

ARCHITECTURE OF THE MAMMALIAN CIRCADIAN REPRESSIVE COMPLEX

Publication No. _____

Clark Jeffrey Rosensweig

The University of Texas Southwestern Medical Center at Dallas, 2017

Supervising Professor: Carla B. Green

PREFACE

Intricate timing systems have evolved to help organisms in all walks of life organize their physiology to the solar day. Mammalian circadian clocks are driven by a transcription/translation feedback loop composed of positive regulators (CLOCK/BMAL1) and repressors (CRY1/2 and PER1/2). To understand what drives periodicity within this clock, I took structural approaches with the hope of identifying atomic-level details that inform behavioral outputs. Despite high sequence identity, null mutations of *Cry1* or *Cry2* have divergent effects on periodicity, accelerating and decelerating the clock speed, respectively. To understand the unique roles of CRY1 and CRY2, we used statistical

coupling analysis to identify co-evolving residues within the CRY protein family. We identified an evolutionary hotspot, an ancestral secondary cofactor-binding pocket, which has been repurposed for direct interaction with CLOCK and BMAL1. Mutations weakening binding between CLOCK/BMAL1 and CRY1 lead to acceleration of the clock, revealing a novel mode of period regulation in the mammalian clock. Subtle divergence between CRY1 and CRY2 at the secondary pocket underlies differences in affinity for CLOCK/BMAL1. The lower affinity interaction with CRY2 is strengthened by co-expression of PER2, suggesting that PER expression limits the length of the repressive phase in CRY2-driven rhythms. In order to better understand PER's role, we collaborated with another lab to solve and validate a structure of CRY2 bound to a fragment of PER. In so doing, we discovered that interaction between PER and CRY is necessary for rhythmic derepression, providing insight into the role of a key interaction in the molecular clockwork.

ACKNOWLEDGEMENTS

A work of this length and depth has always seemed beyond me, but lo and behold, here it is, complete and digitally tangible. Although it appears to be the work of a single author, there are many people who have made this work possible and I am deeply indebted to all of them.

First, I am very grateful to my mentor, Dr. Carla B. Green. When I started my career as a graduate student, I had a very clear picture of what I wanted in a mentor: someone approachable, thoughtful, and engaged in a compelling research program. In Carla, I got all of this and more. She is generous with her time and energy and has a deft touch when it comes to understanding how to develop students into independent investigators. I have been free to pursue my ideas in her lab with the knowledge that there would always be support for me no matter what ledge I decided to jump off. Her door is always open and she is willing to listen and advise on matters scientific and personal. I am deeply indebted to her for her mentorship and friendship.

I also wish to express my sincere gratitude to my dissertation committee members, Dr. Joseph S. Takahashi, Dr. Genevieve Konopka, and Dr. Ryan E. Hibbs. Their insight has been invaluable and together I think we have made interesting and worthwhile discoveries. Their guidance and example have lit the way for me as a young scientist.

This work stands as a monument to the power of great collaborators. I have had the opportunity to work with world-class scientists in my time at UT Southwestern and the collaborative atmosphere fostered here is unlike any place I have ever been. In particular, Dr. Kimberly A. Reynolds has gone well out of her way to help teach me statistical coupling

analysis and create a huge component of my flagship work. Likewise, Dr. Peng Gao, Dr. Yongli Shan, Yogarany Chelliah, Dr. Ryan E. Hibbs, and Dr. Colleen M. Noviello have bent over backwards to teach me considerably difficult things while I peppered them with questions. Without their help, very little of this work would have been possible. I have also had the pleasure of collaborating with several researchers at other institutions. I am still floored by the largesse of our collaborators Dr. Ning Zheng and Dr. Shannon N. Nangle at the University of Washington. Shannon in particular is my scientific better half and I will be forever grateful to her for bringing me on board for our eLife paper. In addition, I want to thank our excellent collaborators at the University of Virginia, Dr. Michael Menaker and Denise Holmes, for their help on a project not described here. My life as a scientist has been greatly enriched by my interactions with Mike and I will never forget his stories from years of fascinating research.

I have had the good fortune to share a lab with a great group of people for many years and I value our friendship highly. Thank you to Dr. Jeremy Stubblefield, Dr. Peng Gao, Dr. Shihoko Kojima, Isara Laothamatas, Yasemin Onder, Dr. Katharina Sewart, Anita Wu, and Cameron Ford for your advice, input, and camaraderie over the years.

Outside of strict collaborations, I am lucky to work with a variety of wonderful, funny, and intelligent people, including (but not limited to) Dr. Seung-Hee Yoo, Dr. Brian Zoltowski, Dr. Shin Yamazaki, Dr. Filipa Rijo-Ferreira, Dr. Victoria Acosta, Dr. Marleen de Groot, Dr. Jennifer Mohawk, Dr. Guocun Huang, Prachi Nakashe, Crystal Bettilyon Walsh, Dr. Sara Ireland, Dr. Daniel J. Araujo, Ashley Anderson, Marissa Co, and Dr. Miles Fontenot, M.D. I would also like to point out especially some of my closest compatriots in

the neuroscience graduate program, Lauren Tyra and Stephanie Hickey. Science is a long and difficult path with only a little bit of success for every failure. Having good friends with which to laugh and complain along the way is of paramount importance. Lauren and Stephanie have always been there for both. Likewise for Lindsay Clark, my earliest grad school friend, structure guru, and purveyor of music and comedy. I am also grateful to her for introducing me to some awesome members of the LA stand up scene.

Finally, amongst friends, Dr. Bradford Casey is in fact a brother. Life occasionally brings us into contact with a fellow traveler, not in a political sense, but rather someone who sees the world as we see the world. Bradford is someone whose intellect and curiosity know no horizon. Without his friendship in graduate school, I think I would have been quite lost. Without the generosity of his spirit, I would have been impoverished. And though he will always demur at his skill as a scientist, we both know the score. There are few better than him.

I would also like to express my gratitude to my original scientific mentor, Dr. David B. Teplow. At the end of college, I thought that I would never work in science or have anything to contribute scientifically. Nearly a year later I found myself interviewing with one of the most warm and generous humans I have ever met. Dave put me back on the path of science and he has continued to mentor me to this day. If I have accomplished anything, it is because Dave has adopted me as his cause and supported my development and for that I am eternally grateful.

Finally, I would like to thank my family for their support. To my wife, Abby: thank you for sharing in all of my triumphs and failures. The highs are sweeter and the lows are

less low because of you. To my brother, Drew: your sense of humor gets me through the weeks. To my parents, Nora and Larry: you are the gold standard. To my cousins, Jennifer and Jeffrey Bond: thank you for making Texas feel like home.

No work occurs in a vacuum. I drove the work presented here, but many, many people contributed in both material and immaterial ways. I am so thankful to everyone in my life for making the past six years an adventure worth doing again. You all made this work possible.

TABLE OF CONTENTS

PRIOR PUBLICATIONS

Rosensweig C, Reynolds KA, Gao P, Laothamatas I, Shan Y, Ranganathan R, Takahashi JS, and Green CB. An evolutionary hotspot defines functional differences between CRYPTOCHROMES. *In preparation for submission to eLife*.

Oguro-Ando A, **Rosensweig C**, Herman E, Nishimura Y, Werling D, Bill BR, Berg JM, Gao F, Coppola G, Abrahams BS, and Geschwind DH. Increased CYFIP1 dosage alters cellular and dendritic morphology and dysregulates mTOR. Mol Psychiatry 2015, 20(9): 1069-78. doi: 10.1038/mp.2014.124

Nangle SN*, **Rosensweig C***, Koike N, Tei H, Takahashi JS, Green CB, and Zheng N. Molecular assembly of the period-cryptochrome circadian transcriptional repressor complex. Elife 2014; 3**,** e03674. doi: 10.7554/eLife.03674.

*authors contributed equally to this work

Gao P, Yoo SH, Lee KJ, **Rosensweig C**, Takahashi JS, Chen BP, and Green CB. Phosphorylation of the Cryptochrome 1 C-terminal Tail Regulates Circadian Period Length. J Biol Chem. 2013, 288(49)**:** 35277–35286. doi: 10.1074/jbc.M113.509604.

Lopes DHJ, Sinha S, **Rosensweig C**, Bitan G. Application of photochemical cross-linking to the study of oligomerization of amyloidogenic proteins. Methods Mol Biol. 2012, 849: 11-21. doi: 10.1007/978-1-61779-551-0_2.

Rosensweig C, Ono K, Murakami K, Lowenstein DK, Bitan G, Teplow, DB. Preparation of stable amyloid β-protein oligomers of defined assembly order. Methods Mol Biol. 2012, 849: 23-31. doi: 10.1007/978-1-61779-551-0_3.

Wang J, Ho L, Zhao W, Ono K, **Rosensweig C**, Chen L, Humala N, Teplow DB, Pasinetti GM. Grape derived polyphenolics prevent Aβ oligomerization and attenuate cognitive deterioration in a mouse model of Alzheimer's disease. J Neurosci. 2008, 28(25): 6388-92. doi: 10.1523/JNEUROSCI.0364-08.2008.

Reichert JM, **Rosensweig CJ**, Faden LB, Dewitz MC. Monoclonal antibody successes in the clinic. Nat Biotechnol. 2005, 23(9): 1073-1078.

LIST OF FIGURES

LIST OF TABLES

LIST OF APPENDICES

LIST OF DEFINITIONS

bHLH – basic Helix-Loop-Helix

BMAL1 – Brain and muscle arnt-like 1

CBD – CRY-binding domain, a C-terminal motif on PER that interacts with CRY

CCE – Cryptochrome C-terminal Extension, often referred to as CRY's tail

CC helix – Coiled coil-like helix in CRY's C-terminus

CKIδ/ε – Casein kinase I δ/ε

CKBD – Casein kinase-binding domain, a region of PER that interacts with CKIδ/ε

CLOCK – Circadian locomotor output cycles kaput

CRY – Cryptochrome

CYC – Cycle, a Bmal1 homolog

FAD – flavin adenine dinucleotide

FBXL3 – F-box and leucine rich repeat protein 3

FBXL21 – F-box and leucine rich repeat protein 21

HAT – Histone acetyltransferase

HMT – Histone methyltransferase

PAS – PER-ARNT-SIM domain

PER – Period

SCF – Skp1-cullin-F-box

SCN – Suprachiasmatic Nucleus

TAD – Transcriptional activation domain

TIM – Timeless

CHAPTER ONE: A Review of the Literature

PERIODICITY, REPRESSION, AND THE MOLECULAR ARCHITECTURE OF THE MAMMALIAN CIRCADIAN CLOCK

A Transcription/Translation Feedback Loop

In biology, as in life, timing is everything. In particular, there are a preponderance of environmental challenges that occur with regularity and require innate timing systems to predict and respond in order to maintain a competitive advantage in the wild. An environmental timing challenge can be relatively simple, for instance needing to predict whether it will be light or dark at any given time while living near the equator, or it can be complex, as in the case of the short-lived marine midge, *Clunio marinus*, which must navigate both lunar and daily cycles to mate and oviposit during extreme low tides at various latitudes (Kaiser et al., 2016). The study of daily cycles, or circadian biology (circa meaning about and dian meaning day), has led to rapid advancement in our understanding of how these endogenous timing systems are generated and perpetuated even in the absence of environmental input.

Discovery of the activators

Although decades of behavioral research preceded, the story of the mammalian molecular clock begins with the discovery of a gene called *Clock*, which encodes a protein

with a basic Helix-Loop-Helix (bHLH) domain and two tandem PER-ARNT-SIM (PAS) domains (King et al., 1997). *Clock* was discovered in a forward genetic mutagenesis screen searching for mice with aberrant period phenotypes (Vitaterna et al., 1994). The mutation identified in this screen, *Clock*-Δ*19*, is semi-dominant and maps to a 5'-splice donor site in intron 19 that causes skipping of exon 19 (King et al., 1997). Heterozygous carriers of the mutation have slightly elongated endogenous periods of 24.5 to 24.8 hours, while homozygous carriers range from roughly 27 to 30 hours (Vitaterna et al., 1994). Shortly after the discovery and cloning of *Clock*, a second bHLH-PAS gene, *Arntl*, was cloned (Hogenesch et al., 1997) and shown to interact with CLOCK in a yeast two-hybrid screen (Gekakis et al., 1998). In the circadian community, *Arntl* is known primarily as *Brain and muscle ARNT-like 1* (*Bmal1*), but sometimes called *Mop3*. CLOCK and BMAL1 were shown to form a heterodimeric transcription factor, which activated transcription from E-box elements in the genome (Gekakis et al., 1998). This role as a transcriptional activator is dependent on an intact exon 19, as CLOCK-Δ19 was unable to induce target gene expression with BMAL1 (Gekakis et al., 1998). In concert, this work suggested that a key feature of the mammalian clock is transcriptional control of gene targets. This finding echoed previous work in fruit flies and the bread mold *Neurospora crassa*, which suggested that endogenous clocks in these organisms are composed of transcription/translation feedback loops in which positive regulators are repressed by products of their own gene targets (Aronson et al., 1994; Hardin et al., 1990).

A simple model takes shape

In the early 1970s, pioneering research in fruit flies by Konopka and Benzer identified several mutations that caused aberrant period phenotypes in eclosion and locomotor activity (Konopka and Benzer, 1971). All three mutations mapped to the same genetic locus and about a decade later the gene, *period*, was cloned by two labs (Bargiello et al., 1984; Bargiello and Young, 1984; Reddy et al., 1984; Zehring et al., 1984). Later work identified *per* as a negative regulator of its own expression (Hardin et al., 1990) along with a binding partner, TIMELESS (TIM) (Sehgal et al., 1995).

Concurrent with the discovery of the heterodimeric transcriptional activator CLOCK/BMAL1, a number of genes with homology to the *Drosophila per* gene were identified and cloned (Albrecht et al., 1997; Shearman et al., 1997; Shigeyoshi et al., 1997; Sun et al., 1997; Tei et al., 1997; Zylka et al., 1998). Expression of this gene family (*Period 1, 2,* and *3*) is oscillatory in an anatomical region of the brain called the suprachiasmatic nucleus (SCN) (Shearman et al., 1997; Sun et al., 1997; Tei et al., 1997; Zylka et al., 1998), which has been shown to function as a master pacemaker (Ralph et al., 1990). Moreover, all three PER proteins were shown to be capable of repressing the transcriptional activity of CLOCK and BMAL1 (Jin et al., 1999; Sangoram et al., 1998). The discovery that the positive arm of the *Drosophila* oscillator is composed of homologs of *Clock* and *Bmal1*, *Clk* and *Cyc* respectively, suggested that the mammalian circadian clock might be composed of the same components as the *Drosophila* clock (Allada et al., 1998; Rutila et al., 1998). However, unlike the molecular oscillator in *Drosophila*, PER proteins have a unique binding partner in mammalian clocks: CRYPTOCHROMEs (CRYs). *Cry1* and *Cry2* were originally

cloned from human cDNAs before mouse homologs were identified (Hsu et al., 1996; Kobayashi et al., 1998). Originally thought to be a mammalian photoreceptor involved in light entrainment of the clock (Thresher et al., 1998), it quickly became apparent that CRYs are necessary components of a functioning clock with a direct, light-independent role in repression of CLOCK/BMAL1-mediated transcription (Griffin et al., 1999; Kume et al., 1999; van der Horst et al., 1999; Vitaterna et al., 1999). Thus, the core mechanism of the mammalian circadian clock is a transcription/translation feedback loop in which CLOCK and BMAL1 regulate the transcription of their repressors, PERs and CRYs (Figure 1-1).

This simple model has been expanded to include an accessory loop in which *Bmal1* expression is regulated by several members of the retinoic acid-related orphan receptor family: *Rora*, *Rorb*, *Rorc*, and *Nr1d1* (*Rev-erb α*) and *Nr1d2* (*Rev-erb β*). RORs function as positive regulators of *Bmal1* expression while both REV-ERBs function as negative regulators, competing with the RORs for a binding site in the *Bmal1* promoter (Guillaumond et al., 2005; Preitner et al., 2002; Sato et al., 2004; Ueda et al., 2002). *Rev-erb α* and *β* are in turn regulated by CLOCK and BMAL1 (Preitner et al., 2002). The REV-ERBs function redundantly in the core clock mechanism. Deletion of either *Rev-erb α* or *β* has a minimal effect on normal clock function, but deletion of both results in either very low amplitude rhythms with a period roughly 2.5 hours shorter than WT or outright locomotor arrhythmicity, reminiscent of *Bmal1*$^{-/-}$ mice (Cho et al., 2012; Liu et al., 2008; Preitner et al., 2002).

In the years since the outlines of the clock began to come together, the portrait has become more complex. A large number of additional clock components have been identified

and characterized. Structures for several of the key proteins have been solved. Network dynamics of the SCN and their contribution to periodicity, rhythmicity, and robustness of the oscillator are better understood. Regardless, one of the most critical questions in trying to understand a timing system remains poorly understood: how is a 24-hour periodicity achieved and what are the key nodes in the molecular network where the period can be tuned?

This work will largely ignore the contributions of the SCN network and post-transcriptional regulation to periodicity to focus on an oft-overlooked facet of the clock: structural dynamics and the formation and function of the repressive complex. In doing so, it will become clear that assembly of the repressive complex on the activators CLOCK and BMAL1 is not only integral to a functional oscillator, but central to determining period.

Structural features of the activation complex

High-resolution structures of the bHLH-PAS domains of CLOCK and BMAL1 have provided insight into how CLOCK and BMAL1 heterodimerize and bind DNA (Huang et al., 2012; Wang et al., 2013). In addition to static structures, conformational dynamics of a protein interaction domain in the C-terminus of BMAL1 have been reported helping to elucidate a key structural mechanism in clock function (Gustafson et al., 2017; Xu et al., 2015). Beyond structural information, several labs have identified post-translational modifications on CLOCK and BMAL1 and additional components of the activator complex. Here I describe these findings and their implications for a mechanistic understanding of the clock.

The CLOCK/BMAL1 heterodimer

CLOCK is an 855 amino acid protein and its structure is defined principally by three major features: an N-terminal bHLH domain immediately succeeded by tandem PAS domains (PAS-A and PAS-B), and the exon 19 region in CLOCK's disordered C-terminal domain (Figure 1-2). Similarly, comprised of 626 amino acids, BMAL1 is also defined by its N-terminal bHLH domain and tandem PAS domains, though its disordered C-terminus contains a transactivation domain (TAD) (Figure 1-2). The primary crystal structure of CLOCK and BMAL1 is composed of the bHLH and PAS domains of each protein (residues 26-384 of CLOCK and 62-447 of BMAL1) (Huang et al., 2012). Notably, all three of these structural features are heavily involved in the heterodimerization of CLOCK and BMAL1 with each domain interacting primarily with its associated partner such that both bHLH domains interact, both PAS-A domains interact, and both PAS-B domains interact. The interactions of the PAS domains are primarily driven by large patches of surface-exposed hydrophobic residues at each interface. The interface between the PAS-A domains is extensive, burying a surface area of nearly 2000 $Å^2$ while the interface between the PAS-B domains is still substantial at roughly 700 $Å^2$. As a result, the heterodimerization of CLOCK and BMAL1 is highly robust to mutations at these interfaces. Minimal effects on heterodimerization and transactivation were observed when single hydrophobic residues were substituted with charged residues at these interfaces. Critically, the two PAS interactions seen in this structure are highly divergent. The PAS-A domains adopt common PAS folds with several α helices surrounding the concave surface of a five-stranded

antiparallel β sheet. An α helix from each PAS-A packs against the β sheet face of the opposing PAS-A (Figure 1-3A). In contrast to the symmetrical interaction between the PAS-A domains, the PAS-B domains interact at a single interface. The BMAL1 PAS-B domain sits atop CLOCK's PAS-B domain forming an interaction between the concave β sheet surface of BMAL1's PAS-B domain and an α helix from CLOCK's PAS-B. Critically, the nature of this embrace leaves a substantial portion of CLOCK's PAS-B domain exposed and available for an additional protein-protein interaction, which we shall return to shortly (Figure 1-3B).

Like other bHLH-PAS proteins, the bHLH domain is used primarily for mediating a direct interaction with target DNA (Wang et al., 2013). CLOCK and BMAL1 have been shown to interact with both canonical (CACGTG) and non-canonical (e.g. CCAATG, CATTGG, CATGTG, AACGTG) E-boxes (Hogenesch et al., 1998; Koike et al., 2012; Panda et al., 2002; Storch et al., 2002; Ueda et al., 2002; Yoo et al., 2005). Wang and colleagues solved a structure of the bHLH domains of CLOCK and BMAL1 bound to a canonical E-box DNA sequence (CACGTG) and found that basic helical regions insert into the major groove of DNA and residues from both CLOCK (R39, E43, R47) and BMAL1 (H77, E81, R85) have specific interactions with this motif (Wang et al., 2013). The authors go on to show that interaction with non-canonical E-boxes often requires an additional hydrophobic interaction between the BMAL1 residue I80 and a flanking thymine next to the E-box (e.g. A<u>CACGTG</u>T, E-box underlined). In addition to specifying DNA targets, the bHLH domains also stabilize the CLOCK/BMAL1 heterodimer through interactions between the two helices of each protein, which form a four-helical bundle (Huang et al., 2012; Wang et al., 2013).

Although the bHLH domains can homodimerize, steric clashes resulting from CLOCK H84 or BMAL1 L125 render homodimers far less stable than the heterodimer, suggesting a mechanism for mutual recognition and preferential formation of the heterodimer (Wang et al., 2013).

CLOCK-specific features

The C-terminal region of CLOCK beyond the PAS-B domain is intrinsically disordered, but contains at least one region of critical importance to normal clock function. The exon 19 region of CLOCK (residues 514-564) falls within a glutamine-rich region of the C-terminus (King et al., 1997). CLOCK has one known paralog, NPAS2, which can serve as a secondary binding partner for BMAL1, rhythmically activating clock-controlled genes like the repressors *Per1*, *Per2*, and *Cry1* (Reick et al., 2001). Interestingly, the exon 19 region of CLOCK represents the only region of sequence similarity between CLOCK and NPAS2 beyond the bHLH-PAS domains (King et al., 1997). Moreover, CLK proteins from Drosophila and the silk moth Antheraea pernyi (dCLK and apCLK respectively) both contain C-terminal sequences with homology to the exon 19 region of CLOCK (Chang et al., 2003; Lee et al., 2016). Deletion of these homologous sequences prevented repressive feedback from dPER and apPER. Lee and colleagues went on to show that deletion of the exon 19 homology region in dCLK impaired interaction with dPER (Lee et al., 2016). This observation extended to the associated mouse proteins. In transiently transfected cells, CLOCK Δ19 showed weakened interaction with all three PER proteins compared with WT CLOCK.

Substantial evidence exists to suggest that CLOCK and BMAL1 effect some of their role as transcription factors through epigenetic regulation, opening chromatin and recruiting several histone-modifying enzymes (DiTacchio et al., 2011; Katada and Sassone-Corsi, 2010; Menet et al., 2014; Nam et al., 2014). One such enzyme, Mixed Lineage Leukemia 1 (MLL1, encoded by *Kmt2a*), promotes transcriptional activity through its histone methyltransferase (HMT) activity (Katada and Sassone-Corsi, 2010). MLL1's HMT activity is specialized for trimethylation of H3K4 (H3K4me3). Katada and Sassone-Corsi demonstrated that there is a circadian rhythm of H3K4me3 at the promoters of clock-controlled genes and MLL1 is essential for rhythmic expression of these genes. Moreover, though recruitment of MLL1 is circadian, its expression is not. Loss of MLL1 results in severely attenuated expression and blunted amplitude of *Dbp* and *Per2* mRNA, two targets of CLOCK and BMAL1. The HMT activity of MLL1 is also regulated in a circadian manner by acetylation, controlled in part by the NAD^+-dependent deacetylase SIRT1 (*Sirt1*) (Aguilar-Arnal et al., 2015). Notably, MLL1 physically interacts with WT CLOCK and BMAL1, but not with CLOCK Δ19 (Katada and Sassone-Corsi, 2010). In concert with the work characterizing the exon 19 region of CLOCK, these data suggest the intriguing possibility that the exon 19 region recruits MLL1 to the activator complex at the start of the active phase to orchestrate a cascade of epigenetic modifications opening chromatin and allowing transcription to begin. Later in the repressive phase, PER proteins negatively feedback onto the activator complex in part by competing with MLL1 to bind the exon 19 region and sequester it from interaction with MLL1, ultimately helping to generate rhythmicity in gene

expression. This potential mechanism might represent a conserved motif in vertebrate and insect clocks, though further study is merited.

In addition to the exon 19 region, the disordered C-terminus of CLOCK also contains a glutamine-rich region with limited sequence similarity to ACTR, a member of the SRC family of histone acetyltransferases (HATs), and ESA1, a member of the MYST family of HATs (Doi et al., 2006). CLOCK was shown to have intrinsic HAT activity, which requires an intact Acetyl-coenzyme A (CoA) binding motif in this region (Doi et al., 2006). CLOCK's HAT activity was shown to be essential to circadian regulation of *Dbp* and *Per1*, potentially through epigenetic regulation of H3K9 and H3K14. Beyond its role in histone acetylation, CLOCK also selectively acetylates its binding partner BMAL1 at residue K537 (Hirayama et al., 2007). Acetylation at this site is critical for recruitment of CRY1 to BMAL1 and for normal cycling behavior through a mechanism addressed in the text below.

While the PAS domains of CLOCK are important for mediating the heterodimerization of CLOCK and BMAL1, the PAS-B domain is also responsible for an interaction with CRY1. In a random mutagenesis screen of CLOCK, Sato and colleagues identified several residues in the PAS-B domain that were responsible for gating physical interaction with CRY1 (Sato et al., 2006). When mutated, residues G332, H360, W362, and E367 disrupted binding with CRY1 and rendered CLOCK resistant to CRY1-mediated repression, suggesting that a physical interaction at this interface is necessary for repressive feedback. In a separate study, Zhao and colleagues found that substitution of the homologous HIF2 residues at positions 361 and 362 of the PAS-B domain (Q361P/W362R) disrupted binding and repressive activity between CLOCK and CRY (Zhao et al., 2007). Notably, the

structure of the CLOCK and BMAL1 bHLH-PAS domains revealed that all of these residues are located on a part of the PAS-B domain that protrudes out from the rest of the structure, making them accessible for a protein-protein interaction (Figure 1-3C) (Huang et al., 2012).

BMAL1-specific features

The bHLH-PAS domains of BMAL1 are primarily used to mediate interactions with DNA and CLOCK, but outside of these domains, there is a single known structural feature of import in the disordered C-terminus of BMAL1: a transactivation domain (TAD) with multiple binding partners. The transcriptional coactivators p300 (*Ep300*) and CREB-binding protein (CBP, *Crebbp*) have been identified as members of the CLOCK/BMAL1 activator complex with potential roles in epigenetic regulation (through domain-specific HAT activity) and recruitment of transcription initiation complex machinery (Etchegaray et al., 2003; Takahata et al., 2000). In particular, p300/CBP enhances transcriptional activation when co-expressed with CLOCK/BMAL1, though this role is dependent on an interaction with the BMAL1 C-terminus (Etchegaray et al., 2003; Takahata et al., 2000). However, co-expression of CRY1 blocked this effect (Etchegaray et al., 2003). Consistent with these data, concurrent reports from two groups identified a region in the distal C-terminus that is critical for both BMAL1-mediated transactivation and CRY1-mediated feedback repression (Kiyohara et al., 2006; Sato et al., 2006). Mutation of BMAL1 A611 or G612 desensitized BMAL1 to CRY1 repression and disrupted binding between the two proteins (Sato et al., 2006). Likewise, BMAL1 constructs truncated at residue 554, 608, and 619 all disrupted binding to CRY1 and resulted in weaker transactivation activity (Kiyohara et al., 2006). Taken together, these data

suggested one or more protein interaction motifs in the final 25-50 residues of the BMAL1 C-terminus.

BMAL1 has a highly conserved paralog, BMAL2, which is nonetheless incapable of rescuing circadian rhythms in *Bmal1*$^{-/-}$ fibroblasts (Xu et al., 2015). Domain swapping rescue experiments demonstrated that a C-terminal region of BMAL1 with a binding motif (IxxLL) for the p300/CBP KIX domain is necessary for normal circadian transcriptional activity. Chemical-shift mapping of the BMAL1 TAD in the presence of CRY1's coiled-coil domain and the CBP KIX domain showed that these two proteins share an overlapping interface on the BMAL1 TAD. Critically, substitutions in and around the IxxLL motif resulted in dramatic changes in periodicity (between 19 and 26 hours) in rescue assays. These changes in period were highly correlated with shifts in the affinity of CRY1 for the TAD with longer periods stemming from higher affinity interactions and shorter periods from lower affinity interactions (Xu et al., 2015). These results suggest that the balance between activator and repressor at this interface is a major node of period regulation in the clock.

Further characterization of the C-terminal TAD revealed that there is a slow conformational switch between cis and trans isomers at a conserved Trp-Pro imide bond in the extreme C-terminus of BMAL1 (Gustafson et al., 2017). Substitution of an alanine at either position of the switch (W624 and P625) locked the TAD into the trans isomer. Trans-locked analogs used in cell-based rescue assays resulted in period shortening of up to 3 hours compared to rescues with WT BMAL1. However, there was no difference in affinity for either CRY1 or the CBP KIX domain with the cis or trans isomers, suggesting an alternate explanation underlying the shift in periodicity for trans-locked mutants. Isomerization of the

switch in BMAL1's TAD occurs over a slow timescale of minutes, but cyclophilins, a family of peptidyl prolyl isomerases (PPIases), can catalyze the isomerization resulting in substantially faster interconversion. Antagonizing the activity of cyclophilins with specific inhibitors results in dose-responsive period lengthening in cycling cell assays, though this effect was reduced in the context of trans-locked TAD mutants. The mechanism underlying these effects on periodicity in the clock is not yet known, but clearly represents an important node for regulation of clock speed.

As stated previously, CLOCK can acetylate BMAL1 at K537 in BMAL1's intrinsically disordered C-terminus (Hirayama et al., 2007). Characterization of the binding affinity between various CRY1/2 and BMAL1 TAD fragments revealed a potential role for this post-translational modification on BMAL1 (Czarna et al., 2011). The C-terminal region of CRY contains a structured coiled coil, which is highly conserved between CRY1 and CRY2, and an intrinsically disordered tail region, which is completely divergent between the two CRYs. Czarna and colleagues purified the C-terminal regions of CRY1 and CRY2, denominated CRY1CCT and CRY2CCT respectively, and measured the affinity of these fragments for a short (residues 577-625) and long (residues 490-625) fragment of the BMAL1 C-terminus. While both CCT constructs bound the short fragment of BMAL1 with ~10 μM affinity, there was a clear difference in affinity between CRY1CCT (~20-40 μM depending on method of analysis) and CRY2CCT (~10 μM) with the longer fragment of BMAL1, which contains the acetylated residue K537. Interestingly, substitution of a glutamine at K537 (K537Q), which mimics an acetylated lysine, resulted in a stronger affinity between CRY1CCT and the long fragment (~10 μM). Whether this observation is

relevant in vivo is unknown, but it raises the question of how acetylation status at BMAL1 K537 might affect the circadian timing mechanism. The work of Xu and colleagues certainly suggests that the balance of affinity between CRY1 and the BMAL1 TAD is an important regulatory node for period length (Xu et al., 2015).

Components of the activator complex

In addition to the previously described components of the circadian activator complex MLL1 and p300/CBP, several other proteins have been identified with roles in the molecular clockwork. Thyroid hormone receptor-associated protein-150 (TRAP150, *Thrap150*) was identified in CLOCK/BMAL1 complexes (Lande-Diner et al., 2013). TRAP150 can function as a coactivator for certain nuclear receptors, but also has roles in RNA splicing and DNA repair. However, in the clock, its role appears to be confined to coactivation with CLOCK and BMAL1. Expression of TRAP150 is controlled in part by CLOCK and BMAL1 through an E-box in its promoter, with mRNA peaking at circadian time (CT) 4, early in the subjective day. TRAP150 physically associates with CLOCK and BMAL1 through an unknown interface and recruits the Mediator complex, a large protein complex that functions as a modulator of the RNA polymerase II preinitiation complex. Depletion of TRAP150 results in low amplitude, long period rhythms and a reduction in RNA polymerase II at E-box sites of clock-controlled genes.

JumonjiC (JmjC) and ARID domain-containing histone lysine demethylase 1a (JARID1a, *Kdm5a*) has also been identified in activator complexes (DiTacchio et al., 2011). DiTacchio and colleagues identified circadian oscillations in histone modifications at histone

3 (H3) lysine 9 (H3K9Ac) and H3K4 (H3K4me3). As previously described, trimethylation at H3K4 is promoted by MLL1 (Katada and Sassone-Corsi, 2010), so the authors focused on the JmjC domain-containing H3K4me3 demethylase family as potential regulators of demethylation at this site. However, JARID1a was found to associate with CLOCK and BMAL1 during the positive phase of the circadian cycle and function as a coactivator for circadian target genes, enhancing the activity of CLOCK and BMAL1 (DiTacchio et al., 2011). This role is inconsistent with a function as a demethylase for H3K4me3 as this epigenetic marker is primarily associated with a poised chromatin state, available for active transcription (Wang et al., 2009). Subsequently, DiTacchio and colleagues demonstrated that JARID1a's demethylase activity is not required in its role as a coactivator (DiTacchio et al., 2011). Rather it functions in the clock primarily as an antagonist of histone deacetylase 1 (HDAC1, *Hdac1*), repressing its activity and increasing acetylation of H3K9 at the Per2 E-box. Deletion of *Jarid1a* results in shorter periods and lower amplitude oscillations in clock-controlled gene expression. Notably, related family members JARID1b (*Kdm5b*) and JARID1c (*Kdm5c*) did not serve as coactivators of CLOCK/BMAL1-mediated transcription, but did function in a repressive capacity by reducing H3K4me3 modifications at the *Per2* promoter.

Photic input to the clock through the activation complex appears to come in part from a signal cascade in which Protein kinase C α (PKCα, *PRKCA*) phosphorylates lysine-specific demethylase 1 (LSD1, *KDM1A*). Phosphorylated LSD1 subsequently helps to recruit CLOCK and BMAL1 to target E-boxes, functioning primarily as a coactivator (Nam et al., 2014). Though its mechanism of action is unknown, its demethylase activity is not involved,

but phosphorylation by PKCα at S112 is necessary. Phosphorylation at this site also occurs rhythmically with a peak at CT8 in the liver, suggesting that it not only mediates photic input to the activation complex, but also functions in normal daily rhythms. However, knock-in mice with S112A substitutions have relatively minor effects on overall clock function. This LSD1 mutant shows attenuated binding with CLOCK and BMAL1 and less recruitment to target promoters, but there is no change in period in locomotor activity rhythms. The most significant behavioral effect is lower amplitude rhythms suggesting that LSD1 primarily reinforces normal clock function.

Structural features of the repressive complex

Our understanding of the molecular details of the circadian clock has accelerated in the last decade due in no small part to a wealth of data on the repressors CRY and PER. Structural details on CRYs and PERs have emerged through crystallographic and NMR studies. Meanwhile, a number of different post-translational modifications have been identified and their roles elucidated to paint a picture of how the repressors are regulated. Finally the size and scope of the circadian repressive complex has been characterized conveying a sense of both the mechanistic basis of repression and the contributions of different elements to timing.

Structural features of the Cry/Photolyase Family

CRYs belong to a family of proteins (the Cry/Photolyase Family (CPF)) with an ancestral role in DNA repair (Chaves et al., 2011). DNA Photolyases (PHLs) catalyze repair

of UV-damaged DNA through a flavin adenine dinucleotide (FAD) cofactor (Kavakli et al., 2017). FAD is complexed in a large cavity in the globular domain that comprises most of the PHL (Park et al., 1995; Tamada et al., 1997). DNA lesions bind at this site and appose the FAD molecule, bringing the two components of the reaction into close proximity for a reduction of the cyclobutane pyrimidine dimer bond in the damaged DNA (Mees et al., 2004). This reaction is dependent on exposure to blue light and the reaction dynamics can be improved by a light-harvesting, variable secondary cofactor bound in a distal pocket on the other side of CPF proteins (Kavakli et al., 2017; Park et al., 1995; Tamada et al., 1997). Secondary cofactors, traditionally either methenyltetrahydrofolate (MTHF) or 8-hydroxy-5-deazaflavin (8-HDF), are complexed in different ways (Park et al., 1995; Tamada et al., 1997). While MTHF extends out of the secondary pocket, 8-HDF is fully enclosed in the cavity.

Though structurally related to PHLs, CRYs are functionally divergent (Park et al., 1995; Xing et al., 2013; Zoltowski et al., 2011). Although mammalian CRYs have been shown to bind FAD like PHLs (Xing et al., 2013), they possess no DNA repair activity (Ozgur and Sancar, 2003). Moreover, though CRYs exist broadly across the domains of life with a diversity of roles, scant evidence exists to suggest that any eukaryotic CRYs complex a secondary cofactor. For instance, despite several attempts to obtain a structure with a secondary cofactor, none of the existing CRY structures contain one, suggesting that CRYs have evolved to function without secondary cofactors (Brautigam et al., 2004; Czarna et al., 2013; Xing et al., 2013; Zoltowski et al., 2011).

On a functional level, animal CRYs can be grouped into two broad classes: type I and type II CRYs. Type I CRYs (also known as *Drosophila*-type *Crys*, insect-like *Crys*, or *Cry-d* (Rubin et al., 2006)) function as circadian photoreceptors with an ancillary role in the molecular clockwork of *Drosophila* and a number of other insects (Emery et al., 1998; Stanewsky et al., 1998; Yuan et al., 2007). Although type I CRYs have been shown to function as direct repressors of CLK and CYC in some peripheral tissues (Krishnan et al., 2001), their primary role is as a photic input to the clock (Emery et al., 1998; Stanewsky et al., 1998). Indeed, type I CRYs bind the *Drosophila* repressor TIM in a light-dependent interaction and mediate its degradation (Koh et al., 2006). Type II CRYs (also known as mammalian type *Crys*, vertebrate-like *Crys*, and *Cry-m* (Rubin et al., 2006)) function primarily as direct repressors of CLOCK and BMAL1 in vertebrates (Shearman et al., 2000b) and CLK and CYC in a subset of insects (Chang et al., 2003; Rubin et al., 2006; Yuan et al., 2007). Notably, insect clock architectures can be grouped into three cohorts: (1) a *Drosophila*-like clock in which CLK and CYC are repressed by PER and TIM with photic input from a type I CRY, (2) a vertebrate-like clock in which CLK and CYC are repressed by PER and a type II CRY, and (3) an integrated clock in which both a type I and type II CRY are present and functional, providing both a photic input to the system and direct repressive input to CLK and CYC. Surprisingly, of the organisms that have been characterized so far, the *Drosophila*-like architecture is least characteristic of insect clocks, as most adopt either a vertebrate-like (bees, ants, red flour beetles) or integrated architecture (monarch butterflies, silk moths, mosquitos) (Chang et al., 2003; Ingram et al., 2012; Rubin et al., 2006; Yuan et al., 2007). It is not yet known how an integrated architecture works at a structural level, but it

is worth noting that at least a subset of insects with vertebrate-like or integrated architectures express a version of CYC that contains a C-terminal TAD with significant homology to mammalian BMAL1, unlike the truncated version of CYC found in Drosophila (Chang et al., 2003; Rubin et al., 2006). These findings suggest that type II CRYs function as direct repressors of CLOCK and BMAL1/CYC in part due to their ability to sequester the BMAL1/CYC TAD as in mice (Xu et al., 2015). Adding further confusion, most vertebrates have at least two type II CRYs, traditionally called CRY1 and CRY2. While the two are structurally quite similar (Czarna et al., 2013; Kobayashi et al., 1998; Xing et al., 2013), there are several key functional differences that will be discussed shortly.

On a structural level, CRYs have a stereotyped architecture consisting primarily of two major domains: a globular photolyase homology region (PHR) and a highly variable intrinsically disordered C-terminal tail (Figure 1-4A) (Czarna et al., 2013; Xing et al., 2013; Zoltowski et al., 2011). The PHR contains several structural features of note: two cavities on opposite sides of the protein where PHLs ancestrally bound FAD (FAD-binding pocket) and the secondary cofactor (secondary pocket) and a C-terminal α-helix, which is often referred to as the coiled coil helix (CC helix) due to structural characteristics common to coiled coils (Figure 1-4A) (Chaves et al., 2006). Furthermore, the PHR can be divided into an N-terminal α/β domain connected to a C-terminal α-helical domain by a flexible interdomain linker (Figure 1-4B) (Czarna et al., 2013; Xing et al., 2013). The surface area of the secondary pocket is made up of residues from both the α/β domain and the α-helical domain, while the FAD-binding pocket is entirely associated with the α-helical domain. The CC helix is notable for its role as a high traffic interface for protein-protein interactions in type II CRYs (Czarna

et al., 2011; Nangle et al., 2014; Schmalen et al., 2014; Xing et al., 2013; Xu et al., 2015) and for its potential role in nuclear localization of type II CRYs (Chaves et al., 2006). Finally, the intrinsically disordered tails of CRYs are highly divergent and represent the clearest region of departure between CRY1 and CRY2 (Figure 1-4C).

CRY1 and CRY2

Broadly speaking, CRY1 and CRY2 play the same role in the mammalian clock, functioning as indispensible and direct repressive components (Kume et al., 1999; Shearman et al., 2000b; van der Horst et al., 1999; Vitaterna et al., 1999). However, the details of their respective roles are far murkier. Genetic knock-out (KO) models demonstrate that deletion of *Cry1* and *Cry2* together results in arrhythmic locomotor behavioral rhythms (van der Horst et al., 1999; Vitaterna et al., 1999). $Cry1^{-/-}$ and $Cry2^{-/-}$ mice maintain rhythmic locomotor activity, but the former cohort have short endogenous free-running rhythms (~22.5 h) while the latter have long periods (~24.5 h) compared to WT mice (van der Horst et al., 1999; Vitaterna et al., 1999). There is evidence that CRY1 plays a more dominant role in the clock than CRY2. SCN explants from $Cry1^{-/-}$ mice maintain oscillatory expression of a PER2::LUC reporter, while explants from peripheral tissues and dispersed fibroblast cultures do not (Liu et al., 2007). Under the same conditions $Cry2^{-/-}$ tissues and fibroblasts remained rhythmic suggesting that intercellular coupling within the SCN manifests a protective role against weak cell autonomous rhythms. Moreover, it supports the conclusion that *Cry1* is more indispensible than *Cry2* in the clock. In further support of this conclusion, work from Khan

and colleagues found that CRY2 was a weaker repressor of CLOCK/BMAL1-mediated transcription (Khan et al., 2012).

The stark divergence in functional character between CRY1 and 2 is surprising given the level of conservation between the two at a structural level. CRY1 and 2 are 66.4% identical and 76.7% similar across an entire alignment, but excluding their completely divergent tails, the PHR domains are 77.4% identical and 88% similar. Of the residues that diverge in the PHR, the largest cluster is a group of superficial residues in the α/β domain, though there is no substantial dataset to date that implicates this particular region of CRY as an area of importance in normal CRY function (Figure 1-5). Alignment of apo structures of CRY1 and CRY2 also suggests that they are highly similar with a root mean square deviation (RMSD) of 0.493 Å and an all-atom RMSD of 2.162 Å (Czarna et al., 2013; Xing et al., 2013).

Due to the high degree of structural conservation, several theories have arisen to explain the divergent periodicity characteristics observed. One possible explanation is that the phase of expression of *Cry1* and *Cry2* plays a role in their unique periodicities. *Cry2* expression is regulated primarily by CLOCK and BMAL1 through E-box elements, but *Cry1* expression relies on both E-box elements in its promoter and a Rev-Erb/ROR-binding element (RRE) in one of its introns (Ueda et al., 2002; Ueda et al., 2005; Ukai-Tadenuma et al., 2011). As a result, peak *Cry1* expression is delayed compared to *Cry2*, *Per1*, and *Per2*, lengthening the period of a circadian luciferase reporter in cell-based rescue assays (Ukai-Tadenuma et al., 2011). Lending credence to this theory, circadian chromatin immunoprecipitation sequencing (ChIP-Seq) analysis of core clock proteins in the mouse

liver identified concurrent peak DNA occupancy for CRY2, PER1, and PER2 in the early evening, but CRY1's peak occupancy occurred in the late night/early morning forming a late repressive complex on its own with CLOCK and BMAL1 (Koike et al., 2012). In contrast, it was recently demonstrated that PER2::LUC rhythms could be rescued in *Cry1*$^{-/-}$/*Cry2*$^{-/-}$ SCN explants following viral transduction of a plasmid expressing either *Cry1* or *Cry2* under the control of *Cry1*'s promoter, but not the intronic RRE (Edwards et al., 2016). Despite the fact that *Cry1* and *Cry2* were expressed under the control of the same promoter element, the rescues displayed period phenotypes characteristic of the previously described single KO mice (i.e., *Cry2* rescues had short periods and *Cry1* rescues had long periods). When the *Bmal1* promoter was used to drive *Cry* expression (i.e., anti-phase to the normal phase of *Cry* expression), the resulting rescues were low in amplitude, and the rhythms were erratic. Ultimately these results suggest that while phasing plays an important role in a robust oscillator, the distinct periodicity differences observed in CRY1/2-driven rhythms appear to be intrinsic to the proteins themselves.

Regulation of CRY stability

An alternative hypothesis is that differences in periodicity between the CRYs are driven by intrinsic differences in stability. The degradation dynamics of CRYs are primarily driven by interactions with two different Skp1-Cul1-F-box (SCF) E3 ubiquitin ligase complexes: SCF^{FBXL3} and SCF^{FBXL21} (Busino et al., 2007; Godinho et al., 2007; Hirano et al., 2013; Siepka et al., 2007; Yoo et al., 2013). Mutations in FBXL3 that disrupt binding to CRYs result in significant period lengthening in vivo (26-27 h) due to the stabilization of

CRY (Busino et al., 2007; Godinho et al., 2007; Siepka et al., 2007). Surprisingly, the opposite phenotype is present in mice with a mutation or deletion of FBXL21 (Hirano et al., 2013; Yoo et al., 2013). Although both complexes possess E3 ligase activity, SCF^{FBXL21} ubiquitinates CRY less efficiently than SCF^{FBXL3} (Hirano et al., 2013; Yoo et al., 2013). In contrast, however, FBXL21 acts as an antagonist of FBXL3 due to its stronger physical interaction with CRY, effectively stabilizing CRY in the presence of FBXL3. Interestingly, while FBXL21 interacts with CRY in both the cytoplasm and nucleus of cells, FBXL3's interaction is entirely nuclear. Thus, FBXL21 functions as the primary E3 ligase for CRY in the cytoplasm whereas in the nucleus it plays a protective role against the primary nuclear E3 ligase FBXL3. Finally, FBXL3 was shown to ubiquitinate eleven lysine residues on CRY1, while FBXL21 targeted a single site, K11, whose side chain forms the back wall of CRY's secondary pocket cavity (Yoo et al., 2013).

CRY stability is also potentially regulated in vivo by several kinases. Adenosine monophosphate-activated protein kinase (AMPK) phosphorylates CRY1 at S71 and S280 (Lamia et al., 2009). Substitution of an alanine at either site to block phosphorylation stabilized CRY1 and substitution of an aspartate to mimic phosphorylation destabilized CRY1. However, a recent dataset assaying substitutions in a large cohort of CRY1 serines and threonines presented a contradictory assessment of the role of these AMPK targets (Ode et al., 2017). In contrast to the previous report, Ode and colleagues found that substitution of an aspartate at S71 significantly increased the half-life of CRY1, but made it a significantly less potent repressor of CLOCK and BMAL1. Perhaps these divergent observations reflect the effects of unknown factors in the cellular environment. CRY1's tail is also the target of

post-translational regulation at S588 (Gao et al., 2013; Papp et al., 2015). S588 is phosphorylated both rhythmically and in response to DNA damage by an unknown kinase. Phosphorylation at this site stabilizes CRY1 by antagonizing its interaction with FBXL3 and promoting an interaction with the deubiquitinase Herpes virus associated ubiquitin-specific protease (HAUSP, *Usp7*).

Revisiting CRY1 and CRY2, a recent report suggests that there is in fact an inherent difference in stability between the two proteins (Li et al., 2016). Based on the *in vivo* phenotypes of *Fbxl3* mutants, one would expect that stabilization of CRY would lead to longer periods (Godinho et al., 2007; Siepka et al., 2007). However, Li and colleagues found that CRY2 is actually more stable than CRY1, which is inconsistent with the notion that their intrinsic periodicity characteristics stem from stability differences (Li et al., 2016). Further complicating this hypothesis is data from Ode and colleagues examining a large group of serine and threonine residues in CRY1 and their role in both stability and periodicity (Ode et al., 2017). A wide range of periods (from 20-34 h) were observed in cell-based rescue assays with various mutants, but there was little correlation between period in the rescue assay and half-life of the protein. In fact, this data reflects an emergent view in circadian biology that the quality of a protein is just as important as the quantity in determining period (Larrondo et al., 2015).

Nuclear localization of CRY

In their work on CRY1 and CRY2, Li and colleagues suggest that the balance between nuclear and cytoplasmic CRY might be determinative for periodicity (Li et al.,

2016). Nuclear import mechanisms for CRYs are still poorly understood, but work from Hirayama et al. suggests that CRY1 and CRY2 have a conserved nuclear localization sequence (NLS) spanning residues 265-282 and 283-300 respectively (Hirayama et al., 2003). CRY1 and CRY2 also appear to contain a less conserved bipartite NLS in their C-terminal tails that requires an intact CC helix (Chaves et al., 2006). The CC helix, the N-terminal NLS, and the C-terminal NLS are each sufficient to direct CRY to the nucleus and at least one is necessary (Chaves et al., 2006). Members of the Importin α/β family (in particular KPNB1) have been implicated in nuclear localization of CRY2, but CRY1 nuclear entry appears to be primarily mediated through an alternative mechanism (Lee et al., 2015; Sakakida et al., 2005). Interestingly, while CRYs are efficiently translocated to the nucleus on their own, the rate of PER nuclear accumulation is significantly increased in the presence of CRY (Lee et al., 2001; Ollinger et al., 2014; Sakakida et al., 2005; Yagita et al., 2002). Modulating the rate of nuclear import of PER and CRY has clear effects on period, suggesting that it could be an important regulator of the overall timing mechanism, though a more thorough understanding of the mechanisms driving nuclear import of the repressors is warranted.

Protein-protein interactions of CRY

Of all of the core clock proteins, the greatest wealth of structural information belongs to CRY. To date, three structures of the CRY1 PHR and five structures of the CRY2 PHR have been solved with various cofactors and binding partners (Czarna et al., 2013; Michael et al., 2017; Nangle et al., 2013; Nangle et al., 2014; Schmalen et al., 2014; Xing et al., 2013).

Additionally, interactions between CRY and the BMAL1 TAD have been characterized in depth by a series of biophysical experiments (Czarna et al., 2011; Gustafson et al., 2017; Xu et al., 2015). Finally, CRYs have been subjected to substantial mutagenic analysis through which residues involved in periodicity, repression, and protein-protein interactions have been identified (Froy et al., 2002; Gao et al., 2013; Khan et al., 2012; Lamia et al., 2009; Li et al., 2016; McCarthy et al., 2009; Michael et al., 2017; Nangle et al., 2014; Ode et al., 2017; Ozber et al., 2010; Sanada et al., 2004; Schmalen et al., 2014; Xing et al., 2013; Yoo et al., 2013). From this bounty, a few major observations have been gleaned.

First, CRY's CC helix is a widely shared interface for protein-protein interactions. Comparison of a structure of the CRY2/FBXL3 complex to a structure of the CRY2/PER2 Cry-binding domain (CBD) complex illuminates an oft-described observation that PER2 stabilizes CRY (Nangle et al., 2014; Xing et al., 2013). Based on these structures, PER2 and FBXL3 have overlapping binding interfaces at the CC helix, suggesting that interaction with CRY is mutually exclusive. PER2 adopts a sinuous, elongated interface with CRY1 and CRY2, wrapping from just above the secondary pocket of CRY to the CC helix before swooping below the helix and coming back up the other side next to the FAD-binding pocket (Nangle et al., 2014; Schmalen et al., 2014). In a curious twist, CRY and PER2 chelate a zinc ion in an intermolecular zinc finger when bound and disruption of this interface destabilizes their interaction, suggesting the potential for redox sensitivity in the core clock mechanism. FBXL3 embraces the CC helix primarily through a curved β-sheet domain, though it also penetrates deep into the FAD-binding pocket with its C-terminal tail (Xing et al., 2013). In fact, its final residue is a tryptophan and the side-chain mimics the aromatic rings of the

flavin moiety usually found in this pocket. FBXL3 activity can be antagonized by a small molecule (KL001) that stabilizes CRY and lengthens the period in cycling cells (Hirota et al., 2012). Comparison of the FBXL3 complex to structures of CRY2 with either FAD or KL001 bound suggest that both molecules stabilize CRY by binding in the FAD-binding pocket and blocking FBXL3's tail from entering the cavity (Nangle et al., 2013; Xing et al., 2013). In addition to FBXL3 and PER2, the CC helix also participates in an interaction with the BMAL1 TAD in a way that is likely to be competitive with both FBXL3 and PER2 (Czarna et al., 2011; Xu et al., 2015). How these interactions are integrated in a dynamic time-keeping mechanism is not fully understood, but likely to be highly informative in understanding the driving molecular features of periodicity.

Emerging evidence also points toward a second major interface at CRY's secondary pocket. A screen for mutations that would weaken CRY's repressive capacity identified three residues along a helix forming one boundary of the secondary pocket (McCarthy et al., 2009). Characterization of one of the mutants (CRY1 R109Q) revealed that it not only weakened CRY1's repressive capacity, but it blocked CRY1's ability to drive rhythms in a rescue assay and diminished binding between CRY and the CLOCK/BMAL1 complex (Nangle et al., 2014). Computational docking studies combined with biochemical characterization of purified CRY1 and CLOCK PAS-B proteins suggests that the secondary pocket is a binding site for the CLOCK PAS-B domain (Michael et al., 2017).

The nature of the interaction between the CRY proteins and the activator complex is still somewhat contentious. Chen and colleagues found that constitutive expression of *Cry1* did not disrupt rhythms in cycling fibroblasts whereas constitutive expression of either *Per1* or

Per2 did (Chen et al., 2009). They demonstrated that co-IP of CRY1 with CLOCK and BMAL1 was barely above baseline levels, but the addition of PER2 made this interaction significantly more robust. PER2 co-immunoprecipitated with CLOCK and BMAL1 without CRY1, suggesting that CRY1 requires PER2 to form a stable complex with CLOCK and BMAL1. However, these data suggest that PER2 does not require CRY1 to form a stable complex. In contrast, work from Ye and colleagues suggests that CRY1 has a direct interaction with CLOCK and BMAL1 even in the absence of PER proteins (Ye et al., 2011). ChIP analysis of the *Per1* and *Per2* promoter in various KO cell lines showed that CRY1 was bound at target promoters even in the absence of endogenous PER. Moreover, CRY1 was competent to repress CLOCK/BMAL1- mediated transcriptional activation without PER. Further work suggested the additional conclusion that CRY and PER function in completely different modes of repression (Ye et al., 2014). CRY binds CLOCK and BMAL1 and directly represses their activity as a "blocking-type" repressor while PER physically removes the complex from DNA as a "displacement-type" repressor. Ultimately, the preponderance of evidence suggests that CRY is directly binding CLOCK and BMAL1 without the express need for PER2, but the nature of PER's role in this interaction is still up for debate.

Taking all of these protein-protein interactions into account, it is easy to view CRY as a nexus bridging multiple components of the circadian complex. Whether the implicit allostery involved in such an intricate web of interactions is a key principle of rhythm generation or merely coincidental is an area for future research. However, what is clear from data collected on the BMAL1 TAD's interaction with CRY is that modulation of these competitive interfaces is likely to be determinative in matters of periodicity (Xu et al., 2015).

Structural features of PER proteins

In sharp contrast with CLOCK, BMAL1, and CRY, structural biology is markedly more challenging in the case of PER proteins. This is due in large part to the fact that PER proteins are large (~1100-1300 residues), intrinsically disordered proteins with just a few structured domains (Albrecht et al., 1997; Sun et al., 1997; Tei et al., 1997; Zylka et al., 1998). Like CLOCK and BMAL1, PER1/2/3 have a set of N-terminal tandem PAS domains (PAS-A and PAS-B), which are primarily used to mediate protein-protein dimerization interactions (Figure 1-6A). Just beyond the PAS domains is a region (from residue 450-763 in PER2) that interacts with the F-box protein β-transducing repeat-containing protein (β-TrCP) and casein kinase 1δ/ε (CKIδ/ε), known as the casein kinase-binding domain (CKBD) (Figure 1-6B) (Eide et al., 2005). C-terminal to this interaction domain is a disordered proline-rich region and at the extreme C-terminus a roughly 100 amino acid binding interface for CRY1/2 known as the Cry-binding domain (CBD) (Nangle et al., 2014; Schmalen et al., 2014). PER3's C-terminus is highly divergent compared to PER1 and PER2 suggesting that it lacks a functional CBD (Zylka et al., 1998).

At present, structures of the PAS domains of all three PERs have been solved as well as structures of the PER2 CBD in complex with CRY1 and CRY2 (Hennig et al., 2009; Kucera et al., 2012; Nangle et al., 2014; Schmalen et al., 2014). The PAS domains of PER1, 2, and 3 all participate in homodimer interactions, primarily mediated by an antiparallel β-sheet interface between PAS-B domains and a conserved tryptophan moiety on a PAS-B loop ($W448_{PER1}$, $W419_{PER2}$, $W359_{PER3}$) that is partially buried in the homodimer (Figure 1-6A)

(Hennig et al., 2009; Kucera et al., 2012). The role of homodimer formation is not yet clear, though disruption of the homodimer interface hastened the mobility of PER2 (but not PER1) in cells (Kucera et al., 2012). PERs have been shown to form large protein complexes in both the cytoplasm and nucleus often containing multiple PER proteins. Perhaps homo- and heterodimerization interactions through the PAS domains are mediating complex formation. PER2's elongated interface with CRY buries 2800 $Å^2$ of solvent accessible surface area, which informs previously observed high affinity interactions between the two (Nangle et al., 2014). However, understanding the contribution of the interaction between the two proteins to the overall mechanism of the clock is complicated by the fact that the interface on CRY overlaps with FBXL3 and BMAL1.

Functional and structural divergence in the mammalian PER family is less obvious than CRY1 and CRY2. PER1 and PER2 are 43% identical and 54% similar; PER1 and PER3 are 33% identical and 45% similar; and PER2 and PER3 are 33% identical and 46% similar. Overall the level of divergence is consistent with a protein family defined primarily by a few structural motifs connected by long intrinsically disordered regions under weak selective pressure. However, despite fairly substantial structural divergence, PER1 and PER2 appear to play relatively redundant roles in the clock. *Per1*$^{-/-}$ and *Per2*$^{-/-}$ mice display reduced circadian amplitude with very minor period differences in light/dark cycles and drift into arrhythmicity after several weeks in constant darkness (Bae et al., 2001). *Per1*$^{-/-}$/*Per2*$^{-/-}$ double KO mice on the other hand are arrhythmic immediately after transition to constant darkness. PER3, in contrast, is functionally dissimilar from PER1 and 2. *Per3*$^{-/-}$ mice maintain circadian amplitude, but have faster endogenous clocks (~0.5 h short) (Shearman et al., 2000a).

Moreover, compound mutants *Per1*$^{-/-}$/*Per3*$^{-/-}$ and *Per2*$^{-/-}$/*Per3*$^{-/-}$ displayed behavioral phenotypes consistent with single KOs (*Per1*$^{-/-}$ or *Per2*$^{-/-}$) (Bae et al., 2001). Thus, PER3 appears to be a superfluous clock component.

Regulation of PER stability

PER protein stability has proven to be every bit as potent a regulator of periodicity as CRY stability. The stability of this repressor first came to the forefront of circadian biology through a spontaneous mutation with a major effect on periodicity (Ralph and Menaker, 1988). A single male golden hamster from the breeding supplier Charles River had an abnormal free-running period of 22 h (Ralph and Menaker, 1988). After this single hamster was bred into a colony, it was discovered that a single mutation (*tau*) was causing this behavioral phenotype and functioned semi-dominantly. Homozygous carriers had dramatically shortened endogenous rhythms of 20 h. After an extensive and laborious process, Lowrey and colleagues identified the mutation as an allele of casein kinase I epsilon (CKIε, *Csnk1e*) with a substitution at a highly conserved residue (R178C) (Lowrey et al., 2000). Although CKIε tau binds PER1 and PER2 comparably to WT, it is less efficient at phosphorylating PER. Further characterization in null and knock-in mice revealed that CKIε *tau* functions essentially as a gain-of-function mutation, accelerating PER protein turnover (Meng et al., 2008). Null mutants were behaviorally inert, likely due to redundant activity in the form of closely related family member CKIδ (*Csnk1d*).

Extensive characterization of CKIδ/ε's interaction with PER has identified a region of PER that gates interaction with CKIδ/ε (Akashi et al., 2002; Eide et al., 2005; Lee et al.,

2004). In PER2, the region from residue 450-763 is broadly where CKIδ/ε binds, but two short segments within this region (582-606 and 731-756) appear to be especially critical for mediating this interaction (Eide et al., 2005). Furthermore, the CKIδ/ε binding domain (CKBD) of PER3 has diverged from that of PER1 and PER2, weakening its interaction with CKIδ/ε (Lee et al., 2004).

Interaction with and phosphorylation by CKIδ/ε is regulated in part by phosphorylation at a priming site ($S662_{hPER2}$/$S659_{mPER2}$) associated with familial advanced sleep phase syndrome (FASPS) (Toh et al., 2001). In turn, phosphorylation by CKIδ/ε at $S478_{mPER2}$ recruits the E3 ligase complex $SCF^{\beta\text{-}TRCP}$, which ubiquitinates PERs and directs them to the proteasome for degradation (Reischl et al., 2007; Shirogane et al., 2005; Zhou et al., 2015). Interestingly, the interplay between these two phosphorylation sites is regulated by temperature and a unique multi-stage decay process (Zhou et al., 2015). Ambient temperature can bias one pathway over the other and result in acceleration or deceleration of PER2 turnover, potentially suggesting a mechanism for temperature compensation in the mammalian clock.

CKIδ/ε kinase activity is antagonized by autophosphorylation of its C-terminus at multiple sites (Gietzen and Virshup, 1999). Activity of the kinase is subsequently regulated by protein phosphatase 5 (PP5, *Ppp5c*), which in turn is inhibited by CRY (Partch et al., 2006). Together with data suggesting that CRY and PER mutually protect each other from degradation, this work supports a mechanism in which PER protects CRY by blocking interaction with FBXL3 and CRY protects PER through a roundabout mechanism in which it antagonizes PP5, blocking dephosphorylation of CKIδ/ε, reducing phosphorylation of PER at

a priming site for β-TRCP interaction, and ultimately reducing ubiquitination and degradation of PER.

In addition to being rhythmically phosphorylated (Lee et al., 2001), PER is also rhythmically acetylated and deacetylated in vivo in part by the NAD^+-dependent deacetylase, SIRT1 (Asher et al., 2008). SIRT1 rhythmically associates with CLOCK, BMAL1, and PER, deacetylating PER in the process and promoting its degradation. Due to the fact that this process is NAD^+-dependent, it represents a functional input from metabolism to the clock. Furthermore, it builds the case along with the temperature-sensitive regulation of PER described above that various external conditions converge on PER, regulating its stability through post-translational modifications and thereby affecting the timing of the clock.

Clearly the combined regulation of repressor stability seems to be the preeminent factor in the timing in the mammalian clock, but the overall concentration of these proteins is secondary to what they actually do. Understanding their function at a mechanistic level will provide key insight into why concentration matters for timing.

The role of PER in the mammalian clock

Despite relatively detailed accounting of regulatory sites, protein interaction domains, and cellular mobility, one of the outstanding questions in circadian biology remains what does PER do? Though reports on the requirement of PER for assembly of a stable repressive complex differ (Chen et al., 2009; Ye et al., 2014; Ye et al., 2011), one detail is clear: CRY is a strong repressor of CLOCK/BMAL1 with or without PER and the reverse is not true (Koike et al., 2012; Shearman et al., 2000b; Ye et al., 2011). These reports implicitly suggest

that CRY must be able to bind CLOCK and BMAL1 and mediate its repressive effects without PER. Furthermore, characterization of nuclear localization of PER and CRY suggests that CRY nuclear import is insensitive to PER, but nuclear import of PER is highly regulated by CRY and CKIδ/ε (Lee et al., 2015; Ollinger et al., 2014; Sakakida et al., 2005; Yagita et al., 2002). Again, these data support a critical, PER-insensitive role for CRYs in the clock, but do little to explain PER's function.

One possible and surprising role for PER may be as a circadian derepressor (Akashi et al., 2014). Coexpression of small amounts of *Per1* and *Per2* attenuated transcriptional repression by CRY in a dose-dependent manner. This response required both the presence of CRY and an intact PER CBD, which precluded PER3 from playing a role in derepression. And perhaps most importantly, full-length PER2 and a small fragment containing the CBD were able to block CRY1 from binding to CLOCK and BMAL1. This finding is perhaps not entirely shocking in the context of known interaction domains on CRY, but it strongly suggests that the PER2 CBD and BMAL1 TAD are in competition. Based on the conflicting data in the literature about PER's role and the assembly of the repressive complex on the activators, a clear study of the kinetics of various domain associations would be valuable in understanding what interactions are important and when.

A final possible role for PER is that of a large scaffolding protein necessary for the assembly of a sizeable repressive complex. Work from a number of groups has identified over 20 different protein components of the repressive complex (detailed in the next section) with various roles and effects on the function of the clock. Some estimates put the size of this complex at roughly 2000 kDa (Kim et al., 2015). Though PER might not mediate every

interaction, it can be found in heterogeneous complexes at various circadian times and has an architecture consistent with other scaffolding proteins (i.e., intrinsically disordered with many small, discrete structured elements throughout).

Components of the repressive complex

The identification of repressive complex components has been an ongoing process for over a decade and, based on the findings, supports the idea that these components can be coarsely sorted into two basic groups: (1) epigenetic regulators and (2) repressors without a clear mechanism of action.

Epigenetic regulators have primarily been identified through immunoprecipitation of PER complexes followed by mass spectrometry (Brown et al., 2005; Duong et al., 2011; Duong and Weitz, 2014; Kim et al., 2014; Padmanabhan et al., 2012; Tamayo et al., 2015). Studies of complex members indicate a progression of epigenetic regulators throughout the active and repressive phases of the clock ultimately leading to cycles of decompaction and compaction of chromatin (Aguilar-Arnal et al., 2013). CLOCK and BMAL1 actually participate in their own repression by associating with the adaptor protein WD repeat-containing protein 76 (WDR76, *Wdr76*), which recruits DNA damage binding protein 1 (DDB1, *Ddb1*) and Cullin-4 (CUL4, *Cul4*) (Tamayo et al., 2015). DDB1-CUL4 then monoubiquitinates histone 2B (H2B) at the promoter of CLOCK/BMAL1 targets, which serves to recruit PER complexes during the repressive phase. siRNA-mediated knock-down of DDB1 or CUL4 shortens the period in cycling fibroblasts. Early in the repressive phase, members of the Mi-2-nucleosome remodeling and deacetylase (NuRD) transcriptional co-

repressor complex are split between CLOCK/BMAL1 and CRY/PER (Kim et al., 2014). Chromodomain-helicase-DNA-binding protein 4 (CHD4, *Chd4*), metastasis-associated 1 family member 2 (MTA2, *Mta2*), and sucrose nonfermenting protein 2 homolog (SNF2H, *Smarca5*) and BRG1 (*Smarca4*) (two members of the SWI/SNF family) are bound to the activators and depletion of CHD4, SNF2H, or BRG1 results in modest period lengthening. The repressive complex on the other hand is bound to Methyl-CpG-binding domain protein 2 (MBD2, *Mbd2*), RbAp48 (*Rbbp4*), GATA zinc finger domain containing 2A (GATAD2a, *Gatad2a*), and HDAC1/2. Depletion of MBD2 shortens the period in cycling cells. Only through interaction of the activator and repressor complexes are all of the NuRD components reconstituted to function as a repressor of CLOCK and BMAL1. The repressive complex also includes polypyrimidine tract-binding protein-associated-splicing factor (PSF, *Sfpq*), which recruits the SIN3A (*Sin3a*)-HDAC1 complex during the repressive phase and modulates the acetylation state at H3K9 and H4K5 (Duong et al., 2011). Depletion of either PSF or SIN3A results in period shortening. Rhythms in H3K27 di- and trimethylation are regulated in part by the polycomb group protein EZH2 (*Ezh2*), which associates with the repressive complex and functions in concert with CRY as a co-repressor (Etchegaray et al., 2006). shRNAs targeted to EZH2 result in arrhythmicity of *Per2-Luc* and *Bmal1-Luc* rhythms. Several other histone methyltransferases have also been identified in the repressive complex including WD repeat-containing protein 5 (WDR5, *Wdr5*) and HP1γ (*Cbx3*)-SUV39H (*Suv39h1*) (Brown et al., 2005; Duong and Weitz, 2014). The details of WDR5's role in the clock are scant, but depletion resulted in the loss of an antiphase rhythm in H3K4 and H3K9 methylation (Brown et al., 2005). The HP1γ-SUV39H complex promotes di- and trimethylation of H3K9 in later

phases of repression (Duong and Weitz, 2014). Interestingly, HDAC1 is recruited to deacetylate H3K9 early in the repressive phase and followed later by HP1γ-SUV39H. Moreover, these repressive complex components appear to be part of distinct complexes separated in a spatiotemporal manner, suggesting either that PER complexes are fluid, with components joining and leaving, or that unique complexes form throughout the repressive phase and interact in a phase-specific manner with CLOCK and BMAL1. In addition to histone modifiers, the repressive complex also contains a number of helicases involved in transcriptional termination (*Ddx5*, *Dhx9*, and *Setx*) (Padmanabhan et al., 2012). During the repressive phase, SETX in particular is recruited to termination sites on clock-controlled genes where it blocks transcriptional termination and causes a build up of RNAP II, thus providing an additional layer of transcriptional regulation. Depletion of SETX causes arrhythmicity in cycling fibroblasts.

Beyond epigenetic regulators, several other co-repressors have been identified. Receptor of activated protein C kinase-1 (RACK1, *Rack1*) recruits Protein kinase C-α (PKCα) to CLOCK and BMAL1 where PKCα phosphorylates BMAL1, repressing its activity (Robles et al., 2010). CLOCK and BMAL1 are also repressed by CLOCK-interacting protein, circadian (CIPC, *Cipc*) (Zhao et al., 2007). CIPC interacts with the exon 19 region of CLOCK through a 50 amino acid region of its C-terminus and potentially regulates the phosphorylation and subsequent destabilization of CLOCK (Yoshitane et al., 2009; Zhao et al., 2007). Depletion of CIPC shortens the period (Zhao et al., 2007). In addition to CRY, BMAL1 has an additional negative regulator interacting with its TAD: CHRONO (*Ciart*, also known as *Gm129*) (Anafi et al., 2014; Annayev et al., 2014; Goriki et al., 2014).

Concurrent reports from three different labs suggest that CHRONO binds to BMAL1 and represses the transcriptional activity of CLOCK and BMAL1. Though the mechanism is not entirely clear, it appears to disrupt BMAL1's interaction with CBP and antagonize circadian acetylation of H3K9 at CLOCK/BMAL1 targets, potentially through an interaction with HDAC1. *Chrono*$^{-/-}$ mice had modestly lengthened locomoter behavioral rhythms in constant darkness (Goriki et al., 2014). Finally, a protein called NONO (*Nono*) is also found in PER complexes and may in fact function as a weak antagonist of the repressors of CLOCK and BMAL1 (Brown et al., 2005). siRNA's targeted to *Nono* result in period shortening.

Concluding thoughts

The wealth of structural analysis that has been performed on mammalian clock proteins has opened windows into the function of the clock. Ultimately, building a model for how a molecular machine works requires an understanding of how the components fit together, which interactions are dynamic, and what the kinetics of those dynamic states are. In the case of the clock, regulation is occurring at many levels, but focusing on the key interactions might tell us about the most important aspect of a timing mechanism: measuring time.

To that end, there are a few key components that appear to drive the clock. (1) CLOCK and BMAL1 must form a stable complex that binds to DNA targets. (2) CLOCK and BMAL1 must be able to recruit the necessary machinery and cofactors for chromatin decompaction and transcription. (3) CRY and PER must bind and sequester the relevant domains of CLOCK and BMAL1 mediating recruitment of cofactors. (4) There must be a

mechanism in place to remove the repressors from the system and allow the cycle to begin anew.

In accounting for the various components of the activator and repressor complexes, it becomes clear that many of them have relatively minor effects on periodicity or overall clock function based on knockdown and knockout studies (Table 1-1). In most cases these components appear to serve in making the clock more robust. In contrast, the most dramatic effects on periodicity and clock function come from stabilizing or destabilizing the repressors (Busino et al., 2007; Godinho et al., 2007; Hirano et al., 2013; Meng et al., 2008; Ralph and Menaker, 1988; Siepka et al., 2007; Yoo et al., 2013) or changing the nature of the interaction at a competitive interface between the repressors and activators (Katada and Sassone-Corsi, 2010; King et al., 1997; Xu et al., 2015). In many ways, these two features of periodicity are two sides of the same coin.

Clearly the intrinsic stability of PER and CRY proteins in a cellular milieu plays a significant role in the timing of the clock. One approach to this idea is to think of how changes in PER and CRY stability affect dynamics at competitive structural interfaces. For instance, if the dissociation constant measured for interaction between CRY1 and the BMAL1 TAD is ~10 μM (Czarna et al., 2011) and the dissociation constant for the CBP KIX domain is ~2 μM (Xu et al., 2015), stabilizing CRY1 is likely to raise the concentration of CRY1 above the threshold necessary for a competitive interaction with the BMAL1 TAD for a longer interval, thus extending the length of the repressive phase of the clock. Likewise, if PER proteins are competing with MLL1 to interact with the CLOCK exon 19 region, then changing the rate of nuclear import is a means of raising the effective concentration of PER

and changing the dynamic of the competition at this interface. It follows that comprehensive models of timing within the clock will need to integrate competitive protein interaction dynamics with measurements of protein stability and mobility to gain insight into how the molecules of the clock achieve precision in timing.

Figures

Figure1-1. Simple model of the mammalian transcription/translation feedback loop.

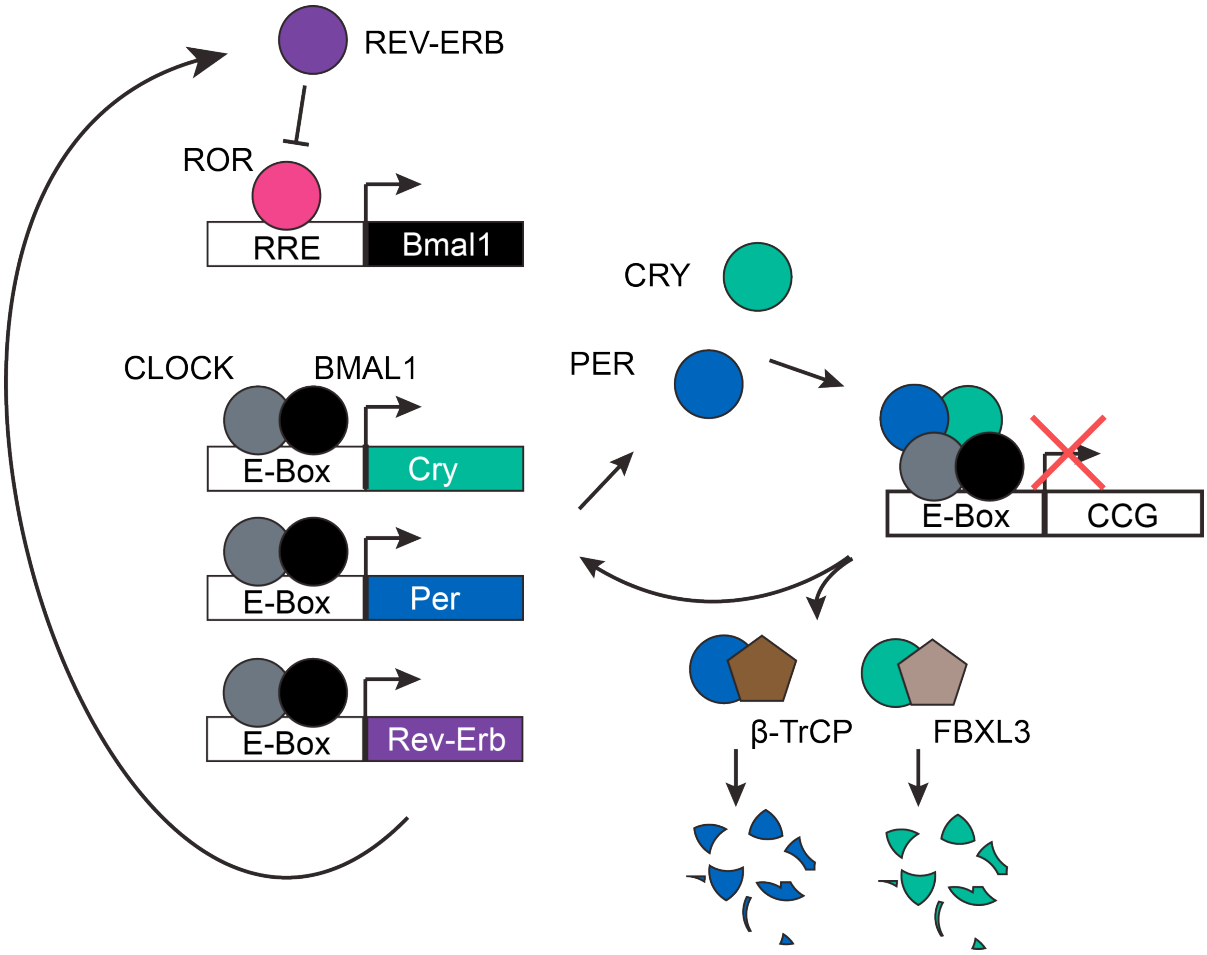

Figure1-1. Simple model of the mammalian transcription/translation feedback loop. CLOCK and BMAL1 bind to E-boxes driving expression of clock-controlled genes (CCG) including their own repressors, CRYPTOCHROME and PERIOD. BMAL1 is also rhythmically expressed as a result of competitive binding at its promoter by the activator ROR and the repressor REV-ERB, which is under the control of CLOCK and BMAL1. Degradation of the repressors, CRY and PER, is mediated by the E3 ubiquitin ligases FBXL3 and β-TrCP respectively. Following degradation of the repressors, the cycle begins again.

Figure 1-2. Molecular architecture of the activators CLOCK and BMAL1.

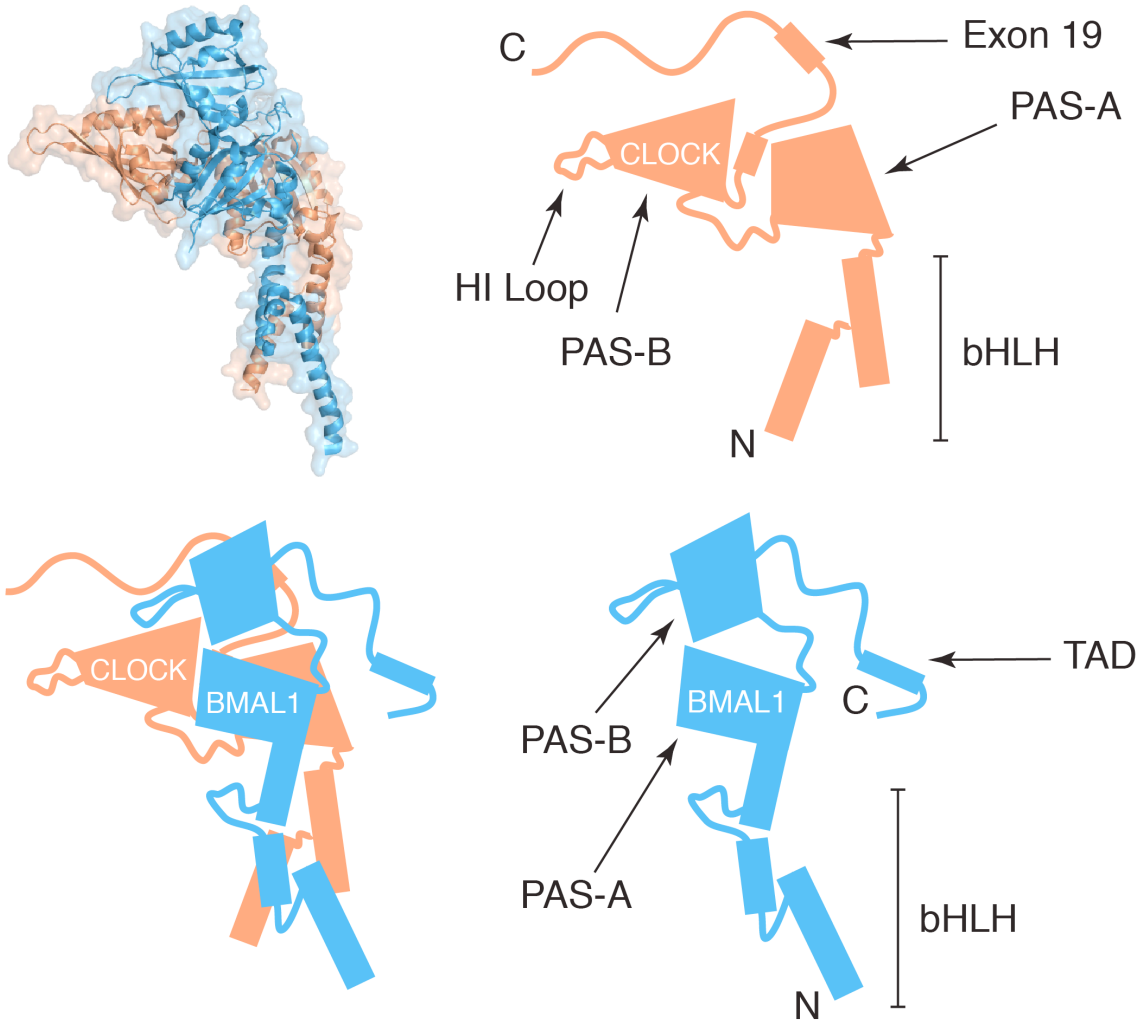

Figure 1-2. Molecular architecture of the activators CLOCK and BMAL1.
On the top left is the crystal structure of the CLOCK/BMAL1 heterodimer (PDB: 4F3L). CLOCK is shown in peach and BMAL1 is shown in blue. Only the bHLH and PAS domains are present in the structure. On the bottom left is a cartoon rendering of the heterodimer based on the structure, but with additional disordered regions drawn in. On the right side are cartoon renderings of the individual members of the heterodimer with important domains labeled: basic Helix-Loop-Helix domain (bHLH), PER-ARNT-SIM domain (PAS), transactivation domain (TAD). N and C termini are labeled with an N and C respectively.

Figure 1-3. CLOCK and BMAL1 PAS domain interactions.

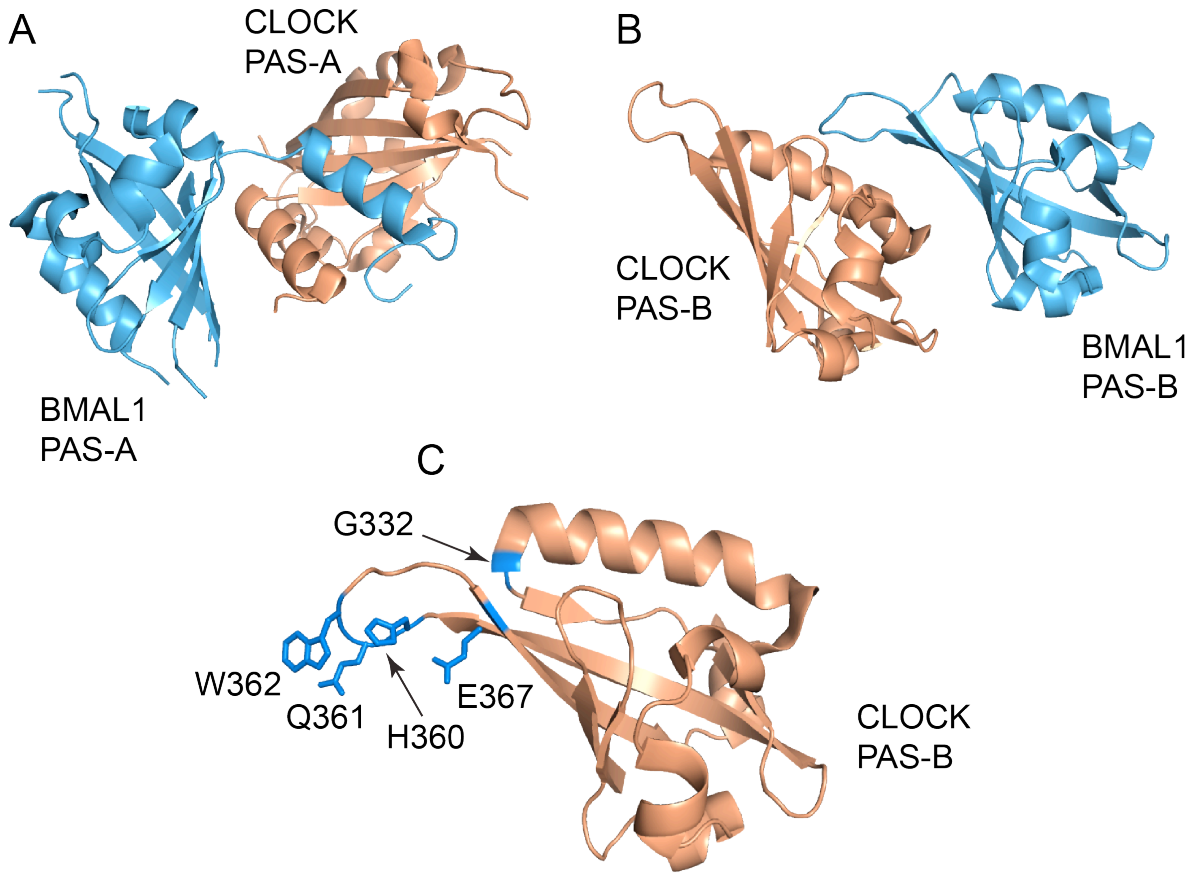

Figure 1-3. CLOCK and BMAL1 PAS domain interactions.
(**A**) The PAS-A domains of CLOCK and BMAL1 have a reciprocal interaction in which the α-helix of one domain binds the β-sheet interface of the other.
(**B**) The PAS-B domains of CLOCK and BMAL1 interact through the β-sheet of BMAL1 and the α-helix of CLOCK, leaving a significant portion of CLOCK's PAS-B available for other protein-protein interactions.
(**C**) Residues identified as important for interaction between the CLOCK PAS-B domain and CRY are highlighted on the PAS-B structure in blue. G332, H360, W362, and E367 were identified in a random mutagenesis screen (Sato et al., 2006) and Q361 and W362 were identified in a directed mutagenesis screen (Zhao et al., 2007).

Figure 1-4. CRYPTOCHROME domain architecture.

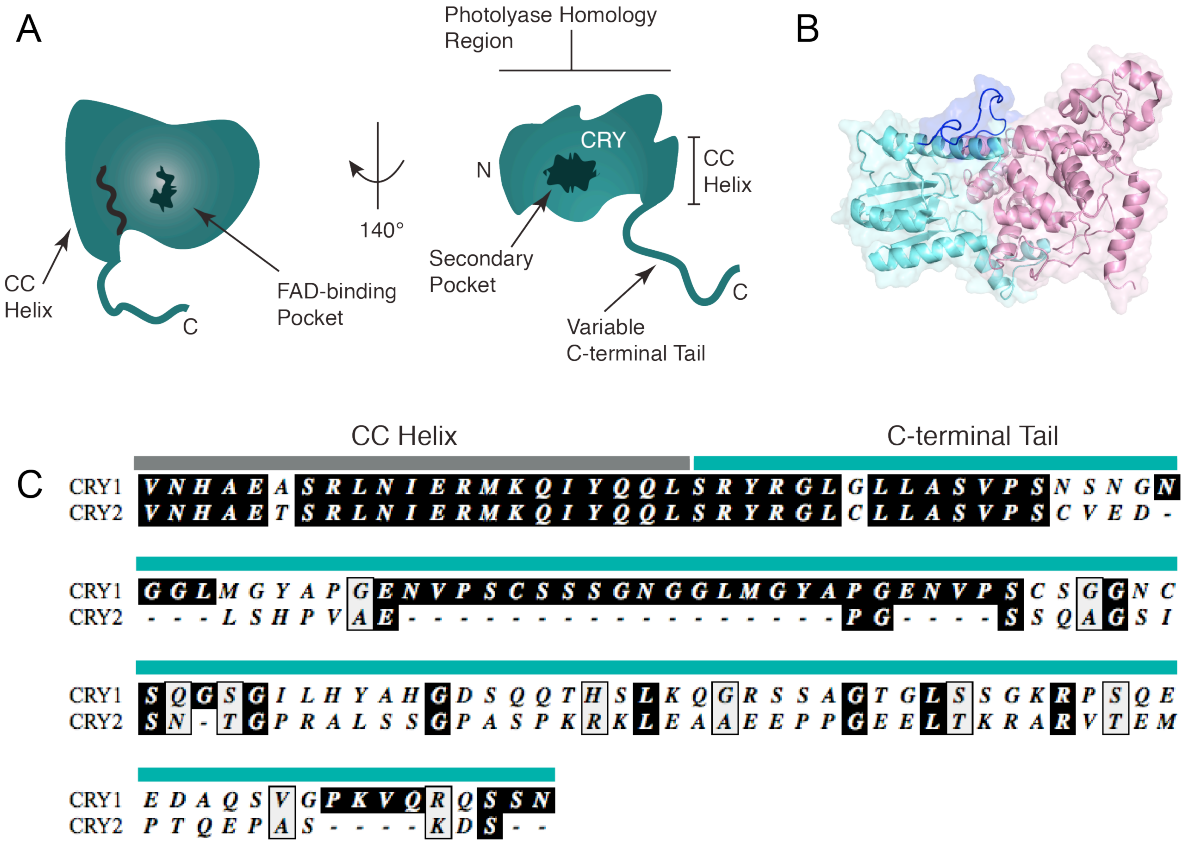

Figure 1-4. CRYPTOCHROME domain architecture.
(**A**) Two cartoon renderings of the CRY structure based on the actual crystal structure of CRY1. Important features of the protein are labeled: coiled coil helix (CC helix), flavin adenine dinucleotide (FAD). N and C termini are labeled.
(**B**) The CRY1 structure (PDB: 5T5X) is colored to show the α/β domain (aquamarine), the interdomain linker (blue), and the α-helical domain. Orientation matches the cartoon on the right in panel A.
(**C**) An alignment of the CC helix and tail of murine CRYs. The alignment was made in MacVector.

Figure 1-5. Divergence between CRY1 and CRY2.

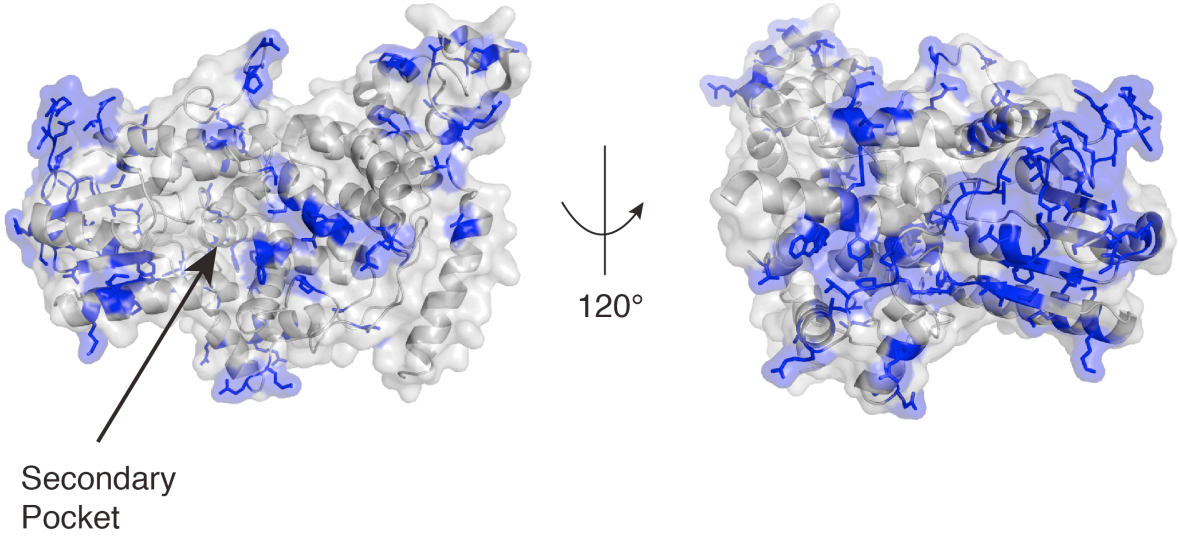

Figure 1-5. Divergence between CRY1 and CRY2.
Two views of the CRY2 PHR structure (PDB: 4I6E) with all of the residues diverging between CRY1 and CRY2 labeled in blue. The vast majority of divergence is in one particular region of the α/β domain shown on the right.

Figure 1-6. PERIOD domain architecture.

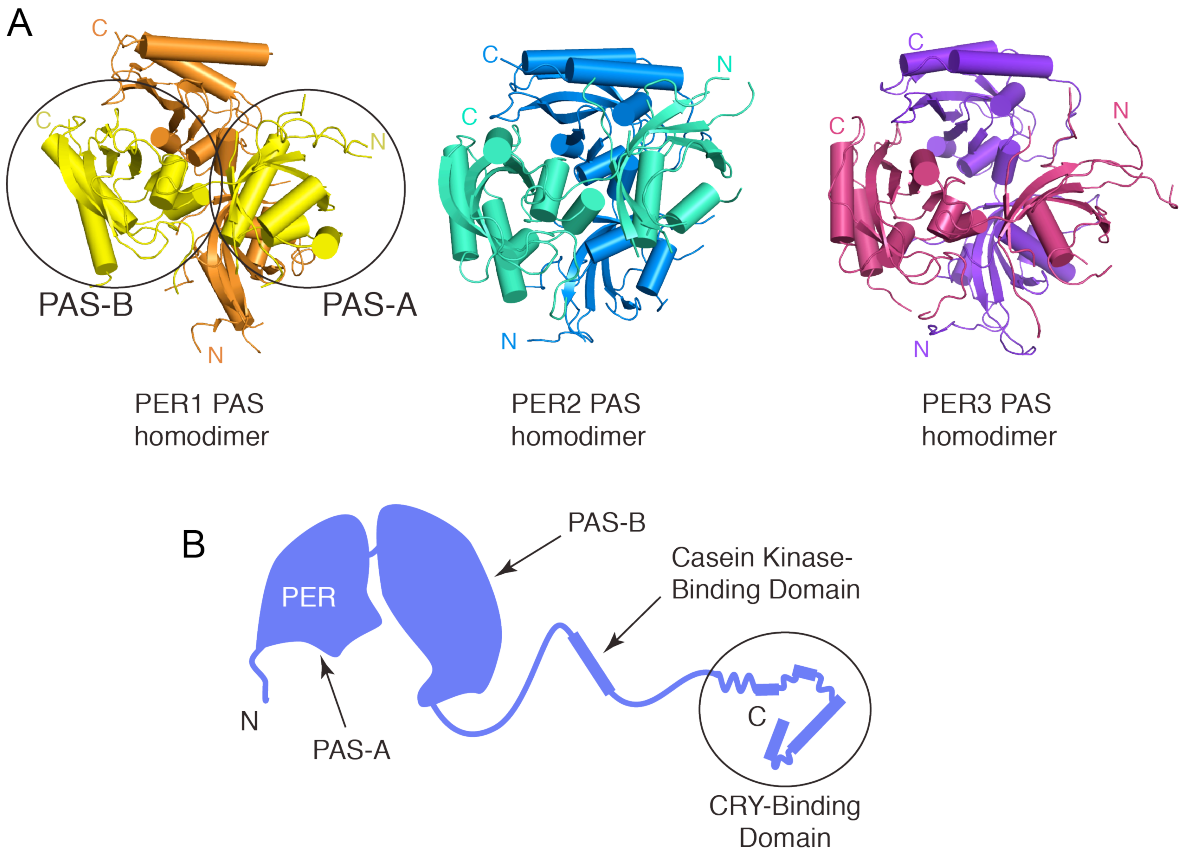

Figure 1-6. PERIOD domain architecture.
(**A**) The PAS domain homodimer structures of PER1, PER2, and PER3. Overall structures are very similar. Each protein homodimerizes in an orthogonal orientation. The PAS-A and PAS-B domains of one PER1 subunit are circled in the figure on the left. N and C termini are labeled for each monomer of each PER complex.
(**B**) A cartoon rendering of PER based very loosely on the few bits of known structure in the PER protein family. Major domains are labeled: PER-ARNT-SIM domains (PAS), casein kinase-binding domain (CKBD), and CRY-binding domain (CBD).

Table 1-1. Effects of depletion or deletion of ancillary clock components on period and amplitude.

Component	Complex Role	Period of KO/KD	Effect on Amplitude	Reference
MLL1	Activator	Arrhythmic		(Katada and Sassone-Corsi, 2010)
TRAP150	Activator	1 h Long	Decreased	(Lande-Diner et al., 2013)
JARID1a	Activator	1 h Short	Decreased	(DiTacchio et al., 2011)
LSD1	Activator	No change	Decreased	(Nam et al., 2014)
DDB1	Repressor	1.5 h Short	No change	(Tamayo et al., 2015)
CUL4	Repressor	2 h Short	No change	(Tamayo et al., 2015)
MTA2	Repressor	2 h Short	Increased	(Kim et al., 2014)
CHD4	Repressor	1-1.5 h Long	Decreased	(Kim et al., 2014)
MBD2	Repressor	0.5 h Short	No change	(Kim et al., 2014)
SNF2H	Repressor	0.5 h Long	Increased	(Kim et al., 2014)
BRG1	Repressor	1.5 h Long	Decreased	(Kim et al., 2014)
PSF	Repressor	1 h Short	No change	(Duong et al., 2011)
SIN3A	Repressor	1 h Short	No change	(Duong et al., 2011)
EZH2	Repressor	Arrhythmic		(Etchegaray et al., 2006)
SUV39H	Repressor	2 h Short	No change	(Duong and Weitz, 2014)
SETX	Repressor	Arrhythmic		(Padmanabhan et al., 2012)
RACK1	Repressor	0.5 h Short	No change	(Robles et al., 2010)
PKCα	Repressor	0.5 h Short	No change	(Robles et al., 2010)
CIPC	Repressor	1 h Short	No change	(Zhao et al., 2007)
CHRONO	Repressor	0.5-1.5 h Long	Decreased	(Anafi et al., 2014; Goriki et al., 2014)
NONO	Repressor	2 h Short	Decreased	(Brown et al., 2005)

CHAPTER TWO: Results

MOLECULAR ASSEMBLY OF THE PERIOD-CRYPTOCHROME CIRCADIAN TRANSCRIPTIONAL REPRESSOR COMPLEX

Note: This chapter appeared in slightly modified form in eLife in 2014. I contributed equally to the work with Shannon N. Nangle. I performed the co-IPs and rescue assays and helped in writing part of the text.

Nangle SN*, Rosensweig C*, Koike N, Tei H, Takahashi JS, Green CB, and Zheng N. Molecular assembly of the period-cryptochrome circadian transcriptional repressor complex. Elife 2014; 3**,** e03674. doi: 10.7554/eLife.03674.
*Authors contributed equally.

Introduction

Life on Earth evolved a self-sustaining molecular timing system that synchronizes cellular activities with the solar day. This endogenous clockwork prepares an organism for periodic environmental fluctuations and coordinates numerous physiological and behavioral processes (Reppert and Weaver, 2002). At the molecular level, the mammalian circadian clock operates through an auto-regulatory transcription-translation feedback loop composed of four core components—the transcriptional activator proteins, CLOCK and BMAL1, and the transcriptional repressors, Periods (PERs) and Cryptochromes (CRYs). The heterodimeric CLOCK and BMAL1 complex acts as the positive arm of the loop by recognizing E-box elements and promoting the expression of clock-controlled genes, including *Per1*, *Per2*, *Cry1*, and *Cry2*. The PER and CRY proteins function as the negative arm of the loop by blocking the activity of CLOCK-BMAL1 and inhibiting the transcription of their own and all other clock-controlled genes. The cyclic accumulation, localization, and

degradation of the PER and CRY proteins are necessary to manifest a 24-hr rhythm (Lowrey and Takahashi, 2011).

Earlier studies suggested that CRYs are the predominant inhibitors of CLOCK-BMAL1 (Griffin et al., 1999; Kume et al., 1999). Independent of PERs, overexpressed CRY1 and CRY2 can each potently inhibit the CLOCK-BMAL1-induced transcription of a luciferase reporter gene in cultured cells (Griffin et al., 1999; Kume et al., 1999). This transcriptional repression activity of CRYs likely occurs through their direct interactions with BMAL1 (Griffin et al., 1999; Partch et al., 2014; Shearman et al., 2000b) and CLOCK (Huang et al., 2012). Despite the important repressor function of CRYs, the PER proteins have been suggested as the rate-limiting factor of the rhythmic negative feedback loop (Lee et al., 2001). With its protein abundance tightly regulated during the circadian cycle, PERs mediate the formation of the PER-CRY complexes and their nuclear localization. Once in the nucleus, PERs might physically bridge CRYs and CLOCK-BMAL1 and promote their interactions (Chen et al., 2009). The critical role of PERs in driving the molecular clock is underscored by the complete loss of circadian rhythmicity upon constitutive overexpression of PERs, but not CRY1, in vitro and in vivo (Chen et al., 2009; McCarthy et al., 2009; Ye et al., 2011).

Periodic degradation of PERs and CRYs represents another crucial step in the negative feedback loop. The F-box proteins, β-TrCP and FBXL3, have been discovered as the key ubiquitin ligases, responsible for promoting the polyubiquitination of PERs and CRYs, respectively (Busino et al., 2007; Godinho et al., 2007; Reischl et al., 2007; Shirogane et al., 2005; Siepka et al., 2007). Phosphorylation of a degron sequence serves as the signal

for PER ubiquitination by β-TrCP (Shirogane et al., 2005), whereas recognition of CRYs by FBXL3 is made through a large protein-interaction interface without the involvement of a canonical degron motif or any post-translational modification (Xing et al., 2013). This CRY-FBXL3 interface is susceptible to disruption by both the CRY cofactor flavin adenine dinucleotide (FAD) and the PER proteins, which have been suggested to control the stability of CRYs by directly competing with FBXL3 (Xing et al., 2013).

Although genetic studies have firmly established a central role of PERs in clock regulation, the molecular mechanisms by which PERs orchestrate the dynamic clock protein network remain elusive. Binding of PERs to CRYs, CLOCK, and BMAL1 have been detected both in vivo and in vitro (Kiyohara et al., 2006; Partch et al., 2014; Ye et al., 2011). However, the role of PER2 in coordinating the repression complex assembly is controversial. In addition, how PER–CRY interaction might interfere with FBXL3 for CRY binding also remains unclear. Here, we report the crystal structure of a PER2–CRY2 complex, which provides the missing structural framework for understanding the multiple functions of PERs in driving the molecular clock.

Results

Characterizing PER-CRY interactions

Mammalian PER1 and PER2 share ~50% sequence identity and a common domain architecture comprised of tandem N-terminal PER-ARNT-SIM (PAS) domains, a central CK1 δ / ε -binding region, and a ~100 amino acid long C-terminal CRY-binding domain (CBD), which is necessary and suf cient for CRY binding (Yagita et al., 2002). The isolated

PER2 CBD can stabilize CRY1/2 in vivo and compete with FBXL3 for CRY1/2 binding in vitro (Chen et al., 2009; Xing et al., 2013). In mouse embryonic fibroblasts (MEFs), overexpression of the PER2-CBD alone was able to completely disrupt the circadian bioluminescence rhythm of the luciferase activity of a *Per2*^{Luc} reporter gene (Chen et al., 2009). To first characterize the PER–CRY interaction, we performed an alanine-scanning mutagenic analysis of the PER2-CBD. We initially targeted stretches of residues strictly conserved among vertebrate PER1/2 orthologs (Figure 2-1, Figure 2-1—figure supplement 1). Surprisingly, none of the 10 single mutants, distributed along the length of the CBD, showed any detectable defect in CRY1 binding. The PER2–CRY1 interaction was only abolished when alanine mutations were simultaneously introduced to two adjacent stretches of residues in the C-terminal, but not N-terminal half of the PER2-CBD (Figure 2-1B). These results suggested an unusual binding mode of the PER2-CBD onto CRYs and the importance of the C-terminal half of the CBD in complex formation.

Overall structure

Mammalian CRY1 and CRY2 paralogs contain a highly similar photolyase-homology region (PHR) and a more diverse Cryptochrome C-terminal Extension (CCE) sequence (Figure 2-1—figure supplement 1). Their PER-binding activity has previously been mapped to the PHR, which is made of an α/β photolyase domain and an α-helical domain (Figure 2-1C). Consistent with their high sequence homology (86%), the crystal structures of CRY1-PHR and CRY2-PHR can be superimposed with a root-mean-square deviation (RMSD) of 0.43 Å out of 377 aligned Cα atoms. To gain structural insights into the general interaction

between PERs and CRYs, we purified a representative PER2-CBD-CRY2-PHR complex and determined its crystal structure at a resolution of 2.8 Å (Table 2-1).

The PER2-CBD adopts a highly extended structure, devoid of a hydrophobic core. It folds into five α-helices of variable length, which are dispersed along an otherwise linear polypeptide (Figure 2-1C). In the crystal, the PER2-CBD meanders along one side of CRY2-PHR and sinuously wraps around the region. With nearly half of the PER2 residues involved in binding, the two proteins bury a total 2800 $Å^2$ of solvent accessible surface area at the interface, which stretches over a distance of more than 215 Å. This unusually extensive interface provides a plausible explanation for the high-affinity binding between the two clock proteins and their insensitivity to mutational disruption.

In comparison to its FBXL3-, KL001-, and FAD-complexed forms, CRY2 adopts the same global fold when bound to the PER2-CBD (Figure 2-4—figure supplement 2). The largest structural variations take place in two local regions, the interface loop next to the FAD-binding pocket and a serine-rich loop neighboring the secondary pocket. The majority of PER2-contacting residues on CRY2 (85%) are strictly conserved between mammalian CRY1 and CRY2, suggesting that the two cryptochrome proteins share a common PER2 binding mode.

Interaction at the CRY2 C-terminal helix

The two stretches of residues, whose alanine mutations abrogated CRY1 binding, are mapped to a loop flanked by two α-helical regions in the C-terminal half of PER2 (Figure 2-1D). The PER2-CBD α3 helix preceding this loop packs against the long CRY2 C-terminal

helix at an approximately 30° angle, while the region C-terminal to the loop locks onto the same CRY2 helix from the other side (Figure 2-1C-D). Together, these PER2-CBD structural elements encircle the CRY2 C-terminal helix like an U-shaped clamp. Arg501 and Lys503 in the CRY2 C-terminal helix have previously been documented to be important for PER2 binding (Ozber et al., 2010). In the crystal, these two positively charged residues of CRY2 project in opposite directions and latch onto the surrounding PER2 regions by forming salt bridges with Asp1167 and Asp1206, respectively (Figure 2-2A). To confirm the critical role of the CRY2 C-terminal helix in binding PERs, we mutated two hydrophobic residues, Ile505 and Tyr506, at the end of this CRY2 helix, which are involved in fixing the α-helix to the rest of the CRY2 α-helical domain (Figure 2-2B). As expected, mutating both residues to aspartate completely abolished the PER2-binding activity of CRY2 (Figure 2-2C). The same effect was also achieved when negative charges were introduced to the side chains of a stretch of four nearby residues (amino acids 1171–1174) in the α3 helix of the PER2-CBD (Figure 2-2B, Figure 2-2—figure supplement 1A). Based on these results, we conclude that the CRY2 C-terminal helix represents a key anchoring site for PER2 binding.

The close interaction between the C-terminal half of PER2-CBD and CRY2 C-terminal helix is immediately reminiscent of the docking mode between FBXL3 and CRY2. In the crystal structure of the FBXL3-CRY2 complex, the leucine-rich repeat (LRR) domain of FBXL3 engages CRY2 at the same site as the PER2-CBD does in the PER2-CRY2 complex. The interface between FBXL3-LRR and CRY2 is also centered around the long C-terminal helix of the Cryptochrome protein. In fact, the CRY2 surface regions involved in contacting FBXL3-LRR and PER2-CBD share extensive overlapping regions (Figure 2-2D).

Superposition analysis reveals that FBXL3 and PER2 cannot be simultaneously engaged with CRY2 without clashing into each other (Figure 2-2—figure supplement 1B). PERs, therefore, have the capability of protecting CRYs from FBXL3-mediated ubiquitination and degradation by directly competing with the ubiquitin ligase for binding CRYs.

Intermolecular zinc finger

Amino acid sequence alignment of vertebrate PER1/2 orthologs reveals that their sequence conservation ends at a CXXC motif near the C-terminus (Figure 2-1A). In the complex structure, these two cysteine (C1210 and C1213) residues face a pair of cysteine and histidine residues in CRY2 (C432 and H491), which are also invariant among vertebrate CRY1/2 proteins (Figure 2-1—figure supplement 1). Together, these four residues sequester a strong density at the center, hinting at the coordination of a Zn^{2+} ion at the end of the PER2–CRY2 interface (Figure 2-3A, Figure 2-3—figure supplement 1A). Indeed, we were able to validate the identity of the Zn^{2+} ion by both anomalous dispersion measurements and inductively coupled plasma mass spectrometry (Figure 2-3—figure supplement 1A-B). Although a Zn^{2+} ion has been previously reported to mediate protein–protein interactions (Somers et al., 1994), to our knowledge, this is the first CCCH-type intermolecular zinc finger that has been identified in a protein complex. Interestingly, the electron density of the PER2 sequence preceding the CXXC motif is not as strong as other regions of the PER2-CBD, suggesting that the intermolecular zinc finger might have evolved to stabilize a flexible region of the PER–CRY interaction by acting as a ‘molecular clasp’.

To assess the role of the intermolecular zinc finger in mediating PER–CRY association, we first tested the CRY2-binding activity of a recombinant mutant PER2-CBD, which lacks the CXXC motif. In comparison to the wild-type polypeptide, the ability of the PER2-CBD mutant to bind CRY2 was substantially compromised (Figure 2-3B). Similarly weakened interaction was also observed in a co-immunoprecipitation assay, in which the CXXC motif of the full-length PER2 protein or the two zinc-coordinating residues of CRY2 were mutated to alanines (Figure 2-2—figure supplement 1A, Figure 2-3C). Together, these results highlight the importance of the intermolecular zinc finger in strengthening the PER–CRY interface.

Secondary pocket

Cryptochromes and DNA photolyases belong to the same superfamily of flavoproteins, whose common PHR fold is characterized by two large surface pockets, one for binding flavin adenine dinucleotide (FAD) and the other for binding a photoantenna cofactor, which is used by light-sensitive photolyases to catalyze FAD-dependent DNA repair (Figure 2-4A) (Glas et al., 2009). Previously, we have identified the FAD-binding pocket as a regulatory ‘hot spot’, which is targeted by FAD, the extreme carboxyl tail of FBXL3, and the clock-modulating small molecule, KL001 (Figure 2-4—figure supplement 1A) (Nangle et al., 2013; Xing et al., 2013). However, the functional significance of the secondary pocket remained unexplored.

In the PER2-CRY2 crystal, the N-terminal half of the PER2-CBD diverges from the FBXL3-binding site of CRY2 and reaches the rim of the secondary pocket after traversing

around the α-helical domain (Figure 2-4A). With a highly conserved sequence, the N-terminal end of the PER2-CBD is embedded in a V-shaped cleft formed between the two globular domains of CRY2-PHR, burying a PER2 tryptophan residue (Trp1139) at the junction (Figure 2-4B, Figure 2-2—figure supplement 1A). One side of the cleft is constructed by a serine-rich loop in CRY2, which we denominated 'serine loop'. Distinct from its surrounding regions, this loop adopts different conformations in several available crystal structures of CRY (Figure 2-4—figure supplement 2). Remarkably, PER2 binding induces yet another distinct structural configuration of the loop, thereby, defining a unique structural state of the local area next to the secondary pocket.

Although CRYs are known to not engage a second cofactor (Xing et al., 2013; Zoltowski et al., 2011), our previous cell-based random mutagenesis screen has identified three residues within this secondary pocket (Gly106 and Arg109 in CRY1, Glu121 in CRY2) (Figure 2-4C), whose missense mutations effectively abolished the repressor activity of CRYs (McCarthy et al., 2009). Among these three residues, Arg109 is exposed to the solvent and decorates one side of the pocket. Co-immunoprecipitation analysis of the R109Q mutant showed that alteration of this single amino acid is sufficient to abrogate CLOCK-BMAL1, but not PER1 or PER2 binding (Figure 2-4D-F). Thus, the secondary pocket of CRYs represents an important docking site for the heterodimeric transcriptional activators. Anchoring of PER2 at the edge of this CRY pocket not only reinforces its function as a previously unrecognized locus for protein–protein interactions, but also suggests a possible role of PERs in modulating the repressor functions of CRYs.

Functional analysis of CRY mutants

To functionally characterize the multiple interfaces on CRYs mapped by the crystal structures, we systematically assessed several representative CRY mutants for their abilities to rescue rhythmicity in *Cry1*$^{-/-}$/*Cry2*$^{-/-}$ MEF cells. Consistent with previous studies, wild-type CRY1 was able to repress the expression of the P(*Per2*)-*Luc* reporter gene and produce robust bioluminescence rhythms. By contrast, the 'IY' mutant of CRY1, which confers severe structural disruption in the C-terminal helix, failed to restore any level of circadian rhythm, although it has the ability to repress CLOCK-BMAL1 as seen by the constitutively low luciferase signal (Figure 2-5A). Because the C-terminal helix of CRYs is a critical region for binding both FBXL3 and PERs, this result underscores the importance of CRY ubiquitination and degradation in establishing clock rhythmicity and suggests the ability of CRY1 to inhibit CLOCK- BMAL1 in a PER-independent manner. In agreement, two CRY1 mutants unable to coordinate zinc, C414A and H473A, were also capable of transcriptional repression, even though their PER-binding activities are largely compromised (Figure 2-5B-C).

We noticed that the two zinc finger CRY1 mutants still sustained circadian rhythms. However, they showed defects in their bioluminescence oscillations (Figure 2-5B-C). Such a phenotype was not observed for a mutant with a nearby residue, Cys412, mutated to alanine, which did not perturb PER or FBXL3 binding as previously documented (Figure 2-5D) (Xing et al., 2013). The contrast between the two zinc finger-defective mutants and the wild-type-like C412A mutant confirms the functional role of the zinc-coordinating residues in the negative arm of the feedback loop.

Consistent with its impaired CLOCK-BMAL1 binding activity, the CRY1 R109Q mutant showed significant derepression in the rescue assay (Figure 2-5E) (McCarthy et al., 2009). This single amino acid mutation highlights the key role of the secondary pocket of CRYs for repression. Intriguingly, double serine to aspartate mutations (S44D S45D) in the nearby serine loop at the opposite side of the CRY secondary pocket completely rescued the circadian rhythm, although the period of the bioluminescence rhythms rescued by the mutant was reliably shorter than the wild-type CRY1 by about 1 hr (Figure 2-5F). In our co-immunoprecipitation experiments, this double serine mutation weakened PER2 binding to a lesser degree than the zinc finger mutations, which did not elicit a similar period-shortening effect (Figure 2-2C). Therefore, the period-shortening effect induced by the double serine mutation is likely specific to the defects of the local PER–CRY interface instead of their overall binding. It is conceivable that PERs might engage with CRYs near the CLOCK-BMAL1 docking site to control a periodicity-related step of negative feedback different from what they do at the predominant PER–CRY interface.

Discussion

Previous studies have established a critical role of PERs in driving the rhythmic negative feedback loop (Reppert and Weaver, 2002). To fulfill this role, PERs have been suggested to act through multiple mechanisms, including mediating CRY nuclear entry, coupling CRYs to CLOCK-BMAL1, and competing with FBXL3 to stabilize CRYs. Our structural and mutagenic analyses of the PER2-CBD-CRY2 complex reveal a surprisingly robust binary assembly, which is resilient to mutational disruption. This stable complex is

enabled by an extended binding mode of the PER2-CBD, which spreads several distinct functional modules over a mostly linear interface. The hallmark of the PER–CRY interactions is its steric incompatibility with the FBXL3–CRY complex, which provides the structural basis for the competition of PERs and the FBXL3 ubiquitin ligase for controlling CRY stability. Interestingly, distant from the FBXL3–CRY interface, PERs also anchor themselves next to the putative CLOCK-BMAL1-binding pocket of CRYs, possibly regulating a specific step of transcriptional repression. Despite intensive genetic and cell-based studies, the precise spatial and temporal steps undertaken by PERs to coordinate transcriptional repression in the molecular clockwork remain unclear. On the one hand, PERs have been reported to be essential for CRYs to interact with CLOCK-BMAL1 (Chen et al., 2009). On the other hand, emerging evidence suggests that PERs binding might interfere with complex formation between CRYs and CLOCK-BMAL1 at certain steps during repression (Akashi et al., 2014; Ye et al., 2011). Conceivably, by interacting with the CRY C-terminal helix, PERs could compete with the C-terminus of the BMAL1 transactivation domain for CRY binding (Czarna et al., 2011). While detailed biochemical studies are necessary to resolve this controversy, our results offer the structural framework for in-depth mechanistic investigations.

Apart from the PER2-CBD-CRY2 complex, the crystal structures of CRY2 have been determined for four additional functional states, apo, FAD-, FBXL3-, and KL001-bound (Nangle et al., 2013; Xing et al., 2013). Together, these structures outline a rich landscape for the functional surfaces of mammalian CRYs, which distinguishes them from other members of the cryptochrome/photolyase superfamily. In their C-terminal α-helical domain, CRYs

feature the conserved FAD-binding pocket, which is also targeted by the FBXL3 C-terminal tail and the clock-modulating drug, KL001. In their N-terminal α/β photolyase domain, CRYs have evolved the secondary pocket into a critical site for CLOCK-BMAL1 binding. Importantly, both CRY surface pockets are demarcated by structural elements with noticeable structural plasticity (Figure 2-4—figure supplement 1 and 2). The FAD-binding pocket is framed by the phosphate-binding loop and the interface loop on opposite edges, whereas the secondary pocket is guarded by the serine loop on one side. With the exception of the phosphate-binding loop, both the interface and serine loop have been shown to directly mediate protein–protein interactions. Lastly, the extreme C-terminal α-helix of the mammalian CRYs presents yet another important surface area, which is responsible for the mutually exclusive binding of FBXL3 and PERs. Remarkably, all these molecular interacting sites likely represent an incomplete functional map of CRYs. Numerous mutants identified in our random mutagenesis screen of functionally deficient CRY1 and CRY2 bear mutations of amino acids located outside these sites (McCarthy et al., 2009). Future structural studies are needed to paint a complete picture of CRY functional surfaces.

Our crystal structure of the PER2-CBD-CRY2 complex unveils a structurally important intermolecular zinc finger, which might function as a stabilizing ‘molecular clasp’. Although the evolutionary significance of the zinc-coordinating residues is apparent, as evidenced by their strict conservation across vertebrates, the functional significance of this unusual binding interface requires further investigation. On the one hand, the intermolecular zinc finger might be an intermediate product of the still evolving PER–CRY interface. On the other hand, it is plausible that this special protein interaction interface confers sensitivity to

the fluctuating abundance of intracellular zinc (Wang et al., 2012), which might serve as a tissue-specific clock-modulating ion.

During the preparation of this manuscript, the complex structure of mammalian CRY1-PHR and PER2-CBD was reported (Schmalen et al., 2014). With high sequence conservation between CRY1 and CRY2, the PER2-CBD adopts a similar CRY-binding mode with a tetrahedral coordination of a zinc ion by an intermolecular CCCH zinc-binding motif. The major structural difference lies at the interface of the N-terminal region of the PER2-CBD and the CRY secondary pocket. The CRY1-bound PER2-CBD fragment contains a residual fusion-protein sequence, which forms an artifactual β-hairpin with the first five amino acids of the PER2-CBD (Figure 2-4—figure supplement 3). In contrast to the PER2-bound CRY2 serine loop, but reminiscent of the *Drosophila* CRY antenna loop (Zoltowski et al., 2011), the otherwise disordered (Czarna et al., 2013) CRY1 serine loop adopts an inward conformation and occludes the secondary pocket. This conformational difference reveals a substantial degree of structural plasticity, which might be necessary for differential binding and regulation at this site. Interestingly, Schmalen and colleagues identified a potential redox sensor involving a disulfide bond near the zinc finger between Cys412 and Cys363, which modulates CRY1-PER2 binding. However, in our circadian reporter assay, we did not detect any difference between the CRY1 wild type and C412A mutant (Figure 2-5D). More in-depth analyses can now exploit the specific structural differences between the two complexes to explain the non-redundant roles of the two *Cryptochrome* proteins.

True to their name, *Period* proteins act as the master timekeepers in the circadian clock pathway, and likely use their multiple functional modules to simultaneously mediate

the negative and positive phases of the clock through CRY stability and CRY-CLOCK-BMAL1 repression complex assembly.

Materials and methods

Recombinant protein purification

The mouse CRY2 (amino acids 1–512) was expressed as a glutathione S-transferase (GST) fusion protein in High Five (Invitrogen, Carlsbad, CA) suspension insect cells and isolated by glutathione affinity chromatography using buffer containing 20 mM Tris–HCl pH 8, 200 mM NaCl, 10% glycerol, 5 mM DTT (dithiothreitol). The protein was cleaved on-column by tobacco etch virus (TEV) protease then purified further by cation-exchange chromatography. Proteolytically stable murine PER2 (amino acids 1095–1215) was expressed as a GST-fusion protein in *Escherichia coli* expression system and isolated through glutathione affinity chromatography using buffer containing 20 mM Tris–HCl pH 8, 300 mM NaCl, 5 mM DTT. The protein was cleaved on-column by TEV protease then purified further by anion-exchange and size-exclusion chromatography. Both proteins were combined, concentrated, and further purified by size-exclusion chromatography using buffer containing 20 mM Tris–HCl pH 8, 300 mM NaCl, 5 mM DTT, 10% glycerol to establish stoichiometric binding.

Crystallization, data collection, and structure determination

The crystals of the CRY2-PER2 complex were grown at 4°C by the hanging-drop vapor diffusion method, using 2 μL protein complex sample mixed 2:1 with reservoir

solution containing 100 mM HEPES pH 7.5, 200 mM NaCl, 15% PEG 3350. Diffraction-quality crystals were subjected to a cryo-protectant procedure by gradually increasing the concentration of ethylene glycol to 25% (vol/vol) and then frozen in liquid nitrogen. The native and zinc anomalous data sets were collected at the BL8.2.1 beamline at the Advanced Light Source of the Lawrence Berkeley National Laboratory. Reflection data were indexed, integrated, and scaled with the HKL2000 (Otwinowski and Minor, 1997). The CRY2-PER2 complex was determined by molecular replacement using CRY2 from the murine CRY2-KL001 complex structure (PDB:4MLP) as the search model. The structural models were manually built, refined, and rebuilt with the programs COOT (Emsley et al., 2010), PHENIX (Adams et al., 2010), and CCP4 (Winn et al., 2011). PER2 was built in following density modification. All figures were made using PyMOL (Schrödinger, LLC). Buried surface area was calculated using CNS (Brunger et al., 1998).

In vitro GST pull down

GST-tagged mCRY2 (amino acids 1–512) was over-expressed in High Five insect cell suspension culture. GST-tagged mPER2 WT (amino acids 1095–1215) and GST-tagged mPER2ΔCXXC (amino acids 1095–1209) were over-expressed in *E. coli* and purified as previously described. Equal volumes CRY2-PHR was incubated with immobilized PER2 at 4°C for 1 hr. Glutathione beads were rigorously washed, and GST-PER2-CRY2 was released from the beads with SDS sample buffer, analyzed by SDS-PAGE and detected by Coomasssie stain.

Co-immunoprecipitation

N-terminal Myc-tagged *Cry2* (0.25 μg) and a C-terminal V5-tagged *Per2* (0.5 μg) were transfected (Fugene 6, Madison, WI) into HEK293 cells. After 48 hr, cells were harvested and lysed by centrifugation. α-MYC-conjugated beads were used to immobilize MYC-CRY2. Beads were washed with buffer containing 50 mM Tris–HCl pH 7.5, 100 mM NaCl, 5% glycerol, 0.5 mM DTT, 0.5% Triton X-100, protease inhibitor (1:50). Protein was released from beads with SDS sample buffer and analyzed by Western blot using α-MYC and α-V5 for CRY2 and PER2, respectively.

Real-time circadian rescue assays

Real-time circadian rescue assays performed as described in (Ukai-Tadenuma et al., 2011). *Cry1*$^{-/-}$/*Cry2*$^{-/-}$ MEFs were plated in 35-mm dishes at a density of 5×10^5 cells per dish. 24 hr later, cells were transfected with FuGene6 with 4 μg of pGL3-P(*Per2*)-*Luc* reporter plasmid and 150 ng of the pMU2-mCry1 expression vector (Ukai-Tadenuma et al., 2011) or mutant forms of this vector. 72 hr after transfection, the cells were synchronized by a 2-hr incubation in medium (DMEM/10% FBS/antibiotics) with dexamethasone (0.1 μM). The medium was then replaced with medium prepared from powdered DMEM without phenol red (Corning 90-013-PB) containing 4.5 g/l glucose and supplemented with 10 mM HEPES pH 7.2, 100 μM luciferin, 1 mM sodium pyruvate, 0.035% sodium bicarbonate, 10% FBS, antibiotics, and 2 mM L-glutamine. Bioluminescence monitoring was performed

using a LumiCycle (Actimetrics, Inc. Wilmette, IL) to record from each dish continuously for ~70 seconds every 10 min using a photomultiplier tube at 37°C.

Figures

Figure 2-1. Overall structure of the murine CRY2-PER2 complex at 2.8 Å.

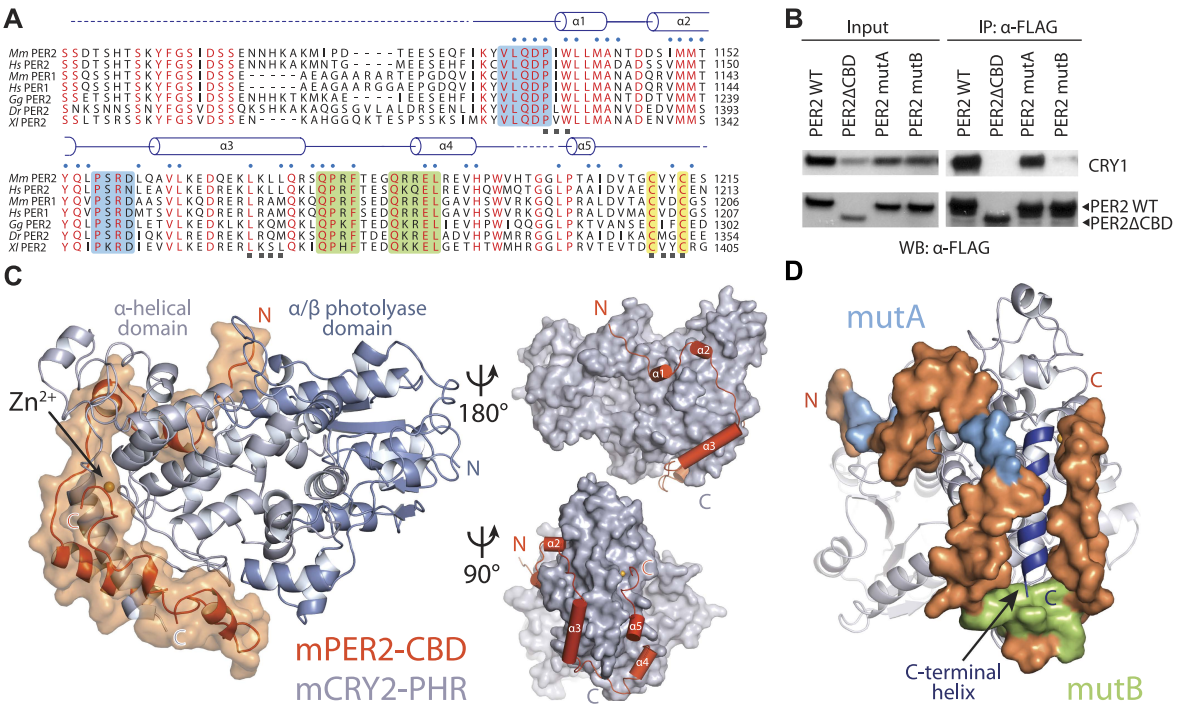

Figure 2-1. **Overall structure of the murine CRY2–PER2 complex at 2.8 Å.**
(**A**) PER2 CBD sequence alignment. 49% of PER2 CBD residues interact with CRY2 (blue dots). The zinc-coordinating residues are conserved throughout vertebrates (highlighted in yellow). Blue and green boxes correspond to the mutA and mutB constructs, respectively, and indicate regions of PER2-CBD that were mutated to alanines. Dashed lines indicate crystallographically disordered regions. Black squares indicate residues mutated under structure guidance.
(**B**) Co-immunoprecipitation of mutant PER2-CBD-FLAG constructs, only mutB was able to abolish CRY1-MYC binding. Western blot of an immunoprecipitaion of COS7 cells transfected with PER2-NLS-FLAG and CRY1-MYC. Proteins were precipitated with α-FLAG and then analyzed by Western blots using α-MYC and α-FLAG.
(**C**) CRY2 PHR (gray) adopts an overall fold identical to its apo and complexed forms (e.g., FAD, FBXL3, and KL001). PER2 CRY-binding domain (CBD) (orange) shows a highly extended binding mode around CRY2. PER2 flanks the CRY2 C-terminal helix and coordinates a zinc ion with CRY2 within a CCCH-type intermolecular zinc finger motif.
(**D**) Crystallographic data identify the location of alanine scanning mutants. Importantly, the mutB construct is centered around the CRY2 C-terminal helix.

Figure 2-1—figure supplement 1. Sequence alignment and structural elements of vertebrate CRY.

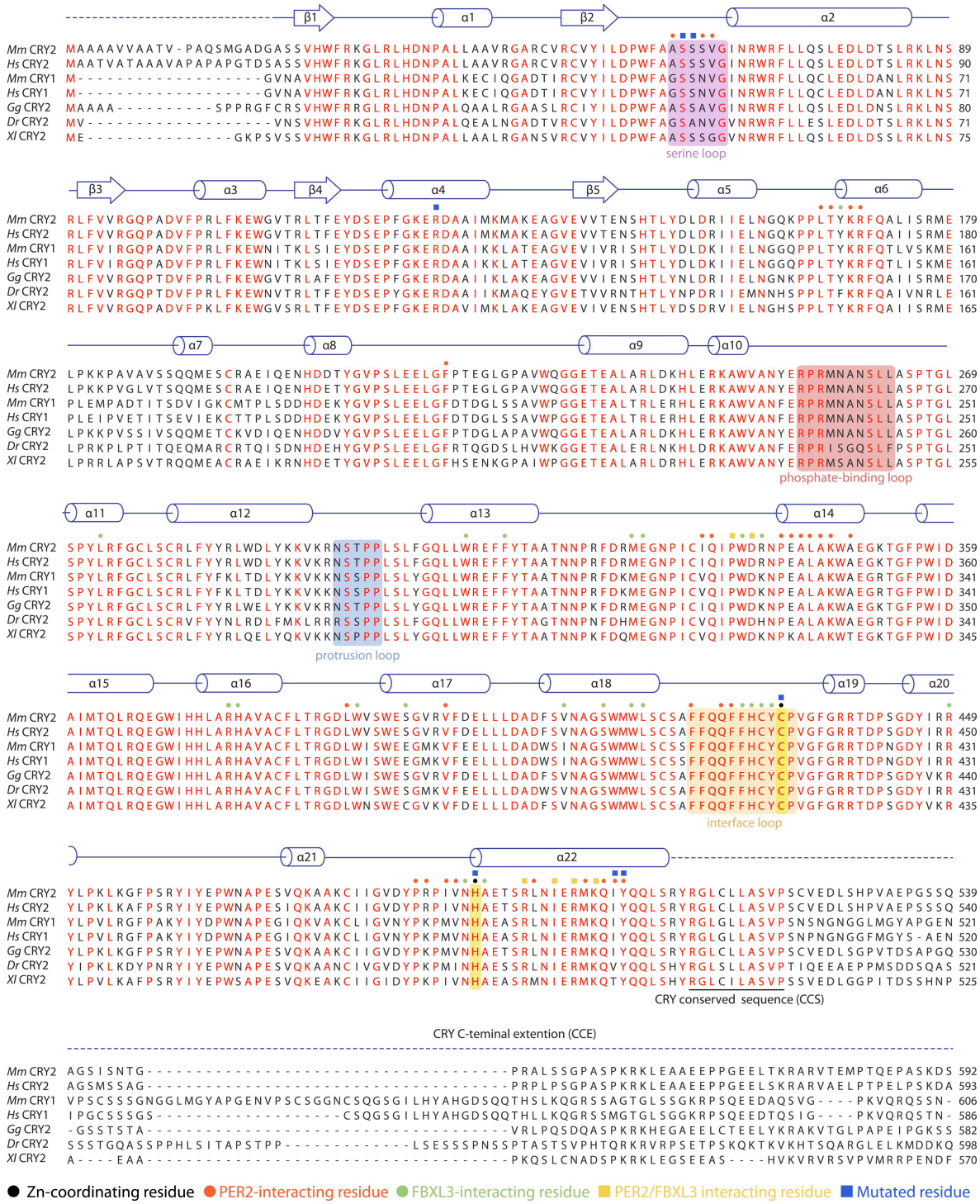

Figure 2-1—figure supplement 1. Sequence alignment and structural elements of vertebrate CRY.

Alignment and secondary structure assignments of CRY2 orthologs from Mus musculus (Mm), Homo sapiens (Hs), Gallus gallus (Gg), Danio rerio (Dr), and Xenopus laevis (Xl). Strictly conserved residues are colored in red. Blue and green dots indicate mPER2-CBD- and hFBXL3-interacting residues, respectively. Yellow squares indicate residues that interact with both PER2 and FBXL3. Black dots indicate residues that are involved in zinc coordination. Colored boxes represent the boundaries of structurally dynamic loops. Dashed line represents the regions outside the PHR.

Table 2-1. Data collection and refinement statistics

CRY2-PER2	
Data collection	
Space group	P41
Cell dimensions	
a, *b*, *c* (Å)	97.67, 97.67, 163.21
α, β, γ (°)	90, 90, 90
Resolution (Å)	2.9 (2.8)
R_{meas}	0.06 (0.8)
$I/\sigma I$	18.8 (2.1)
Completeness (%)	99.6 (98.2)
Redundancy	4.2 (4.2)
Refinement	
Resolution (Å)	42.7–2.8
No. reflections	37541 (3671)
R_{work}/R_{free}	20.5/27.7
No. atoms	9342
Protein	9292
Ligand/ion	2
Water	48
B-factors	97.3
Protein	97.5
Ligand/ion	114.1
Water	66.3
R.m.s. deviations	
Bond lengths (Å)	0.009
Bond angles (°)	1.3

Figure 2-2. CRY2 C-terminal helix is the central locus of both PER2 and FBXL3 interactions.

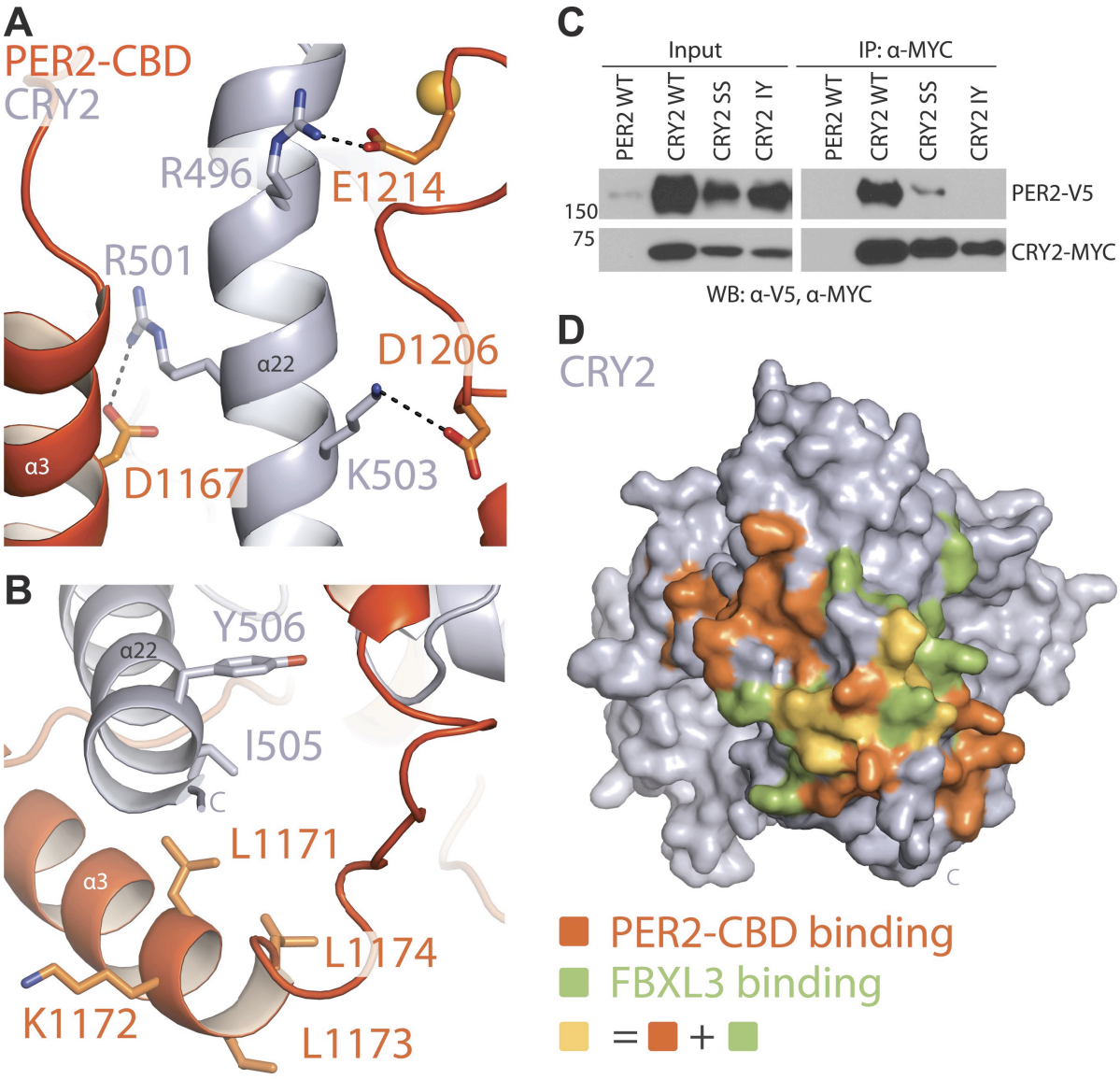

Figure 2-2. CRY2 C-terminal helix is the central locus of both PER2 and FBXL3 interactions.

(**A**) PER2 (orange) forms three salt-bridges along CRY2 C-terminus helix (gray) R501 and K503 have been previously reported as critical binding residues.

(**B**) A close-up view of the PER2-CRY2 interface at the end of CRY2 C-terminal helix. While the upper portion of the CRY2 C-terminal helix maintains ionic interactions with

PER2, the lower is predominantly mediated by hydrophobic interactions. CRY2 and PER2 residues chose for subsequent mutational analysis are shown in sticks.
(**C**) Concurrent mutations of hydrophobic residues on the CRY C-terminal helix (I505D and Y506D) prevent PER-CRY complex formation. Co-immunoprecipitations were performed with transfected full-length PER2-V5 and MYC-CRY2 in HEK293 cells with α-MYC beads and analyzed by Western blotting using α-V5 and α-MYC. See Figure 2-2—figure supplement 1A for corresponding PER2 mutants.
(**D**) Surface mapping of FBXL3- and PER2-binding sites on CRY2. Residues that share contacts with PER2 and FBXL3 are colored in yellow and are clustered along the C-terminal helix. Other residues involved in binding PER2 and FBXL3 are colored in orange and green, respectively.

Figure 2-2—figure supplement 1. Mutational and structural analysis of the PER2-CRY2 interface.

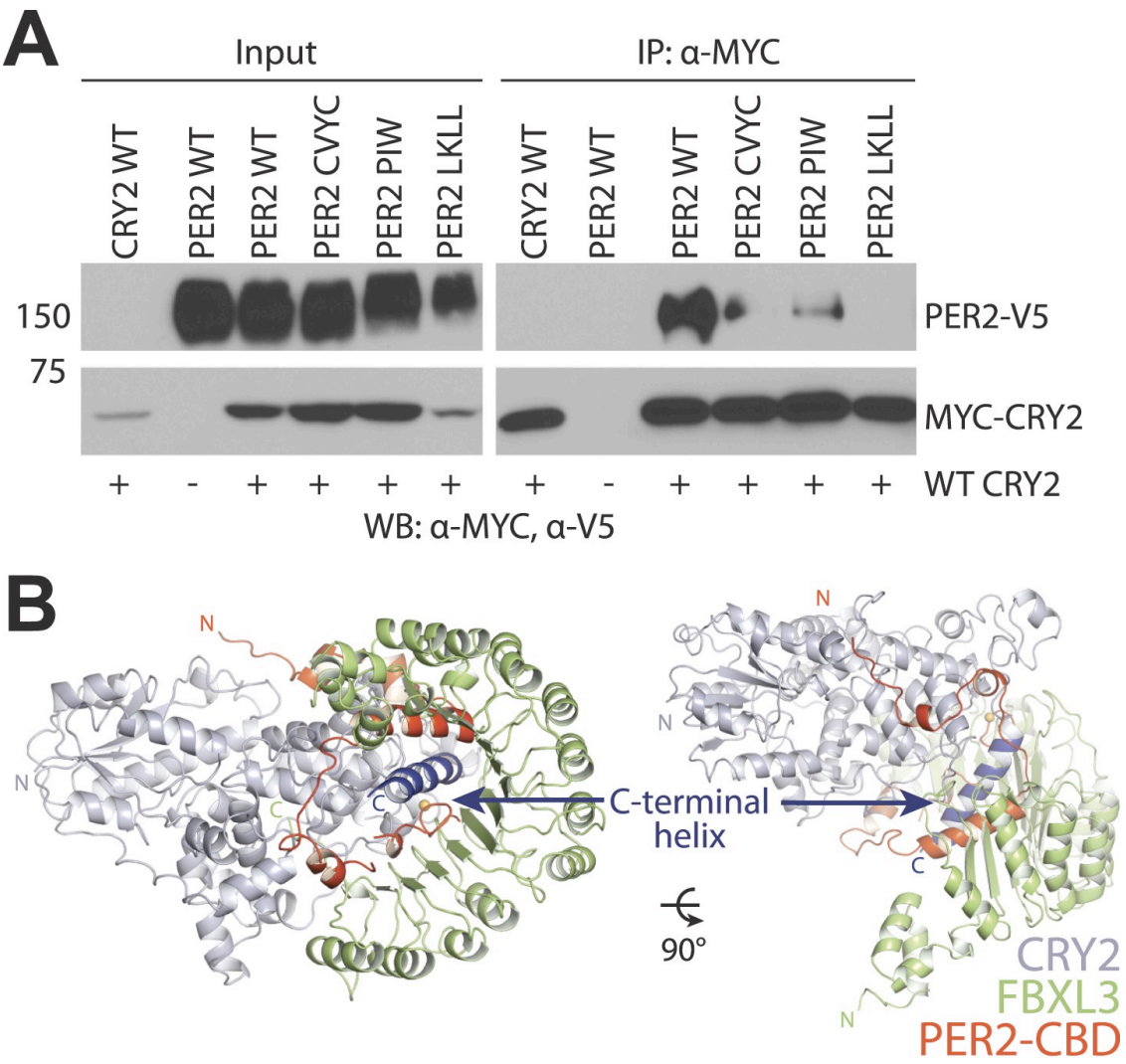

Figure 2-2—figure supplement 1. Mutational and structural analysis of the PER2-CRY2 interface.

(**A**) Diminished PER2-CRY2 interaction was replicated in a co-immunoprecipitation assay, in which the CXXC motif of the full-length FLAG-tagged PER2 protein was mutated to four alanines. Co-immunoprecipitations were performed with transfected full-length PER2-V5 and MYC-CRY2 in HEK293 cells with α-MYC beads.

(**B**) Superimposition analysis demonstrates the direct competition of PER2-CBD (orange) and FBXL3 (green) binding to CRY (gray), which is centered around the CRY2 C-terminal helix (blue).

Figure 2-3. The intermolecular zinc finger is important for PER2–CRY2 complex formation.

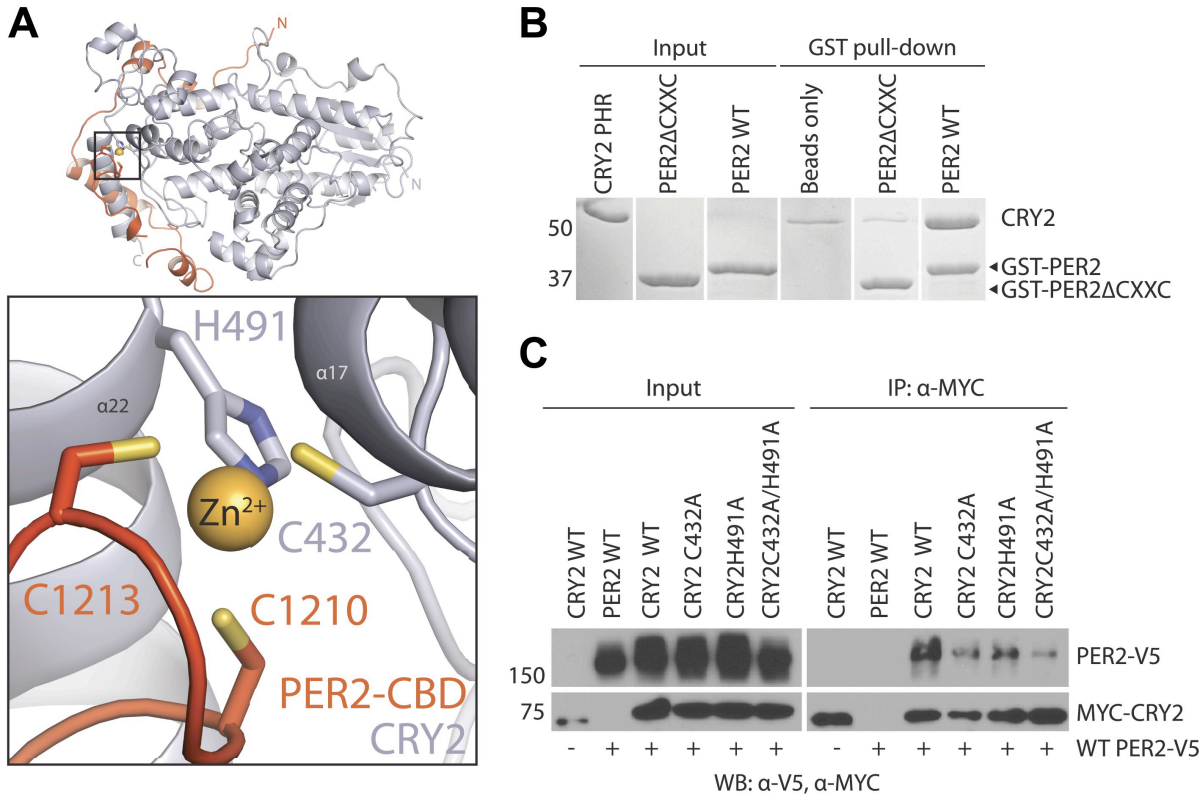

Figure 2-3. The intermolecular zinc finger is important for PER2–CRY2 complex formation.

(**A**) Four conserved, contributing residues from PER2 (C1210 and C1213) and CRY2 (C432 and H491) form a CCCH-type zinc finger.

(**B**) GST-pull-down assay with recombinant GST-tagged PER2ΔCXXC CBD and untagged CRY2-PHR protein show compromised CRY binding in the zinc finger mutant compared to WT PER2-CBD.

(**C**) Similarly diminished interaction was replicated in a co-immunoprecipitation assay. Alanine mutations were introduced to CRY2 zinc-coordinating residues, C432 and H491, individually or in combination. Co-immunoprecipitations were performed with transfected full-length PER2 and CRY2 in HEK293 cells with α-MYC beads.

Figure 2-3—figure supplement 1. Analysis of the intermolecular zinc finger.

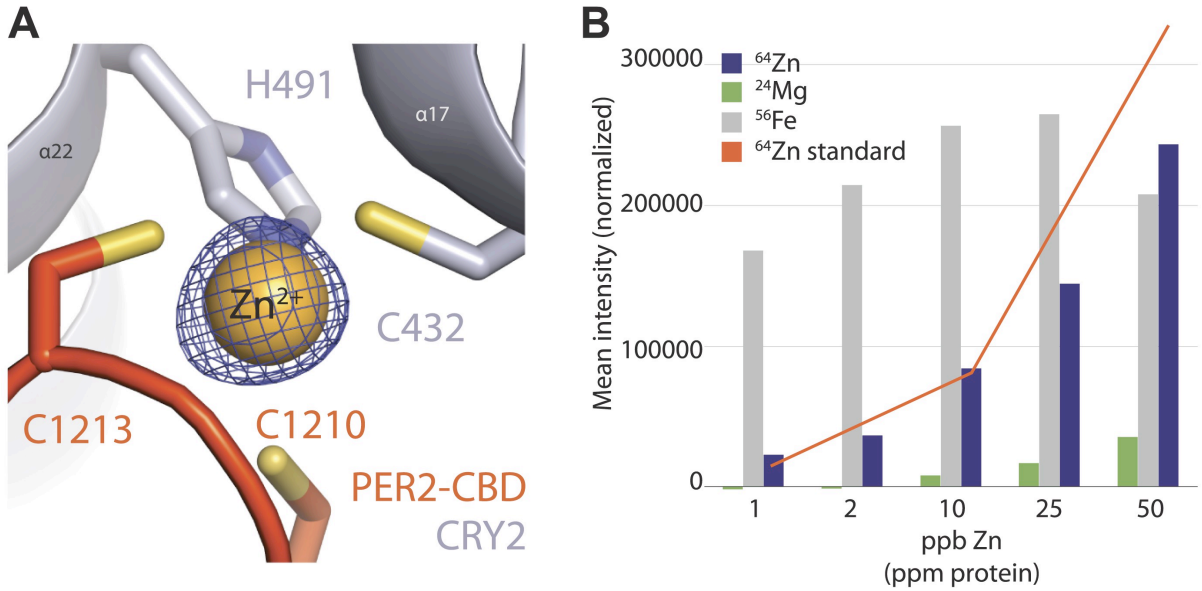

Figure 2-3—figure supplement 1. Analysis of the intermolecular zinc finger.
(**A**) Zinc-coordinating residues of PER2-CBD (orange) and CRY2 (gray) with zinc anomalous signal (λ = 1.284 Å) contoured at 7σ (blue mesh).
(**B**) Inductively coupled plasma mass spectrometric analysis of metal isotopes. Purified PER2-CBD-CRY2 complex was dehydrated, dissolved in concentrated HNO_3 overnight, diluted to 1% vol/vol HNO_3, and titrated. Zn (purple) isotopes (^{64}Zn, ^{66}Zn, ^{67}Zn, ^{68}Zn, ^{70}Zn) were the only ones that showed a greater than sixfold increase in mean signal intensity above the blank, dose-dependent increase, and approximated the predicted intensity of the standard (orange line). ^{24}Mg (green) and ^{56}Fe (gray) are shown as controls.

Figure 2-4. The secondary pocket is involved in CRY-CLOCK-BMAL1 complex assembly and repression.

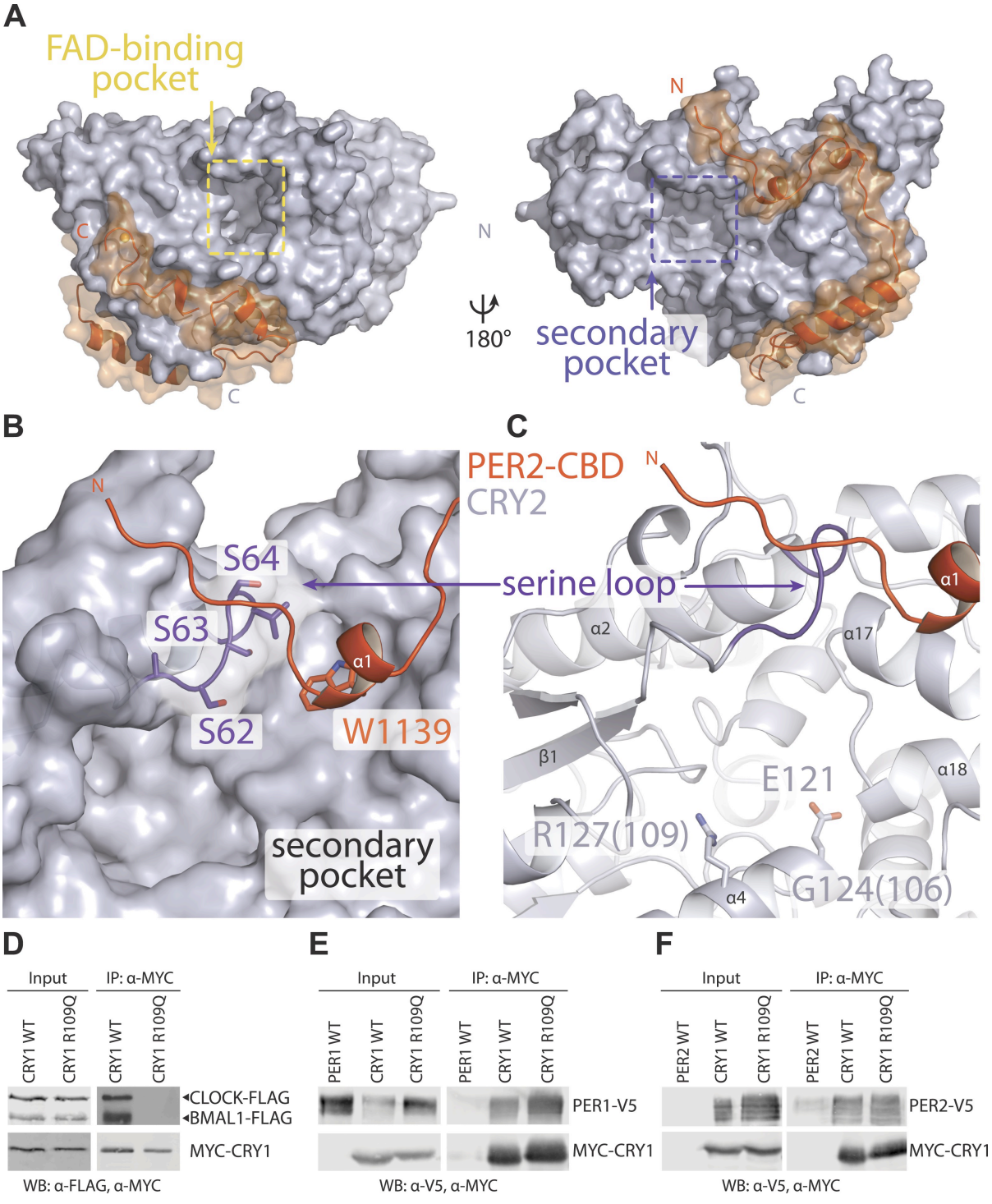

Figure 2-4. The secondary pocket is involved in CRY-CLOCK-BMAL1 complex assembly and repression.
(**A**) Relative positions of the two large pockets on CRY2.
(**B**) Surface representation of CRY2 with side chains of the serine loop shown in sticks. PER2 α1 helix inserts into a hydrophobic cleft. Compared to other CRY2 complexed forms, the serine loop flips up and engages PER2.
(**C**) The serine loop lies opposite to the CRY α4 helix, which together frame the secondary pocket, the α4 helix contains three residues (CRY1 G106R and R109Q, CRY2 E121K), whose mutations result in a weak repression phenotype.
(**D–F**) Co-immunoprecipitation assays show that the CRY1 R109Q mutant is unable to bind CLOCK-BMAL1, but retains PER1 and PER2 binding.

Figure 2-4—figure supplement 1. Locations of structurally plastic loops on CRY2.

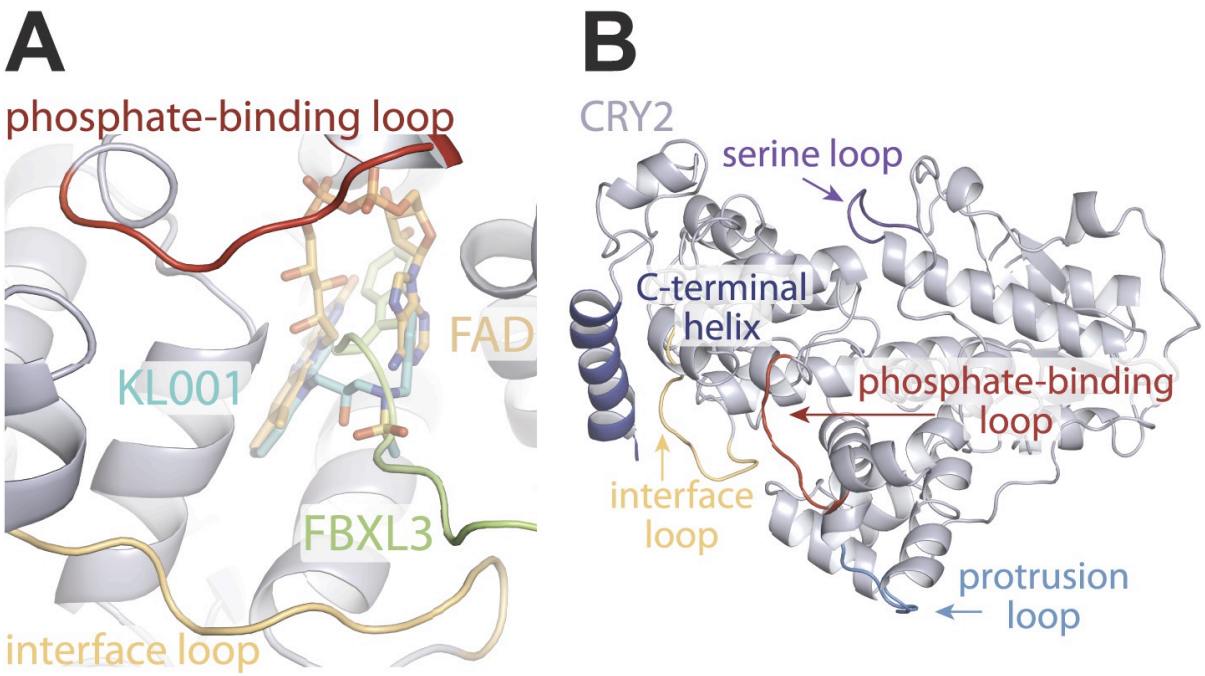

Figure 2-4—figure supplement 1. Locations of structurally plastic loops on CRY2.
(**A**) The phosphate-binding loop and interface loop frame opposite sides of the FAD-binding pocket. Superimposition analysis shows the FAD-binding pocket as a regulatory hotspot, which can bind metabolic cofactor, FAD (yellow), clock-modulating small molecule, KL001 (cyan), and FBXL3 C-terminal tail (green).
(**B**) Locations of CRY2 loops; interface loop (yellow), phosphate-binding loop (red), serine loop (purple), and protrusion loop (light blue), which in light-sensitive CRYs occludes part of the FAD-binding pocket but is pushed outward and maintains an open FAD-binding pocket in vertebrate CRYs.

Figure 2-4—figure supplement 2. CRY-PHR superposition: including CRY1 apo (red), CRY2 apo (light blue), KL001-bound (green), FAD-bound (orange), FBXL3-bound (cyan), and PER2-CBD-bound (gray) CRY.

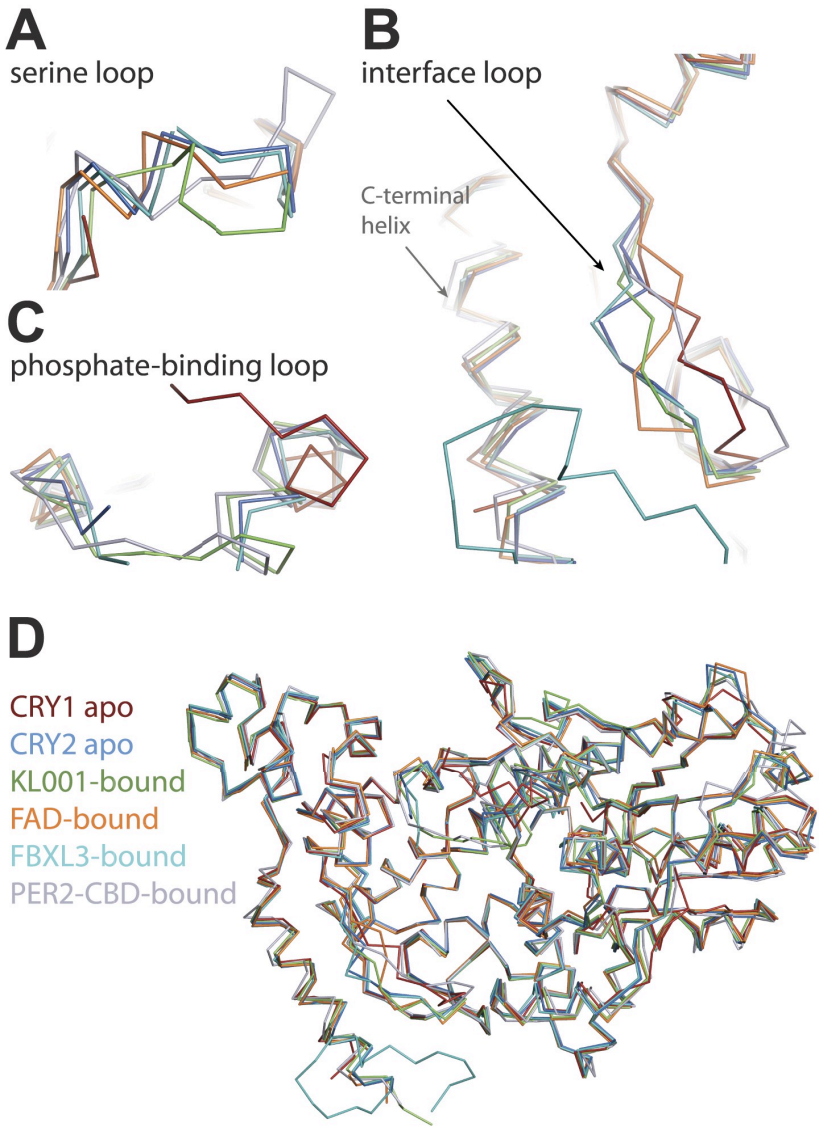

Figure 2-4—figure supplement 2. CRY-PHR superposition: including CRY1 apo (red), CRY2 apo (light blue), KL001-bound (green), FAD-bound (orange), FBXL3-bound (cyan), and PER2-CBD-bound (gray) CRY.
(**A**) Serine loop undergoes a large conformational change after PER2-CBD binding.
(**B** and **C**) The interface loop and phosphate-binding loop are also sites of high structural plasticity.
(**D**) Overall CRY-PHR showing the global structure adopts a common fold.

Figure 2-4—figure supplement 3. Major differences between CRY1-PER2-CBD and CRY2-PER2-CBD complex structures.

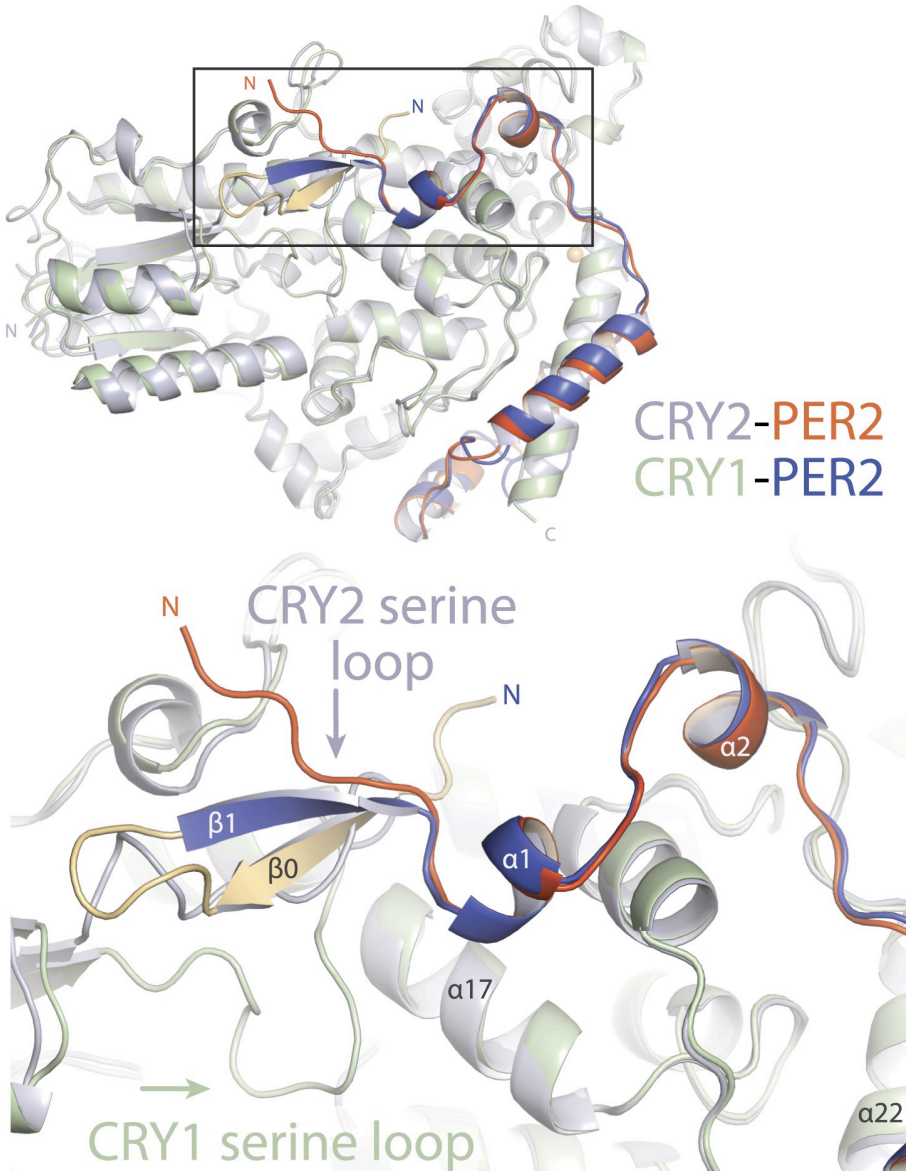

Figure 2-4—figure supplement 3. Major differences between CRY1-PER2-CBD and CRY2-PER2-CBD complex structures.
Superposition of the two structures reveals major structural dissimilarities between the two paralogs at the CRY secondary pocket and a residual fusion-protein sequence (yellow) in CRY1-bound PER2-CBD. The PER2-CBD (dark blue) N-terminus together with the artifactual sequence (AGLEVLFQGPDSM) forms a β-hairpin and induces an inward conformation of the CRY1 (light green) serine loop.

Figure 2-5. Real-time circadian rescue assays.

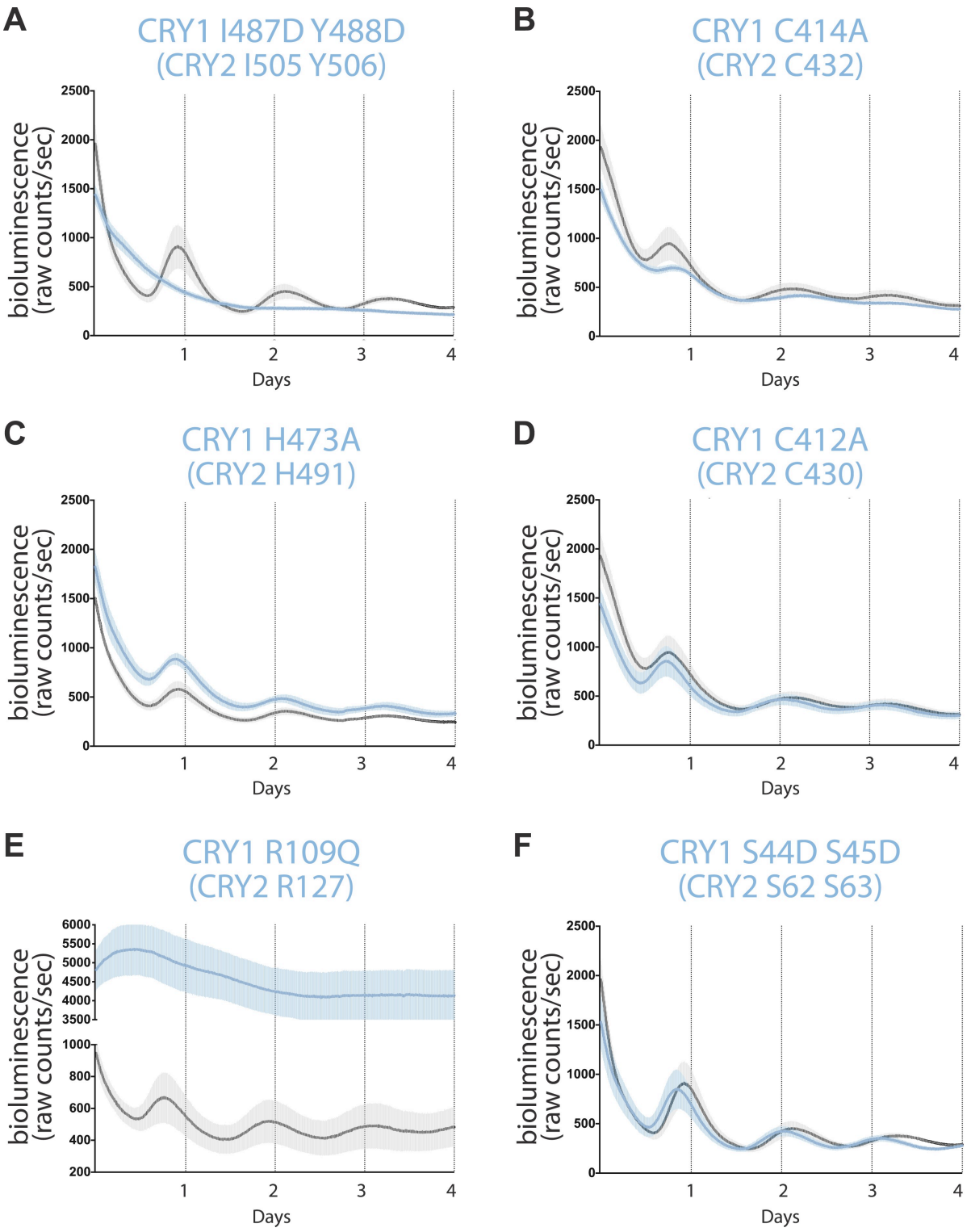

Figure 2-5. Real-time circadian rescue assays.
Cry1$^{-/-}$*/Cry2*$^{-/-}$ MEFs were transfected 24 hr after plating with *dLuc* reporter plasmid and *mCry1* expression or mutant vector. 72 hr after transfection, the cells were synchronized with dexamethasone. Bioluminescence (raw counts/s) monitoring was performed continuously for 70 s every 10 min using a photomultiplier tube at 37°C. Traces are shown as mean ± SEM and are representative of triplicate samples. Mutants are shown in blue and WT control in black. Only CRY1, not CRY2 is able to reconstitute robust circadian rhythmicity.
(**A**) CRY1 I487D Y488D (CRY2 I505 Y506) 'IY' mutant abolishes rhythmicity but maintains repression compared to WT, suggesting that PER is not required for transcriptional repression.
(**B** and **C**) Zinc-coordinating residues on CRY1 C414 and H473 (CRY2 C432 and H491) show blunted rhythm amplitude.
(**D**) A nearby cysteine residue, C412 (CRY2 430), when mutated to alanine, does not show a significantly different phenotype from the WT control.
(**E**) A critical residue on the secondary pocket, CRY1 R109 (CRY2 R127) shows a severely weakened repression phenotype when mutated to a glutamine. Traces are shown as mean ± SEM and are representative of duplicate samples.
(**F**) Mutations of two serine residues in the serine loop, CRY1 S44D S45D (CRY2 S62 S63), show near WT rhythmicity and repression but with a 1-hr shorter period. For all mutants, corresponding CRY2 residues are in parenthesis.

CHAPTER THREE: Results

AN EVOLUTIONARY HOTSPOT DEFINES FUNCTIONAL DIFFERENCES BETWEEN CRYPTOCHROMES

Introduction

Cell autonomous molecular clocks with robust 24-h rhythms have evolved to coordinate physiological processes with daily changes in the environment. At the molecular level, clocks appear to have evolved independently a number of times and are comprised of a variety of different components. In eukaryotes, these clocks are made up of transcription/translation feedback loops (TTFL) with regulatory steps at many levels that tune the period and provide environmental input into the system. In mammals, the TTFL is principally defined by a heterodimeric transcription factor, composed of basic helix-loop-helix (bHLH) PER-ARNT-SIM (PAS) domain-containing proteins CLOCK and BMAL1 (Gekakis et al., 1998; King et al., 1997), which regulates the expression of many targets including the genes encoding the repressors: *Cry 1/2* and *Per 1/2/3* (reviewed in (Gustafson and Partch, 2015)). CRY and PER proteins translocate to the nucleus where they bind and repress CLOCK and BMAL1 activity (reviewed in (Gustafson and Partch, 2015); (Kume et al., 1999)).

Both CRY and PER are necessary to maintain rhythmicity in both cellular and organismal milieus (Bae et al., 2001; Liu et al., 2007; van der Horst et al., 1999; Vitaterna et al., 1999); however, the mechanisms driving repression are poorly understood. Though CRY

appears to be sufficient for repression on its own, PER proteins appear to play a role in promoting CRY interaction with CLOCK/BMAL1 in vivo (Chen et al., 2009). Furthermore, degradation of the repressors is a critical period-determining step mediated primarily by CASEIN KINASE 1δ/ε (CK1δ/ε) and β-TrCP in the case of PER (Shirogane et al., 2005), and FBXL3 and FBXL21 in the case of CRY (Busino et al., 2007; Godinho et al., 2007; Hirano et al., 2013; Siepka et al., 2007; Yoo et al., 2013). However, greater insight into the mechanisms underlying periodicity is lacking, but necessary for targeted development of therapies for circadian disorders.

CRYs offer a unique opportunity to gain insight into the function of the core clock and specifically to better understand how precise timing is achieved. Despite high sequence identity and similarity, CRY1 and CRY2 (which refer to the two CRYs from mice hereafter) have several critical differences. First, CRY1 is a stronger repressor of CLOCK/BMAL1-mediated transcriptional activation (Griffin et al., 1999; Khan et al., 2012). Although deletion of both CRYs results in arrhythmicity, individual null mutations result in short (*mCry*$1^{-/-}$) and long (*mCry2*$^{-/-}$) periods respectively (van der Horst et al., 1999; Vitaterna et al., 1999). Moreover, the CRYs are associated with a highly divergent set of DNA binding complexes within the genome and a substantially different phase of peak binding (Koike et al., 2012). The peak of occupancy for CRY2 is early in the evening in phase with PER1 and PER2, whereas CRY1 occupancy peaks in the late night and early morning, several hours after the peak occupancy of PER1 and PER2 (Koike et al., 2012).

Notably, CRYs evolved from a family of photoactivated DNA-repair enzymes known as photolyases (PHLs) (Ozturk et al., 2007), that catalyze the repair of UV-induced DNA

lesions through two cofactors, a flavin adenine dinucleotide (FAD) molecule in a central pocket, which directly interacts with and repairs the DNA lesion, and a variable secondary cofactor (either methenyltetrahyrdofolate (MTHF) or 8-hydroxy-7,8-didemethyl-5-deazariboflavin (8-HDF)), which functions as a light-harvesting antenna (reviewed in (Sancar, 2008)). In this reaction, the FAD molecule is essential for enzymatic activity while the secondary cofactor is dispensable, but improves the dynamics of the reaction (Ozturk et al., 2007). CRYs have evolved from PHLs to take on both direct and indirect roles in a number of different molecular clock architectures, but only a subset are photoactive and none retain the ability to function as DNA repair enzymes (reviewed in (Chaves et al., 2011)). Although CRYs from all organisms have a stereotyped structure of a conserved photolyase-homology region (PHR), a C-terminal helix, and a highly divergent CRY C-terminal extension known as the tail (reviewed in (Chaves et al., 2011)), intrinsic functional characteristics must derive from demonstrable structural divergence. In particular, animal CRYs, classified into type I and II, play dynamic, but significantly different roles in similar, but distinct clock mechanisms typified by *Drosophila* and mouse clocks respectively (Merbitz-Zahradnik and Wolf, 2015; Ozturk et al., 2007). A key difference between type I and type II CRYs is that only type II CRYs (such as CRY1 and CRY2 in mice) function as direct repressors of their transcriptional activators (Yuan et al., 2007), whereas type I CRYs, such as the single CRY in *Drosophila* (dCRY), function as blue light-sensitive inputs to a TTFL composed of CLOCK and BMAL1 homologs and the repressors PER and TIMELESS (Merbitz-Zahradnik and Wolf, 2015). However, the structural features underlying the divergent role of type I and type II CRYs are poorly understood.

Thus, major open questions include: (1) how do certain mutations in CRY lead to acceleration or deceleration of the clock; (2) what are the functional interfaces on CRY that lead to specific protein-protein interactions; (3) how are functional differences between type I and II CRYs manifested at a structural level; and (4) how do the structural features that differentiate CRY1 and CRY2 manifest divergent functional characteristics? Here, to address these questions, we use Statistical Coupling Analysis (SCA) to identify collectively co-evolving residues in the CRY/PHL family (CPF) and discover an evolutionarily conserved network of residues spanning the FAD-binding pocket and secondary cofactor pocket (Rivoire et al., 2016). Focusing on the secondary pocket, we demonstrate that the interior of the pocket gates interactions with CLOCK and BMAL1 and likely differentiates type I and type II CRYs in their ability to directly repress CLOCK and BMAL1. Furthermore, we show that subtle changes at this pocket result in substantial differences in periodicity in cycling cells due to changes in affinity between CRY1 and CLOCK/BMAL1. Finally, we observe that a few small differences between CRY1 and CRY2 at this surface underlie CRY2's periodicity characteristics, again the result of a weakened affinity for CLOCK/BMAL1. Importantly, these results define a mode of period regulation of the circadian clock that is orthogonal to the canonical model of period regulation arising from the stability of the PER and CRY repressor proteins.

Results

CRYs and PHLs contain a co-evolutionary network of amino acids connecting the FAD-binding pocket to the secondary pocket

The central problem in understanding the structural basis for function in any protein is to deduce the pattern of energetic interactions between amino acid residues. An emerging approach for addressing this difficult problem is the analysis of statistical coevolution. The basic premise of these methods is that the constraints between amino acids that underlie folding and function should be reflected in the coevolution of those amino acid positions in a large and diverse sampling of sequences comprising a protein family. In general, there are two distinct approaches for using coevolution that deduce different relevant features of protein structures. The first comprises a set of methods for contact prediction – DCA, PSICOV, and Gremlin – which use classic tools from statistical physics to identify the minimal set of direct interactions between amino acids that can explain the empirical correlations between sequence positions. The fundamental goal of this approach is to separate the local structural interactions between residues (the contacts) from the indirect, global coevolution that can arise through chains of interacting residues. The second approach is defined by methods such as the statistical coupling analysis (or SCA), which explicitly focus on discovering the conserved collectively evolving groups of amino acids with the premise that these encode the cooperative actions of amino acids underlying protein function – binding, catalysis, and allostery. Here, we apply SCA to probe potential allosteric mechanisms in the CPF proteins.

A central finding of SCA has been the identification of protein sectors: physically contiguous networks of amino acids that often bridge the active site of proteins to allosteric surfaces (Halabi et al., 2009; Suel et al., 2003). Recent work has shown that sector-connected surfaces on the protein are hotspots for allosteric regulation, and has led to the proposal that the sector provides a conserved cooperative mechanism that can be used to evolve new regulation in proteins (Lee et al., 2008; Reynolds et al., 2011). Using mCRY1 as a PSI-BLAST query, 10,000 CRY and PHL protein sequences were identified, collected, filtered by size, and aligned. This alignment was used as the basis for the SCA (For a thorough discussion of the theory and mechanics of the SCA, please see (Rivoire et al., 2016)). The initial alignment was trimmed to remove highly gapped positions and, subsequently, highly gapped sequences before the sequences were weighted based on their identity to other sequences in the alignment (described in greater detail in Methods), resulting in a final alignment of 3,619 sequences composed of 460 positions. Plotting a histogram of all of the pairwise sequence identities suggests a trimodal distribution of similarities: a small group of sequences sharing a roughly 45% sequence identity, and two larger groups sharing approximately 25% and 33% sequence identity (Figure 3-1A). However, careful examination of the sequence similarity matrix suggests many small subgroups of sequences with much higher pairwise identities (>70%) (Figure 3-1B). Position specific conservation values (D_i) (Figure 3-1C) and pairwise conservation values (shown in the weighted correlation matrix in Figure 3-1D) were calculated as a way of assessing both independent and interdependent properties for each position in the alignment. Finally, eigenspectrum decomposition was

performed on the weighted correlation matrix to determine the network of significantly co-evolving positions in the alignment (Figure 3-1E and Figure 3-1—table supplement 1).

The CRY2 sequence from *Mus musculus* was used as the reference sequence for the SCA due to the fact that several loop regions are more complete in the CRY2 structure than in the CRY1 structure, which allows for better mapping of the results of the SCA. Performing the SCA, we discovered a physically contiguous network of amino acids spanning the active site of the PHL family, the FAD-binding pocket (Figure 3-2A), and extending to several surface accessible positions including the secondary cofactor pocket (Figure 3-2B). Thus, the regions surrounding CRY's two major cavities show correlated patterns of sequence variation over the course of CPF evolution. This is consistent with the fact that the FAD access cavity is known to have undergone a change in surface potential, altering interactions with DNA lesions (reviewed in (Chaves et al., 2011)). Moreover, the CPF has interacted with a number of different secondary cofactors in various binding modes (Figure 3-2—figure supplement 1A) (Park et al., 1995; Tamada et al., 1997), and many family members do not appear to complex a secondary cofactor at all (Brautigam et al., 2004; Czarna et al., 2013; Xing et al., 2013; Zoltowski et al., 2011). Critically, SCA is more predictive of allosterically connected surface residues in co-evolutionary networks than a simple analysis of positional conservation, which often predicts primarily residues in the protein core. This feature of SCA is apparent when comparing the network of residues identified by positional conservation (using a permissive cutoff (D_i >1.5)) (Figure 3-2—figure supplement 1B and 1C) to the network identified by the SCA (Figure 3-2—figure supplement 1D).

Because the SCA network is identified by examining correlations in sequence variation across the entire alignment, the finding of a sector connecting the secondary pocket to the FAD-binding site indicates that this interaction is conserved across the CPF proteins and is not an idiosyncratic feature of the PHL domains. However, CRYs no longer function as DNA repair enzymes suggesting that network features have been repurposed for new functions. In support of this idea, we mapped the network of SCA residues onto structures of the CRY2/PER2 CRY-Binding Domain (CBD) complex (Figure 3-2C) and the CRY2/FBXL3 complex (Figure 3-2D) (Nangle et al., 2014; Xing et al., 2013). Both PER2 and FBXL3 interact extensively with the FAD-binding pocket (where DNA lesions directly interact with PHLs) and with network residues around CRY2's C-terminal α-22 helix. This observation suggests that in the absence of an enzymatic role in DNA repair, functional interfaces have been repurposed for new roles in protein-protein interactions.

The secondary pocket of vertebrate CRYs is a binding interface for the CLOCK/BMAL1 heterodimer

The SCA data suggest that multiple functional domains from PHLs have been repurposed for new functions in CRYs. Existing CRY structures lack secondary cofactors in the secondary pocket despite attempts to obtain structures with these ligands (Brautigam et al., 2004; Zoltowski et al., 2011). It has been hypothesized that co-evolutionary networks can be used cooperatively to evolve new protein functions (Lee et al., 2008; Reynolds et al., 2011). Given that other critical PHL surfaces have been subsumed for protein-protein interactions in CRYs, we hypothesized that the secondary pocket may also have been

repurposed. A number of residues at the surface of the secondary pocket (Figure 3-3A) were identified as part of the co-evolutionary network in the SCA. We previously identified three of these residues (E103 (E121 in CRY2), G106, and R109) in a targeted screen for mutations in CRY1 and CRY2 that weaken their repressive capacity (McCarthy et al., 2009). Moreover, we showed that one of the mutants identified in the screen (CRY1 R109Q) diminishes the affinity between the CLOCK/BMAL1 heterodimer and CRY1 (Nangle et al., 2014).

In order to test the predictions from the SCA, we tested the importance of specific residues around the secondary pocket, including those predicted to be co-evolving and those that were not. We focused first on the α4 helix between E103 and R109 of CRY1, where many (E103, P104, F105, G106, R109), but not all (K107, E108) amino acids were identified in the SCA (Figure 3-3A). To test whether changes in these residues alter CRY1's function in the circadian clock, we used a rescue assay originally developed by Ukai-Tadenuma and colleagues (Ukai-Tadenuma et al., 2011). When expressed under the control of its endogenous promoter and an intronic element, *mCry1* can rescue rhythms in a bioluminescent reporter (*Luciferase (Luc)* driven by a *Per2* promoter) in *Cry1*$^{-/-}$/*Cry2*$^{-/-}$ mouse embryonic fibroblasts (Figure 3-3B). We tested two mutations identified in the screen described above (E103K and G106R) and an additional mutant chosen to be less disruptive of the local protein environment (F105A) due to the more conservative mutation and the solvent-exposed nature of the wild-type residue. We found that none of the mutants were able to rescue rhythmicity, resulting in high constitutive LUC activity indicative of unchecked transcriptional activity by CLOCK and BMAL1 (Figure 3-3C). In addition, all three mutants had severe deficits in their ability to co-immunoprecipitate (co-IP) the

CLOCK/BMAL1 heterodimer, but bound PER2 comparably to wild-type CRY1 (Figure 3-3D and Figure 3-3—figure supplement 1). Since PER2 adopts an extended binding interface with CRY1 and CRY2 (Nangle et al., 2014; Schmalen et al., 2014), these data suggest that mutations at the "lower" (relative to the orientation shown here) interface (α4) of the secondary pocket cause local disruptions in CRY1's structure rather than global disruption of its protein fold. Additionally, a recent report from Michael and colleagues demonstrated that purified CRY1 R109Q behaved like WT CRY1 on a size-exclusion column, again suggesting that even substantial mutations on this helix are locally, rather than globally, disruptive (Michael et al., 2017).

In contrast, even severe mutations of the non-network residues at positions 107 (K107E) and 108 (E108K) of CRY1 did not impair CRY1's ability to rescue rhythms (Figures 3-3E and 3-3F), and these mutants interacted strongly with CLOCK, BMAL1 and PER2 (Figure 3-3D and Figure 3-3—figure supplement 1), suggesting that these residues are not critical for binding to CLOCK and BMAL1. Consistent with this interpretation, K107 and E108 are superficial residues with side chains that neither gate access nor form any part of the surface of the interior of the pocket. Based on these results, we suggest that the interior of the secondary pocket is a critical interface for interactions between CRYs and their repressive targets CLOCK and BMAL1, consistent with another recent report (Michael et al., 2017)**.**

Evolution at the secondary pocket defines a critical difference between insect-like CRYs and vertebrate-like CRYs

The two types of ancestral animal CRYs (type I and type II) can be found in various combinations in different animals. For example, some insects have only a type I CRY (*Drosophila*), some have only a type II CRY (the honeybee, *Apis mellifera*), and some have both (the monarch butterfly, *Danaus plexippus*). We hypothesized that an evolving interface for direct interaction between CRY and core clock components might underlie this evolutionary divergence. Our finding that the secondary pocket is an interface for binding between CLOCK and CRY led us to look carefully at other residues in the secondary pocket identified in the SCA. In addition to the "lower" helical boundary of the pocket discussed above (α4), a subset of residues was identified in a flexible loop forming the "upper" boundary of the pocket (located between β2 and α2 in CRY1). An alignment of the α4 helix residues and the "upper" loop residues from various vertebrate and insect sequences reveals that the α4 helix is largely conserved, but the loop is highly divergent between the two groups (Figure 3-4A and Figure 3-4—figure supplement 1). Moreover, a conserved glycine in the type II vertebrate-like CRY population (position 106 in CRY1) is a conserved tryptophan in the type I CRY population (Figures 3-4A, Figure 3-4—figure supplement 1). Structural comparison between CRY2 (for which the "upper" loop has been solved) and dCRY reveals that this tryptophan protrudes into and fills much of the cavity of the secondary pocket in dCRY (Figure 3-4B). Furthermore, in the absence of a ligand, a more structured "upper" loop in CRY2 causes the pocket to adopt an open and exposed conformation suitable for a potential protein-protein interaction. All type II CRY proteins

examined retain the sequence features of the "upper" and "lower" boundaries of this pocket, suggesting that it might be a major site of differentiation between type I and II proteins.

We tested the hypothesis that differences at these two interfaces partially underlie the more direct role of CRY in vertebrate clocks. Single amino acid substitutions in CRY1 of the divergent residues at positions identified in the SCA (P39G, F41S, G106W) caused either weakly repressive, short period rescues (P39G) or arrhythmicity (F41S, G106W) (Figures 3-4C and 3-4D). Substitution at a convergent residue (D38A) from the SCA network also resulted in no rescue (Figure 3-4C). All of these substitutions resulted in attenuated interactions with CLOCK and BMAL1, though P39G retains the strongest interaction (Figure 3-4E and Figure 3-4—figure supplement 2). Interactions with PER2 were mostly intact, though there was a trend toward a weakened interaction between PER2 and the F41S and G106W substitutions (Figure 3-4E and Figure 3-4—figure supplement 2). Taken together, these data suggest that the secondary pocket of type II CRYs has evolved a more accessible conformation through which CRY interacts with the CLOCK/BMAL1 heterodimer. This interaction defines a critical feature of vertebrate-like clocks and likely underlies, at least in part, the direct role of CRY in vertebrate-like clocks.

The secondary pocket interface can tune periodicity and repressivity

In addition to the residues on the "upper" and "lower" boundaries of the secondary pocket, multiple residues in the "upper right corner" of the pocket were identified in our SCA network (Figure 3-5A). We hypothesized that they might also play a role in binding to CLOCK and BMAL1, so we mutated the residues to alanines and tested them in our rescue

assay. All three mutant CRY1s (R51A, E382A and F257A) rescued rhythms with dramatically shortened periods compared to the wild-type rescue (Figures 3-5B, 3-5C, and 3-5D). Moreover, the E382A and F257A rescues had higher amplitude rhythms and were less repressive overall as shown by their increased luminescence signal (Figure 3-5B). Acceleration and deceleration of the clock have consistently been associated with changes in the degradation rate of the repressors, CRY and PER (Gao et al., 2013; Meng et al., 2008; Siepka et al., 2007; Yoo et al., 2013). In order to test whether substitutions at these residues were causing a change in the degradation rate of CRY, we expressed a CRY1::LUC fusion protein in HEK-293A cells and treated with cycloheximide to block new protein synthesis, monitoring the decay in luminescence as a reporter for protein degradation. Introducing a mutation that stabilizes CRY1 (S588D) (Gao et al., 2013) led to deceleration of the rate of luminescence signal decay (Figure 3-5—figure supplement 1A and 1B). This finding is consistent with a recent report in which the half-lives of 36 CRY1 mutants, including S588D, were determined using a similar construct that faithfully reported a wide range of degradation rates (Ode et al., 2017). However, none of the short period pocket mutants (R51A, F257A, E382A) affected the rate of decay (Figures 3-5E and 3-5F).

We hypothesized that these period-shortening pocket mutations modulate the affinity between the CLOCK/BMAL1 heterodimer and CRY1. Though there was a trend towards weaker interaction, co-immunoprecitation of CLOCK and BMAL1 in the presence of overexpressed PER2 was not significantly affected (Figure 3-5G and Figure 3-5—figure supplement 1C) and none of the mutants showed significant changes in PER2-binding when overexpressed only with PER2 (Figure 3-5H and Figure 3-5—figure supplement 1D).

However, when overexpressed with just CLOCK and BMAL1, some of these mutants showed a significant decrease in interaction with CLOCK and BMAL1 in proportion to overall shortening of the rescue period (Figure 3-5I and Figure 3-5—figure supplement 1E). These results imply that mutations in the secondary pocket can modulate the affinity between CRY1 and the CLOCK/BMAL1 heterodimer, which in turn tunes the period of the oscillation. This effect is most obvious without PER2, suggesting that the shortened period in these mutants might stem from an increasing requirement of PER co-expression to stabilize the repressive interaction of CRY with CLOCK and BMAL1.

Subtle divergence in the secondary pocket underlies the dramatic periodicity differences in CRY1- and CRY2-driven rhythms

One of the outstanding mysteries in circadian biology is the profound difference in periodicity of free-running rhythms between Cry1-/- and Cry2-/- mice. Cry1-/- mice have short endogenous periods (~22.5 h) and Cry2-/- mice have long endogenous periods (~24.6 h) (van der Horst et al., 1999; Vitaterna et al., 1999). Moreover, CRY1 functions as a stronger repressor of CLOCK/BMAL1-mediated transcriptional activation (Griffin et al., 1999; Khan et al., 2012). Using the Cry1 promoter to drive Cry2 expression in Cry1-/-/Cry2-/- mouse embryonic fibroblasts, Khan et al. reported that they were unable to rescue rhythms with WT Cry2. However, if they swapped residues 313-426 of CRY1 for the homologous residues in CRY2, this chimeric CRY2 was able to rescue rhythms. This experiment suggests that some set of differential residues within this domain is likely to play a critical role in driving repression of CLOCK/BMAL1-mediated transcriptional activation. There are only 12

residues that are different between CRY1 and CRY2 in this 113 amino acid domain. Intriguingly, 5 of those residues (E376/S394, M378/V396, K379/R397, E382/D400, and W390/F408) are located superficially at the "right" boundary of the secondary pocket (Figure 3-6A) and the amino acid changes are conservative. Moreover, 4 out of 5 of the residues were identified as part of the SCA network (E376/S394, M378/V396, E382/D400, and W390/F408). Given our finding that substitutions in this region of CRY1 can cause substantial shortening of the period of the circadian oscillation, we hypothesized that several subtle changes at this interface might underlie the shorter period in clocks driven only by CRY2. Converting any of these five residues in CRY1 individually to its CRY2 homolog had a minimal effect on the periodicity of the rescue (Figure 3-6—figure supplement 1A and 1B) with the greatest effect observed in E376S and W390F rescues, which were accelerated by roughly an hour per day (Figure 3-6—figure supplement 1B). However, combinatorial conversion of any of these residues to their CRY2 homologs led to increasingly short rescue periods, including the three residues that had no effect at the individual level (M378V/K379R/E382D, i.e., CRY1 3m) (Figures 3-6B and 3-6C). Mutating all five residues in concert (CRY1 5m) led to the most substantial shortening compared to WT (24.4 h vs. 26.9 h) (Figure 3-6C). Examination of the residues contributing to the surface area of the pocket shows that in addition to the five residues identified above, there are only two other divergent residues: G43/A61 and N46/S64 (Figure 3-6A). Mutation of both residues also led to an accelerated rescue rhythm compared to WT CRY1 (Figure 3-6—figure supplement 1C and 1D). Furthermore, combinatorial mutation of these residues also resulted in a corresponding weaker repression of CLOCK/BMAL1 transcriptional activation as

demonstrated by the higher overall luminescence in these rescues (Figure 3-6—figure supplement 1C).

Cry2 can rescue rhythms with short periods consistent with in vivo data

Khan et al. demonstrated that even under the control of the *Cry1* promoter, *Cry2* was unable to rescue rhythms in *Cry*-deficient cells. We reasoned that if the seven residues at this pocket differentiate CRY1 and CRY2 at a functional level, then mutation of all seven together in CRY1 should cause it to fail to rescue rhythms. As a control for this experiment, full-length, WT *Cry2* was cloned into the *Cry1* rescue vector. However, we found that both the seven-residue pocket mutant (CRY1 7m) and CRY2 were competent to rescue rhythms (Figure 3-6D). Moreover, both CRY1 7m and CRY2 produced rhythms with significantly shortened periods (23.48 h and 22.97 h, respectively) compared to WT CRY1 (27.25 h) (Figure 3-6E), consistent with in vivo data from $Cry1^{-/-}$ mice, which also have short periods of ~22.5 h (van der Horst et al., 1999; Vitaterna et al., 1999). Compared to WT CRY1, both CRY2 and CRY1 7m were substantially derepressed and had higher amplitude oscillations. These results suggest that subtle divergence at this interface is a major driver of period differences in CRY1- or CRY2-driven rhythms. To test this hypothesis further, all seven residues in CRY2 were converted to their CRY1 homologs (denoted CRY2 7m). The effect of these mutations was again additive (Figure 3-6—figure supplement 1E and 1F), and resulted in a significant lengthening of the period (24.22 h) and an increase in repression compared to WT CRY2 (Figures 3-6D and 3-6E), though these effects were more modest than the CRY1 7m mutant.

Given that we were using the same cell line as Khan et al. and a nearly identical *Cry2* rescue construct, we were surprised to see a strong rescue by CRY2. One notable difference in our two methodologies is the synchronization agent, which was either 10 μM forskolin (Fsk) in Khan et al. or 0.1 μM dexamethasone (Dex) in our experiments. Both Fsk and Dex have been shown to synchronize dispersed fibroblast cultures through separate signaling pathways (adenylate cyclase and glucocorticoid signaling respectively) (Balsalobre et al., 2000a; Balsalobre et al., 2000b). We found that Dex treatment consistently resulted in high amplitude *Cry2* rescues, but rescues with *Cry2* were highly variable following Fsk treatment. Fsk was sometimes able to induce rhythms in *Cry2* rescues, especially at higher concentrations (100 μM), but always with rapid damping dynamics compared to Dex-synchronized rescues (data not shown). Ultimately, we could not clearly determine the reason underlying diverging reports of *Cry2*'s capacity to rescue rhythms (Khan et al., 2012; Li et al., 2016; Patke et al., 2017).

To determine whether the pocket architecture affects the intrinsic stability of CRY1 and CRY2, we measured the half-life of CRY1, CRY2, CRY1 7m, and CRY2 7m and found that, consistent with a previous report, CRY2 is more stable than CRY1 (Li et al., 2016) (Figures 3-6F and 3-6G). However, neither CRY1 7m nor CRY2 7m differed significantly from CRY1 or CRY2, respectively, in half-life, suggesting that the period differences seen in the rescue assays were not due to changes in stability. Moreover, we found no correlation between half-life and period for any of the mutant residues in the secondary pocket that rescue rhythms (Figure 3-6H). We also performed rescues with *Cry1*, *Cry2*, *Cry1 7m*, and *Cry2 7m* over a broad range of doses (25 ng to 1200 ng of rescue vector) and found a small

effect of dose on period length (Figure 3-6—figure supplement 2). However, the results consistently show a difference between *Cry1* and the other rescues at all doses, suggesting that differences in DNA dosage are not driving the divergent periods.

PER2 facilitates stable CRY2:CLOCK:BMAL1 complexes

Since some of the mutations in the secondary pocket caused dramatic acceleration of the clock by attenuating the interaction between CRY1 and CLOCK/BMAL1 (Figure 3-5I), we tested whether this was also the case for the short period rhythms in the CRY2 rescues. When co-expressed with PER2, both CRY1 and CRY2 had a strong interaction with CLOCK and BMAL1, with no significant differences between the two (Figure 3-7A and Figure 3-7—figure supplement 1A). CRY2 7m had a similarly robust interaction, but CRY1 7m demonstrated an attenuated interaction with CLOCK. There were no clear differences in interaction with PER2 when co-IPed with or without overexpressed CLOCK and BMAL1 (Figure 3-7A, 3-7B, and Figure 3-7—figure supplement 1A and 1B). However, when co-IPs were performed without overexpressed PER2, both CRY1 7m and CRY2 displayed a weakened interaction with CLOCK and BMAL1 compared to WT CRY1 (Figure 3-7C and Figure 3-7—figure supplement 1C). In contrast, CRY2 7m had a significantly stronger interaction with CLOCK and BMAL1 compared to CRY1 7m and CRY2 and a significantly stronger interaction with BMAL1 compared to CRY1 (Figure 3-7C and Figure 3-7—figure supplement 1C). Together these data suggest that in the context of other structural features, a CRY1-like pocket strengthens the interaction with CLOCK and BMAL1 when PER2 is not

present. However, the presence of PER2 equalizes the interaction between CLOCK/BMAL1 and CRY1, CRY2, and CRY2 7m.

Based on several recent reports characterizing the interaction between CRY and CLOCK (Michael et al., 2017) and CRY and BMAL1 (Xu et al., 2015), it is likely that the secondary pocket is gating the interaction between the heterodimer primarily through a direct interaction with CLOCK. To test whether CRY1 has a stronger interaction than CRY2 with CLOCK in a cellular milieu, we performed a reciprocal two-color bimolecular fluorescence complementation (BiFC) competition assay (Figure 3-7D). In this assay, a C-terminal Cerulean (CerC) fragment can interact with either a N-terminal Venus (VenN) or N-terminal Cerulean (CerN) fragment to produce fluorescence in the Venus or Cerulean range respectively. A CerC-CLOCK construct containing the PAS A and PAS B domains was expressed with VenN- and CerN-tagged CRYs and we found that CRY1, regardless of its tag, interacted with CLOCK more strongly than CRY2 (Figures 3-7E and 3-7F), which suggests that the interactions seen in our co-IPs are relevant *in vivo*. These data strongly support the idea that the seven unique residues at the secondary pocket of CRY1 and CRY2 are critical for gating a strong physical interaction with CLOCK and BMAL1. They also suggest that expression of PER restricts the phase of repression for CRY2 by facilitating the formation of a stable repressive complex, while CRY1 is able to maintain a repressive complex even as PER levels decrease.

Both the CRY1 pocket architecture and tail are necessary for longer period rescues

Converting CRY1's secondary pocket to a CRY2-like architecture was sufficient to diminish its interaction with CLOCK and BMAL1 and accelerate the clock speed by four hours. However, despite greater gains in interaction with CLOCK and BMAL1, CRY2 7m had only a modest period lengthening effect compared to WT CRY2. The major region of structural divergence between CRY1 and CRY2 is the tail – a highly disordered region with no similarity between the two CRYs. Given that the secondary pocket does not fully account for periodicity differences, we hypothesized that the tail might play an additional role in determining periodicity. To test this hypothesis, we generated chimeric CRY constructs in which either the secondary pocket (CRY1 7m, CRY2 7m) or the tail residues (CRY1 C2T, CRY2 C1T) were swapped (Figure 3-8A). All four constructs generated rescues with intermittent periods (CRY2 C1T: 24.46 h, CRY1 7m: 23.47 h, CRY1 C2T: 24.02 h, CRY2 7m: 24.13 h) between WT CRY1 (26.61 h) and CRY2 (22.89 h) (Figure 3-8B), suggesting that neither the tail nor pocket is sufficient to fully recapitulate the periodicity phenotype of either WT CRY. However, chimeras in which both the pocket and tail were exchanged (Figure 3-8C) were able to rescue rhythms with period and repression characteristics very similar to WT rescues (Figure 3-8D and 3-8E). CRY1 7m C2T, which has both CRY2's pocket and tail, rescued rhythms with significantly shorter period (21.78 h) than WT CRY2 (22.89 h) (Figure 3-8E). In the case of CRY2 7m C1T, which has both CRY1's pocket and tail, the period (26.20 h) was indistinguishable from WT CRY1 (26.61 h) (Figure 3-8E).

Ultimately, these data suggest that both the tail and the pocket contribute to the periodicity of CRYs and both are required to fully capture native period characteristics.

Mapping phenotype to structure

Understanding how CRY's structure informs its activity ultimately requires detailed mapping of structural space in a phenotypic domain. In the course of this work, we mutated 80 residues in CRY1 and tested the mutants in our rescue assay (Table 1). Residues and mutations were chosen based on a number of different factors: some residues were chosen during various iterations of the SCA, some were designed to mimic homologous residues in type I CRYs, some were identified in a previous mutagenesis screen, and a final set came from a previous structure-based collaboration. In general, we chose an alanine mutation where possible. In some cases, mutations were dictated by the mutation discovered in the mutagenesis screen, a desire to mimic a phosphorylation state, or by a desire to disrupt a charged or hydrophobic interface. We present these data here as a resource for the circadian biology community. 102 individual WT rescues run concurrently with the mutants were averaged (mean ± SD: 27.55 ± 0.77 h) and mutants with an average period greater than one standard deviation from WT were sorted into one of three groups: short period rescues (purple), long period rescues (pink), and failure to rescue (blue), while mutants with an average period less than one standard deviation were deemed to have no effect (gray). Mapping the short, long, and failure groups on to CRY1's structure reveals that disruption of the right side of the secondary pocket always results in period shortening (Figure 3-9). Mutations on the "left side and bottom" of the pocket usually cause a failure to rescue,

suggesting that protein-protein contacts in this region of the pocket are vital for normal function. Additionally, a number of residues on the C-terminal α-helix and the left side of the FAD-binding pocket are responsible for long period rescues, while a group of residues on the right side of this pocket result in short periods. One likely possibility is that these groups of residues modulate binding to PER and FBXL3 resulting in changes in stability. Finally, there are other regions of interest with less obvious mechanistic roles both on the underside and top of CRY. Mutation of the residues on the underside largely results in period lengthening, while mutation of the cluster of residues from G212 to L218 leads to either arrhythmicity or long periods. Ultimately, this mapping suggests other potential interfaces on CRY that are as yet uncharacterized.

Discussion

CRY's evolution into a role as a direct repressor of CLOCK and BMAL1-mediated transcriptional activation suggests that specific structural changes have resulted in critical functional advantages. Much focus has been placed on the FAD-binding pocket of this family and significant work has emphasized the role of FAD in the function of plant CRYs and type I animal CRYs. Moreover, structural work from the past few years highlights the extent to which this pocket has been repurposed for protein-protein interactions with FBXL3 and PER2 (Nangle et al., 2014; Schmalen et al., 2014; Xing et al., 2013). Here we describe how a hotspot of evolutionary changes in the CPF lineage, the secondary pocket, has also been repurposed for a crucial protein-protein interaction with the CLOCK/BMAL1 heterodimer. Previous data demonstrated that CRY's C-terminal α-helix and tail form a functionally

important, high affinity (~1-10 μM) complex with BMAL1's TAD (Czarna et al., 2013; Czarna et al., 2011; Xu et al., 2015). Additionally, mutations on CLOCK's HI loop cause a complete abrogation of binding between CLOCK and CRY (Huang et al., 2012; Sato et al., 2006; Xu et al., 2015) and a recent report suggests that CLOCK's PAS B domain, which contains the HI loop, interacts directly with the secondary pocket (Michael et al., 2017). Taken together with our results, these data suggest a model in which a high affinity interaction between CLOCK's HI loop and CRY at the secondary pocket brings CRY into proximity with the BMAL1 TAD to create a sustained repressive complex through allostery. Tuning the affinity between CRY's C-terminal α-helix and the BMAL1 TAD was shown to have a substantial effect on the period of the oscillation (Xu et al., 2015). Similarly, we found that mutations in the secondary pocket that strengthen the interaction with CLOCK and BMAL1 lengthen the period of the oscillation and mutations that weaken the interaction predominantly shorten the period. Critically, the effects on period were independent of CRY's degradation rate. Historically, spontaneous and induced mutations in fly (Kloss et al., 1998; Li and Rosbash, 2013; Martinek et al., 2001; Price et al., 1998) and mammalian (Busino et al., 2007; Godinho et al., 2007; Hirano et al., 2016; Hirano et al., 2013; Lowrey et al., 2000; Meng et al., 2008; Ralph and Menaker, 1988; Siepka et al., 2007; Xu et al., 2005; Yoo et al., 2013) genomes have helped to identify clock components that affect periodicity primarily by modulating the rate of decay of repressors. Our work demonstrates that the affinity of the core clock proteins for one another plays an important orthogonal role in determining periodicity.

The structural underpinning of striking phenotypic differences in *Cry1*$^{-/-}$ and *Cry2*$^{-/-}$ mice has long been mysterious. At a behavioral level, deletion of one or the other leads to a dramatically different output, but molecular analysis suggests a similar functional role. Amidst high sequence identity and similarity between the two proteins, no obvious structural differences present themselves as possible drivers of functional dissimilitude beyond the divergent tails. The data presented here strongly suggest that the functionality of these proteins stems in large part from the accumulation of subtle structural differences at the secondary pocket, which reduce the strength of the interaction between CRY2 and the CLOCK/BMAL1 heterodimer. Strikingly, co-expression of mPER2 markedly improved the strength of the interaction between both CRY2 and the CRY1 7m mutant and the CLOCK/BMAL1 heterodimer. In concert with previous work demonstrating concurrent temporal occupancy for CRY2, PER1, and PER2 in chromatin association (Koike et al., 2012), our data suggest that CRY2 requires either PER1 or PER2 to form a stable repressive complex with CLOCK and BMAL1, restricting its repressive phase to the phase of PER expression. CRY1, due to its stronger physical interaction with CLOCK/BMAL1, is capable of forming a stable complex without a PER (Figure 3-10). How PER proteins mediate this stabilizing interaction is still unknown and a question for further exploration. In principle, this idea is similar to an idea from studies of circadian rhythms in *Neurospora crassa*, which posited that overall protein levels of the repressor FRQ do not determine period, but the levels of functional FRQ were highly determinant of period (Larrondo et al., 2015). Likewise, if CRY2 is unable to bind CLOCK and BMAL1 without PER, then in the absence of PER, CLOCK and BMAL1 are functionally blind to CRY2's presence.

One potential criticism of this model is that it discounts the dose response experiments in Figure 3-6—figure supplement 2, which suggest that higher concentrations of CRY1 and CRY2 lead to shorter periods. In seeming contradiction, we suggest that a higher concentration of CRY1 would maintain a repressive state longer and delay the start of a new cycle of transcription, while higher levels of CRY2 would be irrelevant as PER2 is degraded. However, it is difficult to interpret the results of the dose response experiments due to the fact that CRY will inhibit its own transcription. As a result, there is likely a floor and a ceiling for CRY expression in this system and increasing amounts of DNA merely change the dynamics of CRY expression, altering the rate at which either CRY reaches its ceiling rather than the ceiling itself.

Ukai-Tadenuma et al. demonstrated that a *ROR*-binding element (RRE) in an intron of the *mCry1* gene body is necessary for the delayed repressive phase of CRY1 (Ukai-Tadenuma et al., 2011). A recent report by Edwards and colleagues, in contrast, showed that a small fragment of the *mCry1* promoter not including the RRE was sufficient to drive rhythmic expression of either CRY1 or CRY2 in brain slices containing the suprachiasmatic nucleus (SCN), a brain region that functions as a master oscillator (Edwards et al., 2016). Moreover, they found that *Cry1* and *Cry2* were individually sufficient for rescue in *Cry1*$^{-/-}$/ *Cry2*$^{-/-}$ *SCN* and drove rhythmic output characteristic of *Cry2*$^{-/-}$ (long periods) or *Cry1*$^{-/-}$ (short periods) animals respectively. Our results, in concert with these two reports, suggest that more work is necessary to understand the contributions of transcription, protein-protein interaction dynamics, degradation, and intercellular coupling to periodicity in CRY1- and

CRY2-driven rhythms. However, it is likely that each of these characteristics of the clock function as nodes for regulation of periodicity.

Our rescue data demonstrate that divergence at the secondary pocket drives a great deal of the repressive strength and periodicity differences between the two CRYs. However, it is also clear from rescues with CRY2 7m that this divergent structural feature cannot fully explain the differences in periodicity. The CRY1 tail and secondary pocket are together necessary and sufficient to fully convert CRY2's rescue profile to a CRY1-like profile. We have developed a mechanistic understanding of the secondary pocket's contribution to periodicity, but the mechanism underlying the tail's contribution is still unknown. It is, however, interesting to view the results of the chimera rescues in an evolutionary context. Exchanging either the tail or secondary pocket between the two CRYs invariably resulted in near 24 h rhythms, suggesting that in organisms with a single repressive CRY, such as the honeybee, one or the other of these features, but not both, is likely to remain intact. Given the low level of conservation in C-terminal tails, it is tempting to speculate that the delay characteristic of the CRY1 tail is in fact a gain of function mutation specific to organisms with two repressive CRYs. The nature of this function is a fertile area for future research.

Materials and Methods

Resources

Key resources used in this study are shown in Appendix E along with manufacturer details (where relevant). Primers used in this study are shown in Appendices A through D.

Experimental Model and Subject Details

Cry1$^{-/-}$*/Cry2*$^{-/-}$ mouse embryonic fibroblasts and HEK-293A were grown in Dulbecco's Modified Eagle Medium (DMEM) containing 10% Fetal Bovine Serum and 1x Pen/Strep antibiotics at 37°C under 5% CO_2. LumiCycle recording medium was prepared from powdered DMEM without phenol red containing 4.5 g/L glucose and supplemented with 10 mM HEPES pH 7.2, 100 μM luciferin, 1 mM sodium pyruvate, 0.035% sodium bicarbonate, 10% FBS, 1x Pen/Strep antibiotics, and 2 mM L-glutamine. LumiCycle recordings were performed at 37°C.

Statistical Coupling Analysis (SCA)

Approximately ten thousand CRY and PHL sequences were collected from NCBI on March 30, 2016 using the full-length mCRY1 protein sequence (GenBank Accession ID: AAH85499.1) as a search sequence for a PSI-BLAST. PSI-BLAST parameters were adjusted from default to include an Expect Threshold of 0.01, a PSI-BLAST Threshold of 0.005, and a minimum sequence identity of 20%. PSI-BLAST was performed iteratively for two rounds before the sequences were downloaded. The sequences were initially filtered by size using a custom python script to remove sequences smaller than 400 or larger than 800 residues. Remaining sequences were subjected to an initial alignment using the alignment tool MUSCLE (Edgar, 2004) locally for two iterations. Extraneous header information was removed using a custom python script before performing a secondary alignment using Promals3D with six additional structure sequences (Cyclobutane Pyrimidine Dimer (CPD) PHL from *E. coli*, CPD PHL from *A. nidulans*, 6-4 PHL from *A. thaliana*, CRY from *D.*

melanogaster, and CRY1 and CRY2 from *M. musculus* (Czarna et al., 2013; Hitomi et al., 2009; Park et al., 1995; Pei et al., 2008; Tamada et al., 1997; Xing et al., 2013; Zoltowski et al., 2011). Using a custom python script, GI numbers were collected from each header in a separate file for use in the annotation step of the SCA. SCA calculations were performed using the pySCA toolbox as described (Rivoire et al., 2016). The annotation step was performed through NCBI using the GI numbers on April 17, 2016. The initial alignment of 9,719 sequences consisted of 4,344 independent positions. The alignment underwent preprocessing during which highly gapped positions were removed. After removing highly gapped *positions*, remaining highly gapped *sequences* were removed using a set cutoff. Sequences with too great of a fractional identity to the reference sequence were also removed. Finally, each sequence was weighted based on the number of sequences with an identity above 80% to the given sequence. This final weighting step allows an effective number of sequences (M') to be computed based on the remaining number of actual sequences (M). After all of the preprocessing steps, the final alignment contained 3,619 sequences representing 2,425 effective sequences composed of 460 positions. Critically, an alignment should be large and diverse enough to give reasonable estimates of amino acid frequencies. 2,425 effective sequences is well above the suggested minimum of 100 effective sequences needed to obtain a reasonable estimate (Rivoire et al., 2016). During these processing steps, default parameters were used and residues were mapped to the CRY2 structure (PDB: 4I6E) (Xing et al., 2013). Following initial calculation steps, the workflow was performed in an ipython notebook.

The alignment comprises a heterogeneous group of sequences with substantial sequence similarity. The content of the alignment is 2,841 bacterial sequences, 147 archaeal sequences, and 626 eukaryotic sequences.

Position specific conservation values (D_i) were calculated identifying a region from roughly position 300 to 400 of the alignment that has the highest level of positional conservation (Figure 3-1C). However, there are clearly other regions of high conservation, including the α/β domain of the PHR (~1-150) and two local maxima between 200 and 300. Pairwise conservation values between each position and all other positions were calculated as a measure of the frequency of coevolution between all pairs of amino acids in the alignment. The weighted correlation matrix (ordered here by primary structure) for this alignment suggests that what we see at the level of positional conservation is similar to what we see by looking at pairwise correlations (Figure 3-1D). Finally, in order to identify distinct, independent correlated groups of positions within the protein, spectral decomposition was performed on the matrix of pairwise correlations and 21 significant independent components (ICs) were identified. The ultimate aim of SCA is to break a protein family into maximally independent coevolving units and then ascertain the architecture of how those units are connected. However, no clear cut divisions in the ICs presented themselves, so all of the residues were grouped into a single network shown in the matrix in Figure 3-1E and the table in Figure 3-1—table supplement 1.

Site-Directed Mutagenesis

Mutagenesis was performed using both the QuikChange II XL kit and, with a few modifications, the Q5 Site-Directed Mutagenesis kit. Manufacturer instructions were followed for QuikChange mutagenesis. See Appendix A for QuikChange primers. For Q5 Site-Directed Mutagenesis, primers were designed using the NEBaseChanger tool (http://nebasechanger.neb.com/). Template DNA was mixed with 2X Q5 PCR Master Mix and the primers shown in Appendix B before being subjected to polymerase chain reaction (PCR). Following PCR, 1 μL of each PCR product was combined with 2X Quick Ligation buffer and ligase, along with 1 μL of T4 Polynucleotide Kinase, and 1 μL of DpnI in a total of 10 μL. The ligation reaction was incubated at room temperature for five minutes and 5 μL of product were used to transform DH5α competent cells. Colonies were selected for culturing and miniprep, and mutations were verified by Sanger sequencing.

Gibson Assembly Cloning

CRY tail chimera rescue vectors were generated by Gibson Assembly cloning using NEBuilder HiFi DNA Assembly kit. Briefly, the rescue vector containing *Cry1*, *Cry2*, *Cry1 7m*, or *Cry2 7m* was linearized by PCR with primers, which also removed the coding sequence for residues 499-606 of *Cry1* and *Cry1 7m* or residues 517-593 of *Cry2* and *Cry2 7m*. The C-terminal Myc tag was left intact. The coding sequences for the tail regions of *Cry1* (residues 499-606) and *Cry2* (residues 517-593) were amplified by PCR using primers that would generate overlaps between the amplified tail product and the linearized target vectors. PCR products were purified using the QIAquick PCR Purification kit and combined

with inserts and linearized target vectors in a 2:1 molar ratio. These combined products were then treated with NEBuilder HiFi DNA Assembly master mix containing an exonuclease, DNA polymerase, and DNA ligase to induce assembly of the final vector. This solution was incubated at 50°C for 15 minutes and the products were used to transform DH5α competent cells. Colonies were selected for culturing and miniprep, and insertions were verified by Sanger sequencing. See Appendix D for primers used in Gibson Assembly Cloning.

Real Time Bioluminescence Rescue Assays

Real-time circadian rescue assays were performed essentially as described (Ukai-Tadenuma et al., 2011). 4 x 10^5 *Cry1*$^{-/-}$/*Cry2*$^{-/-}$ mouse embryonic fibroblasts were plated in 35 mm tissue culture dishes and transfected the same day with 4 μg of a luciferase reporter (pGL3-P(*Per2*)-Luc) (Ueda et al., 2002) and 150 ng of a *Cryptochrome* rescue vector (pMU2-P(*Cry1*)-(intron336)-Cry-Myc, modified with a C-terminal MYC tag) (Ukai-Tadenuma et al., 2011) using FuGENE 6. 72 h after transfection, the cells were synchronized by exchanging growth medium for growth medium supplemented with 0.1 μM dexamethasone and returned to the incubator for 2 h. The medium was then replaced by LumiCycle recording medium and the plates were sealed with vacuum grease and cover glass and transferred to the LumiCycle. Bioluminescence monitoring was performed using a LumiCycle to record from each dish continuously for 70 s every 10 min using a photomultiplier tube at 37°C. Rescue results were processed using the LumiCycle Analysis software package. The first 10 h of recording were discarded and period, amplitude, phase, and damping rate were calculated using a damped sine wave based on a running average fit

for each plate of cells. Rescues were considered arrhythmic if the goodness-of-fit for the damped sine wave was less than 80%. Subsequent data were corrected for background noise in each photomultiplier tube channel, which was measured by monitoring an untransfected plate of cells for 24 hours and averaging the signal. All CRY1 and CRY2 mutants were run with WT CRY1 as an internal control. In some cases, multiple experiments were combined in the data shown if there were positive internal controls for each dataset. Rescues were excluded only in cases where the transfection did not work, which was obvious based on both a very weak or non-existent luminescence signal and the lack of induction of luminescence shortly after synchronization. Appropriate replicate size was determined empirically from extensive use of these assays in previous work (Nangle et al., 2014).

Vector Construction

Large sequences were cloned into existing vectors through megaprimer mutagenesis. Briefly, the insert was copied from a source vector by PCR (using PfuUltra II Fusion HS DNA polymerase with primers containing roughly 30 bp of overlap in either direction with the insertion site in the target vector and 30bp of overlap with the insert. Following primary PCR, PCR products were purified using the QIAquick kit, and 400 ng of purified product used as a megaprimer for a secondary PCR with the target vector serving as a template. PCR products were treated with DpnI for several hours, then DH5α competent cells were transformed with 5 μL. Colonies were selected for culturing and miniprep and insertions were verified by Sanger sequencing. *P. pyralis luciferase* was fused directly to the C-terminus of *Cry1* and *Cry2* in the pCMV-Tag3C-Myc vector. Full-length *Cry2* was inserted

at the exact location in pMU2-P(*Cry1*)-(intron336)-*Myc* where *Cry1* was deleted. See Appendix C for primers used in megaprimer mutagenesis.

Immunoprecipitation

HEK-293A cells were seeded in 6-well tissue culture plates at a density of 4 x 10^5 cells per well. Cells were transfected the same day with FuGENE 6. The following constructs were used for all transfections: p3X-FLAG-CMV-10-*mBmal1*, p3X-FLAG-CMV-10-*mClock*, pCMV-Myc-*Cry1* (McCarthy et al., 2009), pCMV-Myc-*Cry2* (McCarthy et al., 2009), and pcDNA3.1-*mPer2*-V5 (Lee et al., 2004). For immunoprecipitations involving all four clock components, cells were transfected with 45 ng of *mBmal1*, 1.5 μg of *mClock*, 600 ng of *mPer2*, and 150 ng of either *Cry1*, *Cry2*, or mutants thereof, in a total of 2.295 μg of DNA. Empty vector (pcDNA3.1-A) was used to even out DNA cocktails. For immunoprecipitations of only BMAL1, CLOCK, and CRY, cells were transfected with 45 ng of *mBmal1*, 1.5 μg of *mClock*, and 150 ng of *Cry* plasmid in a total of 1.695 μg of DNA. Finally, for immunoprecipitations of PER and CRY alone, cells were transfected with 600 ng of *mPer2* or 300 ng of *Cry* in a total of 900 ng of DNA. After 48 h, cells were lysed in 200 μL of TGED buffer (50 mM Tris–HCl pH 7.5, 100 mM NaCl, 5% glycerol, 0.5 mM DTT, 0.5% Triton X-100, protease inhibitor (1:50)) for 30 min before a 10 min centrifugation to remove cellular detritus. 10% of the supernatant solution was saved for use as input and the remainder was incubated for 3 h with 40 μL of anti-MYC-conjugated beads to immobilize MYC-CRY. Beads were washed with 1 ml of TGED buffer twice. Protein was released from beads by boiling in 50 μL of SDS sample buffer (26.3 mM Tris-HCl pH 6.8, 4.2% glycerol,

0.84% SDS, 10.5% β-mercaptoethanol, 0.21 mg/mL bromophenol blue) and analyzed by immunoblot using anti-MYC, anti-V5, and anti-FLAG-HRP for CRY, PER2, and CLOCK/BMAL1, respectively. Blots were imaged on radiography film with Clarity ECL Substrate. Appropriate replicate size was determined empirically from extensive use of these assays in previous work (Nangle et al., 2014).

Real-Time Bioluminescence Degradation Assays

HEK-293A cells were plated in 35 mm tissue culture dishes at a density of 4 x 10^5 cells per well. Cells were transfected (FuGENE 6) same day with 500 ng of a *Cry-Luc* fusion construct (pCMV-*Myc-Cry1-Luc* or pCMV-*Myc-Cry1-Luc*) and 200 ng of an EGFP construct (pEGFP) as a transfection control. 48 h after transfection, medium was exchanged for LumiCycle recording medium supplemented with cycloheximide (100 μg/ml). Plates were transferred to the LumiCycle and bioluminescence was monitored from each dish continuously for ~70 s every 10 min using a photomultiplier tube at 37°C. Data were corrected for background noise from the photomultiplier tube as described above. The first 10 h of recording were normalized to the first data point and half-life was determined by nonlinear, one-phase exponential decay analysis.

Alignments

CRY alignments for Figures 3-4 and Figure 3-4—figure supplement 1 were performed with CLC Main Workbench 7 using default settings for the slow alignment mode. Sequences were accessed and downloaded from NCBI.

Bimolecular Fluorescence Complementation

Full-length Venus (Ex515/Em528) and Cerulean (Ex433/Em475) have been described previously (Meyer et al., 2006). Based on published reports (Hu et al., 2002; Hu and Kerppola, 2003), truncated Venus and Cerulean fragments in the pEGFP-C1 (Clontech) backbone were created as CerN (1-155 aa), CerC (156-239 aa), and VenN (1-155 aa) by site-directed mutagenesis PCR as previously reported (Yoo et al., 2013). PCR-amplified *Cry1* and *Cry2* cDNAs were inserted into the NheI and AgeI sites upstream of the coding region of CerN and VenN. Full-length *Clock* cDNA was amplified by PCR with an N-terminal Sac2 site and a C-terminal blunt polymerization end and ligated into Sac2 and Sma1 sites in CerC. Residues 2-88 and 396-855 of *Clock* were deleted from the construct by site-directed mutagenesis.

For BiFC competition experiments, 25 ng H2B-mRFP1 (Li et al., 2007) was mixed with 200 ng CerC-Clock (89-395), 10 ng p3X-Flag-Bmal1, 200 ng of Cry1-VenN or Cry1-CerN, and 200 ng of Cry2-CerN or Cry2-VenN in a total of 735 ng of DNA. 8 x 10^4 HEK-293A cells were plated in each well of a 24-well black Visiplate . On the same day, cells were transfected with FuGENE 6. Plates were washed with PBS once 48-60 hours after transfection, fixed with 4% paraformaldehyde in PBS for 15 min, then immersed in PBS. A control well for background fluorescence was transfected with non-complementary BiFC vectors (200 ng Cry1-VenN, 200 ng Cry2-CerN, 25 ng H2B-mRFP1). Controls for normalization of the competition experiments were transfected with single complementation

pairs (25 ng H2B-RFP1, 200 ng CerC-Clock (89-395), 10 ng p3X-Flag-Bmal1, and 200 ng of Cry2-CerN or Cry2-VenN in a total of 735 ng of DNA).

Fluorescence images were acquired on a Deltavision Personal DV Imaging System equipped with an inverted 10x (for quantification) or 20x (for publication images) 0.45NA UPLFL objective and a Microtiter stage on an Olympus IX71 microscope. Four locations in each well were selected and autofocused with RFP1 fluorescence. Single layer images for quantification or 20-layer Z stacks with 1 mm steps for deconvolution and presentation were scanned in the channel sequence of RFP (Ex575/25; Em632/60), YFP (Ex513/17; Em559/34), and CFP (Ex438/24; Em465/30) filter sets with the Z step first. Image stacks were deconvoluted with the Softworx deconvolution module and maximal intensity Z projections of layers were built.

For quantification of BiFC competition results, original image files were imported to and organized by ImageJ (NIH), and exported image sequences were pushed through a custom pipeline run by Cellprofiler. Briefly, the nuclei were first recognized based on RFP fluorescence, and then inverse-masked with strong aggregates in the Venus and Cerulean channels. Mean Venus and Cerulean intensity values of each masked nucleus were measured. About 40-120 cells were identified and measured in each image, and the average values of cells in one image were obtained for further normalization and statistical analysis. Background intensity values from Venus and Cerulean channels were subtracted from competition experiment intensity values. Background subtracted competition values were then normalized to background subtracted intensity values from single complementation

wells. Four images from each well were averaged and the experiments were replicated three times.

Quantification and Statistical Analysis

Statistical parameters are reported in the Figure Legends and indicated in the Figures where appropriate. Unpaired t-tests with Welch's correction were performed by GraphPad Prism software. Welch's t-test was chosen to compare the period means and half-life means because we do not know whether the various mutant populations have equal variances to the WT protein. Protein half-lives were determined by normalizing each luminescence value of a given sample to the initial luminescence reading, then fitting a one-phase decay curve to the resulting data in GraphPad Prism.

Data and Software Availability

Custom scripts used in processing the SCA data, the alignment used for the SCA, the annotated SCA notebook, and the SCA database file are all available upon request. The custom data pipeline for CellProfiler is available upon request.

Figures

Figure 3-1. Statistical coupling analysis identifies a co-evolving network of residues in the CRY/PHL family.

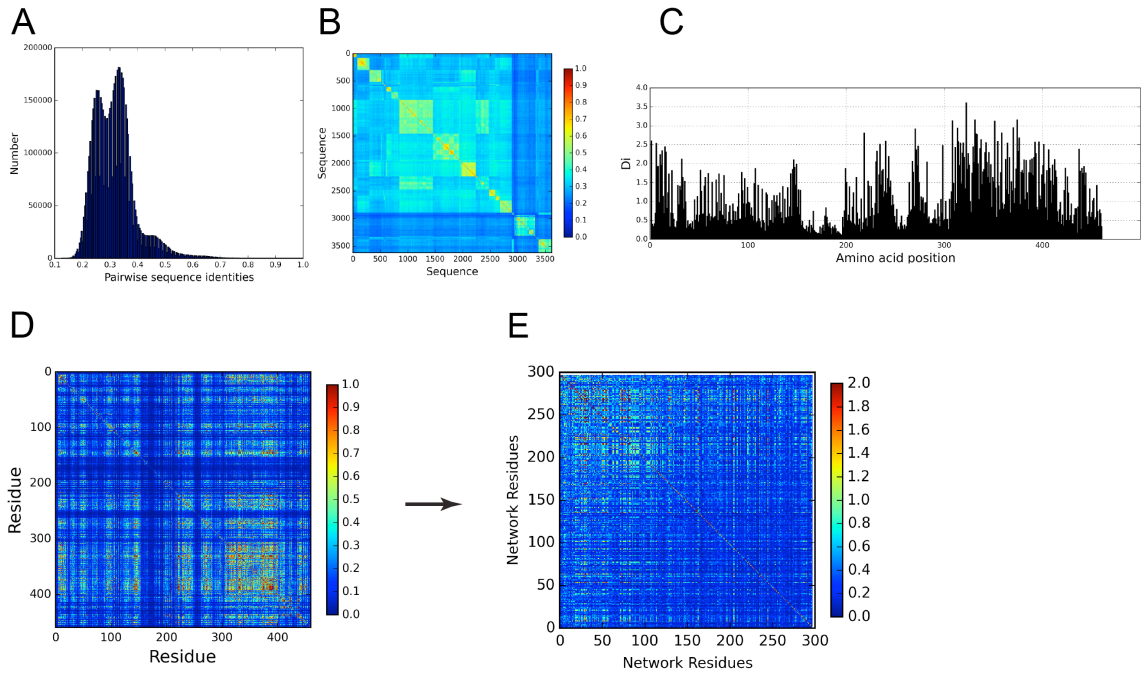

Figure 3-1. Statistical coupling analysis identifies a co-evolving network of residues in the CRY/PHL family.
(**A**) Frequency distribution of pairwise sequence identities for every sequence compared to every sequence. The distribution is trimodal with local maxima at roughly 0.25, 0.33, and 0.45.
(**B**) A sequence similarity matrix shows that the multiple sequence alignment can be grouped into sets of sequences with higher similarity, perhaps representative of specific subsets of CRYs and PHLs.
(**C**) Position specific conservation values (D_i) plotted for each position within the alignment. Positions are numbered by primary structure within the alignment, not as direct positions in mCRY2.
(**D**) Weighted correlation matrix displaying pairwise correlation scores for each position by each position.
(**E**) Shows a submatrix of Figure 3-1D containing selected top-scoring positions from an eigenspectrum decomposition. The matrix displays pairwise correlation scores for each position by each position. The residues selected here represent a network of co-evolving residues in the CPF identified by SCA.

Figure 3-1—table supplement 1. SCA sector positions.

Sector	Assigned Positions
CRY2 residues	26, 27, 28, 29, 30, 31, 32, 33, 34, 35, 36, 37, 38, 39, 41, 42, 43, 49, 51, 52, 53, 54, 55, 56, 57, 59, 60, 63, 66, 68, 69, 70, 71, 72, 73, 74, 75, 76, 77, 79, 80, 84, 89, 90, 91, 93, 94, 96, 98, 101, 103, 105, 106, 108, 110, 111, 114, 115, 116, 117, 118, 119, 120, 121, 122, 123, 124, 127, 128, 131, 132, 135, 139, 140, 142, 144, 145, 147, 150, 152, 153, 154, 155, 156, 158, 161, 163, 164, 166, 167, 168, 169, 170, 171, 172, 173, 174, 183, 187, 213, 215, 220, 228, 230, 231, 232, 235, 238, 239, 242, 258, 260, 261, 265, 266, 267, 268, 269, 270, 271, 272, 273, 274, 275, 276, 277, 278, 279, 280, 281, 282, 283, 284, 298, 304, 305, 307, 308, 310, 311, 312, 313, 314, 315, 316, 317, 318, 320, 321, 322, 328, 329, 333, 334, 336, 337, 338, 340, 341, 345, 347, 348, 349, 350, 351, 352, 353, 354, 355, 356, 357, 358, 359, 360, 361, 362, 363, 364, 365, 366, 368, 369, 370, 371, 372, 373, 374, 375, 376, 377, 378, 379, 380, 381, 382, 383, 384, 385, 387, 388, 389, 390, 391, 392, 393, 394, 396, 398, 399, 400, 401, 402, 403, 404, 405, 406, 407, 408, 409, 410, 411, 412, 413, 414, 415, 416, 417, 418, 419, 420, 421, 422, 423, 424, 425, 426, 427, 428, 429, 430, 431, 432, 433, 434, 435, 436, 437, 439, 440, 441, 442, 444, 446, 447, 448, 449, 450, 451, 452, 453, 454, 455, 457, 458, 460, 461, 462, 463, 465, 466, 468, 469, 481, 483, 484, 485, 487, 488, 489, 490, 491, 492, 494, 495, 497, 498, 499, 501, 502, 503
Homologous CRY1 residues	8, 9, 10, 11, 12, 13, 14, 15, 16, 17, 18, 19, 20, 21, 23, 24, 25, 31, 33, 34, 35, 36, 37, **38**, **39**, **41**, 42, 45, 48, 50, **51**, 52, 53, 54, 55, 56, 57, 58, 59, 61, 62, 66, 71, 72, 73, 75, 76, 78, 80, 83, 85, 87, 88, 90, 92, 93, 96, 97, 98, 99, 100, 101, 102, **103**, 104, **105**, **106**, 109, 110, 113, 114, 117, 121, 122, 124, 126, 127, 129, 132, 134, 135, 136, 137, 138, 140, 143, 145, 146, 148, 149, 150, 151, 152, 153, 154, 155, 156, 165, 169, 195, 197, 202, 210, 212, 213, 214, 217, 220, 221, 224, 240, 242, 243, 247, 248, 249, 250, 251, 252, 253, 254, 255, 256, **257**, 258, 259, 260, 261, 262, 263, 264, 265, 266, 280, 286, 287, 289, 290, 292, 293, 294, 295, 296, 297, 298, 299, 300, 302, 303, 304, 310, 311, 315, 316, 318, 319, 320, 322, 323, 327, 329, 330, 331, 332, 333, 334, 335, 336, 337, 338, 339, 340, 341, 342, 343, 344, 345, 346, 347, 348, 350, 351, 352, 353, 354, 355, 356, 357, 358, 359, 360, 361, 362, 363, 364, 365, 366, 367, 369, 370, 371, 372, 373, 374, 375, **376**, **378**, 380, 381, **382**, 383, 384, 385, 386, 387, 388, 389, **390**, 391, 392, 393, 394, 395, 396, 397, 398,

	399, 400, 401, 402, 403, 404, 405, 406, 407, 408, 409, 410, 411, 412, 413, 414, 415, 416, 417, 418, 419, 421, 422, 423, 424, 426, 428, 429, 430, 431, 432, 433, 434, 435, 436, 437, 439, 440, 442, 443, 444, 445, 447, 448, 450, 451, 463, 465, 466, 467, 469, 470, 471, 472, 473, 474, 476, 477, 479, 480, 481, 483, 484, 485

Figure 3-2. Statistical coupling analysis of the CRY/PHL family suggests an evolving role for the secondary pocket.

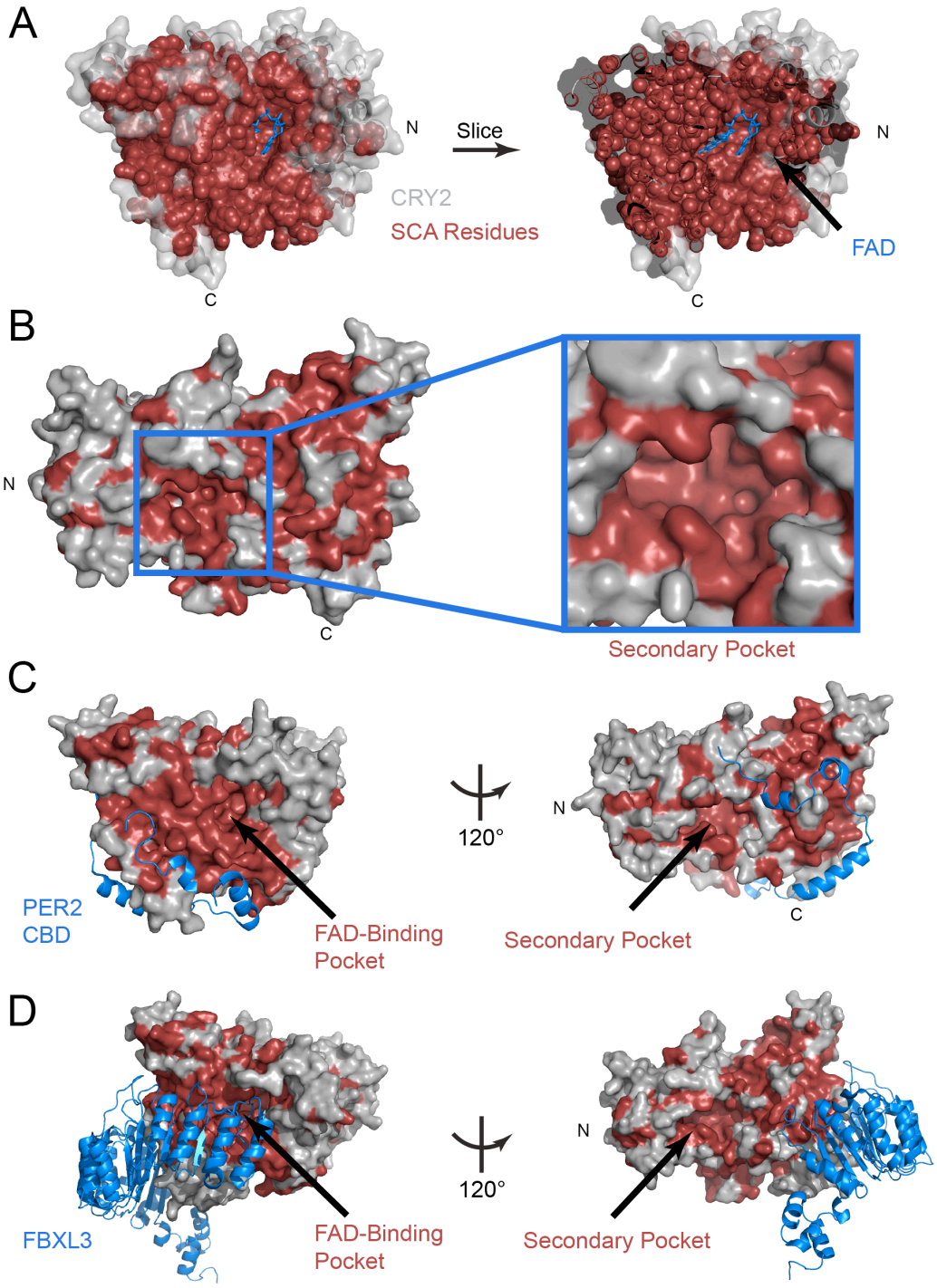

Figure 3-2. Statistical coupling analysis of the CRY/PHL family suggests an evolving role for the secondary pocket.
(**A**) The structure of CRY2 (PDB: 4I6E) is shown in gray with SCA-identified residues colored in red. An FAD molecule is shown in the binding pocket in blue. A coronal slice through the center of the protein is shown on the right.
(**B**) Shows a view of the secondary pocket of CRY2, colored as in Figure 3-2A. Inset is a magnification of this surface demonstrating that these surface exposed residues are a part of this co-evolutionary network.
(**C**) Shows two views of the CRY2/PER2 CRY-binding domain (CBD) complex (PDB: 4U8H). The PER2 CBD is shown as a blue cartoon helix and CRY2 is colored as in Figure 2A. The figure on the left depicts the FAD-binding pocket and the α-22 C-terminal helix of CRY2 while the figure on the right is rotated to show the side of CRY2 containing the secondary pocket. PER2 interacts heavily with residues forming the SCA network.
(**D**) Two views of the FBXL3/CRY2 complex (PDB: 4I6J) with FBXL3 in blue and CRY2 colored as in Figure 2A. The view at the left shows FBXL3's C-terminal tail penetrating into CRY2's FAD-binding pocket, demonstrating the degree to which this critical interaction depends on SCA network residues. The view on the right shows a rotated CRY2, depicting the extent of FBXL3's embrace of the α-22 C-terminal helix of CRY2 and its interaction with SCA network residues.

Figure 3-2—figure supplement 1. SCA identifies allosterically connected surface positions that simple conservation analysis does not.

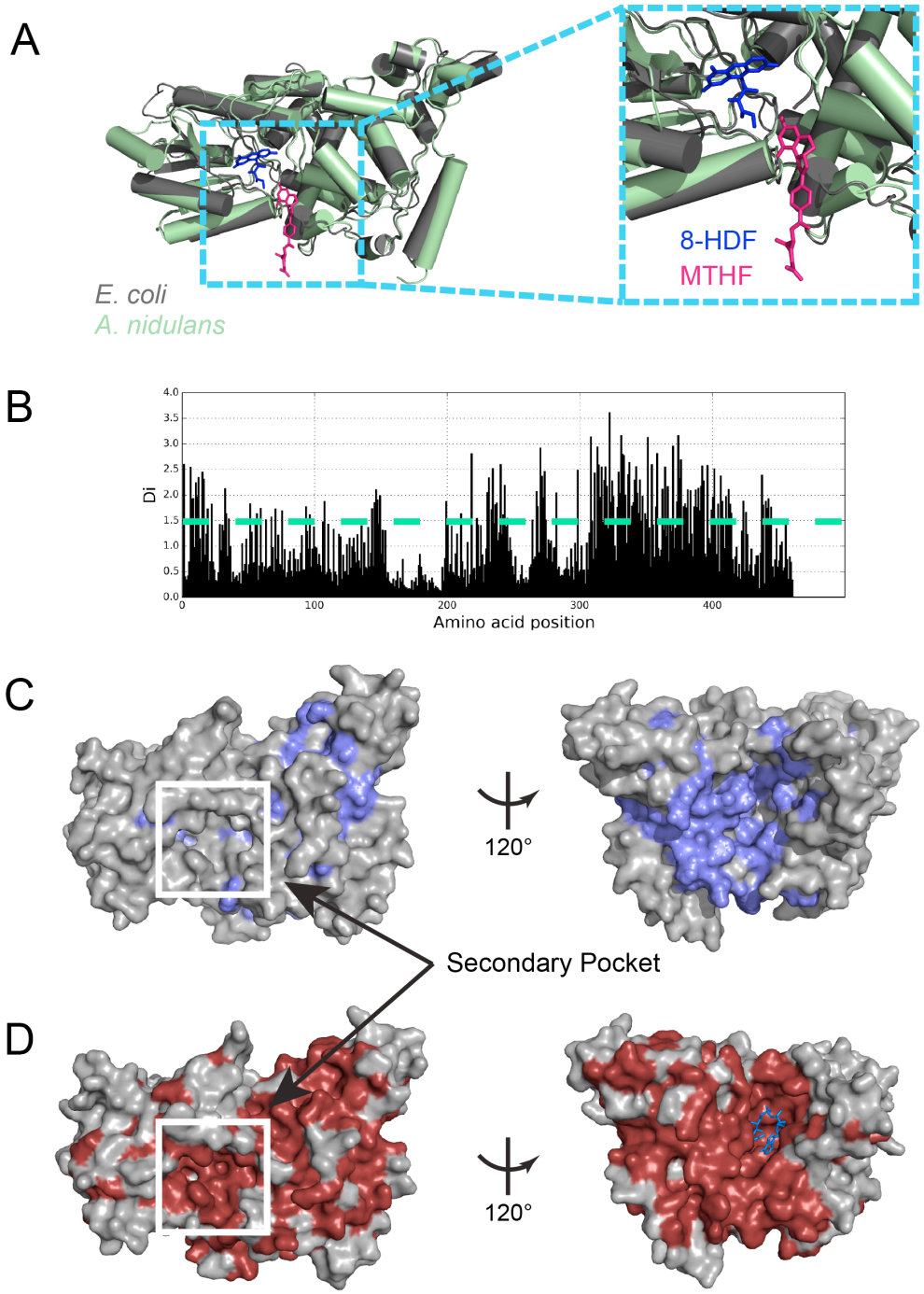

Figure 3-2—figure supplement 1. SCA identifies allosterically connected surface positions that simple conservation analysis does not.
(**A**) Shows an alignment of two photolyase structures with their secondary cofactors. The cyclobutane-pyrimidine dimer (CPD) photolyase from *Escherichia coli* (PDB: 1DNP) is shown in gray with its secondary cofactor 5,10-methenyltetrahydrofolate (MTHF) in pink. The CPD photolyase from the cyanobacterium *Anacystis nidulans* (PDB: 1QNF) is shown in light green with its secondary cofactor 7,8-didemethyl-8-hydroxy-5-deazariboflavin (8-HDF) shown in blue. Inset is a magnified view of the secondary pocket highlighting both the structural diversity in this region of the protein family and the divergent ways that secondary cofactors are bound. Structures were aligned in PyMOL.
(**B**) The positional conservation graph from Figure 3-1C is shown with a line demarcating a D_i value of 1.5 as a cutoff for positional conservation.
(**C**) Positions meeting the $D_i > 1.5$ cutoff are mapped onto the CRY2 structure in blue. These positions primarily identify the protein core and not surface-accessible residues compared to the SCA network shown in (C).
(**D**) CRY2 is shown in gray with SCA network residues shown in red and FAD shown in blue.

Figure 3-3. The lower helical boundary of CRY's secondary pocket gates interaction with CLOCK.

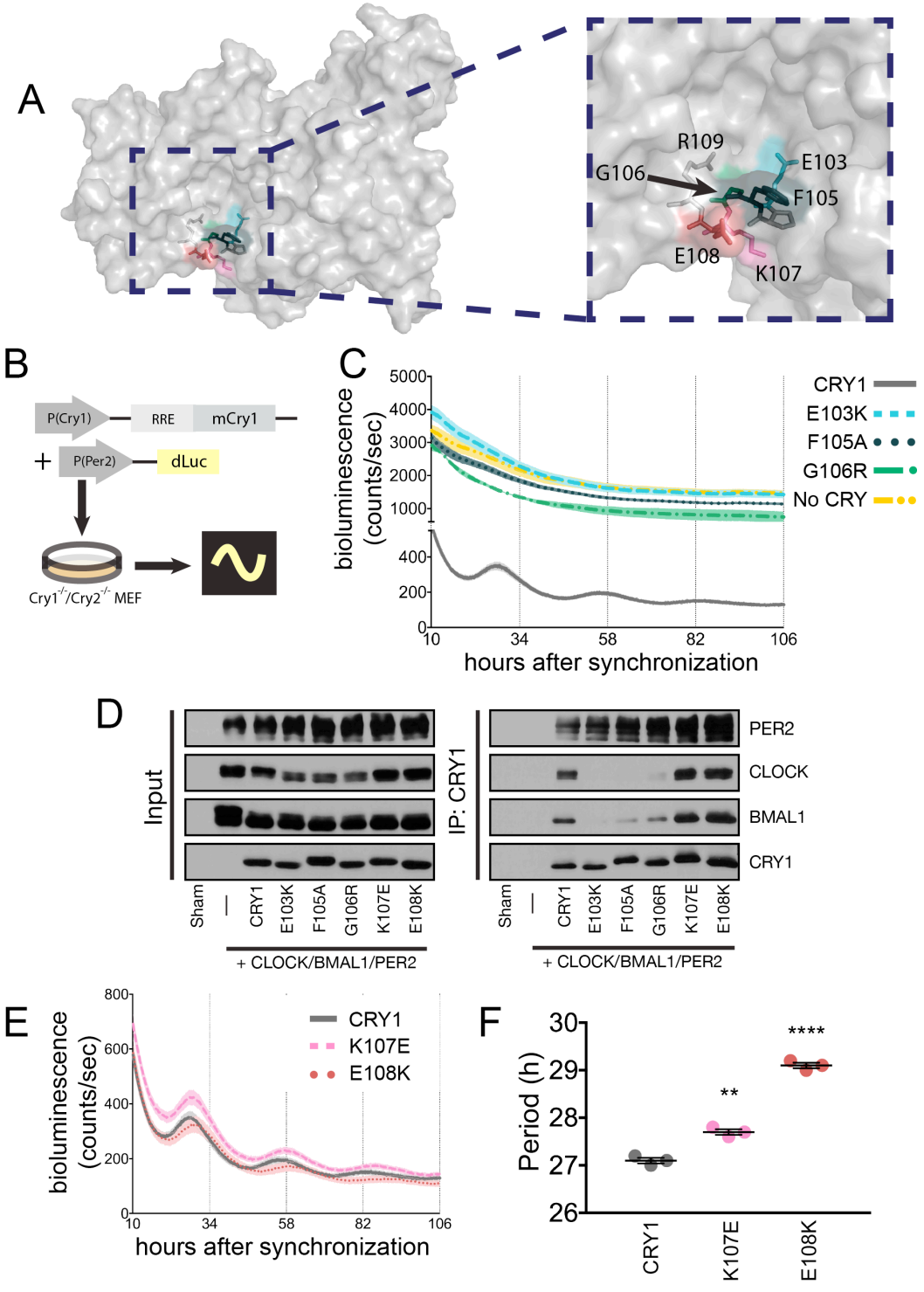

Figure 3-3. The lower helical boundary of CRY's secondary pocket gates interaction with CLOCK.

(**A**) A surface view of the structure of CRY1 (PDB: 5T5X) with the lower helix of the secondary pocket shown as sticks and relevant residues color-coded for the rest of the figure. Inset is a magnified view of this helix with residues labeled.

(**B**) Schematic of *Cry1* rescue assay. RRE is a ROR Response Element necessary for delayed expression of CRY.

(**C**) Rescue assays with CRY1 mutants identified in the SCA (n = 3/condition, reflective of 6 plates from two independent experiments) shown as means ± SEM.

(**D**) Co-IP assay with PER2, CLOCK, BMAL1, and various CRY1 mutants. Multiple bands in PER2, CLOCK, and BMAL1 lanes are indicative of posttranslational modifications on these proteins. Blot is representative of at least three independent experiments.

(**E**) Rescue assays for two CRY1 residues not identified in the SCA (n = 3/condition, reflective of 6 plates from two independent experiments) shown as means ± SEM.

(**F**) Period plot for the data shown in E. Asterisks show significance by unpaired t-test with Welch's correction (**, $p = 0.0018$, ****, $p < 0.0001$).

Figure 3-3—figure supplement 1. Quantification of co-immunoprecipitation experiments.

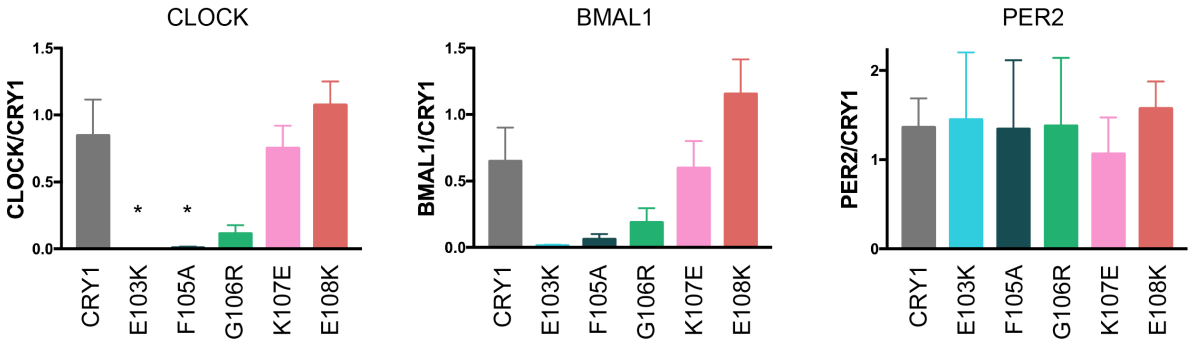

Figure 3-3—figure supplement 1. Quantification of co-immunoprecipitation experiments.
Graphs show respectively the ratio of CLOCK, BMAL1, and PER2 to CRY1 in the IP blot from three independent experiments. Quantification was performed by densitometric analysis with ImageJ. Asterisks show significance of the CLOCK/CRY ratio compared to WT by unpaired t-test with Welch's correction (E103K, *, $p = 0.0346$ and F105A, *, $p = 0.0357$).

Figure 3-4. Structural differences at the secondary pocket differentiate type I and type II CRYs functionally.

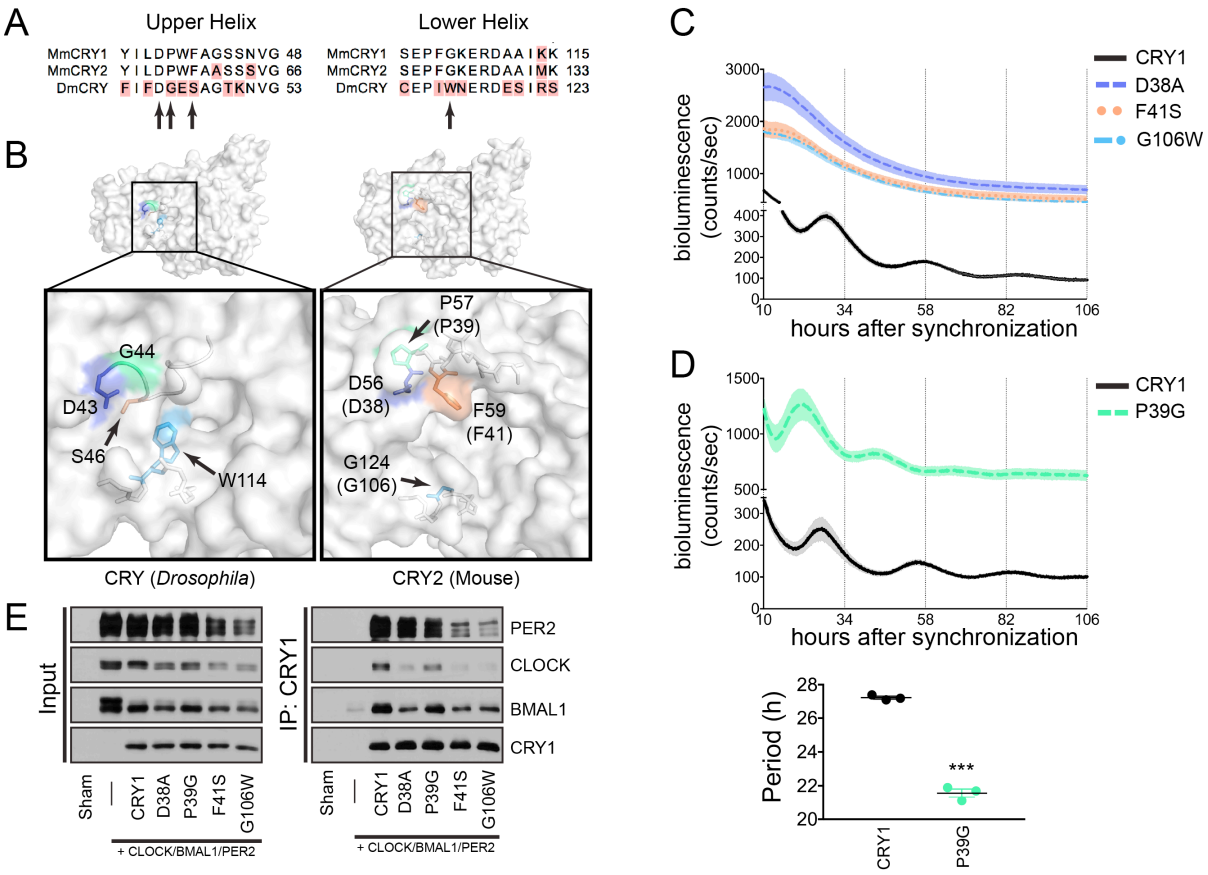

Figure 3-4. Structural differences at the secondary pocket differentiate type I and type II CRYs functionally.

(**A**) Alignment of the amino acids in the upper and lower helical boundaries of the secondary pocket of CRYs from *Mus musculus* (Mm) and *Drosophila melanogaster* (Dm). Residues examined in Fig. 3 indicated by arrows. Red shading indicates disagreement with consensus.
(**B**) Surface view of the secondary pocket of dCRY (PDB: 4GU5) and CRY2 (PDB: 4I6E). Orthologous residues identified in the SCA in dCRY and mCRY2 are shown in teal and purple respectively. CRY1 residues are shown in parentheses.
(**C**) Rescue assays for mutants of three residues in CRY1 identified in the SCA (n = 3/condition, reflective of 9 (D38A), 12 (F41S), and 9 (G106W) plates from 3-4 independent experiments) shown as means ± SEM.
(**D**) Rescue assay for CRY1 P39G (n = 3, reflective of 6 total plates from two independent experiments) shown as mean ± SEM. Period plot for rescues in (D) shown in the plot below.

Mean ± SEM indicated by bars. Asterisks show significance by unpaired t-test with Welch's correction (***, p = 0.0006).
(**E**) Co-IP assay with PER2, CLOCK, BMAL1, and various CRY1 mutants. Blot is representative of at least 3 independent experiments.

Figure 3-4—figure supplement 1. Conserved structural features of vertebrate-like clocks.

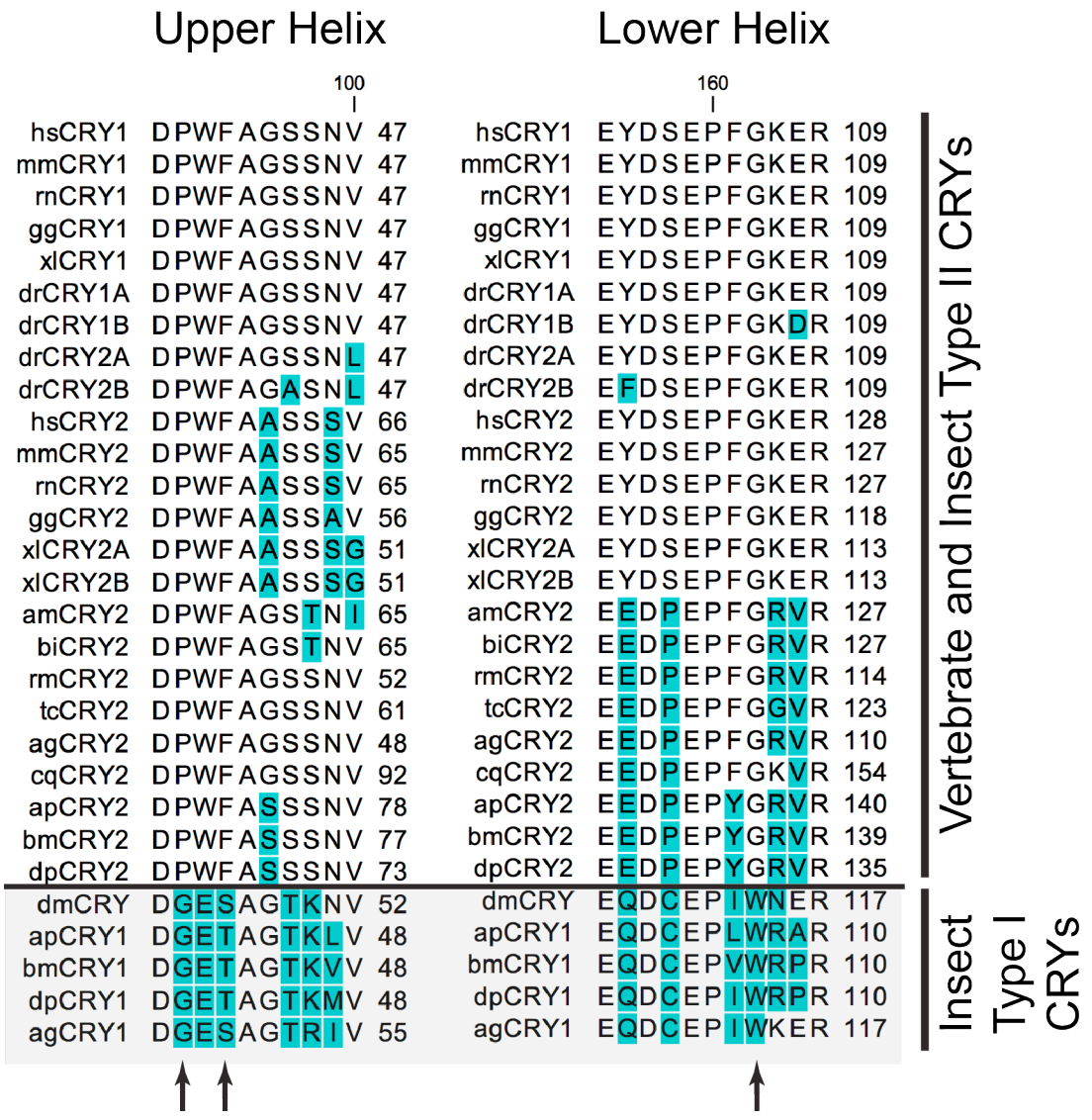

Figure 3-4—figure supplement 1. Conserved structural features of vertebrate-like clocks.

Shows an alignment of the upper and lower boundaries of the secondary pocket from type I and type II CRYs. Position within the alignment is indicated by the number at the top and position within each primary sequence is indicated by the number at the right of each sequence. Arrows at the bottom indicate residues that are highly conserved within each group and divergent between the two groups, further explored in Figure 4. Green shading indicates

divergence from consensus sequence. Abbreviations: hs (*Homo sapiens*, human), mm (*Mus musculus*, mouse), rn (*Rattus norvegicus*, rat), gg (*Gallus gallus*, chicken), xl (*Xenopus laevis*, African clawed frog), dr (*Danio rerio*, zebrafish), am (*Apis mellifera*, western honey bee), bi (*Bombus impatiens*, eastern bumblebee), rm (*Rhyparobia maderae*, madeira cockroach), tc (*Tribolium castaneum*, red flour beetle), ag (*Anopheles gambiae*, marsh mosquito), cq (*Culex quinquefasciatus*, southern house mosquito), ap (*Antheraea pernyi*, Chinese tussar moth), bm (*Bombyx mori*, domesticated silk moth), dp (*Danaus plexippus*, monarch butterfly), dm (*Drosophila melanogaster*, fruit fly).

Figure 3-4—figure supplement 2. Quantification of co-immunoprecipitation experiments.

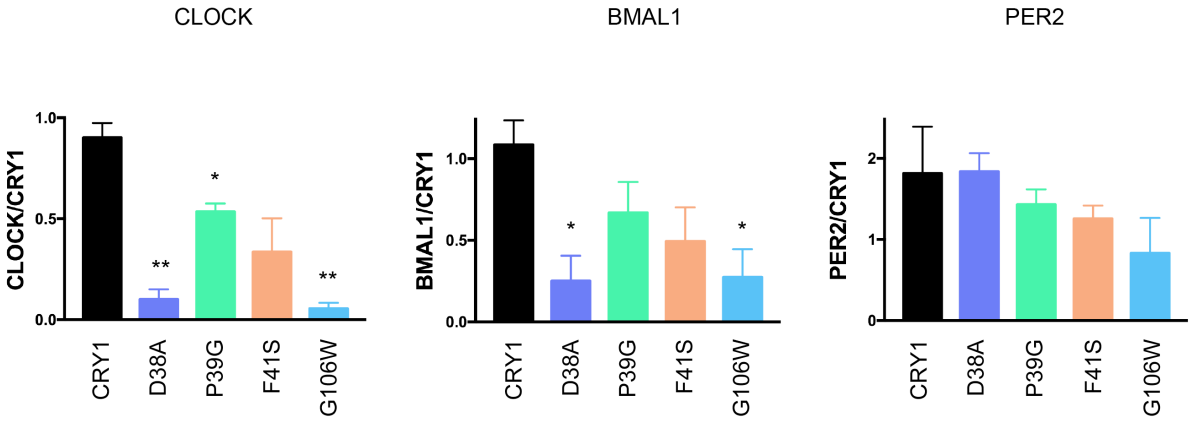

Figure 3-4—figure supplement 2. Quantification of co-immunoprecipitation experiments.
Graphs show respectively the ratio of CLOCK, BMAL1, and PER2 to CRY1 in the IP blot from three independent experiments. Quantification was performed by densitometric analysis with ImageJ. The CLOCK/CRY ratios of D38A (**, p = 0.0014), P39G (*, p = 0.0198), and F41s (**, p = 0.0030) were significantly different from WT by unpaired t-test with Welch's correction. The BMAL1/CRY ratios of D38A (*, p = 0.0180) and G106W (*, p = 0.0245) were significantly different from WT by unpaired t-test with Welch's correction.

Figure 3-5. Weakened interaction between CRY1 and CLOCK/BMAL1 dramatically shortens the period in rescue assays.

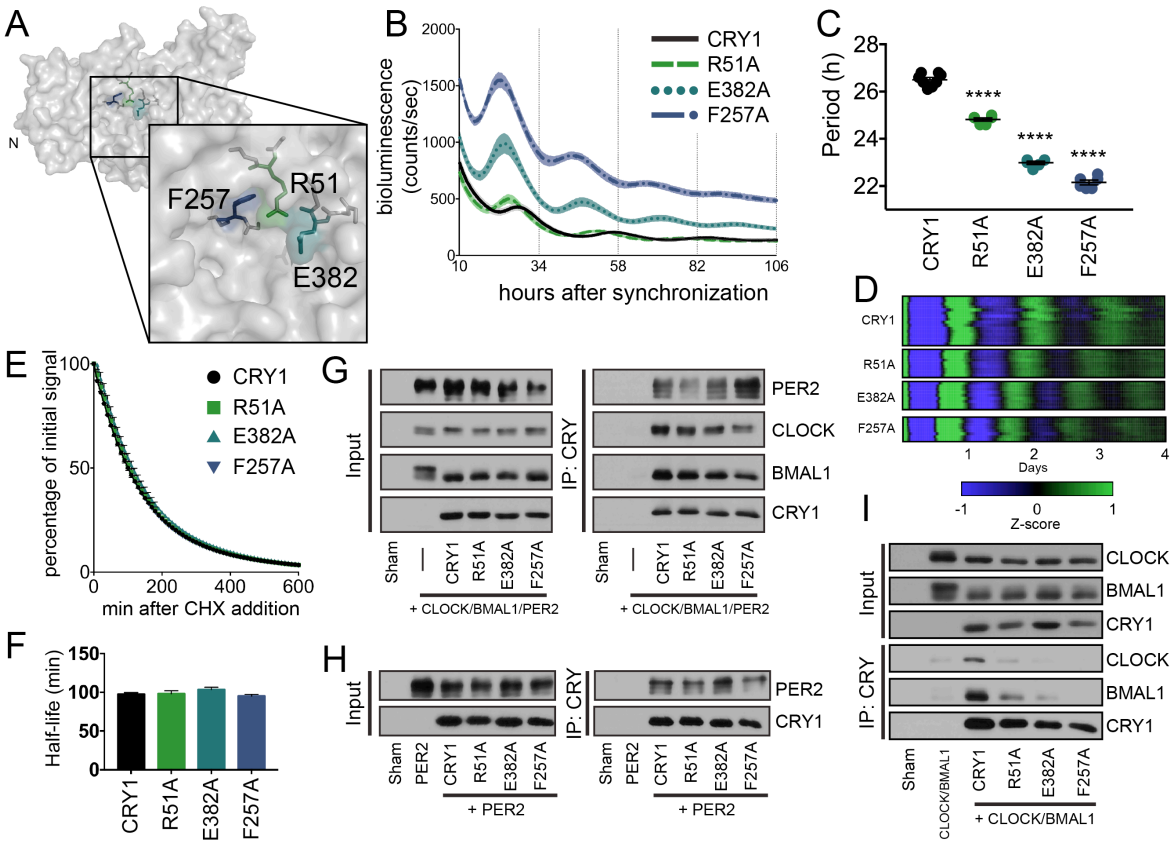

Figure 3-5. Weakened interaction between CRY1 and CLOCK/BMAL1 dramatically shortens the period in rescue assays.

(**A**) Surface view of CRY1 (PDB: 5T5X) with an inset magnification of the secondary pocket. Residues R51, E382, and F257 are labeled and colored in green, teal, and navy blue.

(**B**) Rescue assays performed with WT, R51A, E382A, and F257A CRY1 (n = 8, 6, 6, and 6/condition, respectively, reflective of 9 (R51A), 15 (E382A), and 12 (F257A) plates from 3-5 independent experiments), shown as means ± SEM.

(**C**) Period plot for rescues shown in (B). Mean ± SEM indicated by bars. Asterisks indicate significance by unpaired t-test with Welch's correction (****, $p < 0.0001$).

(**D**) Heat maps of CRY1 and mutant rescues demonstrate period and phase differences over multiple cycles. Raw data were baseline subtracted and z-scores were calculated, then scaled

to a range of -1 to 1. The data from 16 WT, 9 R51A, 9 E382A, and 8 F257A plates are shown.

(**E**) Degradation assay with CRY1::LUC and mutants (n = 3/condition). Samples were normalized to initial luminescence signal. Half-life was determined by fitting a one-phase decay curve to the data.

(**F**) Half-lives from (E) shown as means + SEM. No significant difference between WT and mutants by unpaired t-test with Welch's correction (R51A: $p = 0.8245$; E382A: $p = 0.0660$; F257A: $p = 0.2029$)

(**G**) Co-IP assay with PER2, CLOCK, BMAL1, and CRY1 mutants. Blot is representative of three independent experiments.

(**H**) Co-IP assay with PER2 and CRY1 mutants. Blot is representative of three independent experiments.

(**I**) Co-IP assay with CLOCK, BMAL1, and CRY1 mutants. Blot is representative of three independent experiments.

Figure 3-5—figure supplement 1. Validation of CRY1::LUC fusion construct and quantification of co-immunoprecipitation experiments.

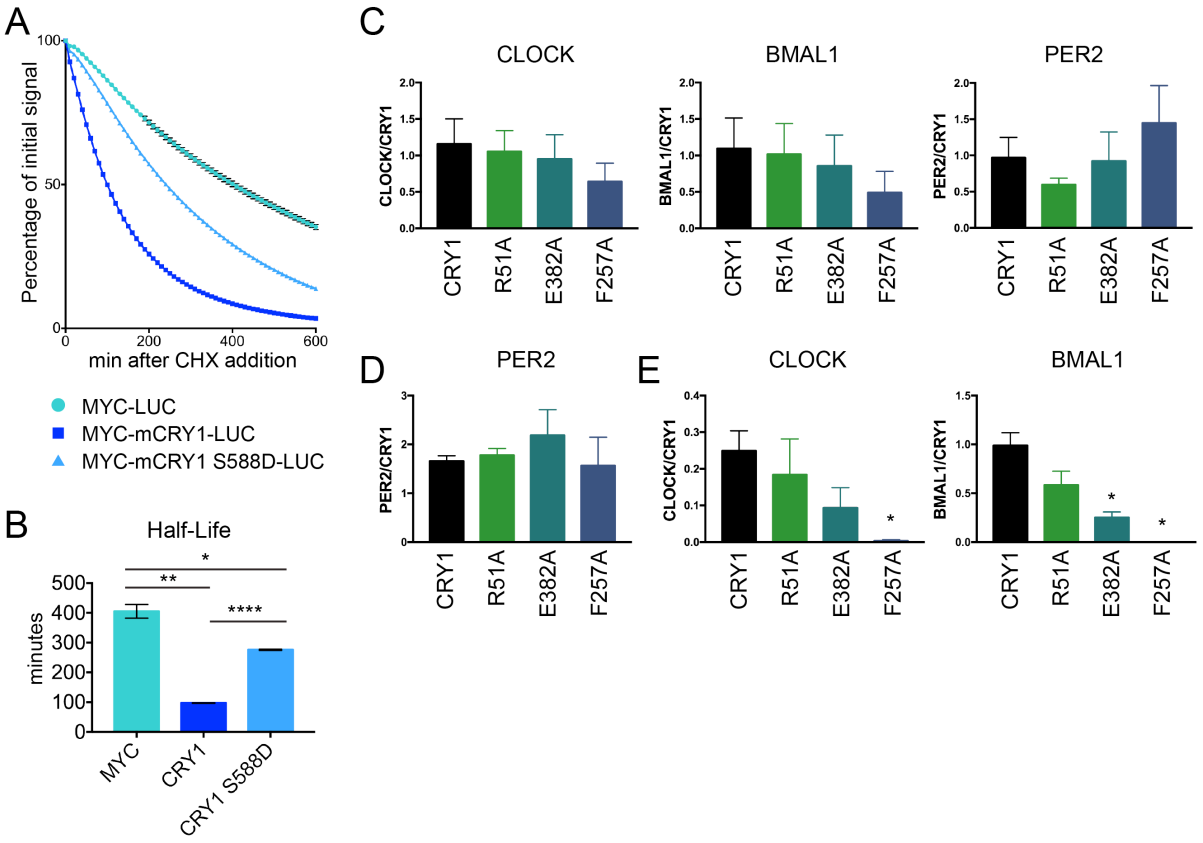

Figure 3-5—figure supplement 1. Validation of CRY1::LUC fusion construct and quantification of co-immunoprecipitation experiments.
(**A**) A *Luc* gene was fused to the C-terminus of a *Myc-Cry1* expression vector. MYC-CRY1-LUC was constitutively expressed in 293A cells for 48 hours before treatment with cycloheximide and the decay in luminescence was monitored as a reporter for protein degradation. Shown here are the WT vector and two controls to demonstrate the efficacy of the approach (n = 3/condition). Samples were normalized to their initial luminescent signal and graphed as the decay from that initial signal. Shown as mean ± SEM. MYC-LUC is a fusion of the MYC tag to LUC. The CRY1 S588D mutation has been previously shown to stabilize CRY1 (Gao et al., 2013; Papp et al., 2015).
(**B**) Half-lives are shown as mean ± SEM. Half-life was determined by fitting a one-phase decay curve to the data in (A). Asterisks show significance by unpaired t-test with Welch's correction (*, $p = 0.0297$, **, $p = 0.0055$, ****, $p < 0.0001$).

(**C**) Graphs show respectively the ratio of CLOCK, BMAL1, and PER2 to CRY1 in the IP blots from three independent experiments. Quantification was performed by densitometric analysis with ImageJ.
(**D**) Shows the ratio of PER2 to CRY1 in the IP blots from three independent experiments, quantified by densitometric analysis with ImageJ.
(**E**) Two graphs that show respectively the ratio of CLOCK and BMAL1 to CRY1 in the IP blots from three independent experiments, quantified by densitometric analysis with ImageJ. The CLOCK/CRY ratio of F257A (*, $p = 0.0464$) was significantly different from WT by unpaired t-test with Welch's correction. The BMAL1/CRY ratios of E382A (*, $p = 0.0173$) and F257A (*, $p = 0.0168$) were significantly different from WT by unpaired t-test with Welch's correction.

Figure 3-6. Subtle divergence between CRY1 and CRY2 at the secondary pocket largely dictates periodicity differences between the two repressors.

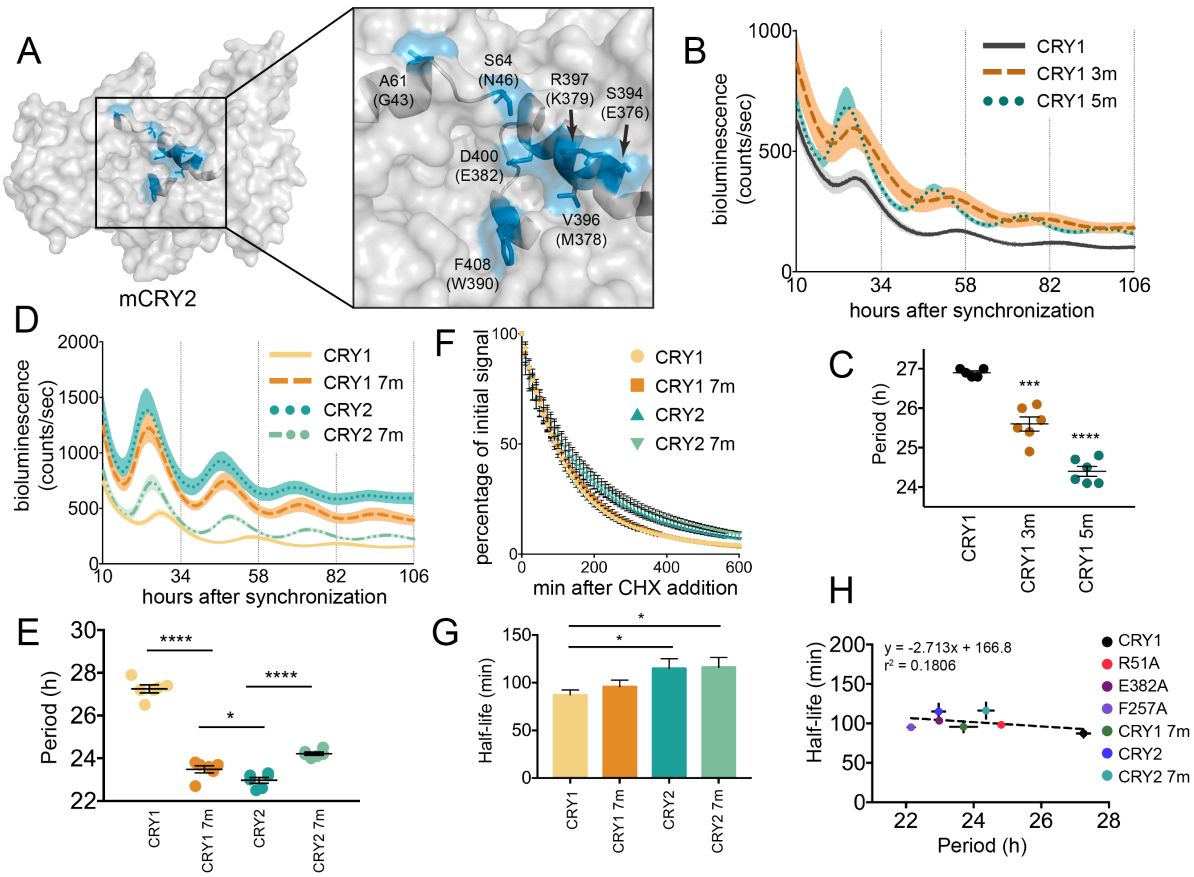

Figure 3-6. Subtle divergence between CRY1 and CRY2 at the secondary pocket largely dictates periodicity differences between the two repressors.
(**A**) Surface view of the secondary pocket in CRY2 (PDB: 4I6E) with the seven divergent paralogous residues of CRY1 and CRY2 colored blue and labeled. CRY1 residues are shown in parentheses.
(**B**) Rescue assays performed with WT CRY1, CRY1 3m (CRY1 M378V/K379R/E382D), and CRY1 5m (CRY1 E376S/M378V/K379R/E382D/W390F) shown as means ± SEM (n = 5, 6, 6/condition, reflective of 18 plates each from 6 independent experiments).
(**C**) Period plot of rescues in (B). Mean ± SEM indicated by bars. Asterisks show significance by unpaired t-test with Welch's correction (***, $p = 0.0005$, ****, $p < 0.0001$) compared to WT.

(**D**) Rescue assays performed with WT CRY1, CRY1 7m (CRY1 G43A/N46S/E376S/M378V/K379R/E382D/W390F), WT CRY2, and CRY2 7m (CRY2 A61G/S64N/S394E/V396M/R397K/D400E/F408W) (n = 6/condition, reflective of 30 (CRY1 7m), 33 (CRY2), and 24 (CRY2 7m) plates from ≥8 independent experiments) shown as means ± SEM.
(**E**) Period plot of rescues in (D). Mean ± SEM indicated by bars. Asterisks show significance by unpaired t-test with Welch's correction (*, $p = 0.0387$, ****, $p < 0.0001$).
(**F**) Degradation assay with CRY1::LUC and CRY2::LUC and mutants (n = 6/condition, 2 independent experiments). Samples were normalized to the initial luminescent signal.
(**G**) Half-lives shown as means + SEM. Half-life was determined by fitting a one-phase decay curve to the data. Asterisks show significance by unpaired t-test with Welch's correction (*, $p < 0.05$ (CRY2 vs CRY1: $p = 0.0407$; CRY2 7m vs CRY1: $p = 0.0376$), ns (CRY1 7m vs CRY1: $p = 0.3484$; CRY2 7m vs CRY2: $p = 0.9348$; CRY2 vs CRY1 7m: $p = 0.1483$; CRY2 7m vs CRY1 7m: $p = 0.1331$)).
(**H**) Correlation plot of period versus half-life for the various pocket mutant rescues. Half-lives and periods shown as means ± SEM. Linear regression shown as a dotted line. The slope's deviation from zero was not significant ($p = 0.3418$).

Figure 3-6—figure supplement 1. Differences in CRY1 and CRY2 rescues are due to concerted effects of multiple mutations.

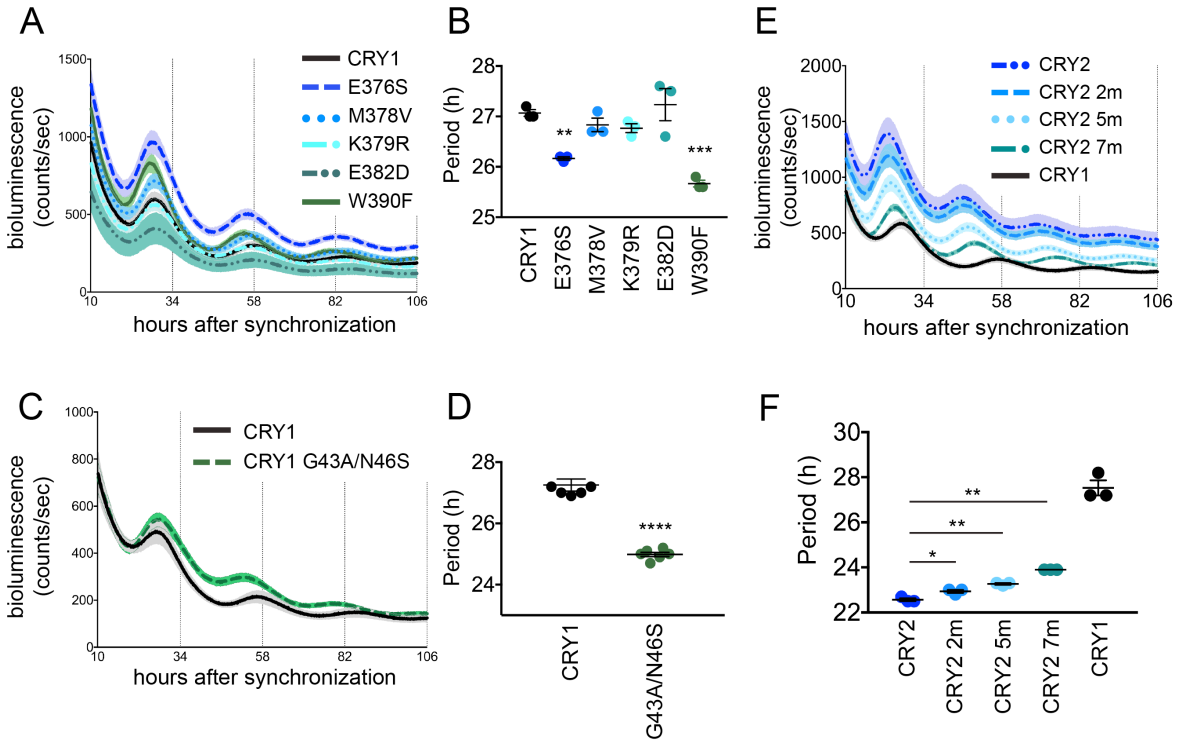

Figure 3-6—figure supplement 1. Differences in CRY1 and CRY2 rescues are due to concerted effects of multiple mutations.

(**A**) Rescue assays performed with WT CRY1, and five single mutations of CRY1: E376S, M378V, K379R, E382D, W390F (n = 3/condition, representative of 9 (K379R, E382D), 12 (E376S, M378V), and 15 (W390F) plates from 3-5 independent experiments) shown as mean ± SEM.

(**B**) Period plot of rescues in (A). Mean ± SEM indicated by bars. Asterisks show significance by unpaired t-test with Welch's correction (**, p = 0.0013, ***, p = 0.0001, ns (M378V: p = 0.2173; K379R: p = 0.0576; E382D: p = 0.6553)).

(**C**) Rescue assays performed with WT CRY1 and a double mutation of CRY1, G43A/N46S (n = 6/condition, representative of 12 plates from 4 independent experiments) shown as mean ± SEM.

(**D**) Period plot of rescues in (C). Mean ± SEM indicated by bars. Asterisks show significance by unpaired t-test with Welch's correction (****, p < 0.0001).

(**E**) Rescue assays performed with WT CRY1, WT CRY2, CRY2 2m (CRY2 A61S/S64N), CRY2 5m (CRY2 S394E/V396M/R397K/D400E/F408W), and CRY2 7m (CRY2 A61G/S64N/S394E/V396M/R397K/D400E/F408W) shown as means ± SEM (n =

3/condition, reflective of 3 (CRY2 2X), 6 (CRY2 5X), 24 (CRY2 7X), and 33 (CRY2) plates from 1, 2, 8, and 11 independent experiments respectively).
(**F**) Period plot of rescues in (E). Mean ± SEM indicated by bars. Asterisks show significance by unpaired t-test with Welch's correction compared to WT CRY2 (*, $p = 0.0177$, **, $p < 0.01$ (CRY2 5m: $p = 0.0028$; CRY2 7m: $p = 0.0025$; CRY1: $p = 0.0034$)).

Figure 3-6—figure supplement 2. Rescue vector dosage does not underlie period differences in *Cry1/Cry2* rescues.

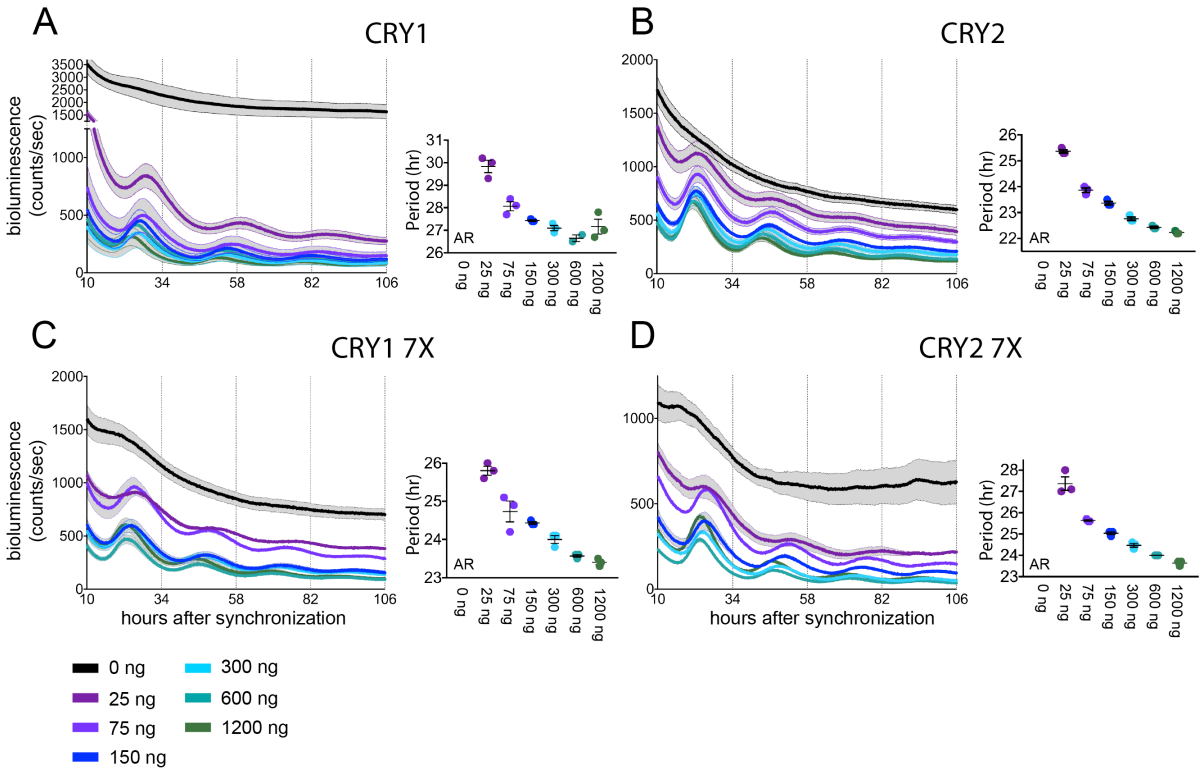

Figure 3-6—figure supplement 2. Rescue vector dosage does not underlie period differences in *Cry1/Cry2* rescues.

(**A**) Rescue assays performed with WT CRY1 (n = 3/dosage). *Cry1*$^{-/-}$/*Cry2*$^{-/-}$ MEFs were transfected with various amounts of rescue vector in a total of 5.2 µg of plasmid DNA. Mean ± SEM shown for each condition. The rescue period for each condition is shown in the graph to the right as mean ± SEM.

(**B**) Rescue assays performed with WT CRY2 (n = 3/dosage). *Cry1*$^{-/-}$/*Cry2*$^{-/-}$ MEFs were transfected with various amounts of rescue vector in a total of 5.2 µg of plasmid DNA. Mean ± SEM shown for each condition. The rescue period for each condition is shown in the graph to the right as mean ± SEM.

(**C**) Rescue assays performed with CRY1 7X (n = 3/dosage). *Cry1*$^{-/-}$/*Cry2*$^{-/-}$ MEFs were transfected with various amounts of rescue vector in a total of 5.2 µg of plasmid DNA. Mean ± SEM shown for each condition. The rescue period for each condition is shown in the graph to the right as mean ± SEM.

(**D**) Rescue assays performed with CRY2 7X (n = 3/dosage). *Cry1*$^{-/-}$/*Cry2*$^{-/-}$ MEFs were transfected with various amounts of rescue vector in a total of 5.2 µg of plasmid DNA. Mean

± SEM shown for each condition. The rescue period for each condition is shown in the graph to the right as mean ± SEM.

Figure 3-7. CRY2 requires PER to form a stable complex with mCLOCK and mBMAL1.

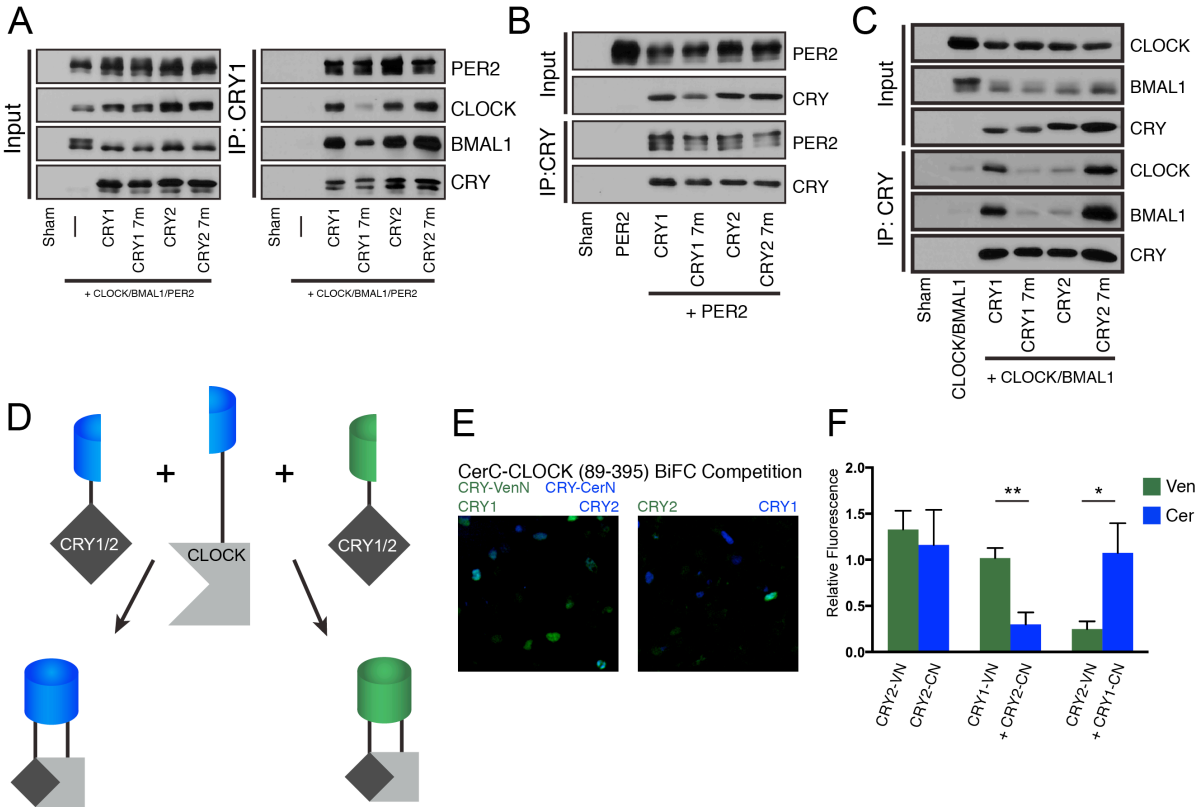

Figure 3-7. CRY2 requires PER to form a stable complex with mCLOCK and mBMAL1.

(**A**) Co-IP assay with mPER2, mCLOCK, mBMAL1, and CRY1, CRY2, or pocket-switched mutants. Multiple bands in mPER2, mCLOCK, and mBMAL1 lanes are indicative of posttranslational modifications on these proteins. The upper band is CRY, the lower band is a nonspecific band recognized by the V5 antibody used to probe for mPER2. Blot is representative of three independent experiments.

(**B**) Co-IP assay with mPER2 and CRY1, CRY2, or pocket-switched mutants. Blot is representative of three independent experiments.

(**C**) Co-IP assay with mCLOCK and mBMAL1, and CRY1, CRY2, or pocket-switched mutants. Blot is representative of three independent experiments.

(**D**) Schematic of bimolecular fluorescence complementation competition assay. A CLOCK construct (residues 89-395) is N-terminally tagged with a C-terminal fragment of Cerulean,

which can interact with either an N-terminal fragment of Venus or Cerulean to produce yellow or blue fluorescence. CRY1 or CRY2 fused to these N-terminal fragments compete to bind CerC-CLOCK and fluorescence is used as a readout in the competition for binding. (**E**) Reciprocal two-color, three-way bimolecular fluorescence complementation (BiFC) in 293A cells using CerC-CLOCK (89-395) complementation with CRY1-VenN + CRY2-CerN or CRY1-CerN + CRY2-VenN. Pseudocoloring: Venus (Green), Cerulean (Blue). (**F**) Quantification of BiFC results. Bar graphs show the mean + SEM of six biological replicates from two independent experiments. Asterisks show significance by unpaired t-test with Welch's correction (*, $p = 0.0494$, **, $p = 0.0017$).

Figure 3-7—figure supplement 1. Quantification of co-immunoprecipitation experiments.

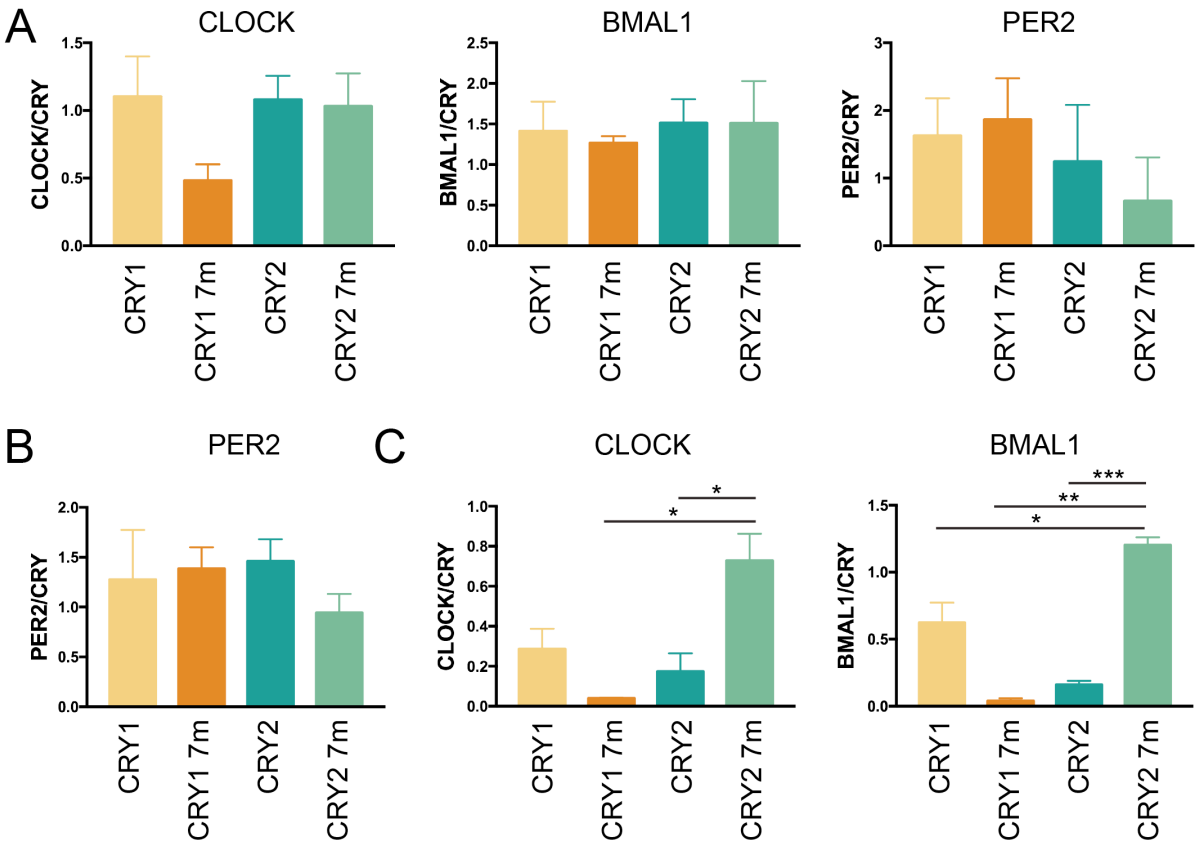

Figure 3-7—figure supplement 1. Quantification of co-immunoprecipitation experiments.

(**A**) Graphs show respectively the ratio of CLOCK, BMAL1, and PER2 to CRY in the IP blot from three independent experiments (related to Figure 7A). Quantification was performed by densitometric analysis with ImageJ.

(**B**) Shows the ratio of PER2 to CRY1 in the IP blots from three independent experiments (related to Figure 7B), quantified by densitometric analysis with ImageJ.

(**C**) Two graphs that show respectively the ratio of CLOCK and BMAL1 to CRY1 in the IP blots from three independent experiments (related to Figure 7C), quantified by densitometric analysis with ImageJ. The CLOCK/CRY ratio of CRY2 7m compared to CRY1 7m and CRY2 (*, p = 0.0365 and 0.0336 respectively) was significantly different by unpaired t-test with Welch's correction. The BMAL1/CRY ratio of CRY2 7m compared to CRY1, CRY1 7m, and CRY2 (*, p = 0.0464, **, p = 0.0010, ***, p = 0.0005) was significantly different by

unpaired t-test with Welch's correction. The BMAL1/CRY ratio of CRY1 to CRY1 7m and CRY2 was not significant, but trending towards significance by unpaired t-test with Welch's correction ($p = 0.0576$ and 0.0846 respectively).

Figure 3-8. Both the CRY1 pocket and tail are required to recapitulate the long period length of *Cry1* rescues.

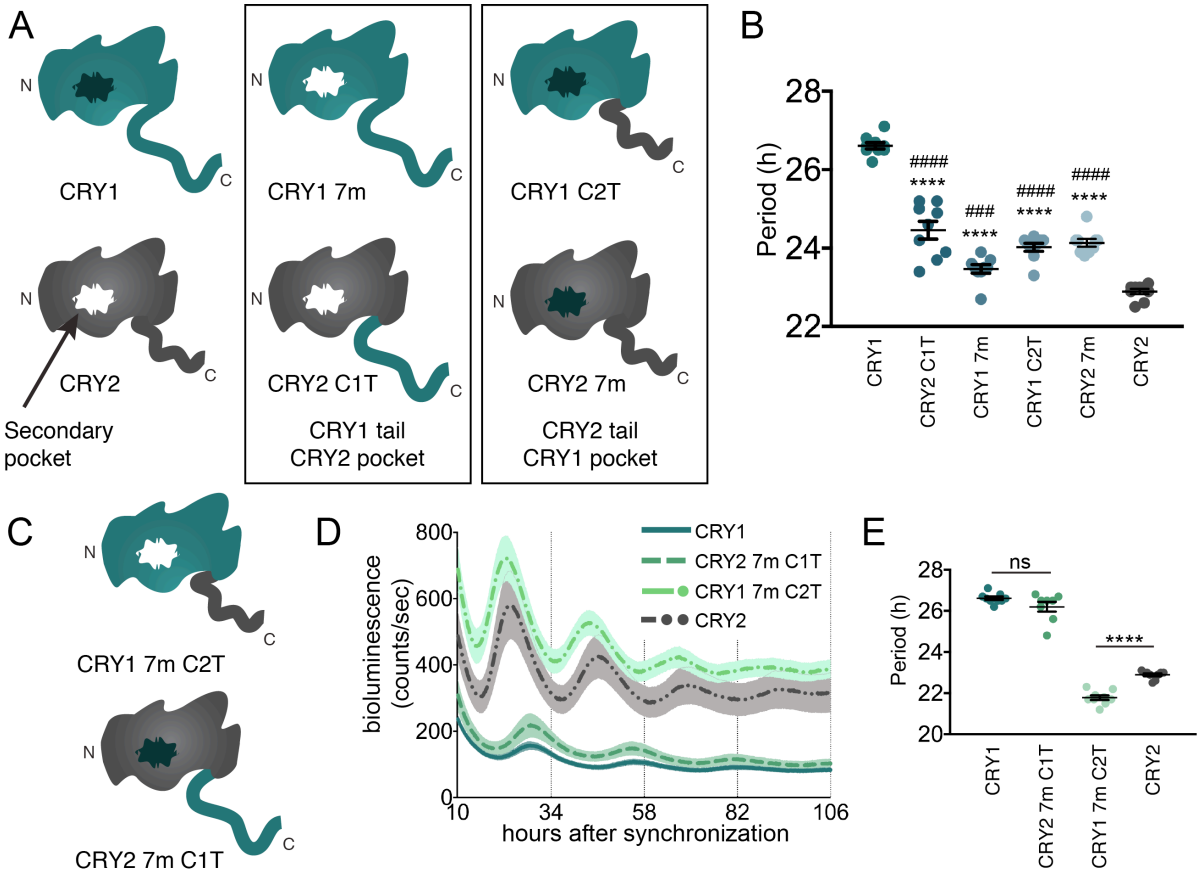

Figure 3-8. Both the CRY1 pocket and tail are required to recapitulate the long period length of *Cry1* rescues.

(**A**) Models of chimeric CRYs used in the experiments in this figure. CRY1- and CRY2-like pockets are shown in black and white respectively. The first column shows WT CRY1 and CRY2; the second column shows CRYs with CRY1 tails and CRY2-like pockets; the final column shows CRYs with CRY2 tails and CRY1-like pockets.

(**B**) Shows a period plot from experiments in which either the tail or pocket of CRY1 and CRY2 was exchanged for its paralog. Data shown here as mean ± SEM (n = 9 plates/condition from 3 independent experiments. Asterisks show significance by unpaired t-test with Welch's correction compared to WT CRY1 (****, $p < 0.0001$). Hashes denote significance by unpaired t-test with Welch's correction compared to WT CRY2 (###, $p = 0.0006$, ####, $p < 0.0001$).

(**C**) Models depicting CRY chimeras in which both the pocket and tail have been exchanged for paralogous residues.
(**D**) Rescue assays performed with WT CRY1, CRY2 7m C1T (CRY2 7m with CRY1 tail (res 499-606)), CRY1 7m C2T (CRY1 7m with CRY2 tail (res 517-593)), and WT CRY2 shown as mean ± SEM (n = 9 plates/condition from 3 independent experiments).
(**E**) Period plot of the data shown in panel (D). Mean ± SEM indicated by bars. Asterisks show significance by unpaired t-test with Welch's correction (****, $p < 0.0001$).

Table 3-1. Period of CRY1 mutants in rescue assay.

Residue Mutation	Period	Residue Mutation	Period	Residue Mutation	Period	Residue Mutation	Period
K11E	25.33 ± 0.21 h	Y100A	30.1 ± 0.17 h	D38A	AR	N50A	27.93 ± 0.31 h
P39G	21.57 ± 0.42 h	E108K	29.1 ± 0.1 h	F41S	AR	K107E	27.7 ± 0.1 h
G43A/N46S	24.98 ± 0.17 h	G121R	29.57 ± 1.79 h	L55D	AR	T118A	27.43 ± 0.21 h
R51A	24.82 ± 0.17 h	S129A	28.4 ± 0.52 h	E103K	AR	E332K	27.27 ± 0.85 h
H130E	25.53 ± 0.28 h	D134A	28.73 ± 0.50 h	F105A	AR	F337A	27.57 ± 1.11 h
T131F	24.6 ± 0 h	L135D	30.4 ± 0.2 h	G106R	AR	F337D	26.93 ± 0.47 h
L132E	24.23 ± 0.21 h	E216K	28.33 ± 0.15 h	G106W	AR	T345A	28.1 ± 0.46 h
Y133D	25.57 ± 0.07 h	L218F	29.87 ± 0.12 h	R109Q	AR	R348A	28.17 ± 0.32 h
G204D	26.53 ± 0.25 h	Y254D	29.17 ± 0.60 h	T149E	AR	L436A	27.1 ± 0.26 h
R227A	20.8 ± 0.1 h	R263A	32.4 ± 1.04 h	G212R	AR	F439A	28.13 ± 0.06 h
R236A/R238A	25.13 ± 0.15 h	F410A	32.97 ± 1.79 h	E214K	AR	I444A	27.9 ± 0.35 h
F257A	22.15 ± 0.25 h	H411A	35.5 ± 0.14 h	T215A	AR	M470A	27.93 ± 0.45 h
G288R*	22.03 ± 0.93 h*	V416K	30.1 ± 0.66 h	A217T	AR	V471A	27.07 ± 0.15 h
D307A	23.2 ± 0.52 h	G419D	29.23 ± 0.06 h	C259Y	AR		
A331E	26.44 ± 0.77 h	K485A	30.1 ± 0.35 h	E294K	AR		
G333D	25.87 ± 0.15 h			G336D	AR		
E350K	24.1 ± 0 h			P338L	AR		
E376S/M378V/K379R/E382D/W390F	24.4 ± 0.31 h			D341A	AR		
E382A	22.98 ± 0.16 h			F409A**	AR		
E383A	24.9 ± 0.17 h			A474K**	AR		
L384A	26.57 ± 0.21 h			R483A**	AR		
S391A	26.4 ± 0.26 h						
L436D	24.97 ± 1.23 h						
F439D	24.17 ± 1.36 h						
I444D	26.7 ± 0.36 h						
*Sustains rhythms for only two cycles				**Represses without rescuing rhythms			

Table 3-1. Period of CRY1 mutants in rescue assay.
All of the mutants tested in our cycling cell rescue assay are shown grouped by phenotype. Short period rescues are shown in purple, long period rescues are shown in pink, mutants that failed to rescue rhythms are shown in blue, and mutants that had no effect are shown in gray. Phenotypes were determined by averaging all of the WT control rescues (>100) and determining the average (27.55 h) and standard deviation (0.77 h). Mutants with an average period > 1 standard deviation from the WT average were sorted into the appropriate group. Mutants were determined to be arrhythmic if we could not achieve a goodness of fit for the data ≥ 80% using a running average damped sine wave fit. Each mutant period is representative of at least 3 biological replicates.

Figure 3-9. A phenotypic map of CRY1 highlights regions of interest in period determination.

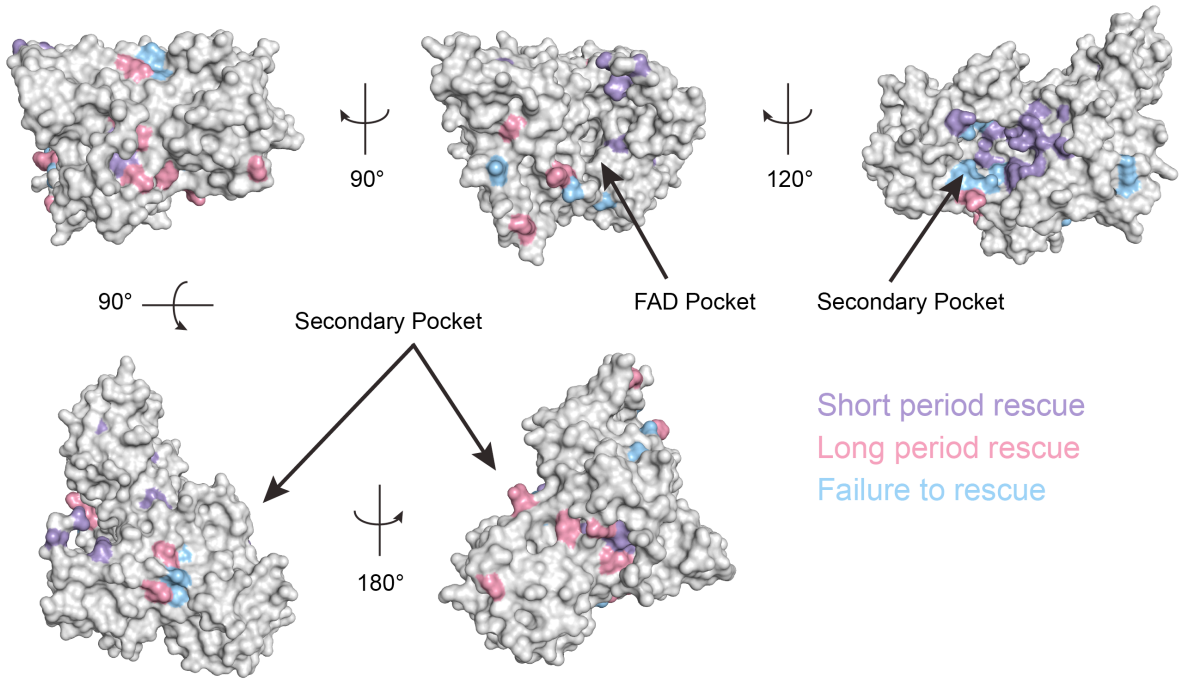

Figure 3-9. A phenotypic map of CRY1 highlights regions of interest in period determination.
Five different surface views of CRY1 (PDB: 4K0R). Based on the data shown in Table 1, residues were colored based on the phenotype of mutants in the rescue assay. Short period rescues were colored purple; long period rescues were colored pink; and mutants that failed to rescue rhythms were colored blue. The bottom row shows the topside and underside of CRY1 on the left and right respectively.

Figure 3-10. Periodicity in the mammalian circadian clock depends on both the latent stability of the ternary complex and degradation dynamics.

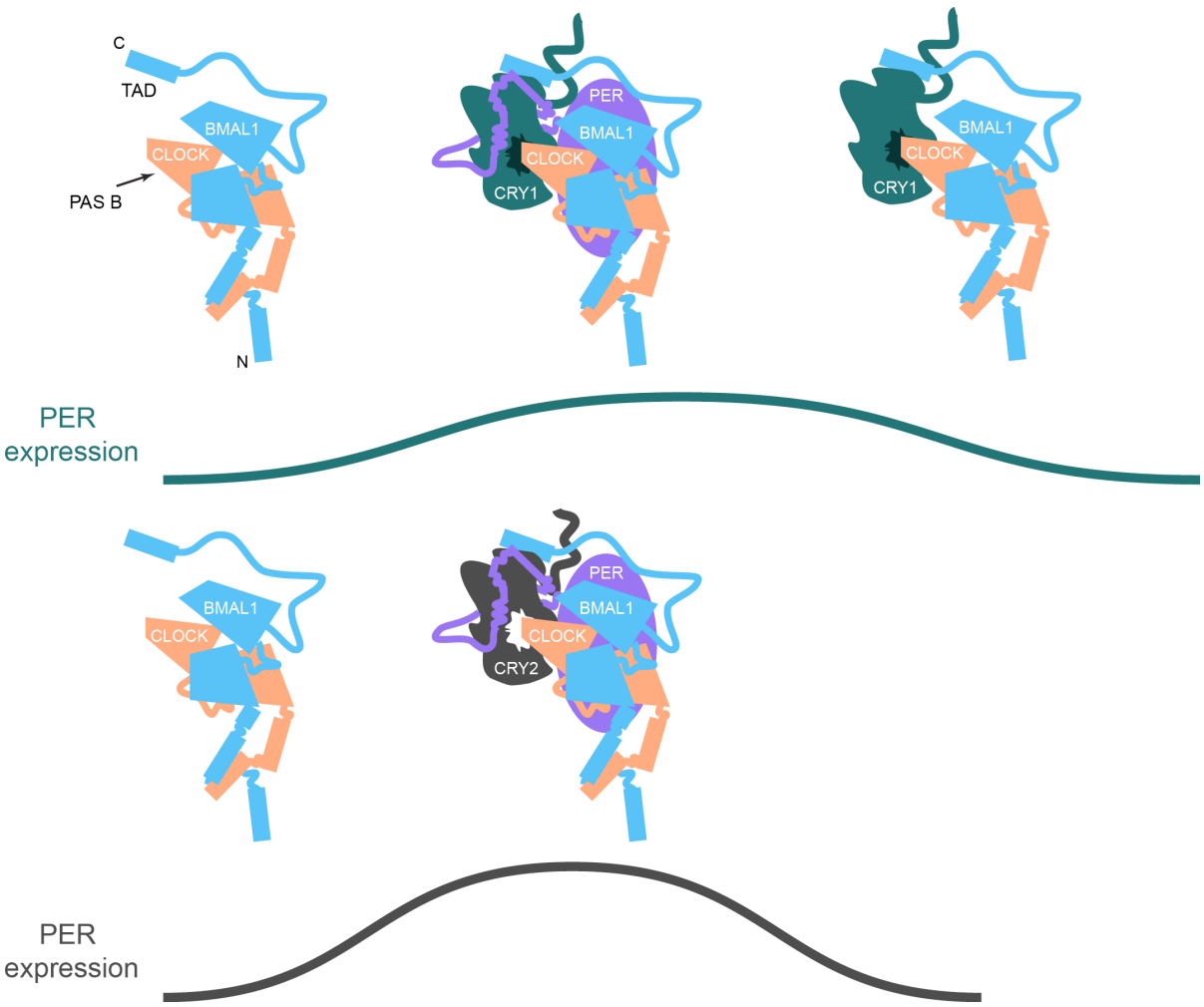

Figure 3-10. Periodicity in the mammalian circadian clock depends on both the latent stability of the ternary complex and degradation dynamics.
In the model shown here, cartoons are based on existing structures. During the rising phase of the oscillation, the BMAL1 TAD is free to recruit transcriptional components. As production of the repressors begins, CRY1 and CRY2 form a PER-dependent complex with CLOCK and BMAL1, allosterically interacting with BMAL1's TAD through C-terminal regions and with the CLOCK PAS B domain through the secondary pocket. Through these interactions, the activity of the CLOCK/BMAL1 heterodimer is suppressed. CRY2's

repressive window is shortened due to its weakened ability to bind CLOCK and BMAL1 without PER. Later in the repressive phase, CRY1 is predominantly bound to CLOCK in a PER-independent interaction and sequesters the BMAL1 TAD. At all times, CRYs are subject to degradation primarily through interaction with FBXL3, eventually leading to renewal of the active phase of the clock.

CHAPTER FOUR: Conclusions and Recommendations

PROPOSED APPROACHES TO UNDERSTANDING THE CONTRIBUTION OF STRUCTURAL DYNAMICS TO CLOCK FUNCTION

Introduction

In these studies, I collaborated with structural biologists to solve and validate the structure of CRY2 in complex with the PER2 CBD. Additionally, I took a computational approach to identify a network of coevolving residues in the CPF proteins and showed that an evolutionary hotspot, the secondary pocket, is a key interface for binding to CLOCK and BMAL1. Moreover, I collected evidence that suggests that subtle divergence between CRY1 and 2 at the secondary pocket underlies some of the phenotypic differences in periodicity found in *Cry1*$^{-/-}$ and *Cry2*$^{-/-}$ mice. The data presented here support a model in which PER proteins stabilize the interaction between CRY2 and the CLOCK/BMAL1 heterodimer to a greater extent than CRY1, suggesting that the periodicity of CRY2-driven rhythms is partially the result of a restricted repressive window confined to the phase of PER expression. Despite this effort, a number of outstanding questions remain about how the repressors contribute to periodicity within the clock.

Contribution of secondary pocket architecture

The work presented here suggests that the secondary pocket architecture found in type II CRYs is critical for direct repression of CLOCK and BMAL1. However, more work is needed to determine whether this feature is *the* critical evolutionary step separating type I and II CRYs or perhaps one of a number of complementary evolutionary changes that converged on a direct repressive role for type II CRYs. Notably, the HI loop in CLOCK's PAS-B domain is conserved even in *Drosophila*, but CYCLE proteins have diverged in insects with some containing a BMAL1-like TAD and others (in particular, *Drosophila*) having a truncated C-terminus without a TAD (Rutila et al., 1998). It is possible too that type I CRYs have undergone uncharacterized evolutionary changes to make them more suitable binding partners for BMAL1's TAD. One way to test this hypothesis is to collect a variety of *Cry* gene sequences from insects and test their ability to rescue rhythms in mammalian fibroblasts lacking endogenous *Cry*. One might expect that type II CRYs from insects would be competent to drive rhythms in a mammalian system due to the strong relationship to mammalian CRYs, but it is certainly possible that the secondary pocket architecture of type II CRYs is merely a necessary though insufficient component of normal repressive activity. Developing a panel of chimeric CRYs built from type I and type II CRYs from both insect and vertebrate sources will be useful for this enterprise.

The seven divergent residues between CRY1 and CRY2 in the secondary pocket appear to play an outsized role in mediating physical interactions with CLOCK and BMAL1. However, it is not entirely clear how these residues stabilize or destabilize the ternary

complex, especially due to the fact that the changes are relatively conservative. Hydrophobic character is largely intact, as is overall charge character. Thus, the results presented here suggest that rather than a global change of the character of the pocket, these residues are mediating very specific interactions, likely with CLOCK's PAS-B domain (Michael et al., 2017). Understanding what these interactions are and how they mediate binding at this interface will likely require solving the structure of CRY bound to one or more other components, though this approach is obviously non-trivial. One alternative approach with the potential to provide similar insight with less hand-wringing is to purify and bind CRY and the CLOCK PAS-B domain, then covalently cross-link the complex, subject it to limited proteolysis, and perform mass spectrometry on the resulting protein fragments. This approach potentially offers the opportunity to identify residue-residue contacts at this interface and provide insight into the role of the divergent residues.

A surprising finding from the multiple structures of CRY1 and CRY2 published in the last few years is that the residues forming the "upper loop" (CRY1: 38-48, CRY2: 56-66) of the secondary pocket are ordered in every CRY2 structure and disordered in nearly every CRY1 structure, including two different apo structures solved in different space groups (Czarna et al., 2013; Michael et al., 2017). The upper loop is only ordered in the CRY1/PER2 CBD structure, which contains an artifactual PER2 structure right at the point of interaction with the upper loop of the secondary pocket making the results difficult to interpret (Schmalen et al., 2014). In contrast, the upper loop adopts an ordered, short helical structure in every CRY2 structure, including structures of the FBXL3 and PER2 CBD complexes and the structures bound to KL001 and FAD (Nangle et al., 2013; Nangle et al., 2014; Xing et al.,

2013). The two regions are primarily conserved, but there is a glycine to alanine and asparagine to serine divergence in the CRY2 structure. To speculate a bit, one wonders whether the glycine to alanine substitution in particular is responsible for stabilizing the region in CRY2 and in turn whether such a conformational change in this region might play a role in periodicity. It is certainly possible that locking this loop in place disrupts an otherwise slow conformational switch that delays interaction between CRY1 and CLOCK. The rescues presented in this work demonstrate that a double mutant in this loop (CRY1 G43A/N46S) accelerates the speed of the clock. Further characterization of this feature, especially through crystallography may provide insight into the association between CRY1 and CLOCK.

One interesting observation about insect type II CRYs in the context of CRY1/2 differences is that insect type II CRYs for the most part preserve the CRY1 secondary pocket architecture at the seven divergent sites. Amongst type II CRYs from butterflies, wasps, bees, moths, cockroaches, beetles, ants, and mosquitoes, divergence is seen only in two of the seven residues compared to CRY1, homologous to CRY1 G43 and CRY1 E382. A subset of these insect type II CRYs substitute a serine for the glycine observed in CRY1 and a different subset substitute an aspartate for the glutamate, just like CRY2. Ultimately, this observation suggests that in organisms with a single repressive CRY, the architecture of the secondary pocket supports the stronger repressive characteristics of CRY1. How the secondary pocket architecture integrates with other repressive interfaces on CRY in diverse species is a question for future interrogation.

The role of the tail

The chimera data reported here suggest that CRY1's tail plays a role in lengthening the period of the oscillation in fibroblast rescues. Moreover, it suggests that together the secondary pocket architecture and tail of CRY1 are necessary and sufficient to generate the long periods characteristic of WT CRY1. The next logical question following this finding is what the tail is doing to result in this delay.

One possibility is that the CRY1 tail is involved in mediating a protein-protein interaction with a known clock component like PER or BMAL1. Indeed, there is plenty of data indicating that CRY's CC helix is intimately involved in binding to both PER and BMAL1 (Nangle et al., 2014; Schmalen et al., 2014; Xu et al., 2015). There is additional evidence to suggest that the tails of CRY1 and 2 might have differential effects on the affinity of CRY for the BMAL1 TAD (Czarna et al., 2011). Notably, the authors of the latter study suggested that the lower affinity of CRY1's tail for the BMAL1 TAD was gated by acetylation of BMAL1 at K537. This observation suggests the tantalizing possibility that sequestration of the BMAL1 TAD by CRY1 is temporally gated by post-translational modification of BMAL1 by CLOCK's intrinsic HAT activity (Hirayama et al., 2007). However, Czarna and colleagues also demonstrated that substitution of an alanine at any of a trio of acidic residues in the CRY1 tail (E590, E591, and D592) increased the affinity of the tail for the BMAL1 TAD (Czarna et al., 2011). I tested the possibility that this would also affect periodicity by making these mutations individually or as a triple mutant and found that rescues with any of the four constructs had no significant effect on either periodicity or amplitude (data not shown). Regardless, a clear experiment to test this hypothesis would be

to generate two cell lines, a *Bmal1*$^{-/-}$ line and a *Bmal1*$^{-/-}$/*Cry1*$^{-/-}$ line, and perform rescues with either WT *Bmal1* or *Bmal1 K537Q* constructs. If acetylation at this site gates interaction with CRY1, then rescues with the two constructs should result in different periods in the *Bmal1*$^{-/-}$ line, but not in the *Bmal1*$^{-/-}$/*Cry1*$^{-/-}$ line.

In addition to affecting known protein-protein interactions in the clock, it is also possible that the tail mediates interactions with unknown clock components. To test for this possibility, one could express either WT or ΔTail CRY1 in a cycling cell line and perform IPs followed by mass spectrometry. Comparing the hit lists from each group might help to identify proteins specifically interacting with CRY1 through its C-terminal tail.

A third possibility is that the tail is involved in nuclear localization of CRY, an idea that is supported by work from Chaves and colleagues (Chaves et al., 2006). In fact, recent work suggests that the CRY1 and CRY2 tails underlie differences in nuclear localization dynamics (Li et al., 2016). Thus, a simple and meaningful experiment to perform is to express the various CRY chimeras that I have generated under the control of a constitutive promoter and look at the balance of nuclear localization in response to the various CRY1 or CRY2 features. Understanding the balance of CRY nuclear localization should provide insight into some of the structural features informing periodicity. However, a more complicated experiment is merited to fully elucidate cellular localization dynamics. Live cell imaging with various CRY chimeras fused to fluorescent proteins would not only capture the balance of cellular localization, but clarify the actual spatiotemporal dynamics of CRY localization, which is more relevant to understanding the function of the clock. Öllinger and colleagues provide a reasonable example for how to perform these experiments in their study

of PER cellular mobility (Ollinger et al., 2014), though one potential innovation is to express CRY under the control of its own promoter. Smyllie and colleagues took this experimental design a step further by generating a knock-in mouse with a PER2::VENUS fusion, which was used for live imaging and quantification of intracellular dynamics (Smyllie et al., 2016). Ideally, creating knock-in fusions of CRY1 and CRY2 would be valuable for understanding the intracellular dynamics of the two repressors, though even with CRISPR-Cas9, generating various chimeras would be difficult if not impossible.

One final possibility is that the C-terminal tail is playing a role in CRY1's stability. Again, this is an easily testable hypothesis. Using the luciferase fusion constructs that I generated, tail deletions of CRY1 and CRY2 can be produced and compared against each other as well as WT CRY1 and CRY2 in the degradation assay described earlier in this dissertation.

In addition to understanding what the tail is doing, it will be necessary to understand what aspect of the tail contributes to this role. Conceptually, it makes sense to first determine the role of the tail then identify the structural component that facilitates that role. However, once this initial determination has been made, it should be relatively straightforward to address this question. A number of factors could be involved including (but not limited to) the charge characteristics of the tail, the length of the tail, potential structured regions within this intrinsically disordered landscape, and potential binding epitopes within the tail. All of these possibilities can be tested by either deletion or mutagenesis of small sections of the tail and subsequent evaluation in the assay used to identify the role of the tail. Furthermore, it will be valuable to the circadian biology community to apply the lessons of this work to

understanding how this region of CRY specifies period not just in mice, but in a wide variety of organisms. How do the divergent tails in insect type II CRYs inform periodicity within those organisms? How does the C-terminus of mouse CRY1 compare to human or rat CRY1 given that it has undergone a short genome duplication in this region? Recent work characterizing a prevalent human mutation in the CRY1 tail (deletion of exon 11) suggests that it could in fact play a role of some kind (Patke et al., 2017).

Architecture of the repressive complex

The finding presented here that PER2 is necessary to stabilize the interaction between CRY2 and the CLOCK/BMAL1 heterodimer illuminates a controversy in the field, namely whether PER is necessary for CRY to bind to CLOCK/BMAL1 or CRY is necessary for PER to bind (Chen et al., 2009; Ye et al., 2011). The answers suggested by this work are (1) CRY2 requires PER to stably interact with CLOCK and BMAL1, but (2) CRY1 complexes CLOCK/BMAL1 by itself, in an interaction that is further stabilized in the presence of PER. Given this finding, a key question moving forward is how PER stabilizes the repressive complex from a structural perspective.

One simple approach to this question is breaking PER into pieces and identifying what pieces stabilize the complex by performing co-IPs as in the work presented here. Interestingly, Akashi and colleagues found that coexpression of PER1 or PER2 with CRY1 resulted in attenuation of CRY1's repressive capacity (Akashi et al., 2014). This effect was evident with full-length proteins, but not with truncated proteins missing their CBD. It was also evident using just the CBD. The authors showed that this effect was mediated by

competition between the CBD and BMAL1 for CRY1 and demonstrated that full-length PER2 and its CBD disrupted formation of the ternary complex using immunopurified *in vitro*-translated proteins. Although somewhat contradictory to my own work, this data suggests that the CBD is not sufficient to stabilize the repressive complex and may even inhibit its formation. Despite my own observation that full-length PER2 stabilizes the repressive complex in co-IPs of transiently transfected proteins, I found in a pilot experiment that the CBD disrupted the binding between CRY and the CLOCK/BMAL1 heterodimer (data not shown). Surprisingly, I found in the same pilot that a PER2 ΔCBD construct also disrupted this binding (data not shown). Although this experiment should be repeated, it suggests two things in concert with the data from Akashi et al. First, a minimal construct for stabilization of the repressive complex likely includes the PER2 CBD and some or all of the protein N-terminal to the CBD. Second, stabilization may be a dynamic process not captured in co-IPs from transiently transfected cells.

Consistent with the second conclusion, Ye and colleagues argued that CRY and PER repress the activity of CLOCK and BMAL1 through two different modes (Ye et al., 2014). CRY participates in "blocking-type" repression, essentially sequestering the BMAL1 TAD while leaving CLOCK and BMAL1 bound to DNA, and PER participates in "displacement-type" repression, removing the whole complex from DNA. In this context, it is important to think of the repressive complex not as a static structure, but as a network of competitive interfaces. In this network, allosteric interactions can be stabilizing or destabilizing. The former is probably best exemplified by a dual interaction between CRY and the CLOCK/BMAL1 heterodimer through both the secondary pocket and the CC helix. A stable

interaction will be slow to dissociate since CRY is held at two structurally distinct locations. It is possible that PER plays a role in this network by stabilizing one interaction while destabilizing another. A distinct possibility is that, when bound to the complex through another domain, the PER CBD competes with the BMAL1 TAD for an overlapping interface on the CRY CC helix. Through this interaction, the PER CBD would be able to facilitate the disengagement of CRY by blocking one of the two interfaces CRY uses to engage CLOCK and BMAL1.

Studying protein dynamics of a complex is challenging, but a first step is characterizing some of the known competitive interactions. In this case, NMR-based studies of the competition between the PER CBD and BMAL1 TAD may provide insight into how this critical CRY interface functions in the context of the complex. Additionally, recent work suggests that PER is interacting with CLOCK through its exon 19 domain, also implicated in binding to CIPC and MLL1 (Katada and Sassone-Corsi, 2010; Lee et al., 2016; Zhao et al., 2007). Characterization of this competitive interface is also of paramount importance in deciphering the molecular details of the clock. As we have seen recently, biophysical characterization of small domains of the clock can provide great insight into atomic level details even as a structure of the full complex remains elusive (Xu et al., 2015).

The work presented here also has implications for future work on a structure of the full complex. If PER is helping to stabilize the ternary complex, defining the minimal PER construct capable of performing this action is a first step toward identifying the potential components needed to lock the complex into a static form. Based on the work presented here and in the broader literature, one of the challenges in solving a structure of the complex is

that some of the crucial domains mediating this interaction are likely to be intrinsically disordered outside of the complex. There are four reasonable approaches to addressing this problem in crystallographic studies. First, testing deletion constructs that will be used for crystallography in transient transfection co-IPs before the arduous process of purifying proteins and setting up crystal screens should help to define the minimal components necessary for a stable complex. Clearly the BMAL1 TAD is crucial for binding CRY, but the long disordered C-terminus preceding it might not be. Removing as much of this region as possible while still preserving the interaction with CRY will likely be crucial for nucleating and growing nicely ordered crystals that diffract well. Whether CRY's tail is also involved in this interaction is still an open question. Likewise, finding a PER construct that stabilizes the complex with a minimum of disordered regions is critical. Second, an accounting of all the interactive surfaces in the quaternary complex will provide a guide as to what protein regions can be deleted with minimal effect on complex formation. Obviously the bHLH-PAS domains of CLOCK and BMAL1 are critical for heterodimer formation, the BMAL1 TAD is important for interaction with CRY, as is CLOCK's PAS-B domain. Recent work suggests that CLOCK's exon 19 region is important for binding to PER (Lee et al., 2016), but it is unknown what regions of PER mediate this interaction, nor is it clear whether PER is interacting with CLOCK or BMAL1 at additional sites. Ultimately, the most stable structure will likely be one that maintains the most native interactions while jettisoning extraneous disordered domains. Third, it might be necessary to determine whether there are additional proteins that stabilize this complex. Luckily, an exhaustive accounting of repressive complex components is already in progress, primarily in the Weitz lab. Screening these components

for a role in stabilizing the repressive complex should be relatively straightforward. Finally, given the conflicting data in the literature regarding the roles of PER and CRY in stabilizing the repressive complex, one gets the sense that there is a dynamic process unfolding over the course of the circadian cycle driven to some extent by shifting protein-protein interactions. Thus, in order to capture a relatively stable (and hopefully single-state) protein complex, expressing the components together and purifying the complex will likely be important. Of course this strategy has previously been employed successfully in crystallizing the CLOCK/BMAL1 bHLH-PAS heterodimer (Huang et al., 2012). This approach is especially important in trying to capture PER in the complex. Due to its elongated, intrinsically disordered structure, PER is likely to only adopt a more defined structure in complex with other protein-binding partners. Thus, purifying more than a small domain of PER by itself is probably impossible.

The role of PER proteins

The findings presented in this work demonstrate the profound importance of having a tractable, high-throughput rescue assay to gain insight into the structural underpinnings of core clock function. The biggest open question in circadian biology is still the precise role of PER proteins in the molecular clockwork. Facilitating inquiry into PER's role is of paramount importance to the future of circadian biology. As such, a high priority for future researchers should be the development of a high-throughput *Per* rescue assay. A recent attempt at developing a *Per* rescue assay was somewhat successful, but very low-throughput

in its design (Tamiya et al., 2016). However, as a proof of principle, this work suggests that a breakthrough is within reach.

Perhaps the most fascinating aspect of PER's role in the clock has to do with the timing of its expression. Of all the clock components tested, only PER expression must be rhythmic (Chen et al., 2009). However, the reason behind this observation is still elusive. It could be that PER is necessary to rhythmically stabilize CRY's interaction with CLOCK and BMAL1 as Chen and colleagues suggest (Chen et al., 2009). Alternatively, rhythmic expression of PER might be necessary to destabilize the activator/repressor complex and remove it from DNA (Ye et al., 2014). Some of the data presented here suggests that the latter idea may be closer to the truth. I found that a mutation that strongly disrupts binding between CRY1 and PER2 (CRY1 I487D/Y488D) was highly repressive in rescue assays, but failed to cycle. One interpretation of this experiment is that CRY1 can bind and repress CLOCK and BMAL1, but requires PER to disengage from the complex. However, I also observed in a pilot experiment that this particular CRY1 mutant is highly stabilized compared to WT CRY1 (data not shown), suggesting the alternative explanation that CRY is not degraded efficiently, locking the system into a hyperrepressive state. Yet comparison of the half-life of this mutant to CRY1 S588D demonstrates that its half-life is roughly 100 minutes less (Gao et al., 2013). Despite this fact, CRY1 S588D rescues are robustly rhythmic, supporting the idea that the hyperrepressive rescues generated by CRY1 I487D/Y488D result from something more than stabilization of CRY.

I favor a model in which PER plays a dynamic role in the repressive complex, paradoxically stabilizing and destabilizing the complex through shifting interactions with

competitive interfaces. Such a model helps to address conflicting reports of PER's role in structural interactions of the core clock proteins. Testing this model, on the other hand, is infinitely more complicated than generating it in the first place. An initial approach might be to mine the data from recent structural work for mutations that will disrupt particular PER interactions and combine that information with the assay used in Ye et al.'s report of displacement-type repression by PER (Ye et al., 2014). In this work, the authors fused an estrogen receptor to ectopically expressed PER2 to create an inducible nuclear entry system for PER2 in *Per1*$^{-/-}$/*Per2*$^{-/-}$ fibroblasts. Through this construct, they were able to look at dynamic effects of PER2 nuclear entry. Ye and colleagues used this system to further characterize PER domains and interactions and showed that both the CBD and CKIδ/ε-binding domain were necessary for dissociation of the activator/repressor complex from DNA four hours after initial induction of PER2 nuclear entry. The PAS domains were not necessary for this activity. Using this system, a fine-grained analysis utilizing both specific residue mutagenesis and more frequent sampling should provide further insight into PER dynamics in the repressive complex.

A final model for the mammalian molecular clock

Synthesizing data from the literature and the work reported here, a working model for the molecular clock involves both a number of characterized interfaces and a highly dynamic complex. In the activation phase, CLOCK and BMAL1 bind through their bHLH and PAS domains, recruiting MLL1 through an interaction with CLOCK's exon 19 and p300/CBP through an interaction with BMAL1's TAD (Huang et al., 2012; Katada and Sassone-Corsi,

2010; Xu et al., 2015). MLL1 methylates H3K4 and p300/CBP acetylate histones opening chromatin and facilitating transcription (Etchegaray et al., 2003; Katada and Sassone-Corsi, 2010; Takahata et al., 2000). p300/CBP also recruit additional transcriptional machinery along with TRAP150 (Etchegaray et al., 2003; Lande-Diner et al., 2013; Takahata et al., 2000). Recruitment of JARID1a during the positive phase antagonizes HDAC1, maintaining an acetylated histone state at H3K9 (DiTacchio et al., 2011). Also during the active phase, CLOCK and BMAL1 bind to WDR76, recruiting the DDB1-CUL4 complex to monoubiquitinate H2B, resulting in subsequent recruitment of PER complexes to clock-controlled genes during the repressive phase (Tamayo et al., 2015). Throughout the active phase, CLOCK and BMAL1 transcriptional activation promotes the expression of CRY and PER proteins, which accumulate in the cytoplasm and stabilize each other through an interaction between their C-termini (Nangle et al., 2014; Schmalen et al., 2014), and eventually translocate into the nucleus in part due to interaction with CKIδ/ε and the importin protein KPNB1 (Lee et al., 2015; Ollinger et al., 2014; Sakakida et al., 2005; Yagita et al., 2002). CRY associates with the CLOCK PAS-B domain through its secondary pocket, as shown in this work and the work of Michael et al. (Michael et al., 2017), and with BMAL1's TAD through its CC helix and tail (Czarna et al., 2011; Xu et al., 2015). This interaction sequesters the BMAL1 TAD, preventing it from interacting with p300/CBP, and also potentially disrupts the PAS-B interface of the CLOCK/BMAL1 heterodimer (Michael et al., 2017; Xu et al., 2015). Concurrently, PER interacts with CLOCK's exon 19 domain through an unknown structural motif, potentially sequestering this domain from interaction with MLL1 (Lee et al., 2016). Consistent with the work presented here, CRY2 reaches its peak

occupancy on DNA in the early evening due to stabilization of its interaction with CLOCK and BMAL1 by PER1 and PER2 (Koike et al., 2012). During this phase, PER1 and 2 assemble a large complex containing a number of histone modifying enzymes, which result in deacetylation of histones (Anafi et al., 2014; Annayev et al., 2014; Duong et al., 2011; Goriki et al., 2014; Kim et al., 2014) and methylation of H3K9 and H3K27 (Duong and Weitz, 2014; Etchegaray et al., 2006) at clock-controlled target genes and compaction of the chromatin to prevent additional transcription. CRY2, PER1, and PER2 are eventually degraded through interactions with FBXL3, FBXL21, CKIδ/ε, and β-TRCP (Busino et al., 2007; Godinho et al., 2007; Hirano et al., 2013; Shirogane et al., 2005; Siepka et al., 2007; Yoo et al., 2013). Finally, a late repressive complex forms in which CRY1 forms a strong interaction between its secondary pocket and the CLOCK PAS-B domain as well as its CC helix and the BMAL1 TAD. CLOCK's exon 19 is free to recruit MLL1 during this timeframe facilitating chromatin decompaction and a poised state ready for transcription following the degradation of CRY1.

Finally, to revisit a point from the introduction to this work, a surprising number of protein-protein interfaces in the circadian complex are shared between multiple binding partners. In essence, this sort of architecture makes sense as an intrinsic mechanism for what is essentially a timing system. At these interfaces, typified by the BMAL1 TAD, the CRY CC helix, and the CLOCK exon 19 region, the dynamics of the competitive interactions are likely playing a very large role in determining periodicity, much more so than some of the fine tuning occurring at other layers of regulation, such as posttranscriptional regulation and epigenetic regulation. Indeed, many of the largest shifts in period *in vivo* result from

mutations that disrupt the balance of negative regulators in the nucleus either by destabilizing PER or stabilizing CRY (Busino et al., 2007; Godinho et al., 2007; Ralph and Menaker, 1988; Siepka et al., 2007). Critically, we see the same dramatic shifts in periodicity when changing the rules of the interaction rather than the levels of CRY and PER, as shown in my work characterizing the interface between CRY and CLOCK at the secondary pocket and the work by Xu and colleagues characterizing the interface between CRY and the BMAL1 TAD (Xu et al., 2015). Thus, future attempts to build a coherent model of clock function and timing should focus on understanding the dynamics and kinetics of the interactions at these interfaces.

APPENDICES

APPENDIX A
Primers for Agilent site-directed mutagenesis

Mutation	*Forward Primer (3' --> 5')*	*Reverse Primer (3' --> 5')*
Cry1 K11E	GTGAACGCCGTGCACTGGTTCCGAGAGGGACTC	GTTGTCGTGGAGCCGGAGTCCCTCTCG
Cry1 E103K	ATCACTAAACTCTCAATTGAGTATGATTCTAAGCCT	ATCTCGTTCCTTCCCAAAAGGCTTAGAATC
Cry1 G106R	GTATGATTCTGAGCCTTTTAGGAAGGAACGAGATGCAGC	GCTGCATCTCGTTCCTTCCTAAAAGGCTCAGAATCATAC
Cry1 K107E	GAGTATGATTCTGAGCCTTTTGGGGAGGAA	GATAGCTGCATCTCGTTCCTCCCCAA
Cry1 R109Q	GCCTTTTGGGAAGGAACAAGATGCAGCTATCAAGAAG	CTTCTTGATAGCTGCATCTTGTTCCTTCCCAAAAGGC
Cry1 T118A	GAACGAGATGCAGCTATCAAGAAGCTGGCTGC	ACTTCCACGCCAGCCTCAGCAGCCAGCTTCTT
Cry1 G121R	CTATCAAGAAGCTGGCTACTGAGGCTCG	GACGATGACTTCCACGCGAGCCTCAGTA
Cry1 G204D	GGCTTTGATACAGATGACCTGTCCTCTGCAGTG	CACTGCAGAGGACAGGTCATCTGTATCAAAGCC
Cry1 G212R	GCCTGTCCTCTGCAGTGTGGCCAAGAGGA	TGTAAGTGCCTCAGTTTCTCCTCTTGGCCA
Cry1 E214K	GTGTGGCCAGGAGGAAAAACTGAGGCACTTAC	GTAAGTGCCTCAGTTTTTCCTCCTGGCCACAC
Cry1 E216K	GCCAGGAGGAGAAACTAAGGCACTTACACGTTTG	CAAACGTGTAAGTGCCTTAGTTTCTCCTCCTGGC
Cry1 A217T	TGGCCAGGAGGAGAAACTGAGACGCTT	ATGCCTTTCCAAACGTGTAAGCGTCTCAGT
Cry1 L218F	AGGAGGAGAAACTGAGGCATTTACA	AATGCCTTTCCAAACGTGTAAATGCCT
Cry1 R236A/R238A	CCTGGGTGGCAAACTT	GCAGGGAGTTTGCATT

	TGAAGCACCTGCAATG AATGCAAACTCCCTGC	CATTGCAGGTGCTTCA AAGTTTGCCACCCAGG
Cry1 Y254D	GCCCAACTGGACTCAG TCCTGATCTCCGC	CCGACATGATAAACAA CCAAAGCGGAGATCAG G
Cry1 F257A	AGTCCTTATCTCCGCG CTGGTTGTTTATC	AGATAAGGACTGAGTC CAGTTGGGC
Cry1 C259Y	GTCCTTATCTCCGCTT TGGTTATTTATCATGTC GGCTG	CAGCCGACATGATAAA TAACCAAAGCGGAGAT AAGGAC
Cry1 E332K	TGGCCAAATGGGCAAA AGGCCG	GGGAAGCCTGTCCGG CCTTTTG
Cry1 G333D	CCAAATGGGCAGAAGA CCGGACAGGCTTCC	GGAAGCCTGTCCGGT CTTCTGCCCATTTGG
Cry1 F337A	CAGAAGGCCGGACAG GCGCCCCGTGGATTG	AGCTGAGTCATGATGG CGTCAATCCACGGGG CG
Cry1 P338L	CGGACAGGCTTCCTGT GGATTGACGCC	GGCGTCAATCCACAGG AAGCCTGTCCG
Cry1 D341A	ACAGGCTTCCCGTGGA TTGCCGCCAT	TGACGAAGCTGAGTCA TGATGGCGGCAATC
Cry1 T345A	CGTGGATTGACGCCAT CATGGCTC	TCCTGACGAAGCTGAG CCATGATG
Cry1 E350K	GCCATCATGACTCAGC TTCGTCAGAAGGGC	TGGCTAAATGGTGGAT CCAGCCCTTCTGAC
Cry1 F409A	CTGTCCTGCAGTTCCT TTTTTCAGCAAGCTTTT CACT	CCACAGGGCAGTAGC AGTGAAAAGCTTGCTG
Cry1 H411A	GCAGTTCCTTTTTTCA GCAATTTTTTGCCTGC TACTGCCCTG	CAGGGCAGTAGCAGG CAAAAAATTGCTGAAA AAAGGAACTGC
Cry1 G419D	GCCCTGTGGGTTTTGA TAGGAGGACAGATCCC	GGGATCTGTCCTCCTA TCAAAACCCACAGGGC

APPENDIX B
Primers for NEB site-directed mutagenesis

Mutation	*Forward Primer (3' --> 5')*	*Reverse Primer (3' --> 5')*
Cry1 D38A	TATATCCTCGCCCCCTGGTTCG	GACGCAGCGGATGGTGTC
Cry1 P39G	TATCCTCGACGGCTGGTTCGCCGG	TAGACGCAGCGGATGGTG
Cry1 F41S	GACCCCTGGTCCGCCGGCTCT	GAGGATATAGACGCAGCGGATGGTG
Cry1 G43A/N46S	TCCAGCGTGGGCATCAACAGGTGG	AGAGGCGGCGAACCAGGGGTCGA
Cry1 N50A	CGTGGGCATCGCCAGGTGGCGATTTTTG	TTGGAAGAGCCGGCGAAC
Cry1 R51A	GGGCATCAACGCGTGGCGATTTTTGCTTCAG	ACGTTGGAAGAGCCGGCG
Cry1 L55D	GTGGCGATTTGATCTTCAGTGTCTTGAG	CTGTTGATGCCCACGTTG
Cry1 Y100A	CTCAATTGAGGCTGATTCTGAGCCTTTTG	AGTTTAGTGATGTTCCATTC
Cry1 F105A	GAGATGCAGCTATCAAGAAG	GTTCCTTCCCAGCAGGCTCAG
Cry1 G106W	TGAGCCTTTTTGGAAGGAACG	GAATCATACTCAATTGAGAGTTTAG
Cry1 E108K	TTTTGGGAAGAAACGAGATGC	GGCTCAGAATCATACTCAATTG
Cry1 S129A	CGTGCGCATTGCACATACACTG	ATGACTTCCACGCCAGCC
Cry1 H130E	GCGCATTTCAGAGACACTGTATGAC	ACGATGACTTCCACGCCA
Cry1 T131F	CATTTCACATTTCCTGTATGACCTGGACAAGATC	CGCACGATGACTTCCACG
Cry1 L132E	TTCACATACAGAGTATGACCTGGACAAGATC	ATGCGCACGATGACTTCC
Cry1 Y133D	ACATACACTGGATGACCTGGAC	GAAATGCGCACGATGACTTC
Cry1 D134A	ACACTGTATGCCCTGGACAAG	ATGTGAAATGCGCACGATG

Cry1 L135D	ACTGTATGACGATGAC AAGATCATAGAACTC	GTATGTGAAATGCGCA CG
Cry1 T149E	GCCACCTCTAGAGTAT AAAAGGTTTCAGACTC TC	TGTCCGCCATTGAGTT CTATG
Cry1 T215A	AGGAGGAGAAGCTGA GGCACTTAC	GGCCACACTGCAGAG GAC
Cry1 R227A	GCATTTGGAAGCAAAG GCCTGG	CTTTCCAAACGTGTAA GTG
Cry1 R263A	TTTATCATGTGCGCTG TTTTATTTCAAACTAAC	CAACCAAAGCGGAGAT AAG
Cry1 G288R	TTCTCTTTATAGGCAAC TCCTGTG	AGGGGAGGGGAACTA TTC
Cry1 E294K	CCTGTGGCGTAAATTT TTTTATAC	AGTTGCCCATAAAGAG AAAG
Cry1 D307A	CCACGCTTTGCCAAAA TGGAAG	GTTGTTTGTGGCTGCT GT
Cry1 A331E	GCCAAATGGGAAGAAG GCCGG	CAGAGCCTCGGGGTT CTTG
Cry1 G336D	GGCCGGACAGACTTC CCGTGG	TTCTGCCCATTTGGCC AGAG
Cry1 F337D	CCGGACAGGCGACCC GTGGATT	CCTTCTGCCCATTTGG CC
Cry1 R348A	GACTCAGCTTGCTCAG GAGGGCTG	ATGATGGCGTCAATCC AC
Cry1 E376S	CAGCTGGGAATCAGG GATGAAGGTC	ATCCACAGGTCACCAC GA
Cry1 E376S/M378V/K379R/E382D/W390F	GTTACTGCTTGATGCA GATTTTAGCATAAATG CTGGAAGTTG	TCATCAAAGACCCTCA CCCCTGATTCCCAGCT GATCCACAG
Cry1 M378V	GGAAGAAGGGGTGAA GGTCTTTG	CAGCTGATCCACAGGT CAC
Cry1 M378V/K379R/E382D	CTTTGATGAGTTACTG CTTGATGCAG	ACCCTCACCCCTTCTT CCCAGCTGATC
Cry1 K379R	GAAGGGATGAGGGTC TTTGAAG	TTCCCAGCTGATCCAC AG
Cry1 E382A	AAGGTCTTTGCAGAGT TACTGCTTG	CATCCCTTCTTCCCAG CTG
Cry1 E382D	AGGTCTTTGATGAGTT ACTGCTTG	TCATCCCTTCTTCCCA GC
Cry1 E383A	GTCTTTGAAGCGTTAC TGCTTG	CTTCATCCCTTCTTCC CAG

Cry1 L384A	CTTTGAAGAGGCACTG CTTGATGC	ACCTTCATCCCTTCTTC C
Cry1 W390F	GATGCAGATTTCAGCA TAAATGCTG	AAGCAGTAACTCTTCA AAGAC
Cry1 S391A	TGCAGATTGGGCCATA AATGCTGG	TCAAGCAGTAACTCTT CAAAG
Cry1 F410A	TCAGCAATTTGCTCAC TGCTACTG	AAAAAGGAACTGCAGG AC
Cry1 V416K	CTACTGCCCTAAGGGT TTTGGTAG	CAGTGAAAAAATTGCT GAAAAAAG
Cry1 L436A	TTTACCTGTCGCAAGA GGCTTCC	TAACGCCTAATATAGT CTCC
Cry1 L436D	TTTACCTGTCGATAGA GGCTTCCCTG	TAACGCCTAATATAGT CTCC
Cry1 F439A	CCTAAGAGGCGCCCCT GCAAAATATATC	ACAGGTAAATAACGCC TAATATAG
Cry1 F439D	CCTAAGAGGCGACCCT GCAAAATATATC	ACAGGTAAATAACGCC TAATATAG
Cry1 I444A	TGCAAAATATGCCTAC GATCCTTGGAATG	GGGAAGCCTCTTAGGA CAG
Cry1 I444D	TGCAAAATATGACTAC GATCCTTGGAATG	GGGAAGCCTCTTAGGA CAG
Cry1 M470A	CCCCAAACCGGCGGT GAACCATG	TAATTAACTCCTATCAA ACACTTG
Cry1 V471A	AAACCGATGGCGAACC ATGCTG	GGGGTAATTAACTCCT ATCAAAC
Cry1 A474K	GGTGAACCATAAGGAG GCAAGCAG	ATCGGTTTGGGGTAAT TAAC
Cry1 R483A	GAATATTGAAGCAATG AAGCAGATCTATCAGC AG	AGTCTGCTTGCCTCAG CA
Cry1 K485A	TGAAAGAATGGCGCAG ATCTATCAGC	ATATTCAGTCTGCTTG CC
Cry1 S588D	GAAGCGTCCTGATCAG GAAGAGGATGCCCAG	CCACTGCTGAGGCCG GTG
Cry2 A61G/S64N	TCGAATGTGGGCATCA ACCGATGGAG	GGAGCCCGCGAACCA CGGGTCGA
Cry2 V396M/R397K/D400E	ATTTGAAGAGCTGCTC CTGGATGCC	ACCTTCATCCCGCTCT CCCAGCTGAC
Cry2 S394E/V396M/R397K/D400E/F406W	GCTGCTCCTGGATGCC GATTGGAGTGTGAATG CAGGCAGC	TCTTCAAATACCTTCAT CCCTTCCTCCCAGCTG ACCCAGAG

pMU2-P(Cry1)-(intron336)-mCry1-Myc: Addition of Myc tag to C-term in rescue vector	AGCGAAGAAGATCTGTGAATCTATGTCGGGTGCG	AATCAGTTTCTGTTCGTTACTGCTCTGCCGCTG
pMU2-P(Cry1)-(intron336)-Myc: Deletion of mCry1 coding sequence from Myc-tagged rescue vector	GAACAGAAACTGATTAGCG	AATACCCATAATAGCTGTTTG
pCMV-Tag3C-Myc-dLuc: Deletion of mCry1 coding sequence from pCMV-Tag3C-Myc-mCry1-dLuc vector	ATGGAAGACGCCAAAAAC	TTGATATCGAATTCCTGCAG
CerC/VenC-Clock 1-395: Deletion of C-terminal residues of mClock after aa 395 in pEGFP-C1 vector	TGATCATAATCAGCCATACC	AAGAGACTCTTCAATGCC
CerC/VenC-Clock 89-395: Deletion of N-terminal residues of mClock (1-395) from aa 2-88 in pEGFP-C1 vector	CAGTCAGATGCTAGTGAGATTCGACAG	CATGCCCGCGGTACCGTC

APPENDIX C
Primers for megaprimer mutagenesis

Final Vector	*Primary PCR Vector*	*Forward Primer (3' --> 5')*	*Reverse Primer (3' --> 5')*	*Secondary PCR Vector*
pMU2-P(*Cry1*)-(intron336)-mCry2-Myc	pCMV-Tag3C-Myc-*mCry2*	CTAGATGGCAAACAGCTATTATGGGTATTATGGCGGCGGCTGCTGTGGTGGCAGCGACG	CAGATCTTCTTCGCTAATCAGTTTCTGTTCGGAGTCCTTGCTTGCTGGCTCTTGGGTAGG	pMU2-P(Cry1)-(intron336)-Myc
pCMV-Tag3C-Myc-mCry1-dLuc	pGL3-P(*Per2*)-dLuc	GGCCCCAAAGTCCAGCGGCAGAGCAGTAACATGGAAGACGCCAAAAACATAAAGAAAGGC	CTTAATTAATTAAGGTACCGGGCCCCCCCTCGAGTTACACGGCGATCTTTCCGCCCTTCTTGGC	pCMV-Tag3C-Myc-*mCry1*
pCMV-Tag3C-Myc-mCry2-dLuc	pGL3-P(*Per2*)-dLuc	CCTACCCAAGAGCCAGCAAGCAAGGACTCCATGGAAGACGCCAAAAACATAAAGAAAGGC	AATTAAGGTACCGGGCCCCCCCTCGAGTCATTACACGGCGATCTTTCCGCCCTTCTTGGC	pCMV-Tag3C-Myc-*mCry2*

APPENDIX D
Primers for Gibson Assembly

Target Vector for Linearization	*Forward Primer (3' --> 5') for linearization*	*Reverse Primer (3' --> 5') for linearization*
pMU2-P(*Cry1*)-(intron336)-mCry1-Myc	GAACAGAAACTGATTAGCGAAGAAGATCTG	TAGCCCTCTGTACCGGGAAAG
pMU2-P(*Cry1*)-(intron336)-mCry1 7m-Myc	GAACAGAAACTGATTAGCGAAGAAGATCTG	TAGCCCTCTGTACCGGGAAAG
pMU2-P(*Cry1*)-(intron336)-mCry2-Myc	GAACAGAAACTGATTAGCGAAG	GAGTCCCCGGTATCTCGAC
pMU2-P(*Cry1*)-(intron336)-mCry2 7m-Myc	GAACAGAAACTGATTAGCGAAG	GAGTCCCCGGTATCTCGAC

Insert PCR Starting Vector	*Forward Primer (3' --> 5') to PCR insert*	*Reverse Primer (3' --> 5') to PCR Insert*
pMU2-P(*Cry1*)-(intron336)-mCry1-Myc	TGTCGAGATACCGGGGACTCGGTCTTCTCGCCTCGGTC	TCGCTAATCAGTTTCTGTTCGTTACTGCTCTGCCGCTG
pMU2-P(*Cry1*)-(intron336)-mCry2-Myc	TTTCCCGGTACAGAGGGCTATGTCTATTGGCATCTGTCCC	TCGCTAATCAGTTTCTGTTCGGAGTCCTTGCTTGCTGG

APPENDIX E
Key Resources Table

REAGENT or RESOURCE	SOURCE	IDENTIFIER
Antibodies		
EZview Red anti-c-myc Affinity Gel (Rabbit polyclonal anti-c-Myc)	Sigma-Aldrich	E6654
Mouse monoclonal anti-Myc	Cell Signaling	2276S
Mouse monoclonal anti-V5	Thermo Fisher Scientific	R960-25
Mouse monoclonal anti-Flag M2-Peroxidase	Sigma-Aldrich	A8592
Anti-Mouse IgG, HRP-linked Secondary	Cell Signaling	7076S
Chemicals, Peptides, and Recombinant Proteins		
Dexamethasone	Sigma-Aldrich	D4902
Forskolin	Sigma-Aldrich	F3917
Ampicillin	Sigma-Aldrich	A9518
Kanamycin	Sigma-Aldrich	K0129
Chloramphenicol	Sigma-Aldrich	C0378
Quick Ligase	New England Biolabs	M2200
DpnI	New England Biolabs	R0176
T4 Polynucleotide Kinase	New England Biolabs	M0201
Cycloheximide	Sigma-Aldrich	C4859
Protease Inhibitor Cocktail	Sigma-Aldrich	P8340
FuGENE 6	Promega	E2692
Dulbecco's Modified Eagle Medium (DMEM)	Thermo Fisher Scientific	11965-092
Fetal Bovine Serum	Sigma-Aldrich	F0926-500ML
Penicillin/Streptomycin Antibiotics	Thermo Fisher Scientific	15070-063
Powdered DMEM without phenol red	Corning	90-013-PB
HEPES buffer	Thermo Fisher Scientific	15630
D-Luciferin Firefly, sodium salt monohydrate	Biosynth	L8240
Sodium Pyruvate	Thermo Fisher Scientific	11360-070
Sodium Bicarbonate	Thermo Fisher Scientific	25080
L-glutamine	Thermo Fisher Scientific	25030
PfuUltra II Fusion HS DNA	Agilent Technologies	600670

polymerase		
Trizma base	Sigma-Aldrich	T1503
Sodium Chloride	Sigma-Aldrich	S7653
Glycerol	Thermo Fisher Scientific	BP229-1
Dithiothreitol (DTT)	Sigma-Aldrich	D9779
Triton X-100	Sigma-Aldrich	T8787
Sodium Dodecyl Sulfate	Sigma-Aldrich	L4509
β-mercaptoethanol	Thermo Fisher Scientific	AC125472500
Bromophenol Blue	Sigma-Aldrich	B5525
Tween 20	Sigma-Aldrich	P1379
Critical Commercial Assays		
QuikChange II XL Site-Directed Mutagenesis Kit	Agilent Technologies	200521
Q5 Site-Directed Mutagenesis Kit	New England Biolabs	E0554S
2X Q5 PCR Master Mix	New England Biolabs	M0494S
NEBuilder HiFi DNA Assembly Master Mix	New England Biolabs	E2621
Qiaprep Spin Miniprep Kit	Qiagen	27106
QIAquick PCR Purification Kit	Qiagen	28104
Clarity Western ECL Substrate	BioRad	170-5060
Deposited Data		
NCBI non-redundant protein sequence database	National Center for Biotechnology Information	https://www.ncbi.nlm.nih.gov/protein
CPD Photolyase from E. coli	PDB: 1DNP	www.rcsb.org
CPD Photolyase from A. nidulans	PDB: 1QNF	www.rcsb.org
6-4 Photolyase from A. thaliana	PDB: 3FY4	www.rcsb.org
CPD Photolyase from T. thermophilus	PDB: 2J07	www.rcsb.org
CRY from D. melanogaster	PDB: 4GU5	www.rcsb.org
CRY1 from M. musculus	PDB: 4K0R	www.rcsb.org
CRY2 from M. musculus	PDBs: 4I6E, 4I6G	www.rcsb.org
CRY2 and FBXL3 complex from M. musculus	PDB: 4I6J	www.rcsb.org
CRY1 and PER2 Cry-Binding Domain from M. musculus	PDB: 4CT0	www.rcsb.org
CRY2 and PER2 Cry-Binding	PDB: 4U8H	www.rcsb.org

Domain from M. musculus		
CRY1 from M. musculus	PDB: 5T5X	www.rcsb.org
Experimental Models: Cell Lines		
Cry1-/-/Cry2-/- mouse embryonic fibroblasts	(Ukai-Tadenuma et al., 2011)	
HEK 293A	Thermo Fisher Scientific	R70507
Recombinant DNA		
pMU2-P(Cry1)-(intron336)-mCry1-Myc	Modified from (Ukai-Tadenuma et al., 2011)	
pMU2-P(Cry1)-(intron336)-mCry2-Myc	Modified from (Ukai-Tadenuma et al., 2011)	
pCMV-tag3c-Myc-mCry1	(McCarthy et al., 2009)	
pCMV-tag3c-Myc-mCry2	(McCarthy et al., 2009)	
pCMV-tag3c-Myc-mCry1-dLuc	Modified from (McCarthy et al., 2009)	
pCMV-tag3c-Myc-mCry2-dLuc	Modified from (McCarthy et al., 2009)	
pGL3-P(Per2)-dLuc	(Sato et al., 2006)	
p3XFlag-CMV-10 DEST-mBmal1	Full-length mBmal1 cDNA cloned into p3XFlag-CMV-10 at attB1 and attB2 sites using Gateway cloning system.	Backbone: Sigma Aldrich E4401
p3XFlag-CMV-10-mClock	Full-length mClock cDNA cloned into p3XFlag-CMV-10 at NotI and BglII sites.	Backbone: Sigma Aldrich (E4401)
pcDNA3.1-mPer2-V5	(Kume et al., 1999)	
mCry1-CerN and mCry1-VenN	(Yoo et al., 2013)	
mCry2-CerN and mCry2-VenN	(Yoo et al., 2013)	
CerC-Clock (89-395)	Full-length Clock cDNA cloned into Sac2 site and Sma1 sites in CerC vector from (Huang et al., 2012). Deletions made by site-directed mutagenesis.	Backbone: pEGFP-C1 from Clontech (632470)
H2B-mRFP1	(Li et al., 2007)	
Software and Algorithms		
pySCA v6.2	(Rivoire et al., 2016)	https://github.com/reynoldsk/pySCA

Python 2.7.9	Python Software Foundation	https://python.org
IPython 3.0.0	(Pérez and Granger, 2007)	https://ipython.org
Custom scripts for SCA processing (alnFilterSeqSize.py, alnParseGI.py, alnReplaceHeaders.py, Header fixing script)	This paper	Available upon request
MUSCLE	(Edgar, 2004)	http://drive5.com/muscle/
Promals3D	(Pei et al., 2008)	http://prodata.swmed.edu/promals3d/promals3d.php
Protein BLAST	National Center for Biotechnology Information	https://blast.ncbi.nlm.nih.gov/Blast.cgi
GraphPad Prism	GraphPad Software, Inc.	http://www.graphpad.com
		Version 7.0a Mac
CellProfiler	(Kamentsky et al., 2011)	cellprofiler.org Version 2.1.1 Mac
MacPyMol	The PyMOL Molecular Graphics System, Schrödinger, LLC.	PyMOL v1.7.0.3 Enhanced for Mac OS X
ImageJ	NIH, USA	https://imagej.nih.gov/ij
LumiCycle Analysis	Actimetrics	http://actimetrics.com/downloads/lumicycle/
		Version 2.40
softWoRx	GE Healthcare	Version 6.5.1
CLC Main Workbench 7	Qiagen	Version 7.7.2
Other		
Deltavision Personal DV Imaging System	GE Healthcare	
Olympus IX71 microscope		
LumiCycle	Actimetrics	LumiCycle

Black Visiplates	Perkin-Elmer

BIBLIOGRAPHY

Adams, P.D., Afonine, P.V., Bunkoczi, G., Chen, V.B., Davis, I.W., Echols, N., Headd, J.J., Hung, L.W., Kapral, G.J., Grosse-Kunstleve, R.W.*, et al.* (2010). PHENIX: a comprehensive Python-based system for macromolecular structure solution. Acta crystallographica Section D, Biological crystallography *66*, 213-221.

Aguilar-Arnal, L., Hakim, O., Patel, V.R., Baldi, P., Hager, G.L., and Sassone-Corsi, P. (2013). Cycles in spatial and temporal chromosomal organization driven by the circadian clock. Nature structural & molecular biology *20*, 1206-1213.

Aguilar-Arnal, L., Katada, S., Orozco-Solis, R., and Sassone-Corsi, P. (2015). NAD(+)-SIRT1 control of H3K4 trimethylation through circadian deacetylation of MLL1. Nature structural & molecular biology *22*, 312-318.

Akashi, M., Okamoto, A., Tsuchiya, Y., Todo, T., Nishida, E., and Node, K. (2014). A positive role for PERIOD in mammalian circadian gene expression. Cell reports *7*, 1056-1064.

Akashi, M., Tsuchiya, Y., Yoshino, T., and Nishida, E. (2002). Control of intracellular dynamics of mammalian period proteins by casein kinase I epsilon (CKIepsilon) and CKIdelta in cultured cells. Molecular and cellular biology *22*, 1693-1703.

Albrecht, U., Sun, Z.S., Eichele, G., and Lee, C.C. (1997). A differential response of two putative mammalian circadian regulators, mper1 and mper2, to light. Cell *91*, 1055-1064.

Allada, R., White, N.E., So, W.V., Hall, J.C., and Rosbash, M. (1998). A mutant Drosophila homolog of mammalian Clock disrupts circadian rhythms and transcription of period and timeless. Cell *93*, 791-804.

Anafi, R.C., Lee, Y., Sato, T.K., Venkataraman, A., Ramanathan, C., Kavakli, I.H., Hughes, M.E., Baggs, J.E., Growe, J., Liu, A.C.*, et al.* (2014). Machine learning helps identify CHRONO as a circadian clock component. PLoS biology *12*, e1001840.

Annayev, Y., Adar, S., Chiou, Y.Y., Lieb, J.D., Sancar, A., and Ye, R. (2014). Gene model 129 (Gm129) encodes a novel transcriptional repressor that modulates circadian gene expression. The Journal of biological chemistry *289*, 5013-5024.

Aronson, B.D., Johnson, K.A., Loros, J.J., and Dunlap, J.C. (1994). Negative feedback defining a circadian clock: autoregulation of the clock gene frequency. Science *263*, 1578-1584.

Asher, G., Gatfield, D., Stratmann, M., Reinke, H., Dibner, C., Kreppel, F., Mostoslavsky, R., Alt, F.W., and Schibler, U. (2008). SIRT1 regulates circadian clock gene expression through PER2 deacetylation. Cell *134*, 317-328.

Bae, K., Jin, X., Maywood, E.S., Hastings, M.H., Reppert, S.M., and Weaver, D.R. (2001). Differential functions of mPer1, mPer2, and mPer3 in the SCN circadian clock. Neuron *30*, 525-536.

Balsalobre, A., Brown, S.A., Marcacci, L., Tronche, F., Kellendonk, C., Reichardt, H.M., Schutz, G., and Schibler, U. (2000a). Resetting of circadian time in peripheral tissues by glucocorticoid signaling. Science *289*, 2344-2347.

Balsalobre, A., Marcacci, L., and Schibler, U. (2000b). Multiple signaling pathways elicit circadian gene expression in cultured Rat-1 fibroblasts. Current biology : CB *10*, 1291-1294.

Bargiello, T.A., Jackson, F.R., and Young, M.W. (1984). Restoration of circadian behavioural rhythms by gene transfer in Drosophila. Nature *312*, 752-754.

Bargiello, T.A., and Young, M.W. (1984). Molecular genetics of a biological clock in Drosophila. Proceedings of the National Academy of Sciences of the United States of America *81*, 2142-2146.

Brautigam, C.A., Smith, B.S., Ma, Z., Palnitkar, M., Tomchick, D.R., Machius, M., and Deisenhofer, J. (2004). Structure of the photolyase-like domain of cryptochrome 1 from Arabidopsis thaliana. Proceedings of the National Academy of Sciences of the United States of America *101*, 12142-12147.

Brown, S.A., Ripperger, J., Kadener, S., Fleury-Olela, F., Vilbois, F., Rosbash, M., and Schibler, U. (2005). PERIOD1-associated proteins modulate the negative limb of the mammalian circadian oscillator. Science *308*, 693-696.

Brunger, A.T., Adams, P.D., Clore, G.M., DeLano, W.L., Gros, P., Grosse-Kunstleve, R.W., Jiang, J.S., Kuszewski, J., Nilges, M., Pannu, N.S.*, et al.* (1998). Crystallography

& NMR system: A new software suite for macromolecular structure determination. Acta crystallographica Section D, Biological crystallography *54*, 905-921.

Busino, L., Bassermann, F., Maiolica, A., Lee, C., Nolan, P.M., Godinho, S.I., Draetta, G.F., and Pagano, M. (2007). SCFFbxl3 controls the oscillation of the circadian clock by directing the degradation of cryptochrome proteins. Science *316*, 900-904.

Chang, D.C., McWatters, H.G., Williams, J.A., Gotter, A.L., Levine, J.D., and Reppert, S.M. (2003). Constructing a feedback loop with circadian clock molecules from the silkmoth, Antheraea pernyi. The Journal of biological chemistry *278*, 38149-38158.

Chaves, I., Pokorny, R., Byrdin, M., Hoang, N., Ritz, T., Brettel, K., Essen, L.O., van der Horst, G.T., Batschauer, A., and Ahmad, M. (2011). The cryptochromes: blue light photoreceptors in plants and animals. Annual review of plant biology *62*, 335-364.

Chaves, I., Yagita, K., Barnhoorn, S., Okamura, H., van der Horst, G.T., and Tamanini, F. (2006). Functional evolution of the photolyase/cryptochrome protein family: importance of the C terminus of mammalian CRY1 for circadian core oscillator performance. Molecular and cellular biology *26*, 1743-1753.

Chen, R., Schirmer, A., Lee, Y., Lee, H., Kumar, V., Yoo, S.H., Takahashi, J.S., and Lee, C. (2009). Rhythmic PER abundance defines a critical nodal point for negative feedback within the circadian clock mechanism. Molecular cell *36*, 417-430.

Cho, H., Zhao, X., Hatori, M., Yu, R.T., Barish, G.D., Lam, M.T., Chong, L.W., DiTacchio, L., Atkins, A.R., Glass, C.K.*, et al.* (2012). Regulation of circadian behaviour and metabolism by REV-ERB-alpha and REV-ERB-beta. Nature *485*, 123-127.

Czarna, A., Berndt, A., Singh, H.R., Grudziecki, A., Ladurner, A.G., Timinszky, G., Kramer, A., and Wolf, E. (2013). Structures of Drosophila cryptochrome and mouse cryptochrome1 provide insight into circadian function. Cell *153*, 1394-1405.

Czarna, A., Breitkreuz, H., Mahrenholz, C.C., Arens, J., Strauss, H.M., and Wolf, E. (2011). Quantitative analyses of cryptochrome-mBMAL1 interactions: mechanistic insights into the transcriptional regulation of the mammalian circadian clock. The Journal of biological chemistry *286*, 22414-22425.

DiTacchio, L., Le, H.D., Vollmers, C., Hatori, M., Witcher, M., Secombe, J., and Panda, S. (2011). Histone lysine demethylase JARID1a activates CLOCK-BMAL1 and influences the circadian clock. Science *333*, 1881-1885.

Doi, M., Hirayama, J., and Sassone-Corsi, P. (2006). Circadian regulator CLOCK is a histone acetyltransferase. Cell *125*, 497-508.

Duong, H.A., Robles, M.S., Knutti, D., and Weitz, C.J. (2011). A molecular mechanism for circadian clock negative feedback. Science *332*, 1436-1439.

Duong, H.A., and Weitz, C.J. (2014). Temporal orchestration of repressive chromatin modifiers by circadian clock Period complexes. Nature structural & molecular biology *21*, 126-132.

Edgar, R.C. (2004). MUSCLE: multiple sequence alignment with high accuracy and high throughput. Nucleic acids research *32*, 1792-1797.

Edwards, M.D., Brancaccio, M., Chesham, J.E., Maywood, E.S., and Hastings, M.H. (2016). Rhythmic expression of cryptochrome induces the circadian clock of arrhythmic suprachiasmatic nuclei through arginine vasopressin signaling. Proceedings of the National Academy of Sciences of the United States of America *113*, 2732-2737.

Eide, E.J., Woolf, M.F., Kang, H., Woolf, P., Hurst, W., Camacho, F., Vielhaber, E.L., Giovanni, A., and Virshup, D.M. (2005). Control of mammalian circadian rhythm by CKIepsilon-regulated proteasome-mediated PER2 degradation. Molecular and cellular biology *25*, 2795-2807.

Emery, P., So, W.V., Kaneko, M., Hall, J.C., and Rosbash, M. (1998). CRY, a Drosophila clock and light-regulated cryptochrome, is a major contributor to circadian rhythm resetting and photosensitivity. Cell *95*, 669-679.

Emsley, P., Lohkamp, B., Scott, W.G., and Cowtan, K. (2010). Features and development of Coot. Acta crystallographica Section D, Biological crystallography *66*, 486-501.

Etchegaray, J.P., Lee, C., Wade, P.A., and Reppert, S.M. (2003). Rhythmic histone acetylation underlies transcription in the mammalian circadian clock. Nature *421*, 177-182.

Etchegaray, J.P., Yang, X., DeBruyne, J.P., Peters, A.H., Weaver, D.R., Jenuwein, T., and Reppert, S.M. (2006). The polycomb group protein EZH2 is required for mammalian circadian clock function. The Journal of biological chemistry *281*, 21209-21215.

Froy, O., Chang, D.C., and Reppert, S.M. (2002). Redox potential: differential roles in dCRY and mCRY1 functions. Current biology : CB *12*, 147-152.

Gao, P., Yoo, S.H., Lee, K.J., Rosensweig, C., Takahashi, J.S., Chen, B.P., and Green, C.B. (2013). Phosphorylation of the cryptochrome 1 C-terminal tail regulates circadian period length. The Journal of biological chemistry *288*, 35277-35286.

Gekakis, N., Staknis, D., Nguyen, H.B., Davis, F.C., Wilsbacher, L.D., King, D.P., Takahashi, J.S., and Weitz, C.J. (1998). Role of the CLOCK protein in the mammalian circadian mechanism. Science *280*, 1564-1569.

Gietzen, K.F., and Virshup, D.M. (1999). Identification of inhibitory autophosphorylation sites in casein kinase I epsilon. The Journal of biological chemistry *274*, 32063-32070.

Glas, A.F., Maul, M.J., Cryle, M., Barends, T.R., Schneider, S., Kaya, E., Schlichting, I., and Carell, T. (2009). The archaeal cofactor F0 is a light-harvesting antenna chromophore in eukaryotes. Proceedings of the National Academy of Sciences of the United States of America *106*, 11540-11545.

Godinho, S.I., Maywood, E.S., Shaw, L., Tucci, V., Barnard, A.R., Busino, L., Pagano, M., Kendall, R., Quwailid, M.M., Romero, M.R.*, et al.* (2007). The after-hours mutant

reveals a role for Fbxl3 in determining mammalian circadian period. Science *316*, 897-900.

Goriki, A., Hatanaka, F., Myung, J., Kim, J.K., Yoritaka, T., Tanoue, S., Abe, T., Kiyonari, H., Fujimoto, K., Kato, Y.*, et al.* (2014). A novel protein, CHRONO, functions as a core component of the mammalian circadian clock. PLoS biology *12*, e1001839.

Griffin, E.A., Jr., Staknis, D., and Weitz, C.J. (1999). Light-independent role of CRY1 and CRY2 in the mammalian circadian clock. Science *286*, 768-771.

Guillaumond, F., Dardente, H., Giguere, V., and Cermakian, N. (2005). Differential control of Bmal1 circadian transcription by REV-ERB and ROR nuclear receptors. Journal of biological rhythms *20*, 391-403.

Gustafson, C.L., Parsley, N.C., Asimgil, H., Lee, H.W., Ahlbach, C., Michael, A.K., Xu, H., Williams, O.L., Davis, T.L., Liu, A.C.*, et al.* (2017). A Slow Conformational Switch in the BMAL1 Transactivation Domain Modulates Circadian Rhythms. Molecular cell *66*, 447-457 e447.

Gustafson, C.L., and Partch, C.L. (2015). Emerging models for the molecular basis of mammalian circadian timing. Biochemistry *54*, 134-149.

Halabi, N., Rivoire, O., Leibler, S., and Ranganathan, R. (2009). Protein sectors: evolutionary units of three-dimensional structure. Cell *138*, 774-786.

Hardin, P.E., Hall, J.C., and Rosbash, M. (1990). Feedback of the Drosophila period gene product on circadian cycling of its messenger RNA levels. Nature *343*, 536-540.

Hennig, S., Strauss, H.M., Vanselow, K., Yildiz, O., Schulze, S., Arens, J., Kramer, A., and Wolf, E. (2009). Structural and functional analyses of PAS domain interactions of the clock proteins Drosophila PERIOD and mouse PERIOD2. PLoS biology *7*, e94.

Hirano, A., Shi, G., Jones, C.R., Lipzen, A., Pennacchio, L.A., Xu, Y., Hallows, W.C., McMahon, T., Yamazaki, M., Ptacek, L.J.*, et al.* (2016). A Cryptochrome 2 Mutation Yields Advanced Sleep Phase in Human. eLife *5*.

Hirano, A., Yumimoto, K., Tsunematsu, R., Matsumoto, M., Oyama, M., Kozuka-Hata, H., Nakagawa, T., Lanjakornsiripan, D., Nakayama, K.I., and Fukada, Y. (2013). FBXL21 regulates oscillation of the circadian clock through ubiquitination and stabilization of cryptochromes. Cell *152*, 1106-1118.

Hirayama, J., Nakamura, H., Ishikawa, T., Kobayashi, Y., and Todo, T. (2003). Functional and structural analyses of cryptochrome. Vertebrate CRY regions responsible for interaction with the CLOCK:BMAL1 heterodimer and its nuclear localization. The Journal of biological chemistry *278*, 35620-35628.

Hirayama, J., Sahar, S., Grimaldi, B., Tamaru, T., Takamatsu, K., Nakahata, Y., and Sassone-Corsi, P. (2007). CLOCK-mediated acetylation of BMAL1 controls circadian function. Nature *450*, 1086-1090.

Hirota, T., Lee, J.W., St John, P.C., Sawa, M., Iwaisako, K., Noguchi, T., Pongsawakul, P.Y., Sonntag, T., Welsh, D.K., Brenner, D.A.*, et al.* (2012). Identification of small molecule activators of cryptochrome. Science *337*, 1094-1097.

Hitomi, K., DiTacchio, L., Arvai, A.S., Yamamoto, J., Kim, S.T., Todo, T., Tainer, J.A., Iwai, S., Panda, S., and Getzoff, E.D. (2009). Functional motifs in the (6-4) photolyase crystal structure make a comparative framework for DNA repair photolyases and clock cryptochromes. Proceedings of the National Academy of Sciences of the United States of America *106*, 6962-6967.

Hogenesch, J.B., Chan, W.K., Jackiw, V.H., Brown, R.C., Gu, Y.Z., Pray-Grant, M., Perdew, G.H., and Bradfield, C.A. (1997). Characterization of a subset of the basic-helix-loop-helix-PAS superfamily that interacts with components of the dioxin signaling pathway. The Journal of biological chemistry *272*, 8581-8593.

Hogenesch, J.B., Gu, Y.Z., Jain, S., and Bradfield, C.A. (1998). The basic-helix-loop-helix-PAS orphan MOP3 forms transcriptionally active complexes with circadian and hypoxia factors. Proceedings of the National Academy of Sciences of the United States of America *95*, 5474-5479.

Hsu, D.S., Zhao, X., Zhao, S., Kazantsev, A., Wang, R.P., Todo, T., Wei, Y.F., and Sancar, A. (1996). Putative human blue-light photoreceptors hCRY1 and hCRY2 are flavoproteins. Biochemistry *35*, 13871-13877.

Hu, C.D., Chinenov, Y., and Kerppola, T.K. (2002). Visualization of interactions among bZIP and Rel family proteins in living cells using bimolecular fluorescence complementation. Molecular cell *9*, 789-798.

Hu, C.D., and Kerppola, T.K. (2003). Simultaneous visualization of multiple protein interactions in living cells using multicolor fluorescence complementation analysis. Nature biotechnology *21*, 539-545.

Huang, N., Chelliah, Y., Shan, Y., Taylor, C.A., Yoo, S.H., Partch, C., Green, C.B., Zhang, H., and Takahashi, J.S. (2012). Crystal structure of the heterodimeric CLOCK:BMAL1 transcriptional activator complex. Science *337*, 189-194.

Ingram, K.K., Kutowoi, A., Wurm, Y., Shoemaker, D., Meier, R., and Bloch, G. (2012). The molecular clockwork of the fire ant Solenopsis invicta. PloS one *7*, e45715.

Jin, X., Shearman, L.P., Weaver, D.R., Zylka, M.J., de Vries, G.J., and Reppert, S.M. (1999). A molecular mechanism regulating rhythmic output from the suprachiasmatic circadian clock. Cell *96*, 57-68.

Kaiser, T.S., Poehn, B., Szkiba, D., Preussner, M., Sedlazeck, F.J., Zrim, A., Neumann, T., Nguyen, L.T., Betancourt, A.J., Hummel, T.*, et al.* (2016). The genomic basis of circadian and circalunar timing adaptations in a midge. Nature *540*, 69-73.

Kamentsky, L., Jones, T.R., Fraser, A., Bray, M.A., Logan, D.J., Madden, K.L., Ljosa, V., Rueden, C., Eliceiri, K.W., and Carpenter, A.E. (2011). Improved structure, function

and compatibility for CellProfiler: modular high-throughput image analysis software. Bioinformatics *27*, 1179-1180.

Katada, S., and Sassone-Corsi, P. (2010). The histone methyltransferase MLL1 permits the oscillation of circadian gene expression. Nature structural & molecular biology *17*, 1414-1421.

Kavakli, I.H., Baris, I., Tardu, M., Gul, S., Oner, H., Cal, S., Bulut, S., Yarparvar, D., Berkel, C., Ustaoglu, P.*, et al.* (2017). The Photolyase/Cryptochrome Family of Proteins as DNA Repair Enzymes and Transcriptional Repressors. Photochemistry and photobiology *93*, 93-103.

Khan, S.K., Xu, H., Ukai-Tadenuma, M., Burton, B., Wang, Y., Ueda, H.R., and Liu, A.C. (2012). Identification of a novel cryptochrome differentiating domain required for feedback repression in circadian clock function. The Journal of biological chemistry *287*, 25917-25926.

Kim, J.Y., Kwak, P.B., Gebert, M., Duong, H.A., and Weitz, C.J. (2015). Purification and analysis of PERIOD protein complexes of the mammalian circadian clock. Methods in enzymology *551*, 197-210.

Kim, J.Y., Kwak, P.B., and Weitz, C.J. (2014). Specificity in circadian clock feedback from targeted reconstitution of the NuRD corepressor. Molecular cell *56*, 738-748.

King, D.P., Zhao, Y., Sangoram, A.M., Wilsbacher, L.D., Tanaka, M., Antoch, M.P., Steeves, T.D., Vitaterna, M.H., Kornhauser, J.M., Lowrey, P.L.*, et al.* (1997). Positional cloning of the mouse circadian clock gene. Cell *89*, 641-653.

Kiyohara, Y.B., Tagao, S., Tamanini, F., Morita, A., Sugisawa, Y., Yasuda, M., Yamanaka, I., Ueda, H.R., van der Horst, G.T., Kondo, T.*, et al.* (2006). The BMAL1 C terminus regulates the circadian transcription feedback loop. Proceedings of the National Academy of Sciences of the United States of America *103*, 10074-10079.

Kloss, B., Price, J.L., Saez, L., Blau, J., Rothenfluh, A., Wesley, C.S., and Young, M.W. (1998). The Drosophila clock gene double-time encodes a protein closely related to human casein kinase Iepsilon. Cell *94*, 97-107.

Kobayashi, K., Kanno, S., Smit, B., van der Horst, G.T., Takao, M., and Yasui, A. (1998). Characterization of photolyase/blue-light receptor homologs in mouse and human cells. Nucleic acids research *26*, 5086-5092.

Koh, K., Zheng, X., and Sehgal, A. (2006). JETLAG resets the Drosophila circadian clock by promoting light-induced degradation of TIMELESS. Science *312*, 1809-1812.

Koike, N., Yoo, S.H., Huang, H.C., Kumar, V., Lee, C., Kim, T.K., and Takahashi, J.S. (2012). Transcriptional architecture and chromatin landscape of the core circadian clock in mammals. Science *338*, 349-354.

Konopka, R.J., and Benzer, S. (1971). Clock mutants of Drosophila melanogaster. Proceedings of the National Academy of Sciences of the United States of America *68*, 2112-2116.

Krishnan, B., Levine, J.D., Lynch, M.K., Dowse, H.B., Funes, P., Hall, J.C., Hardin, P.E., and Dryer, S.E. (2001). A new role for cryptochrome in a Drosophila circadian oscillator. Nature *411*, 313-317.

Kucera, N., Schmalen, I., Hennig, S., Ollinger, R., Strauss, H.M., Grudziecki, A., Wieczorek, C., Kramer, A., and Wolf, E. (2012). Unwinding the differences of the mammalian PERIOD clock proteins from crystal structure to cellular function. Proceedings of the National Academy of Sciences of the United States of America *109*, 3311-3316.

Kume, K., Zylka, M.J., Sriram, S., Shearman, L.P., Weaver, D.R., Jin, X., Maywood, E.S., Hastings, M.H., and Reppert, S.M. (1999). mCRY1 and mCRY2 are essential components of the negative limb of the circadian clock feedback loop. Cell *98*, 193-205.

Lamia, K.A., Sachdeva, U.M., DiTacchio, L., Williams, E.C., Alvarez, J.G., Egan, D.F., Vasquez, D.S., Juguilon, H., Panda, S., Shaw, R.J.*, et al.* (2009). AMPK regulates the circadian clock by cryptochrome phosphorylation and degradation. Science *326*, 437-440.

Lande-Diner, L., Boyault, C., Kim, J.Y., and Weitz, C.J. (2013). A positive feedback loop links circadian clock factor CLOCK-BMAL1 to the basic transcriptional machinery.

Proceedings of the National Academy of Sciences of the United States of America *110*, 16021-16026.

Larrondo, L.F., Olivares-Yanez, C., Baker, C.L., Loros, J.J., and Dunlap, J.C. (2015). Circadian rhythms. Decoupling circadian clock protein turnover from circadian period determination. Science *347*, 1257277.

Lee, C., Etchegaray, J.P., Cagampang, F.R., Loudon, A.S., and Reppert, S.M. (2001). Posttranslational mechanisms regulate the mammalian circadian clock. Cell *107*, 855-867.

Lee, C., Weaver, D.R., and Reppert, S.M. (2004). Direct association between mouse PERIOD and CKIepsilon is critical for a functioning circadian clock. Molecular and cellular biology *24*, 584-594.

Lee, E., Cho, E., Kang, D.H., Jeong, E.H., Chen, Z., Yoo, S.H., and Kim, E.Y. (2016). Pacemaker-neuron-dependent disturbance of the molecular clockwork by a Drosophila CLOCK mutant homologous to the mouse Clock mutation. Proceedings of the National Academy of Sciences of the United States of America *113*, E4904-4913.

Lee, J., Natarajan, M., Nashine, V.C., Socolich, M., Vo, T., Russ, W.P., Benkovic, S.J., and Ranganathan, R. (2008). Surface sites for engineering allosteric control in proteins. Science *322*, 438-442.

Lee, Y., Jang, A.R., Francey, L.J., Sehgal, A., and Hogenesch, J.B. (2015). KPNB1 mediates PER/CRY nuclear translocation and circadian clock function. eLife *4*.

Li, Y., and Rosbash, M. (2013). Accelerated degradation of perS protein provides insight into light-mediated phase shifting. Journal of biological rhythms *28*, 171-182.

Li, Y., Xiong, W., and Zhang, E.E. (2016). The ratio of intracellular CRY proteins determines the clock period length. Biochemical and biophysical research communications *472*, 531-538.

Li, Y., Yu, W., Liang, Y., and Zhu, X. (2007). Kinetochore dynein generates a poleward pulling force to facilitate congression and full chromosome alignment. Cell research *17*, 701-712.

Liu, A.C., Tran, H.G., Zhang, E.E., Priest, A.A., Welsh, D.K., and Kay, S.A. (2008). Redundant function of REV-ERBalpha and beta and non-essential role for Bmal1 cycling in transcriptional regulation of intracellular circadian rhythms. PLoS genetics *4*, e1000023.

Liu, A.C., Welsh, D.K., Ko, C.H., Tran, H.G., Zhang, E.E., Priest, A.A., Buhr, E.D., Singer, O., Meeker, K., Verma, I.M.*, et al.* (2007). Intercellular coupling confers robustness against mutations in the SCN circadian clock network. Cell *129*, 605-616.

Lowrey, P.L., Shimomura, K., Antoch, M.P., Yamazaki, S., Zemenides, P.D., Ralph, M.R., Menaker, M., and Takahashi, J.S. (2000). Positional syntenic cloning and functional characterization of the mammalian circadian mutation tau. Science *288*, 483-492.

Lowrey, P.L., and Takahashi, J.S. (2011). Genetics of circadian rhythms in Mammalian model organisms. Advances in genetics *74*, 175-230.

Martinek, S., Inonog, S., Manoukian, A.S., and Young, M.W. (2001). A role for the segment polarity gene shaggy/GSK-3 in the Drosophila circadian clock. Cell *105*, 769-779.

McCarthy, E.V., Baggs, J.E., Geskes, J.M., Hogenesch, J.B., and Green, C.B. (2009). Generation of a novel allelic series of cryptochrome mutants via mutagenesis reveals residues involved in protein-protein interaction and CRY2-specific repression. Molecular and cellular biology *29*, 5465-5476.

Mees, A., Klar, T., Gnau, P., Hennecke, U., Eker, A.P., Carell, T., and Essen, L.O. (2004). Crystal structure of a photolyase bound to a CPD-like DNA lesion after in situ repair. Science *306*, 1789-1793.

Menet, J.S., Pescatore, S., and Rosbash, M. (2014). CLOCK:BMAL1 is a pioneer-like transcription factor. Genes & development *28*, 8-13.

Meng, Q.J., Logunova, L., Maywood, E.S., Gallego, M., Lebiecki, J., Brown, T.M., Sladek, M., Semikhodskii, A.S., Glossop, N.R., Piggins, H.D*., et al.* (2008). Setting clock speed in mammals: the CK1 epsilon tau mutation in mice accelerates circadian pacemakers by selectively destabilizing PERIOD proteins. Neuron *58*, 78-88.

Merbitz-Zahradnik, T., and Wolf, E. (2015). How is the inner circadian clock controlled by interactive clock proteins?: Structural analysis of clock proteins elucidates their physiological role. FEBS letters *589*, 1516-1529.

Meyer, P., Saez, L., and Young, M.W. (2006). PER-TIM interactions in living Drosophila cells: an interval timer for the circadian clock. Science *311*, 226-229.

Michael, A.K., Fribourgh, J.L., Chelliah, Y., Sandate, C.R., Hura, G.L., Schneidman-Duhovny, D., Tripathi, S.M., Takahashi, J.S., and Partch, C.L. (2017). Formation of a repressive complex in the mammalian circadian clock is mediated by the secondary pocket of CRY1. Proceedings of the National Academy of Sciences of the United States of America *114*, 1560-1565.

Nam, H.J., Boo, K., Kim, D., Han, D.H., Choe, H.K., Kim, C.R., Sun, W., Kim, H., Kim, K., Lee, H.*, et al.* (2014). Phosphorylation of LSD1 by PKCalpha is crucial for circadian rhythmicity and phase resetting. Molecular cell *53*, 791-805.

Nangle, S., Xing, W., and Zheng, N. (2013). Crystal structure of mammalian cryptochrome in complex with a small molecule competitor of its ubiquitin ligase. Cell research *23*, 1417-1419.

Nangle, S.N., Rosensweig, C., Koike, N., Tei, H., Takahashi, J.S., Green, C.B., and Zheng, N. (2014). Molecular assembly of the period-cryptochrome circadian transcriptional repressor complex. eLife *3*, e03674.

Ode, K.L., Ukai, H., Susaki, E.A., Narumi, R., Matsumoto, K., Hara, J., Koide, N., Abe, T., Kanemaki, M.T., Kiyonari, H.*, et al.* (2017). Knockout-Rescue Embryonic Stem Cell-Derived Mouse Reveals Circadian-Period Control by Quality and Quantity of CRY1. Molecular cell *65*, 176-190.

Ollinger, R., Korge, S., Korte, T., Koller, B., Herrmann, A., and Kramer, A. (2014). Dynamics of the circadian clock protein PERIOD2 in living cells. Journal of cell science *127*, 4322-4328.

Otwinowski, Z., and Minor, W. (1997). Processing of X-ray diffraction data collected in oscillation mode. Methods in enzymology *276*, 307-326.

Ozber, N., Baris, I., Tatlici, G., Gur, I., Kilinc, S., Unal, E.B., and Kavakli, I.H. (2010). Identification of two amino acids in the C-terminal domain of mouse CRY2 essential for PER2 interaction. BMC molecular biology *11*, 69.

Ozgur, S., and Sancar, A. (2003). Purification and properties of human blue-light photoreceptor cryptochrome 2. Biochemistry *42*, 2926-2932.

Ozturk, N., Song, S.H., Ozgur, S., Selby, C.P., Morrison, L., Partch, C., Zhong, D., and Sancar, A. (2007). Structure and function of animal cryptochromes. Cold Spring Harbor symposia on quantitative biology *72*, 119-131.

Padmanabhan, K., Robles, M.S., Westerling, T., and Weitz, C.J. (2012). Feedback regulation of transcriptional termination by the mammalian circadian clock PERIOD complex. Science *337*, 599-602.

Panda, S., Antoch, M.P., Miller, B.H., Su, A.I., Schook, A.B., Straume, M., Schultz, P.G., Kay, S.A., Takahashi, J.S., and Hogenesch, J.B. (2002). Coordinated transcription of key pathways in the mouse by the circadian clock. Cell *109*, 307-320.

Papp, S.J., Huber, A.L., Jordan, S.D., Kriebs, A., Nguyen, M., Moresco, J.J., Yates, J.R., and Lamia, K.A. (2015). DNA damage shifts circadian clock time via Hausp-dependent Cry1 stabilization. eLife *4*.

Park, H.W., Kim, S.T., Sancar, A., and Deisenhofer, J. (1995). Crystal structure of DNA photolyase from Escherichia coli. Science *268*, 1866-1872.

Partch, C.L., Green, C.B., and Takahashi, J.S. (2014). Molecular architecture of the mammalian circadian clock. Trends in cell biology *24*, 90-99.

Partch, C.L., Shields, K.F., Thompson, C.L., Selby, C.P., and Sancar, A. (2006). Posttranslational regulation of the mammalian circadian clock by cryptochrome and protein phosphatase 5. Proceedings of the National Academy of Sciences of the United States of America *103*, 10467-10472.

Patke, A., Murphy, P.J., Onat, O.E., Krieger, A.C., Ozcelik, T., Campbell, S.S., and Young, M.W. (2017). Mutation of the Human Circadian Clock Gene CRY1 in Familial Delayed Sleep Phase Disorder. Cell *169*, 203-215 e213.

Pei, J., Kim, B.H., and Grishin, N.V. (2008). PROMALS3D: a tool for multiple protein sequence and structure alignments. Nucleic acids research *36*, 2295-2300.

Pérez, F., and Granger, B.E. (2007). IPython: a system for interactive scientific computing. Computing in Science & Engineering *9*, 21-29.

Preitner, N., Damiola, F., Lopez-Molina, L., Zakany, J., Duboule, D., Albrecht, U., and Schibler, U. (2002). The orphan nuclear receptor REV-ERBalpha controls circadian transcription within the positive limb of the mammalian circadian oscillator. Cell *110*, 251-260.

Price, J.L., Blau, J., Rothenfluh, A., Abodeely, M., Kloss, B., and Young, M.W. (1998). double-time is a novel Drosophila clock gene that regulates PERIOD protein accumulation. Cell *94*, 83-95.

Ralph, M.R., Foster, R.G., Davis, F.C., and Menaker, M. (1990). Transplanted suprachiasmatic nucleus determines circadian period. Science *247*, 975-978.

Ralph, M.R., and Menaker, M. (1988). A mutation of the circadian system in golden hamsters. Science *241*, 1225-1227.

Reddy, P., Zehring, W.A., Wheeler, D.A., Pirrotta, V., Hadfield, C., Hall, J.C., and Rosbash, M. (1984). Molecular analysis of the period locus in Drosophila melanogaster and identification of a transcript involved in biological rhythms. Cell *38*, 701-710.

Reick, M., Garcia, J.A., Dudley, C., and McKnight, S.L. (2001). NPAS2: an analog of clock operative in the mammalian forebrain. Science *293*, 506-509.

Reischl, S., Vanselow, K., Westermark, P.O., Thierfelder, N., Maier, B., Herzel, H., and Kramer, A. (2007). Beta-TrCP1-mediated degradation of PERIOD2 is essential for circadian dynamics. Journal of biological rhythms *22*, 375-386.

Reppert, S.M., and Weaver, D.R. (2002). Coordination of circadian timing in mammals. Nature *418*, 935-941.

Reynolds, K.A., McLaughlin, R.N., and Ranganathan, R. (2011). Hot spots for allosteric regulation on protein surfaces. Cell *147*, 1564-1575.

Rivoire, O., Reynolds, K.A., and Ranganathan, R. (2016). Evolution-Based Functional Decomposition of Proteins. PLoS computational biology *12*, e1004817.

Robles, M.S., Boyault, C., Knutti, D., Padmanabhan, K., and Weitz, C.J. (2010). Identification of RACK1 and protein kinase Calpha as integral components of the mammalian circadian clock. Science *327*, 463-466.

Rubin, E.B., Shemesh, Y., Cohen, M., Elgavish, S., Robertson, H.M., and Bloch, G. (2006). Molecular and phylogenetic analyses reveal mammalian-like clockwork in the honey bee (Apis mellifera) and shed new light on the molecular evolution of the circadian clock. Genome research *16*, 1352-1365.

Rutila, J.E., Suri, V., Le, M., So, W.V., Rosbash, M., and Hall, J.C. (1998). CYCLE is a second bHLH-PAS clock protein essential for circadian rhythmicity and transcription of Drosophila period and timeless. Cell *93*, 805-814.

Sakakida, Y., Miyamoto, Y., Nagoshi, E., Akashi, M., Nakamura, T.J., Mamine, T., Kasahara, M., Minami, Y., Yoneda, Y., and Takumi, T. (2005). Importin alpha/beta mediates nuclear transport of a mammalian circadian clock component, mCRY2, together with mPER2, through a bipartite nuclear localization signal. The Journal of biological chemistry *280*, 13272-13278.

Sanada, K., Harada, Y., Sakai, M., Todo, T., and Fukada, Y. (2004). Serine phosphorylation of mCRY1 and mCRY2 by mitogen-activated protein kinase. Genes to cells : devoted to molecular & cellular mechanisms *9*, 697-708.

Sancar, A. (2008). Structure and function of photolyase and in vivo enzymology: 50th anniversary. The Journal of biological chemistry *283*, 32153-32157.

Sangoram, A.M., Saez, L., Antoch, M.P., Gekakis, N., Staknis, D., Whiteley, A., Fruechte, E.M., Vitaterna, M.H., Shimomura, K., King, D.P.*, et al.* (1998). Mammalian circadian autoregulatory loop: a timeless ortholog and mPer1 interact and negatively regulate CLOCK-BMAL1-induced transcription. Neuron *21*, 1101-1113.

Sato, T.K., Panda, S., Miraglia, L.J., Reyes, T.M., Rudic, R.D., McNamara, P., Naik, K.A., FitzGerald, G.A., Kay, S.A., and Hogenesch, J.B. (2004). A functional genomics strategy reveals Rora as a component of the mammalian circadian clock. Neuron *43*, 527-537.

Sato, T.K., Yamada, R.G., Ukai, H., Baggs, J.E., Miraglia, L.J., Kobayashi, T.J., Welsh, D.K., Kay, S.A., Ueda, H.R., and Hogenesch, J.B. (2006). Feedback repression is required for mammalian circadian clock function. Nature genetics *38*, 312-319.

Schmalen, I., Reischl, S., Wallach, T., Klemz, R., Grudziecki, A., Prabu, J.R., Benda, C., Kramer, A., and Wolf, E. (2014). Interaction of circadian clock proteins CRY1 and PER2 is modulated by zinc binding and disulfide bond formation. Cell *157*, 1203-1215.

Sehgal, A., Rothenfluh-Hilfiker, A., Hunter-Ensor, M., Chen, Y., Myers, M.P., and Young, M.W. (1995). Rhythmic expression of timeless: a basis for promoting circadian cycles in period gene autoregulation. Science *270*, 808-810.

Shearman, L.P., Jin, X., Lee, C., Reppert, S.M., and Weaver, D.R. (2000a). Targeted disruption of the mPer3 gene: subtle effects on circadian clock function. Molecular and cellular biology *20*, 6269-6275.

Shearman, L.P., Sriram, S., Weaver, D.R., Maywood, E.S., Chaves, I., Zheng, B., Kume, K., Lee, C.C., van der Horst, G.T., Hastings, M.H.*, et al.* (2000b). Interacting molecular loops in the mammalian circadian clock. Science *288*, 1013-1019.

Shearman, L.P., Zylka, M.J., Weaver, D.R., Kolakowski, L.F., Jr., and Reppert, S.M. (1997). Two period homologs: circadian expression and photic regulation in the suprachiasmatic nuclei. Neuron *19*, 1261-1269.

Shigeyoshi, Y., Taguchi, K., Yamamoto, S., Takekida, S., Yan, L., Tei, H., Moriya, T., Shibata, S., Loros, J.J., Dunlap, J.C.*, et al.* (1997). Light-induced resetting of a

mammalian circadian clock is associated with rapid induction of the mPer1 transcript. Cell *91*, 1043-1053.

Shirogane, T., Jin, J., Ang, X.L., and Harper, J.W. (2005). SCFβ-TRCP controls clock-dependent transcription via casein kinase 1-dependent degradation of the mammalian period-1 (Per1) protein. The Journal of biological chemistry *280*, 26863-26872.

Siepka, S.M., Yoo, S.H., Park, J., Song, W., Kumar, V., Hu, Y., Lee, C., and Takahashi, J.S. (2007). Circadian mutant Overtime reveals F-box protein FBXL3 regulation of cryptochrome and period gene expression. Cell *129*, 1011-1023.

Smyllie, N.J., Pilorz, V., Boyd, J., Meng, Q.J., Saer, B., Chesham, J.E., Maywood, E.S., Krogager, T.P., Spiller, D.G., Boot-Handford, R.*, et al.* (2016). Visualizing and Quantifying Intracellular Behavior and Abundance of the Core Circadian Clock Protein PERIOD2. Current biology : CB *26*, 1880-1886.

Somers, W., Ultsch, M., De Vos, A.M., and Kossiakoff, A.A. (1994). The X-ray structure of a growth hormone-prolactin receptor complex. Nature *372*, 478-481.

Stanewsky, R., Kaneko, M., Emery, P., Beretta, B., Wager-Smith, K., Kay, S.A., Rosbash, M., and Hall, J.C. (1998). The cryb mutation identifies cryptochrome as a circadian photoreceptor in Drosophila. Cell *95*, 681-692.

Storch, K.F., Lipan, O., Leykin, I., Viswanathan, N., Davis, F.C., Wong, W.H., and Weitz, C.J. (2002). Extensive and divergent circadian gene expression in liver and heart. Nature *417*, 78-83.

Suel, G.M., Lockless, S.W., Wall, M.A., and Ranganathan, R. (2003). Evolutionarily conserved networks of residues mediate allosteric communication in proteins. Nature structural biology *10*, 59-69.

Sun, Z.S., Albrecht, U., Zhuchenko, O., Bailey, J., Eichele, G., and Lee, C.C. (1997). RIGUI, a putative mammalian ortholog of the Drosophila period gene. Cell *90*, 1003-1011.

Takahata, S., Ozaki, T., Mimura, J., Kikuchi, Y., Sogawa, K., and Fujii-Kuriyama, Y. (2000). Transactivation mechanisms of mouse clock transcription factors, mClock and mArnt3. Genes to cells : devoted to molecular & cellular mechanisms *5*, 739-747.

Tamada, T., Kitadokoro, K., Higuchi, Y., Inaka, K., Yasui, A., de Ruiter, P.E., Eker, A.P., and Miki, K. (1997). Crystal structure of DNA photolyase from Anacystis nidulans. Nature structural biology *4*, 887-891.

Tamayo, A.G., Duong, H.A., Robles, M.S., Mann, M., and Weitz, C.J. (2015). Histone monoubiquitination by Clock-Bmal1 complex marks Per1 and Per2 genes for circadian feedback. Nature structural & molecular biology *22*, 759-766.

Tamiya, H., Ogawa, S., Ouchi, Y., and Akishita, M. (2016). Rigid Cooperation of Per1 and Per2 proteins. Scientific reports *6*, 32769.

Tei, H., Okamura, H., Shigeyoshi, Y., Fukuhara, C., Ozawa, R., Hirose, M., and Sakaki, Y. (1997). Circadian oscillation of a mammalian homologue of the Drosophila period gene. Nature *389*, 512-516.

Thresher, R.J., Vitaterna, M.H., Miyamoto, Y., Kazantsev, A., Hsu, D.S., Petit, C., Selby, C.P., Dawut, L., Smithies, O., Takahashi, J.S., *et al.* (1998). Role of mouse cryptochrome blue-light photoreceptor in circadian photoresponses. Science *282*, 1490-1494.

Toh, K.L., Jones, C.R., He, Y., Eide, E.J., Hinz, W.A., Virshup, D.M., Ptacek, L.J., and Fu, Y.H. (2001). An hPer2 phosphorylation site mutation in familial advanced sleep phase syndrome. Science *291*, 1040-1043.

Ueda, H.R., Chen, W., Adachi, A., Wakamatsu, H., Hayashi, S., Takasugi, T., Nagano, M., Nakahama, K., Suzuki, Y., Sugano, S., *et al.* (2002). A transcription factor response element for gene expression during circadian night. Nature *418*, 534-539.

Ueda, H.R., Hayashi, S., Chen, W., Sano, M., Machida, M., Shigeyoshi, Y., Iino, M., and Hashimoto, S. (2005). System-level identification of transcriptional circuits underlying mammalian circadian clocks. Nature genetics *37*, 187-192.

Ukai-Tadenuma, M., Yamada, R.G., Xu, H., Ripperger, J.A., Liu, A.C., and Ueda, H.R. (2011). Delay in feedback repression by cryptochrome 1 is required for circadian clock function. Cell *144*, 268-281.

van der Horst, G.T., Muijtjens, M., Kobayashi, K., Takano, R., Kanno, S., Takao, M., de Wit, J., Verkerk, A., Eker, A.P., van Leenen, D., *et al.* (1999). Mammalian Cry1 and Cry2 are essential for maintenance of circadian rhythms. Nature *398*, 627-630.

Vitaterna, M.H., King, D.P., Chang, A.M., Kornhauser, J.M., Lowrey, P.L., McDonald, J.D., Dove, W.F., Pinto, L.H., Turek, F.W., and Takahashi, J.S. (1994). Mutagenesis and mapping of a mouse gene, Clock, essential for circadian behavior. Science *264*, 719-725.

Vitaterna, M.H., Selby, C.P., Todo, T., Niwa, H., Thompson, C., Fruechte, E.M., Hitomi, K., Thresher, R.J., Ishikawa, T., Miyazaki, J.*, et al.* (1999). Differential regulation of mammalian period genes and circadian rhythmicity by cryptochromes 1 and 2. Proceedings of the National Academy of Sciences of the United States of America *96*, 12114-12119.

Wang, D., Hosteen, O., and Fierke, C.A. (2012). ZntR-mediated transcription of zntA responds to nanomolar intracellular free zinc. Journal of inorganic biochemistry *111*, 173-181.

Wang, Z., Wu, Y., Li, L., and Su, X.D. (2013). Intermolecular recognition revealed by the complex structure of human CLOCK-BMAL1 basic helix-loop-helix domains with E-box DNA. Cell research *23*, 213-224.

Wang, Z., Zang, C., Cui, K., Schones, D.E., Barski, A., Peng, W., and Zhao, K. (2009). Genome-wide mapping of HATs and HDACs reveals distinct functions in active and inactive genes. Cell *138*, 1019-1031.

Winn, M.D., Ballard, C.C., Cowtan, K.D., Dodson, E.J., Emsley, P., Evans, P.R., Keegan, R.M., Krissinel, E.B., Leslie, A.G., McCoy, A.*, et al.* (2011). Overview of the

CCP4 suite and current developments. Acta crystallographica Section D, Biological crystallography *67*, 235-242.

Xing, W., Busino, L., Hinds, T.R., Marionni, S.T., Saifee, N.H., Bush, M.F., Pagano, M., and Zheng, N. (2013). SCF(FBXL3) ubiquitin ligase targets cryptochromes at their cofactor pocket. Nature *496*, 64-68.

Xu, H., Gustafson, C.L., Sammons, P.J., Khan, S.K., Parsley, N.C., Ramanathan, C., Lee, H.W., Liu, A.C., and Partch, C.L. (2015). Cryptochrome 1 regulates the circadian clock through dynamic interactions with the BMAL1 C terminus. Nature structural & molecular biology *22*, 476-484.

Xu, Y., Padiath, Q.S., Shapiro, R.E., Jones, C.R., Wu, S.C., Saigoh, N., Saigoh, K., Ptacek, L.J., and Fu, Y.H. (2005). Functional consequences of a CKIdelta mutation causing familial advanced sleep phase syndrome. Nature *434*, 640-644.

Yagita, K., Tamanini, F., Yasuda, M., Hoeijmakers, J.H., van der Horst, G.T., and Okamura, H. (2002). Nucleocytoplasmic shuttling and mCRY-dependent inhibition of ubiquitylation of the mPER2 clock protein. The EMBO journal *21*, 1301-1314.

Ye, R., Selby, C.P., Chiou, Y.Y., Ozkan-Dagliyan, I., Gaddameedhi, S., and Sancar, A. (2014). Dual modes of CLOCK:BMAL1 inhibition mediated by Cryptochrome and Period proteins in the mammalian circadian clock. Genes & development *28*, 1989-1998.

Ye, R., Selby, C.P., Ozturk, N., Annayev, Y., and Sancar, A. (2011). Biochemical analysis of the canonical model for the mammalian circadian clock. The Journal of biological chemistry *286*, 25891-25902.

Yoo, S.H., Ko, C.H., Lowrey, P.L., Buhr, E.D., Song, E.J., Chang, S., Yoo, O.J., Yamazaki, S., Lee, C., and Takahashi, J.S. (2005). A noncanonical E-box enhancer drives mouse Period2 circadian oscillations in vivo. Proceedings of the National Academy of Sciences of the United States of America *102*, 2608-2613.

Yoo, S.H., Mohawk, J.A., Siepka, S.M., Shan, Y., Huh, S.K., Hong, H.K., Kornblum, I., Kumar, V., Koike, N., Xu, M.*, et al.* (2013). Competing E3 ubiquitin ligases govern circadian periodicity by degradation of CRY in nucleus and cytoplasm. Cell *152*, 1091-1105.

Yoshitane, H., Takao, T., Satomi, Y., Du, N.H., Okano, T., and Fukada, Y. (2009). Roles of CLOCK phosphorylation in suppression of E-box-dependent transcription. Molecular and cellular biology *29*, 3675-3686.

Yuan, Q., Metterville, D., Briscoe, A.D., and Reppert, S.M. (2007). Insect cryptochromes: gene duplication and loss define diverse ways to construct insect circadian clocks. Molecular biology and evolution *24*, 948-955.

Zehring, W.A., Wheeler, D.A., Reddy, P., Konopka, R.J., Kyriacou, C.P., Rosbash, M., and Hall, J.C. (1984). P-element transformation with period locus DNA restores rhythmicity to mutant, arrhythmic Drosophila melanogaster. Cell *39*, 369-376.

Zhao, W.N., Malinin, N., Yang, F.C., Staknis, D., Gekakis, N., Maier, B., Reischl, S., Kramer, A., and Weitz, C.J. (2007). CIPC is a mammalian circadian clock protein without invertebrate homologues. Nature cell biology *9*, 268-275.

Zhou, M., Kim, J.K., Eng, G.W., Forger, D.B., and Virshup, D.M. (2015). A Period2 Phosphoswitch Regulates and Temperature Compensates Circadian Period. Molecular cell *60*, 77-88.

Zoltowski, B.D., Vaidya, A.T., Top, D., Widom, J., Young, M.W., and Crane, B.R. (2011). Structure of full-length Drosophila cryptochrome. Nature *480*, 396-399.

Zylka, M.J., Shearman, L.P., Weaver, D.R., and Reppert, S.M. (1998). Three period homologs in mammals: differential light responses in the suprachiasmatic circadian clock and oscillating transcripts outside of brain. Neuron *20*, 1103-1110.